University of Kent

Kent Academic Repository

Steer, Brian (2014) *Selective Characterisation of Engineered Nanoparticles in Aerosols using Nucleation and Optical Techniques.* Doctor of Philosophy (PhD) thesis, University of Kent,.

Downloaded from

https://kar.kent.ac.uk/48699/ The University of Kent's Academic Repository KAR

The version of record is available from

This document version

UNSPECIFIED

DOI for this version

Licence for this version

UNSPECIFIED

Additional information

Versions of research works

Versions of Record

If this version is the version of record, it is the same as the published version available on the publisher's web site. Cite as the published version.

Author Accepted Manuscripts

If this document is identified as the Author Accepted Manuscript it is the version after peer review but before type setting, copy editing or publisher branding. Cite as Surname, Initial. (Year) 'Title of article'. To be published in *Title of Journal* , Volume and issue numbers [peer-reviewed accepted version]. Available at: DOI or URL (Accessed: date).

Enquiries

If you have questions about this document contact ResearchSupport@kent.ac.uk. Please include the URL of the record in KAR. If you believe that your, or a third party's rights have been compromised through this document please see our Take Down policy (available from https://www.kent.ac.uk/guides/kar-the-kent-academic-repository#policies).

University of Kent

Nanoeum

Selective Characterisation of Engineered Nanoparticles in Aerosols using Nucleation and Optical Techniques

Brian Steer

A thesis submitted for the degree of

Doctor of Philosophy

2014

Many thanks are due to my two supervisors:

Adrian Podoleanu – Professor of Biomedical Optics and Head of the Applied Optics Group at the University of Kent. (Biography and Research at UKC)
&
Boris Gorbunov – Technical Director at Naneum Ltd. and visiting professor at the School of Physical Sciences, University of Kent. (www.naneum.com)

Both of whom brought their considerable experience and wisdom to bear while guiding me through my PhD studies. Always able and willing to find time in their busy schedules to offer advice and feedback on my research and thesis preparations, their assistance over the years has been very much appreciated.

In addition I would also like to thank all of those detailed in the closing acknowledgements for their myriad of contributions and assistance towards this work, as well as for providing a great working environment and camaraderie over the years.

Except where otherwise noted, this work is licensed under the
Creative Commons Attribution 4.0 International License.
To view a copy of this license, visit:
http://creativecommons.org/licenses/by/4.0/

Table of Contents

List of Figures

Abbreviations

AAS	Atomic Absorption Spectroscopy
AE	Aerosol Electrometer
AEMSA	Aerosol Electrical Mobility Spectrum Analyser
AES	Atomic Emission Spectroscopy
AF	Air Filter
APM	Aerosol Particle Mass Analyser
APS	Aerodynamic Particle Sizer
AMS	Aerosol Mass Spectrometer
ATOFMS	Aerosol Time-Of-Flight Mass Spectrometer
BAM	Beta Attenuation Monitor
BET	Brunauer, Emmett and Teller
CAMM	Continuous Ambient Mass Monitor
CBED	Convergent Beam Electron Diffraction
CCD	Charge-Coupled Device
CNC	Condensation Nucleus Counter
CNT	Carbon Nanotubes
CPC	Condensation Particle Counter
CPMA	Centrifugal Particle Mass Analyser
CU	Condensation Unit
DC	Direct Current
DEMC	Differential Electrical Mobility Classifier
DLPI	Dekati® Low Pressure Impactor
DLS	Dynamic Light Scattering
DMA	Differential Mobility Analyser
DMAS	Differential Mobility Analysis System
DMS	Differential Mobility Spectrometer
DPT	Differential Pressure Transducer
EAA	Electrical Aerosol Analyser
EAB	Electro-Gravitational Aerosol Balance
EAC	Electrostatic Aerosol Classifier
EAD	Electrical Aerosol Detector
EAS	Electrical Aerosol Spectrometer
EDX	Energy-dispersive X-ray (spectroscopy)
EELS	Electron Energy-Loss Spectroscopy
EEPS	Engine Exhaust Particle Sizer
ELPI	Electrical Low Pressure Impactor

ENP	Engineered Nanoparticles
ESP	Electro-Static Precipitator
FCAE	Faraday Cup Aerosol Electrometer
FCE	Faraday Cup Electrometer
FD	Flow Damper
FIMS	Fast Integrated Mobility Spectrometer
FMPS	Fast Mobility Particle Sizer
HEPA	High-efficiency Particulate Air
HV	High Voltage
ICP	Inductively-Coupled Plasma
ICP-AES	Inductively-Coupled Plasma Atomic Emission Spectroscopy
ICP-MS	Inductively-Coupled Plasma Mass Spectrometry
ICRP	International Commission on Radiological Protection
ISO	International Organization for Standardization
LEAFS	Laser Excited Atomic Fluorescence Spectroscopy
LED	Light-Emitting Diode
LDLS	Localised Dynamic Light Scattering
LIBS	Laser-Induced Breakdown Spectroscopy
MALDI	Matrix-Assisted Laser Desorption/Ionization
MEAS	Miniature Electrical Aerosol Spectrometer
MFM	Mass Flow Meter
MNP	Man-made Nanoparticles
MOUDI	Micro-Orifice Uniform Deposit Impactor
NPL	National Physical Laboratory
NPS	Nanoparticle Spectrometer
NSAM	Nanoparticle Surface Area Monitor
NTP	Normal temperature and pressure
OECD	Organisation for Economic Co-operation and Development
OPC	Optical Particle Counter
PAMS	Portable Aerosol Mobility Spectrometer
PFL	Polarisation Fluctuation Spectroscopy
PIXE	Proton Induced X-ray Emission
PM	Particulate Matter
PMC	Particle Mobility Classifier
PROSPEcT	Ecotoxicology Test Protocols for Representative Nanomaterials in Support of the OECD Sponsorship Programme
RAMS	Real-time Total Ambient Mass Sampler
SAED	Selected Area Electron Diffraction
SEM	Scanning Electron Microscopy

SIGMA	Symmetric Inclined Grid Mobility Analyser
SMPS	Scanning Mobility Particle Sizer
TEM	Transmission Electron Microscopy
TEOM	Tapered-Element Oscillating Microbalance
TOF	Time-Of-Flight
TOF-MS	Time-Of-Flight Mass Spectrometer
TSI	Thermo-Systems Incorporated (originally, name later changed to TSI Incorporated)
WGM	Whispering Gallery Modes
WPMN	Working Party on Manufactured Materials
WRAS	Wide-Range Aerosol Sampler
XRD	X-ray Diffraction
XRF	X-ray Fluorescence

Abstract

The aim of this project is to develop novel approaches for the detection and characterisation of engineered and other potentially harmful nanoparticles in the air. In particular we wish to distinguish specific nanomaterials from the background atmospheric aerosol to provide a means of measuring human exposure to nanomaterials that may present a risk to health. Ideally, solutions should be practically deployable in the field.

The metrics considered for measurement across this project are: size, number, chemical nature and surface area. Two main approaches are chosen to address these requirements: online size selective surface area controlled nucleation, and quantitative assessment of size resolved Raman spectroscopic maps.

The first approach is based on the discovery of a different regime of heterogeneous nucleation. In this case nucleation probability is determined by the surface area of the aerosol rather than the number of nuclei present. A portable DMA has also been developed allowing for the pre-separation of particles according to size in a compact package. Combining this DMA with the novel nucleation technology provides a means of measuring surface area distributions of particles.

Finally, a novel Raman spectroscopic methodology is presented for the chemically specific quantification of aerodynamically size selected samples. Particles are first aerodynamically size segregated from the air in a wide size range sampler. These size fractionated samples are analysed by Raman spectroscopy. Imaging analysis is then applied to Raman spatial maps to provide chemically specific quantification against the substrate as a proxy for background aerosol. Analysing this data in combination with the known deposition efficiency of aerosols in the respiratory tract (provided by the sampling method), can then provide a complete exposure measurement approach.

Chapter 1. Background

1.1. Motivation

The study of nanoparticles and their properties can be traced back as far as Faraday's investigation of colloidal gold in the middle of the 19th century (Faraday, 1857). However, it is only now, at the start of the 21st century, that we have started to see the full emergence of the potential offered by these particles with dimensions small enough to significantly alter their behaviour. Progress in development of both top down and bottom up manufacturing techniques have allowed a greater range and ever more complex nanoparticles to be produced in large quantities. In parallel, advances in developments of analytical techniques for the nano-scale are allowing for greater control of the end product and the discovery and development of ever more applications. Those nanoparticles produced for a specific application shall be referred to in this text as engineered nanoparticles (ENP) and shall be the primary focus here.

ENP can refer to both a nano-form of a traditional compound (e.g. TiO_2, ZnO, CeO_2) or to more complex novel constructions such as carbon nanotubes (CNT) or buckyballs/fullerenes (e.g. C_{60}). Some authors reserve the term ENP for these latter materials. Many industrial processes (e.g. combustion, welding, grinding etc.) also produce nanoparticles as an unintended by-product. Such nanoparticles are often referred to as man-made nanoparticles (MNP).

There is growing concern about the potential health and environmental risks posed by anthropogenic nanoparticles, but especially with regard to ENP due to their uncertain biological activity and recent proliferation. In the last 5 – 10 years there has been an acceleration in the growth of the nanotechnology industry as a wide range of nanomaterials are increasingly becoming incorporated into industrial processes and everyday consumer products (ENRHES, 2007; Meyer *et al*., 2009). The sudden and rapid rise in the production of these materials has led to concerns that the health risks associated with them are not well understood. Due to large specific surface areas, nanomaterials can be highly reactive, and can demonstrate divergent chemical properties from a bulk sample of the same compound. Past experience with health scares such as asbestos would suggest a cautious approach to the widespread incorporation and dispersal of these materials into the environment. However legislation is struggling to keep up with the market driven growth in production, and lacks the knowledge and instrumentation to properly monitor, assess, and derive safe exposure limits for existing and newly emerging nanomaterials. Limitations in our understanding, in addition to underlying political and cultural perspectives, delay the implementation of safety standards globally (Vincent, 1998). In response to this, the OECD set up a Working Party on Manufactured Materials (OECD WPMN) in 2006 to coordinate a global drive to focus on the impact of emerging nanomaterials on the environment and human health and safety.

As part of the UK's responsibilities within this framework, the PROSPEcT (Ecotoxicology Test Protocols for Representative Nanomaterials in Support of the OECD Sponsorship Programme) consortium was established in 2008 under which much of the work contained within this project was carried out. PROSPEcT was a £3.7 million DEFRA funded project which started on 1st January 2009 with the aim to fulfil the UK commitment to the global safety assessment of nanomaterials described by the WPMN. For more information see reference PROSPEcT (2009).

The WPMN identified 14 nanomaterials in total which are considered to be commercially relevant to the global economic impact of nanotechnology. PROSPEcT is tasked with investigating two of these; cerium oxide (CeO_2) and zinc oxide (ZnO) nanoparticles. These are important materials used in a range of industries but particularly as a diesel catalyst and additive in sunscreen respectively. Seven representative samples of these particles have been chosen from various manufacturers worldwide for the PROSPEcT project. In particular, the programme is tasked with adapting or creating test methods to enable the ecotoxicological hazard assessment of these materials in nano form.

While the lead sponsor on these two materials is the UK, the PROSPEcT consortium includes co-sponsors and contributors from all over the world including: Australia, Spain, Germany, USA, Denmark, Netherlands, Switzerland and Japan. The consortium includes universities (e.g. Imperial College London and The University of Exeter in the UK), research and metrology institutes (e.g. National Physical Laboratory) and commercial entities both large (e.g. BASF in Germany) and small (e.g. Naneum Ltd., UK).

Exposure to nanoparticles can occur through a range of different pathways (Klaine *et al*., 2008; Oberdörster *et al*., 2005; Cohen *et al*., 2013) including direct dermal contact, ingestion, injection and inhalation. Dermal exposure can come about via occupational handling of material as well as cosmetics and creams, particularly sunscreens. Although smaller nanoparticles can demonstrate increased penetration through the skin compared to larger particles (Alvarez-Román *et al*., 2004; Shim *et al*., 2004), most do not penetrate beyond the upper layer of epidermis in humans (Gamer *et al*., 2006; Newman *et al*., 2009; Gulson *et al*., 2010; 2012; Labouta and Schneider, 2013). However, penetration is more likely with damaged skin (Zhang *et al*., 2008; Larese *et al*., 2009; Zhou *et al*., 2014). Ingestion can occur due to the increased usage of nanoparticles in pharmaceutical products and as food additives. For example, TiO_2 is a commonly used food colourant (Lomer *et al*., 2000; 2007). In addition, nanoparticles escaping into the environment, for example through waste water, can represent a significant ecotoxicological hazard once they enter the food chain. Injection constitutes a more controlled and specialised exposure pathway via targeted therapeutics utilising nanomaterials. Exposure risks in this case include side effects to the patient as well as potential wider ecological impact if the nanomaterial is not broken down in the body. However at the moment the use of such therapies is still an emerging science and is not yet widespread. Inhalation meanwhile represents perhaps the greatest exposure risk (Politis *et al*., 2008; Vandebriel and De Jong, 2012). As will be discussed later (in Section 1.4.2.1), nanoparticles of a particular size can penetrate deep into the respiratory tract and can enter the bloodstream after depositing in the alveoli of the lungs (Ferin *et al*., 1992; Kreyling *et al*., 2006b; 2009; Morawska *et al*., 2009; Chang, 2010). This is a widespread exposure risk, especially in urban and industrial environments, due to the

prevalence of MNP. In addition it represents an acute occupational exposure risk for those that work with or are involved in the manufacture of ENP. Therefore it is considered that airborne exposure is one of the most important and urgent topics to be addressed in nanoscience.

The principal aim of this project is to develop techniques for detecting airborne ENP. Traditionally in air pollution studies, particulates have been measured as a simple mass fraction below a certain size cut-off, with collection usually carried out by filtration. For example, PM10 indicates a mass of particulate matter collected with a size selective inertial deposition inlet with a 50% cut off at 10 μm in size. In general, especially in highly polluted environments, there will be some correlation between this mass metric and exposure health risks. However, this simple mass measurement is usually not sufficient to properly quantify exposure. A primary challenge to the detection of ENP in the air is their relatively low abundance compared to a larger background of other aerosols (Andreae and Rosenfeld, 2008). Even without any anthropogenic sources, there would still be a background of naturally occurring aerosols formed for example by nucleation of compounds released from vegetation, chemical processes in the atmosphere, attrition, and sea spray (Kulmala and Kerminen, 2008). The concentration of naturally occurring aerosol particles can be quite variable depending on the distance to source, however it is generally in the region of 10 – 1000 cm^{-3} (Mészáros and Vissy, 1974; Anastasio and Martin, 2001; Pöschl, 2005; Tunved *et al*., 2006; Andreae and Rosenfeld, 2008), although can be significantly higher during nucleation burst events over forests (Smirnov, 2006). In an urban environment the additional contribution from MNP (mostly vehicle emissions – Pant and Harrison, 2013) can bring this concentration into the region of 10,000 cm^{-3} (Pöschl, 2005), while in busy city centres road side concentrations can reach as high as 100,000 cm^{-3} (Harrison *et al*., 1999). So while the total number or mass of particles in an environment can be measured with reasonable certainty, this number would tell us little about the potential risk from the aerosol without knowing what fraction of this total is likely to cause a toxic response.

With these requirements in place, it is clear that there is a need for new approaches to measuring aerosols which provide data more relevant to the assessment of exposure and toxicology by discriminating species of interest against a potentially larger background aerosol (Ono-Ogasawara *et al*., 2009; Kuhlbusch *et al*., 2011). In particular this thesis will focus on measuring additional aerosol metrics with a view to providing practical techniques and methodologies for health risk assessments.

If one is primarily interested in the health risks to humans posed by ENP then one must first consider the route of exposure, i.e. deposition in the respiratory tract (Yang *et al*., 2008). Importantly, deposition is determined by the size of particles, and primarily occurs by impaction and settling for larger particles above ~1 μm, and by diffusion for smaller particles less than ~0.1 μm (Mitsakou *et al*., 2005; Park and Wexler, 2007; Hofmann, 2011). Therefore size is the most significant metric for determining exposure, and it will determine if and where particles are likely to deposit in the respiratory tract. Larger particles deposit in the head and throat regions while smaller nanoparticles are more likely to deposit in the lower bronchial sections and alveoli in the lungs. This will be discussed in more detail in Section 1.4.2.1. Particle sizes with the lowest deposition probability in filters (~0.1 – 1 μm), are also least likely to be deposited in the respiratory tract, instead being exhaled (Park and Wexler, 2008). Particles close to these sizes will also have the longest residence time in the air. Although a freshly generated aerosol can

have a distribution peak below 20 nm by number, these particles quickly agglomerate to form smaller numbers of larger particles. Larger micron sized particles on the other hand will be quickly lost through gravitational settling.

1.2. Toxicity of nanoparticles and nano-aerosols

Nanoparticles can exhibit significantly divergent behaviour from the bulk materials they are derived from. They are in general much more reactive, generically due to a much higher surface to volume ratio compared to bulk and also in many cases due to filled electron states close to the valence level (i.e. low work function). It is these characteristics that make nanoparticles so useful in industry. For example, catalytic activity scales with the surface area of the catalyst and hence nanoparticles make for more efficient catalysts (e.g. CeO_2 nanoparticles in diesel fuel). However it is these very same characteristics that make nanoparticles potentially more toxic than their bulk counterparts (Oberdörster *et al*., 1994a; 1995; van Niekerk and Fourie, 2004; Nel *et al*., 2006; Simeonova and Erdely, 2009). As well as divergent chemical behaviour, nanoparticles can exhibit size dependent biological behaviour. For example, the size of a nanoparticle will determine whether it can be engulfed by a macrophage as part of an immune system response or whether it can cross a cell membrane boundary.

Following the proliferation of nanoparticles across industry and even into consumer products, there is growing concern that the potential health and environmental impact of these materials is not well understood. Exposure scientists and toxicologists are hastening to understand the exposure pathways, environmental and biological fate of these materials and what the long term effects could be.

Of particular interest here is the potential exposure to nanoparticles through the inhalation of airborne particulate matter in the form of aerosols. Some understanding of the connection between airborne pollutants and health has existed for centuries (Maynard and Kuempel, 2005; Pope and Dockery, 2006) and the technological wherewithal to study nano-sized aerosols (nano-aerosols) has been in place for many decades. However in the last decade, with the rapid expansion in use of man-made nanoparticles, a much greater interest has developed in understanding the potential exposure and toxicity of nano-aerosols (Oberdörster *et al*., 1994b; Laden *et al*. 2000, 2006; Hoet *et al*., 2004; Kreyling *et al*., 2006a; Ibald-Mulli *et al*., 2009), and in particular how it might differ from the bulk material form. Already numerous studies have confirmed a size dependent toxic response to inhaled aerosol particles (e.g. Ferin *et al*., 1992; Donaldson *et al*., 1998; 2000; Brown *et al*., 2001; Li *et al*., 2002a; Kreyling *et al*., 2009). Toxic effects of nanoparticles on the lung are well documented (Gehr *et al*., 2010; Donaldson and Poland, 2012), with ongoing research focussing on nanoparticle impairment of macrophages (Renwick *et al*., 2001; Möller *et al*., 2002; Lundborg *et al*., 2006) and the ability of nanoparticles to translocate across cell membranes (Oberdörster *et al*., 2002; Kreyling *et al*., 2002; Möller *et al*., 2008; Cohen *et al*., 2014). The latter point has particular importance to the ability of deposited nanoparticles to reach the blood stream and other areas of the body (Oberdörster *et al*., 2004; Kreyling *et al*., 2006b; Kreyling *et al*., 2009).

1.3. ZnO and CeO_2

1.3.1. ZnO applications

ZnO has mainly been used in recent decades as a UV absorber, often in conjunction with TiO_2 (Smijs and Pavel, 2011), as well as considered as a dopant in, or in conjunction with, CeO_2 absorbers (Yabe *et al*., 2001; Li *et al*., 2002b; 2002c; de Lima *et al*., 2009). In particular its use for this purpose in sunscreens has led to much research on its potential exposure risks (Gulson *et al*., 2010; Smijs and Pavel, 2011; Gulson *et al*., 2012; Larner *et al*., 2014), toxicological response (EPA, 2005; Sayes *et al*., 2007; SCCS, 2012; Vandebriel and De Jong, 2012), and eventual environmental fate (Larner *et al*., 2012; Khan *et al*., 2013). Aside from this, ZnO has also come under scrutiny for its potential in a range of proposed applications including as a lasing material (Huang *et al*., 2001; Willander *et al*., 2009), in light-emitting diodes (Tsukazaki *et al*., 2004; Sun *et al*., 2008; Park *et al*., 2010), in gas sensors (Boccuzzi *et al*., 1995; Ryu *et al*., 2003; Wan *et al*., 2004; Liao *et al*., 2007; Qi *et al*., 2008), in transistors (Arnold *et al*., 2003; Goldberger *et al*., 2005; Suh *et al*., 2008), in solar cells (Baxter and Aydil, 2005; Law *et al*., 2005; Suh *et al*., 2007; Cheng *et al*., 2008; Senthil *et al*., 2013), photodetectors (Suehiro *et al*., 2006) and as a "nanogenerator" of electric current (Wang *et al*., 2007). In addition, ZnO has also come under scrutiny as a potential novel optical material in applications such as second harmonic generation (Mehl *et al*., 2010), high Q optical cavities based on whispering gallery modes (Wang *et al*., 2006), and as a photonic sensor of oxygen (Sanchez-Valencia *et al*., 2014). Furthermore, nano-ZnO has also found to be effective for the removal of cadmium from aqueous solutions (Srivastava *et al*., 2013). Further details on ZnO synthesis, properties and applications can be found in the reviews by Wang (2004), Özgür *et al*. (2005), and Moezzi *et al*. (2012).

1.3.2. CeO_2 applications

CeO_2 has been used for many years in a wide range of applications, particularly as a catalyst in the automotive industry to reduce emissions (Lahaye *et al*., 1996; Trovarelli *et al*., 1999; Stanmore *et al*., 2001; Dresselhaus and Thomas, 2001; Jung *et al*., 2005) as well as in glass polishing (Mortensen, 2006), and as a UV absorber (Morimoto *et al*., 1999, also see references in ZnO section above). In addition it has being considered by researchers in a wide range of new applications including gas sensors (Izu *et al*., 2002), corrosion resistant coatings (Ardelean *et al*., 2008; Zhong *et al*., 2008), water treatment (Matatov-Meytal and Sheintuch, 1998), as a component of germanium transistor gates (Dimoulas *et al*., 2007; Galata *et al*., 2007), in solar cells (Corma *et al*., 2004), as a photocatalyst for the generation of hydrogen and oxygen from water (Chung and Park, 1996; Bamwenda *et al*., 2000; 2001) and many others (e.g. see Qian *et al*., 2009; Goharshadi *et al*., 2011). As with ZnO, there has been a push in recent years to investigate any potential health or environmental risks that might emerge from nano-CeO_2 (Park *et al*., 2007; 2008; Gojova *et al*., 2009; van Hoecke *et al*., 2009).

1.3.3. PROSPEcT samples

In total, seven samples were chosen for analysis within the PROSPEcT project representing materials from different manufacturing sources which are widely used in industry. A quick overview of these samples is provided in Table I below along with associated code numbers used for quick reference.

ZnO nanoparticles		**CeO_2 nanoparticles**	
NM-110	Z-COTE – BASF	NM-211	Ceria Dry – Antaria [cerium (IV) oxide precipitated, uncoated, cubic]
NM-111	Z-COTE HP1 – BASF (coated with triethoxycaprylsilane)	NM-212	Nanograin – Umicore [cerium (IV) oxide precipitated, uncoated]
NM-112	Microniser	NM-213	Micron scale – Sigma Aldrich [cerium (IV) oxide]
NM-113	Micron scale – Sigma Aldrich		

Table I. PROSPEcT samples. Code Numbers from the European Repository of NM-Series of Representative Manufactured Nanomaterials.

Figure 1.3–1 provides a couple of examples of how these materials appear under TEM. Typically a wide mix of particle morphologies and sizes are present in any given sample. While freshly generated ENP may have primary particle sizes in the order of 5 – 100 nm, the material will quickly agglomerate in the air up to sub-micron sized particles (e.g. ~100 – 300 nm) which can survive much longer in the air due to their lower diffusion mobility (Eggersdorfer and Pratsinis, 2014). In addition the deposited state as analysed by TEM may not be representative of the airborne state.

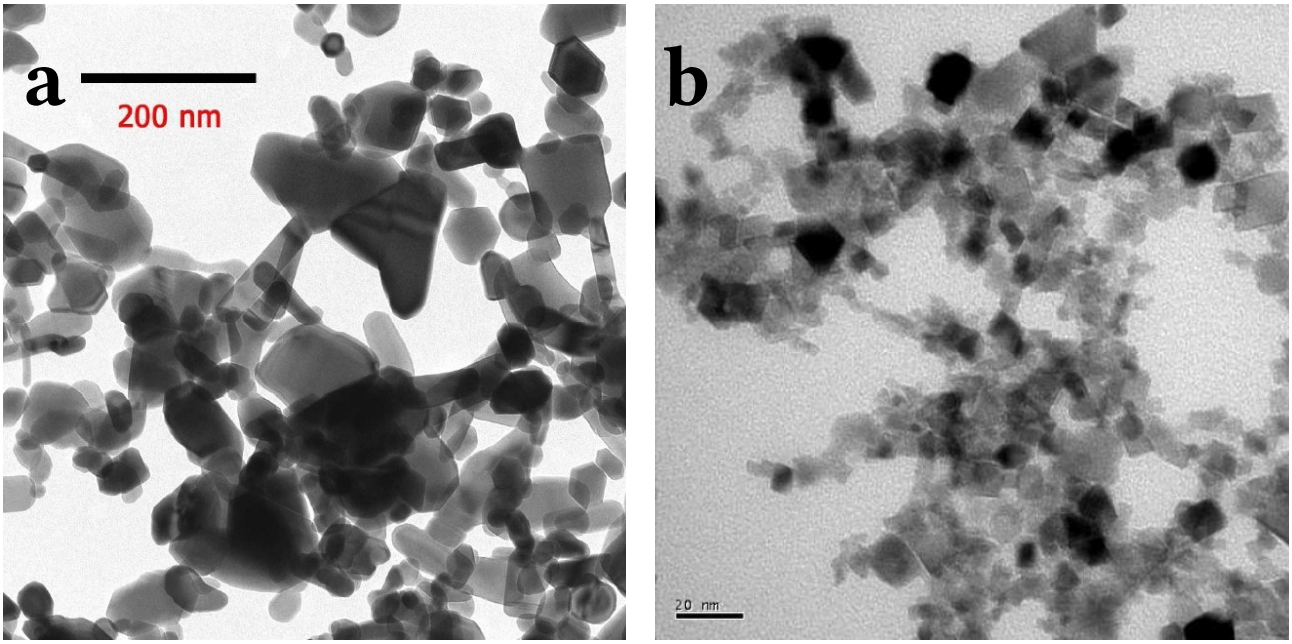

Figure 1.3–1. Example TEM images of (a) ZnO and (b) CeO_2 nanoparticles.

1.4. Existing techniques and metrics

Once particles have been deposited in the respiratory tract, their uptake into the surrounding body tissue will be determined by parameters such as size, aspect ratio and the chemical nature of their surface. Once incorporated, the toxicity of particles will be mainly determined by their underlying chemical nature, and can then be quantified in terms of the mass of each compound present. However the traditional total mass measurements of airborne pollutants alone are not adequate to fully characterise their potential health or environmental impact.

In attempting to make any sort of quantitative assessment of the health risk associated with airborne particulate matter, it is necessary to consider a range of different metrics, such as; size, chemistry, mass, surface area, etc. (Cass *et al*., 2000; Cohen *et al*., 2000; Harrison and Yin, 2000; Oberdörster *et al*., 2005; Maynard and Aitken, 2007; ENRHES, 2009). In recognition of the shortcoming of a simple mass metric, there has been a shift in recent years towards measuring numbers of particles (Peters *et al*., 1997). This is considered to better represent the risk from a given particle distribution as it is a more sensitive measure of the smaller particles present which can penetrate more deeply into the lungs. By comparison, in mass measurements, the contribution of many nanoparticles will still be insignificant by comparison to much lower numbers of much larger microparticles. However, there is still ongoing debate as to what the best approach is for quantifying exposure to aerosols, and the associated risks (Kuhlbusch *et al*., 2011). Clearly, neither a mass nor number metric alone says anything about the chemical nature, and therefore toxicity, of the measured particles; while surface area has also emerged as a strong contender for replacing the tradition mass metric (Sager *et al*., 2008; Sager and Castranova, 2009). The only generally agreed point on metrics by exposure scientists, is that it is preferable to measure as many parameters of a sample

aerosol as practically achievable with the available instrumentation (Powers *et al*., 2007; Rodríguez *et al*., 2012). In addition, numerous studies have called for additional devices to be developed to fill gaps in characterisation techniques currently available (e.g. Maynard and Aitken, 2007; Giechaskiel *et al*., 2014; Kuhlbusch *et al*., 2014).

To gain a better understanding of the potential risks, one must carry out a more detailed survey of the components present. As an introduction to this field we shall first consider the currently available techniques for measuring different aspects of airborne particles.

1.4.1. Mass concentration metrics

Mass has been the most commonly measured metric used in aerosol studies for over a hundred years (Chow, 1995; Walton and Vincent, 1998; Moosmüller *et al.*, 2009), and a large array of different techniques have been applied to its measurement (Chow, 1995; Wilson *et al*., 2002; Solomon and Sioutas, 2008).

The relatively simple and economical approach of gravimetric measurements on filter collected samples has remained a popular approach to this day (e.g. Annibaldi *et al*., 2011). And indeed the simplicity of filter sampling has ensured its continued popularity in compact personal samplers (Baron, 1998; Lidén *et al*., 1998; Aizenberg *et al*., 2000; 2001; Zamengo *et al*., 2009). Most early sampling developments focussed on pre-collection cut-offs, by e.g. impactors, to remove larger particles which could otherwise dominate the final total mass measurement. The exact nature of these cut-offs was found to be very critical to the final result and hence samplers of different designs with only minor specification variation (e.g. cut-off diameters in the tolerance range 10 ± 0.5 μm) could yield quite significantly different results. On top of this, long sampling times were required to achieve measurable mass quantities, followed by removal and offline weighing of the loaded filters. This resulted in a time resolution in the order of a day, and hence was little use in identifying short temporal emissions or diurnal variations. It is also worth noting that all filter based collection methods, including those outlined below, need to consider the potential errors arising from subsequent loss of volatile components or gains due to the condensation of vapours (particularly water).

To overcome the slow response of filter collection and gravimetric approaches, optical methods were developed which could provide a continuous read-out of aerosol mass. Optical scattering research undertaken during the Second World War to investigate atmospheric visibility led to the development of the nephelometer (Waldram, 1945; Ahlquist and Charlson, 1967; Charlson, 1969), which became popular as a mass measurement tool once a correlation between optical scattering and mass had been demonstrated (Charlson *et al*., 1968; Ettinger and Royer, 1972; Waggoner and Weiss, 1980). In this device a beam of light is passed through a scattering volume through which the aerosol flow is passed. Scattering from aerosol particles is then measured by a photometer such as a photomultiplier tube. Background reflections from the internal surfaces of the device are minimised by the use of black paint and one or more apertures placed in front of either the light source or detector. The nephelometer subsequently fell out of favour due to the dependency of total scattering on additional factors such as the index of refraction, especially for smaller particles (Willeke and Brockmann, 1977; Molenar, 2005).

An alternative measurement approach to total scattering is optical absorption (Lin *et al*.,

1973; Clarke *et al*., 1987). As this requires consideration of relative changes in a detected light source, it is less sensitive compared to scattering techniques. Therefore higher sample quantities are required, usually achieved through filter collection. A wide range of schemes have been designed for measuring the optical absorption of aerosols (Moosmüller *et al*., 1997; Bond *et al*., 1999; Petzold and Schönlinner, 2004), however the most commonly used approach is the aethalometer (Hansen *et al*., 1982; 1984). In this instrument, the absorption of a particular wavelength through a filter is measured simultaneously by two photodetectors. One photodetector measures the light transmitted through the collected sample, while the other photodetector measures the light transmitted through a separate part of the filter which is kept clean by means of a transparent mask preventing particle collection. This allows the second photodetector to provide a reference signal such that the difference between the two output signals is a measure of the absorption (or extinction to be precise) of the deposited sample. Aethalometers are sensitive to the most absorbing aerosol component which is usually given the term "black carbon" (Hansen and Novakov, 1990; Weingartner *et al*., 2003; Watson *et al*., 2005; Bond and Bergstrom, 2006). Despite their widespread use and further development as multi-wavelength systems, aethalometers, as with nephelometers, still suffer from difficulties in interpreting their output and linking the values obtained to underlying measurement parameters such as mass. In addition, they exhibit significant short term thermal stability issues, a non-linear change in response with filter prior loading levels, and require situational dependent correction factors for accurate measurements (Arnott *et al*., 2005).

The photoacoustic method allows for the measurement of optical absorption of suspended aerosol particles *in situ* without the need to deposit them on a filter (Terhune and Anderson 1977; Bruce and Pinnick, 1977; Colles *et al*., 1979; Japar and Killenger, 1979; Adams, 1988; 1989; Lack *et al*., 2006). It measures absorption via the energy that is deposited in the sample rather than the extinction of the light beam. This is achieved by passing the aerosol through a resonant acoustic cavity. A laser beam is also introduced and chopped at the resonant frequency of the cavity. Absorption by the aerosol particles leads to heating and thus expansion of the air in the cavity creating pressure pulses. By adjusting the chopper, the pulse frequency can be tuned to the acoustic resonant frequency of the cavity. The resulting acoustic signal is detected by a microphone to provide a continuous output measure of the aerosol absorption. Developments in the technique have focussed on increasing the sensitivity by reducing background absorption and other artefacts (Arnott *et al*., 1999; 2000), as well as creating more compact and portable designs (Petzold and Niessner, 1996; Krämer *et al*., 2000). However, as with any optical absorption based technique, it is still more a measure of particular absorbing aerosol components rather than overall mass.

One of the oldest continuous techniques for measuring aerosol mass, and not reliant on optical interactions, is the Beta Attenuation Monitor (BAM – Nader and Allen, 1960; Lilienfeld, 1970; Jaklevic *et al*., 1981 and references in Chow, 1995). This method measures beta particles (electrons) emitted from a radioactive source (e.g. ^{14}C, ^{147}Pm, ^{85}Kr, ^{63}Ni) after passing through a ribbon filter for collecting aerosol particles. The ribbon filter can be automatically progressed with time, usually in increments of e.g. half an hour, to provide a semi-continuous output. Dual beta detectors are often used where one detector provides a reference reading, either from a clean section of the filter or from the reverse side of the source, to correct for instrumental fluctuations and drift. There is some compositional dependency on the mass dependent electron attenuation,

however it is usually considered to be small or negligible with an empirical relation proportional to $(Z/A)^{4/3}$ where Z is the atomic number and A is the atomic weight (Klein *et al*., 1984; Weingartner *et al*., 2011). Z/A does not deviate significantly from 0.5 for all elements and compounds apart from hydrogen (e.g. see Table 12–2 in Weingartner *et al*., 2011).

Another long-standing mass measurement technique is the Tapered-Element Oscillating Microbalance (TEOM – Patashnick, 1975; Wang *et al*., 1980; Patashnick and Rupprecht, 1983; 1991; Ruppecht *et al*., 1992; Allen *et al*., 1997; Weingartner *et al*., 2011). This method is based on measuring the change in resonance frequency due to the mass of particles being collected on a filter. It is based on earlier works measuring single particle masses with resonant fibres (Patashnick and Hemenway, 1969; Stevens, 1971) and has some similarity in the operating principle to piezoelectric quartz crystal microbalances (Olin and Sem, 1971; Wilson *et al*., 2002), which are limited in use due to the requirement for impaction based sampling. In the TEOM, a conductively coated tapered tube is fixed at the wide end but free to oscillate at the narrow end where a filter is mounted. The oscillation is maintained by means of an electronic feedback system. An LED and photodetector measure the oscillation and feed the signal back to field plates either side of the conductively coated oscillating tube. Sample air is drawn through the tube and, as aerosol particles are deposited on the filter, the change in mass can be detected by the change in resonance frequency of the system. More recently the TEOM has been combined with increasingly complex sample collection techniques and a dual sampling system with a blank/reference microbalance to form the Real-Time Total Ambient Mass Sampler (RAMS – Eatough *et al*., 1999; 2001; 2003). These improvements are aimed at combating some of the short-comings of filter based measurements mentioned previously. Reasonable agreement has been found between the BAM and TEOM methods when measuring atmospheric aerosols (Hauck *et al*., 2004; Schwab *et al*., 2006), while the relative merits of the TEOM, nephelometer, aethalometer and photoacoustic techniques for measuring diesel exhausts are discussed in Moosmüller *et al*. (2001).

The Continuous Ambient Mass Monitor (CAMM – Babich *et al*., 2000; Lee *et al*., 2005a; 2005b) is another filter based method for monitoring aerosol mass which operates by measuring the increase in pressure drop across the collection filter with particle loading.

More recently, techniques have been devised for the online measurement of mass distributions which provide an output based on the balance between electrostatic forces (i.e. the particles electrical mobility) and another mass sensitive force. In the Aerosol Particle Mass Analyser (APM – Ehara *et al*., 1996; Park *et al*., 2003), this second (mass sensitive) force is a centrifugal force, created by passing charged aerosol through the annular operating space between two cylindrical electrodes rotating at the same angular velocity. It is assumed that the air flow moves through the operating space with the same angular velocity as the electrodes, and the voltage polarity on the electrodes is setup to oppose the centrifugal force. In this manner, for a particular voltage on the electrodes, only particles of a particular mass to charge ratio will reach the exit rather than collide with the walls of either electrode. The particles output can be counted with e.g. a condensation particle counter and so adjusting the APM voltage over time will generate a mass distribution of the sample aerosol particles. A differential mobility analyser (described in Section 3.1) can also be included upstream to independently

classify the electrical mobility equivalent diameter. This can be used to provide a density measurement when combined with the APM result (McMurry *et al*., 2002). A refinement of the APM concept was proposed as the Couette centrifugal particle mass analyser (CPMA – Olfert and Collings, 2005; Olfert *et al*., 2006). In this variant it is shown that losses in the system can be reduced by slightly increasing the rotational velocity of the inner electrode relative to the outer electrode. By contrast, the Electro-Gravitational Aerosol Balance (EAB – Ehara *et al*., 2006a; 2006b; Lin *et al*., 2008) employs fixed horizontal parallel plate electrodes such that gravity acts as the mass sensitive balancing force.

Online measurements of total or average mass can also be made by simultaneously measuring electrical mobility and aerodynamic diameter (Ristimäki *et al*., 2002; Moisio and Niemelä, 2002; Lehmann *et al*., 2004), or simply converted from size measuring instruments with assumptions made about the shape and density (e.g. SMPS-APS – Sioutas *et al*., 1999; Shen *et al*., 2002).

A summary of existing techniques will be provided in Section 1.4.8.

1.4.2. Sizing nanoparticles

1.4.2.1. Size dependent deposition in the respiratory tract

When evaluating the health risks of airborne particles, one of the first metrics that must be considered is size. The size of particles determines how they will move in the air and how likely they are to deposit in a certain location. The probability of inhaled particles depositing in the lungs or airways is strongly dependent on their size. Therefore, in the context of human health risks, the impact of particle size is usually considered in light of some lung deposition model – most often that published by the International Commission on Radiological Protection (ICRP) in 1994 (ICRP, 1994 – Fig. 1.4–1). This model shows the deposition probability for different parts of the respiratory tract as a function of particle size.

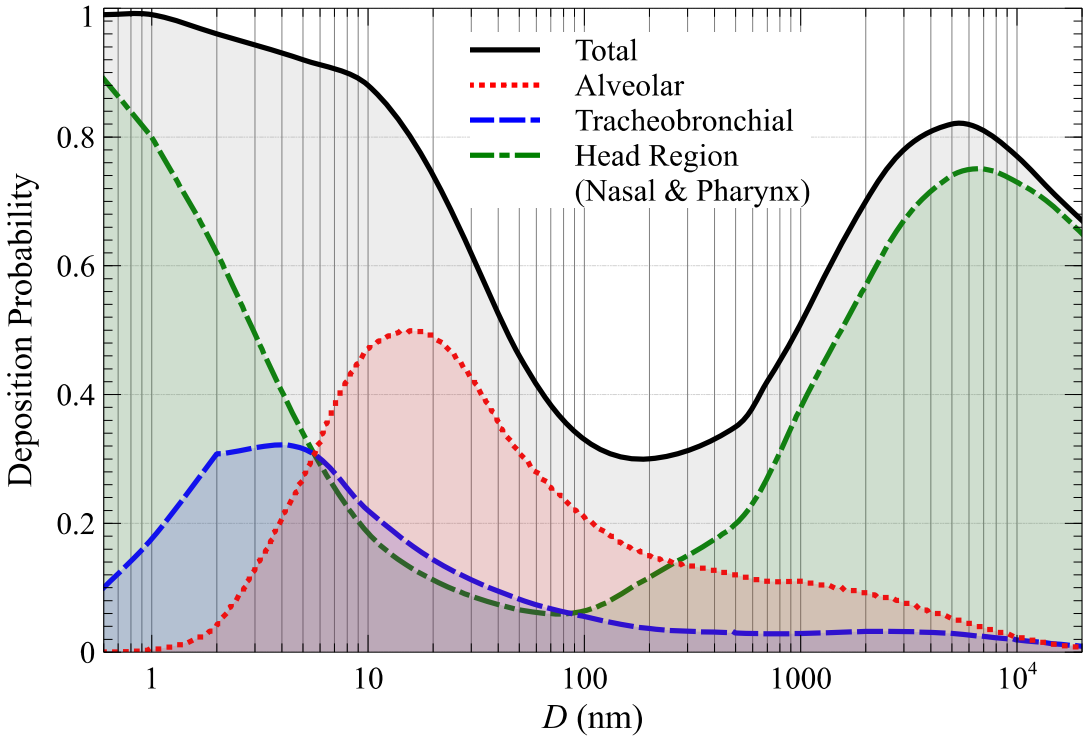

Figure 1.4–1. Deposition probability as a function of particle size for different regions of the respiratory tract. Adapted from data published by the ICRP (1994).

Total deposition efficiency in the respiratory system, similar to that in filters, shows a minimum at ~100 – 300 nm. The capture efficiency increases sharply on either side both towards smaller and larger particles.

Larger particles are lost by impaction due to having enough mass, and therefore momentum, such that they do not so easily follow the air flow around obstructions or corners. The removal of micron scale particles is mostly achieved by hairs (vibrissae) in the nasal cavity. Smaller particles are increasingly captured by diffusion, preferentially in the lower reaches of the lungs (alveolar region) due to the high surface area. The diffusion mobility of small particles increases steeply with decreasing size in the nanometre range, and therefore they are increasingly likely to collide with and become lost to the boundaries of any flow channel. The smallest particles will therefore only travel short distances. This can be seen in the increasing deposition in the head region of Fig. 1.4–1 at the lower end of the scale, with a corresponding drop-off in the deposition in other regions as the particles no longer travel far enough to penetrate so deeply. However nanoparticles > 5 nm are more likely to penetrate further down the respiratory tract and deposit in the alveoli of the lungs. From here they can enter the bloodstream or interfere with oxygen uptake in the lungs and so are of much greater concern as a potential health risk. Particles in the intermediate size range of a few hundred nanometres are less effectively deposited. They do not have enough mass to be as easily lost by impaction as larger particles, nor do they diffuse as effectively as smaller particles. Therefore most of what is inhaled in this size range is simply exhaled again (although the proportion deposited may still be a significant concern). Similarly, this size range demonstrates the highest penetration efficiency through filters, and therefore can be used to characterise the worst case collection efficiency of a filter.

When discussing the "size" of nanoparticles one must in conjunction define the method of measurement. This is usually relayed through the concept of an "equivalent diameter". Any given particle of a given composition and morphology can result in differing measures of its size depending on the method of measurement used. These measures are usually referenced to a conceptual idealised particle with regular attributes, such as spherical morphology and uniform density of 1,000 kg/m^3. So, if we state that a particle has an aerodynamic equivalent diameter of d_A, we mean that it has the same settling velocity as, and hence will be measured by aerodynamic techniques to be the same as, a 1,000 kg/m^3 spherical particle of diameter d_A. Equivalently, a particle with an electrical mobility equivalent diameter of d_E will move in an electrical field with the same velocity as our idealised spherical particle of diameter d_E. For any given particle the measured values of d_A and d_E may not be the same depending on its true composition or shape. To put this another way, an equivalent diameter is the particle's diameter assuming it has certain regular idealised characteristics as its true nature is either unknown or too complex to characterise with a single value. Often the "equivalent" is dropped from the terminology for brevity, such that the terms simplify to "aerodynamic diameter", "electrical mobility diameter" etc. with the "equivalent" implied.

1.4.2.2. Differential mobility analysis

Differential electrical mobility classifiers (DEMC according to ISO standard ISO 15900:2009) commonly known as DMAs (differential mobility analysers) have been used for many years to classify aerosol particles within a narrow range of electrical mobility – e.g. see references in Knutson (1976), Flagan, (1998), Baron and Willeke, (2001), Biskos *et al*. (2005) and Szymanski *et al*. (2009). DMAs may be designed in many different ways, e.g. cylindrical, radial, parallel plate geometry, or indeed any other shape within the bounds of engineering feasibility. Most commercial DMAs are based upon a cylindrical geometry where an electric field is created between two co-axial cylinders following pioneering works of Hewitt (1957), Whitby and Clark (1966) and Knutson and Whitby (1975). With the advent of computer controlled flows and voltages within the DMA, and continuous flow particle detectors like condensation particle counters (CPCs – described in Section 1.4.3.3), commercial differential mobility analysing systems (DMAS) emerged as scanning mobility particle sizers (SMPS – described in Section 1.4.3.4), to record aerosol particle size distributions (Liu *et al*., 1974). DMAs as standalone instruments are often used to produce monodisperse aerosol particles for research and instrument calibration. An overview of traditional cylindrical designs is provided by Intra and Tippayawong (2008).

DMAs and SMPSs have traditionally been large, heavy, desktop devices mainly suitable for laboratory use (e.g. Winklmayr *et al*., 1991; Quant *et al*., 1993; Wiedensohler *et al*., 2012). However, in recent years there has been growing demand for smaller, portable, easy to use instruments that can be freely and easily moved. For example, occupational hygiene and nanotechnology needs can be more easily addressed with a portable SMPS. Portability and ease of use offer a number of advantages including the ability to sample aerosols *in situ*. Instruments can be more easily stored or moved between laboratories or test locations allowing greater flexibility of working arrangements. The size of an SMPS is largely determined by the size of the DMA column which is typically about

500 mm in length (TSI, Grimm). Even a DMA column designed for a limited nano-size range is about 200 mm (Chen *et al*., 1998). Thus, the first step towards a portable SMPS is to design a small DMA.

Of importance to the overall research goals of this project; a DMA represents a first step in honing a method for the specific detection of engineered nanoparticles in the air. Specifically, it gives us control of the metric of size via the electrical mobility equivalent diameter. Combined with other metrics, such as surface area or shape, it can form the basis of a method to classify and distinguish different species of particles.

Portable devices in the current literature include the mini-disk EAC (Li *et al.,* 2009) which is a radial electrostatic classifier with a cumulative (variable cut-off) output, and a hand-held DMA of dual conical design (de la Mora and Kozlowski, 2013), designed for high resolution operation in the range 1 – 30 nm. Miniature devices have also been developed focussed only on ion mobility measurements. These operate on the same principle as DMAs used for particle measurements. Due to the much higher mobility of ions, smaller drift regions are required which greatly helps to facilitate miniaturization. Examples which have achieved this to such a degree as to be compatible with a hand-held device include both planar (Spangler, 2000; Zimmermann *et al.,* 2007; 2008) and cylindrical (Babis *et al.*, 2009) geometries. While interesting in their own right, and useful for the applications they were designed for, none of these devices fit the requirements for a high resolution portable device with a wide enough size range to cover most aerosol particle applications. Other portable DMAs found in recent commercial devices include the TSI Nanoscan 3910 and the Kanomax Portable Aerosol Mobility Spectrometer (PAMS). The Nanoscan utilises a radial type DMA while the design of the PAMS DMA is not disclosed. Therefore, current standalone DMA instruments are either large, expensive, or low resolution. To address the needs of the occupational hygiene, environmental, and atmospheric sciences, a portable high resolution low cost DMA is required. One of the aims of this work is therefore to develop a DMA to bridge the gap in current instrumentation.

1.4.2.3. Size resolved sampling

It is often desirable to sample airborne particles into size-resolved fractions for the purpose of carrying out offline size-resolved gravimetric or chemical analyses. The most common method for doing this is by inertial impaction. Typically this is achieved by positioning an orifice opposite a collecting plate. As the air flow passes through the orifice it will form a high velocity jet which then must turn sharply as it bends around the collection plate. Entrained particles above a certain size will have sufficient inertia such that they do not follow the flow streamlines around the sharp bend, but instead cross the flow and impact on the collection plate. The value which determines whether a particle will impact on the plate or follow the flow around it is the dimensionless parameter known as the Stokes number (*Stk*):

$$Stk = \frac{\rho_p C_C D_p^{\,2} v}{18 \eta r} \tag{1}$$

where ρ_p is the density of the particle, C_c is the Cunningham slip correction factor, D_p is the particle diameter, v is the air velocity, η is the air viscosity, and r is the radius of the

orifice. The particle will impact and be collected if the Stokes number is greater than a critical value, usually ~0.21 – 0.23 (McMurry, 2000a).

Single stage impactors are common for collecting PM samples (e.g. PM10 or PM2.5), with a filter downstream to collect all the particles below the impactor cut-off. However for higher size resolution, cascade impactors (May, 1945; 1982) can be used. In this case there are multiple stages in series, with each subsequent stage having a smaller orifice size and hence higher velocity jets than the preceding stage to give a smaller size cut-off. Ideally all of the particles above the stage 1 cut-off are removed such that only particles larger than the stage 2 cut-off but smaller than the stage 1 cut-off are collected on stage 2. This will continue on through subsequent stages such that stage n will collect particles in the size range between the n and $n - 1$ cut-off diameters. In this manner, a series of size bins can be collected to allow for size resolved analysis of the different fractions. In practice, the cut-off profiles are not perfectly sharp, and will be characterised by a sigmoidal profile rather than a step function with the stage indicated by the particle size where the collection efficiency reached 50% (d_{50}). However, in a well designed cascade impactor the collection profiles are usually steep enough for stage overlap to be negligible. A more serious concern is typically particle bounce, such that impaction does not equal collection, and the particle in question is instead collected on the following stage. While the choice of impactor design and collection substrate can help to alleviate this problem (Chang *et al*., 1999), often a grease or oil is added to the collection substrate to minimise bounce. Although care must be taken to ensure that this does not interfere with subsequent analysis techniques. Stage overloading can still result in newly arriving particles bouncing off those already deposited and should be avoided. In addition, inter-stage losses can also cause measurement errors, although this is usually only a concern at the smallest sizes.
Cascade impactors are effective at collecting micron sized particles and usually have a largest size (first stage) cut-off of ~10 μm (Sanderson *et al*., 2014). However, due to the low inertia of nanoparticles, it is a challenge to design impactors with a d_{50} below ~50 nm. Typically cascade impactors feature a final filter stage to collect all remaining particles smaller than the final stage cut-off. Standard approaches to reducing d_{50} to smaller particle sizes include working at lower pressures where C_c is increased, or to use micro-orifices such that the orifice radius r in Equation (1) is reduced into the micron range. In the first case large pumps are required to generate the low pressures, and the sample may be augmented from its ambient pressure state. While the latter case requires a large multitude of micro-orifices in the final stages, to allow sufficient air flow and sample collection, which can be a challenge to manufacture. However by using such techniques to generate hypersonic jets, the size range of impactors has been extended down to ~5 nm (de la Mora et al., 1990). Commercial examples include the NanoMOUDI range of cascade impactors (as an extension of the original MOUDI – Marple *et al*., 1991) from MSP Corporation which uses micro-orifices to provide a lowest cut-off diameter of 10 nm, and the DLPI from Dekati which is a low pressure impactor providing size classification down to 30 nm. The collection characteristic of these instruments with different collection substrates has been compared by Fujitani *et al*. (2006). Following the work of Keskinen *et al*., (1992), Dekati have also extended this technology with particle charging and electrometer collection stages in the ELPI™ (Marjamäki *et al*., 2000) to provide online size distribution measurements, while the ELPI+™ (Lamminen, 2011; Järvinen *et al*., 2014) extends the size range down to 6 nm.

Characterising aerosol distributions purely by impaction, although useful, does not accurately reflect how particles are deposited in the human respiratory tract. Therefore, cascade impactors do not necessarily provide an accurate representation of health risks across the entire size range. To address this issue, it is desirable to have a collection technique which replicates the deposition characteristics of particles as occurring in the respiratory tract – i.e. mainly impaction deposition at larger sizes and mainly diffusion deposition at smaller sizes. A number of groups have proposed samplers designed to collect particles in ~3 stages representing the major divisions of the respiratory tract (e.g. Madelin, 1992; Li *et al*., 2008; Koehler *et al*., 2009; Koehler and Volckens, 2013). However, it is challenging to develop deposition profiles that accurately reflect the desired response across the entire size range. In addition, some of the collection substrates used (e.g. tubing, glass spheres, foam) are not ideally suited to a full range of offline analysis techniques. For a more accurate, flexible and higher resolution analysis of aerosol health risk, Naneum Ltd. developed the Nano-ID® Select sampler (formerly wide-range aerosol sampler, WRAS – Gorbunov *et al*., 2009). In this instrument an aerosol flow of 20 l/min is first passed through a 7 stage cascade impactor which classifies particles in the size range from 0.25 μm to > 20 μm. The remaining particles are then passed through a diffusion battery (Fuchs *et al*., 1962; Sinclair and Hoopes, 1975a; Cheng *et al*., 1980; Cheng and Yeh, 1980; Knutson, 1999) where they are classified in 5 stages covering the size range from < 2 nm to 250 nm. Different numbers of nylon net filters are used at each stage of the diffusion battery with mesh openings ranging from 11 to 180 μm. Filters typically exhibit a V-shaped deposition curve with a minimum somewhere in the 0.1 – 0.3 μm region. However, by removing all of the larger particles upstream in the cascade impactor, only the lower branch of the deposition curve applies. This results in a monotonic relation between deposition efficiency and particle size that would not otherwise be achieved. The Nano-ID® Select has previously been used to determine mass fractions of lead in crystal glass factories (Gorbunov *et al*., 2009), to characterise the mass distributions of metals resulting from friction stir welding (Pfefferkorn *et al*., 2010), to determine respirable mass concentrations of carbon nanotubes at a commercial production facility (Asbach *et al*., 2014), and to determine exposures to lead and other heavy metals at gun shooting ranges (Lach *et al*., 2014).

Online sizing devices based on the size dependent penetration through diffusion screens have also been devised using both electrometers and condensation particle counters as the measurement approach (Fierz *et al*., 2002; 2009; Feldpausch *et al*., 2006). While additional methods used for the effective sampling of nano-sized aerosol particles include electrostatic (McLean, 1988; Mizuno, 2000; Jaworek *et al*., 2007) and thermal precipitators (Cartwright, 1954; Cartwright *et al*., 1956; Schadt and Cadle, 1957).

1.4.2.4. Online aerodynamic sizing

It is possible to make online measurements of the aerodynamic diameter of particles *in situ* via their lag in response to an accelerating air flow around them. Mazumder and Kirsch (1977) proposed an interesting approach whereby the aerodynamic diameter was determined by measuring the phase lag of particles in response to an acoustic signal. The standard approach however is to accelerate particles through a nozzle and to then measure their velocity close to the nozzle exit. Wilson and Liu (1980) used a laser-

Doppler velocimeter to measure particle velocities. In this scheme, a laser beam is first split to form two coherent beams, which are then focussed to a cross-over point. As particles pass through the interference pattern created at this point, the detected signal intensity is modulated. The particle velocity can then be calculated by multiplying this modulation frequency by the interference fringe spacing. The most commonly used device at present is the commercial TSI Aerodynamic Particle Sizer (APS 3300 series), with a measurement range from 0.5 to 20 μm. In this instrument, velocity measurements are carried out using two parallel laser beams at the nozzle exit to form a time-of-flight detection system.

Note that the parameter measured by an APS is not exactly the same as the standard definition of aerodynamic diameter (related to the settling velocity of the particle). Therefore, some details need to be considered with care in the use and calibration of these instruments (Baron, 1986; Kenny and Lidén, 1991; Tsai *et al*., 2004). Firstly, for larger differential velocities, liquid droplets can be deformed, affecting their drag force and resulting measurement (Secker *et al*., 2000). This can create differences in calibration between liquid and solid particles (Griffiths *et al*., 1986). At higher concentrations, coincidence (Armendariz and Leith, 2002; Peters and Leith, 2003) and recirculation (Stein *et al*., 2002) can cause size-dependent measurement errors, while non-spherical particles can also pose a challenge (Griffiths and Vaughan, 1986; Marshall *et al*., 1990; 1991; Marshall and Mitchell, 1992). For larger sized particles, measurements need to be corrected for density (Wang and John, 1987; 1989; Chen *et al*., 1989). Alternatively the APS can be calibrated beforehand with the same material that is to be measured. However, there will always be some additional uncertainty when measuring unknown or mixed aerosols limiting the accuracy in real-world exposure scenarios.

1.4.3. Number concentration metrics

Counting airborne particles has a long history from cloud chambers and manual counting of microscopy samples (Cunningham, 1873; Walton and Vincent, 1998) to more modern automated optical methods.

1.4.3.1. Optical particle counters

Optical particle counters (OPCs) have been used for many years for the counting and monitoring of particle concentrations in the air of micron and sub-micron sized particles (Willeke and Liu, 1976). In operation, an aerosol flow is focused into a narrow stream and passed through an optical cavity, usually containing a laser diode, mirror, and a detector (e.g. PIN photodiode with collecting lenses to widen the angular response). The mirror and collector share a common axis which is orthogonal to both the light source and aerosol particle stream axes. If there are no particles passing through the OPC, the light is captured in a trap opposite the source and no signal is detected. When a particle traverses the light beam, it scatters the light, which is then detected as a pulse in the mirror and photodetector arrangement. Ideally each pulse should correspond to a single particle, i.e. one particle is counted at a time (single particle counting mode). If the particle concentration gets too high such that more than one particle traverses the light

beam within the gating period of the photodetector, then these particles will be counted as a single event and the response of the OPC will saturate. Some OPCs have the ability to switch into an additional photometric mode whereby the total amount of scattered light is used as a measure of the particle concentration. This allows for higher concentrations to be measured, but is less accurate, and can also cause discontinuities in the data if there is a calibration mismatch at the cross-over between the single particle counting and photometric modes.

OPCs are limited in the smallest size of particle they can detect by the wavelength of light used. Most standard OPCs measure down to ~300 nm and generally provide some low resolution sizing information (e.g. 2 – 5 channels) by use of different thresholds on the scattered light pulse. However, by passing the aerosol through the active cavity of a laser, much higher light intensity can be achieved allowing for detection of particles as small as 50 nm (Gebhart *et al*., 1976). Such instruments are known as Laser Aerosol Spectrometers (Szymanski and Liu, 1986) and can provide high resolution optical sizing across the sub-micron and micron size range.

1.4.3.2. Faraday cup electrometer

One of the most straightforward measurement techniques for counting nanoparticles is to charge them and then measure the current generated when they are deposited in a Faraday cup. This can be achieved for example by passing the aerosol through a conducting filter in the Faraday cup and measuring the current resulting from particles becoming caught in the filter with an electrometer. Such a device is variably known as a Faraday cup aerosol electrometer (FCAE), aerosol electrometer (AE) or Faraday cup electrometer (FCE). It is usually a simple and robust system requiring low maintenance. However there is a trade off in terms of low sensitivity and poor accuracy, especially with larger particles. The challenge of measuring very low currents means that these devices are usually not sensitive to concentrations much below 1,000 cm^{-3}. In addition, these devices have an associated zero-particle current which needs to be accounted for and can be sensitive to temperature fluctuations. Although measuring over longer intervals is preferable for minimising random noise effects, it can also lead to a drift in this base level reading, increasing uncertainty. Averaging of multiple short interval samples could help to avoid having to compromise between random noise and drift, assuming it is possible to re-check and re-adjust for the zero-particle current between samples. Also, to convert the data from current to number of particles, knowledge of the number of charges associated with each particle is required. Depending on the charging mechanism, it may be a safe assumption that particles much less than 100 nm are unlikely to have more than one charge (singularly charged); while at larger particle sizes this will not be the case. With correct knowledge of the charger performance, and another element (such as a DMA) in front of the FCE to provide sizing information, it is possible to correct for the level of multiple charging based on the size distribution measured. However, this is not possible if the FCE is used in isolation and only providing a measure of concentration. Therefore these devices are generally better suited to quick and rough measurements in dirty environments. They are often incorporated into hand-held devices due to their inherently robust and compact nature. In an occupational or environmental exposure setting, they can therefore be useful as indicators of the presence and source of contaminants, allowing more detailed

investigation to be carried out with additional instrumentation. They are less well suited to critical low level applications such as clean room monitoring.

1.4.3.3. Condensation particle counters

Condensation particle counters (CPCs, also known as condensation nucleus counters, CNCs – McMurry, 2000b; Spurny, 2000) allow for the measurement of both smaller nanoparticles and much lower concentrations compared to FCEs. A CPC is composed of two main components; a condensation unit (CU), and an optical particle counter (OPC) as discussed above. The CU is utilised as a pre-enlargement device to overcome the size limitations of OPCs. The CU is comprised of a saturator, as a source of vapour, and a condenser, where the vapour is nucleated onto an aerosol stream of nanoparticles to form droplets large enough to be detected in an OPC. In this manner particles can be detected right down to a few nanometres or less. The details of nucleation and CPCs will be discussed further in Section 3.3.

Condensation counters were reported as early as 1888 by Aitken (Walton and Vincent, 1998; Spurny, 2000; Sem, 2002). However, early devices relied on adiabatic expansion to produce supersaturation conditions, and hence analysis could only be carried out on pulsed volumes. The first commercial continuous flow and single-particle counting CPC, utilising heated saturator and cooled condenser regions, was reported by Agarwal and Sem (1980), based on prior works by Sinclair and Hoopes (1975b), and Bricard *et al*. (1976). This design was further developed by Stolzenburg and McMurry (1991) by incorporating the mixing type design as proposed by Kousaka *et al*. (1982) in which a separate saturated sheath air flow is mixed with the aerosol flow before entering the condenser. In this manner the response to small nanoparticles < 20 nm was improved, achieving a 50% counting efficiency cut-off of 3 nm. Generally the size of droplet formed in a CPC is independent of the size of the nucleating particle. However some correlation can be found at the smallest detectable particle sizes of ~10 nm or less. This effect has been exploited by using pulse height analysis in the OPC for the sizing of nucleation mode particles (Wiedensohler *et al*., 1993; 1994; Marti *et al*., 1996; O'Dowd *et al*., 2004).

As the particles detected by a CPC do not need to be charged, and with the single particle counting functionality provided by the OPC back-end, CPCs can offer a much more sensitive measure of nanoparticle concentrations compared to FCEs. However they usually require a regular re-supply of working fluid, and, depending on the design, may not be suitable for portable applications. Tilting of CPCs can cause the working fluid to run into flow paths and can, for example, damage the OPC. In addition, the common choices of butanol and isopropanol as working fluids can create unpleasant fumes requiring suitable ventilation.

1.4.3.4. Electrical mobility particle sizers

The counting technology of a CPC (or FCE) can be combined with the sizing classification of a DMA to form an instrument which measures size distributions of airborne particles. This is usually referred to as a "scanning mobility particle sizer" (SMPS) or more recently as a "differential mobility analysis system" (DMAS) in the

ISO nomenclature.

SMPS instruments were a natural development following on from the measurement of the output of a DMA. It was recognised early on in their development that the output of a DMA could provide measures of aerosol size distributions across the nano and sub-micron range with good resolution and minimal disturbance of their natural state (Knutson, 1976). Automatic computer control and synchronisation of a CPC collector with stepped DMA voltages led to the commercialisation of such systems as "differential mobility particle sizers" (Keady *et al.*, 1984). Depending on the resolution and range required, the process of stepping through each DMA voltage and measuring the output could be quite time consuming, even if run by an automated system. It was found that this process could be sped up considerably by instead scanning through the range of voltages required with an exponential ramp and monitoring the output continuously (Wang and Flagan, 1990). With correct consideration of the correlation between measurement time and DMA voltage, the mobility of the particles measured by the CPC is reliably known. This system was then commercialised by TSI as a "scanning mobility particle sizer" (Quant *et al.*, 1993). Since then not a lot has changed in the fundamental approach of SMPS instruments. The size range of DMAs has been extended further into the nano range (Chen *et al.*, 1996), and limitations on minimising the scan time further have been explored (Tokonami and Knutson, 2000; Shah and Cocker, 2005). In addition, the effects of different measurement conditions such as humidity (Ristovski *et al.*, 1998) and carrier gas (Schmid *et al.*, 2002) have been investigated and the system has been extended for application in low pressure systems (Ober *et al.*, 2002).

Electrometers are less commonly used in SMPS instruments in comparison to CPCs. However, they have found widespread use in instruments in which multiple electrometer stages are incorporated into the body of a DMA type device. Such instruments have no particle output but instead each electrometer stage collects a certain sub-set of mobility trajectories within the device. In this manner, the entire mobility range is measured in parallel. This allows for the measurement of particle size distributions on a much faster time scale, albeit with lower resolution and sensitivity compared to an SMPS. The earliest such instrument was the Electrical Aerosol Spectrometer (EAS), developed by Tammet and co-workers in the 1970s (see references in Tammet *et al.*, 2002). However the modern successor to this instrument is known as the Fast Mobility Particle Sizer (FMPS), licensed by TSI from Airel Ltd. The FMPS can measure a 16 channel per decade size distribution in 1 second covering a size range from 5.6 to 560 nm. More specialised instruments include the Cambustion DMS50 and DMS500 (Biskos *et al.*, 2003; 2005; Symonds *et al.*, 2007) and the TSI Engine Exhaust Particle Sizer (EEPS – very similar to FMPS but with higher sampling rate) all used for measuring exhaust particle distributions from engine emissions.

Other devices based on the EAS principle include the Miniature Electrical Aerosol Spectrometer (MEAS – Ranjan and Dhaniyala, 2007; 2008), a compact, low resolution device suitable for portable applications, which utilises an ESP (electro-static precipitator) pre-filtration system to allow differential classification with only one flow, and the Symmetric Inclined Grid Mobility Analyzer (SIGMA – Tammet, 2011), a high flow device for measuring positive and negative air ions.

Another approach to fast measurements of mobility spectra is the Fast Integrated Mobility Spectrometer (FIMS – Kulkarni and Wang, 2006a; 2006b; Olfert *et al.*, 2008;

Wang, 2009). This device in effect combines DMA and CPC technologies into one. Charged particles are separated into different trajectories in a classification region which also utilises a sheath flow saturated with working fluid. These separated trajectories are then maintained through a subsequent condenser region and the positions of the resulting condensed droplets are imaged with laser illumination and a CCD camera. The Aerosol Electrical Mobility Spectrum Analyzer (AEMSA – Ahn and Chung, 2010) is a similar device that allows for the simultaneous measurement of both positively and negatively charged particles.

1.4.4. Surface measurements

Numerous studies to date have shown a strong correlation between aerosol surface area and specific health effects such as tissue damage in the lung (see references summarised in Maynard and Kuempel, 2005; Szymanski and Allmaier, 2009). Efforts to measure the surface area of particles stretch back many decades. An early example is the work of Talbot (1966, 1967) who proposed a technique which involved measuring the far-field diffraction pattern created by apertures in a metal film. The apertures could be formed by depositing the metal film over previously deposited particles on a glass slide such that when the particles were removed the resulting apertures would roughly correspond to projections of the particles. The photomultiplier current measured in this setup was then related back to either a total or respirable surface area by means of different optical filters representing different conversion functions.

The standard method for measuring the surface area of powder samples has for many years been to use gas adsorption, known as the BET method following the works of Brunauer, Emmett and Teller (Brunauer *et al*., 1938; Gregg and Sing, 1982). Many studies have shown a correlation between BET measured surface area and toxic response (e.g. Lison *et al*., 1997; Stoeger *et al*., 2005; Singh *et al*., 2007; Warheit *et al*., 2007; LeBlanc *et al*., 2010). However, it is not suited to online measurements, and requires either measurement of powder samples before aerosolisation, or measurement of samples collected by e.g. impaction. It is unclear how well this measurement corresponds to the airborne surface area, especially when applied to powder samples with much of the primary particle surface area buried within the volume of the powder.

Another long-standing offline technique is to measure particle surface area from images recorded by electron microscopy (typically TEM – e.g. Bau *et al*., 2003). Compared to BET which only measures total surface area, this method has the advantage of being able to relate measurements to individual particles and build up a graph of the surface area distribution. However, this method is only reliable for uniform and smooth spherical particles. For more complex morphologies, the restrictions imposed by only measuring a two dimensional projection become more significant. In addition, more consideration is required to deposit the requisite particle samples onto TEM grids.

One of the earliest methods for measuring the surface of particles in an airborne state is the epiphaniometer (Baltensperger *et al*., 1988; Gäggeler *et al*., 1989; Rogak *et al*., 1991). In this device, aerosol particles are drawn through a chamber containing an ^{227}Ac source. One of the decay products from this source is the lead isotope ^{211}Pb which attaches to particles passing through the chamber. Unattached ^{211}Pb is removed by diffusion in a capillary tube and the particles are then collected on a filter. The amount

of deposited ^{211}Pb on the filter is then measured by an α-detector which measures the α emissions of its daughter nuclide ^{211}Bi. The attachment rate of the ^{211}Pb to aerosol particles (and therefore the instrument response) was found to be proportional to d^2 for small particle diameters with $d < 100$ nm, and proportional to d for particles larger than 3 μm, with a transition zone at intermediate sizes. In general, the property measured by this attachment rate is termed the "active" or "Fuchs" surface area, and is given by $\pi.d^x$ where x varies between 1 and 2 depending on the particle diameter (Fuchs, 1964; Pandis *et al*., 1991; Keller *et al*., 2001). Although the epiphaniometer has been used with some success for the measurement of atmospheric aerosols (Shi *et al*., 2001), it has not found widespread use nor is it currently commercially available. The radioactive source required in its operation makes it ill-suited to occupational exposure measurements in the workplace. In addition, the 36 minute half-life of ^{211}Pb acts like a damping constant on the response such that it is better suited to long term field monitoring applications rather than bursts of industrial pollutants.

To overcome the difficulty in using radioactive sources, the contemporary method for measuring the active surface area of aerosols is by diffusion charging. In this case ions replace the radioactive gas, and the charge collected in an electrometer is used to measure the attachment rate of ions to the aerosol particles. Instruments based on measurements of diffusion charging rates include the LQ1-DC from Matter Engineering (discontinued), the Electrical Aerosol Detector 3070A (EAD), Nanoparticle Surface Area Monitor 3550 (NSAM) and AeroTrak 9000 from TSI Inc., as well as the DC 2000CE from EcoChem Analytics. The LQ1-DC, EAD and DC 2000CE have responses defined by their individual charger performance but are inherently similar in giving an active surface area response with diameter power x values between 1 and 2. The NSAM (Shin *et al*., 2006) and AeroTrak instrument include additional ion trap potentials to augment the response to make it similar over a certain size range to the alveolar or tracheo-bronchial deposition functions (investigated with the EAD by Fissan *et al*., 2006). There has been much debate in recent years about the exact nature of the response of these instruments and its potential correlation to health risks. Very briefly, and in chronological order, the major results reported in this area in recent years are as follows with responses to diameter (d^x) characterised by values of the power x:

- Weber *et al*. (1996) reported an attachment rate of lead isotopes to agglomerates proportional to the agglomerate diameter to the power of 1.47 in the range 70 – 200 nm.
- Woo *et al*. (2001) and Wilson *et al*. (2003) found an EAD response of $x = 1.16$ using atmospheric aerosol.
- Jung and Kittelson (2005) found that the LQ1-DC and EAD had x values of 1.36 and 1.13 respectively when measuring NaCl particles in the range 30 – 150 nm and calculated that the Fuchs (active) surface area gives $x = 1.39$ over the same size range.
- Ku and Maynard (2005) investigated the LQ1-DC and EAD and found they both had a response close to the geometric surface area with $x = 2$ below 100 nm with monodisperse silver agglomerate aerosols. A good match was also found to SMPS and TEM measures of surface area in this size range. The response of the

LQ1-DC decreased to a power of 1.6 when the size range increased to 20 – 200 nm or 1.5 when considering 80 – 200 nm.

- Wilson *et al*. (2007) investigated how well the response of the EAD correlated to the estimated deposited surface area in the lung. They found that the correlation to deposited surface area reached a maximum for values of diameter power *x* between 1.1 and 1.6 and concluded that the "EAD should provide a useful indicator of fine particle surface area deposited in the lung".
- Asbach *et al*., (2008) concluded that the NSAM does accurately reflect the alveolar and tracheo-bronchial responses between 20 and 400 nm, at least for spherical particles.
- Szymanski and Allmaier, G. (2009) found a good correlation between measured and calculated alveolar and tracheo-bronchial deposition fractions with the NSAM between ~10 and 200 nm.
- Ku (2010) reported that the surface area responses of the DC 2000CE and LQ1-DC in the size range from 100 – 900nm were proportional to the mobility diameter to the power of 1.22 and 1.38 respectively. This led to deviations from the geometric surface area (power $x = 2$) of up to 94%.
- Ku and Kulkarni (2012) found that diffusion charging instruments could underestimate the surface area compared to BET and a tandem mass plus TEM technique by a factor of 3 – 10.

Most of these results are roughly consistent with the underlying postulation that as the particle size is increased through the transition regime, the response of instruments sensitive to the active surface area will demonstrate decreasing values of *x* between the limits of 2 and 1 corresponding to the purely free molecular and continuum regimes respectively. However, the result from Jung and Kittelson (2005) for the LQ1-DC (x = 1.36 for 30 – 150 nm particles) does not fit with this trend when compared to subsequent measurements (x = 1.5 for 80 – 200 nm particles and x = 1.38 for 100 – 900 nm particles) by Ku and colleagues (2005, 2010).

Another technique sensitive to surface area is photoelectric charging (Schmidt-Ott and Federer, 1981; Burtscher *et al*., 1982). Particles are exposed to UV light and the resulting emitted electrons or positively charged particles can be measured with an electrometer. The resulting signal will depend on the chemical nature of the surface as well as the total surface area exposed. Therefore the interpretation of the results is too uncertain to be generally useful. However, it has found application in measurements of exhaust aerosols from combustion engines, in particular due to its sensitivity to polyaromatic hydrocarbons (Burtscher, 1992). Matter *et al*. (1998; 1999) measured a linear response in the photoelectric signal compared to that obtained from diffusion charging, with the slope dependent on the type of combustion source measured. The combination of these two techniques is suggested as a useful characterisation approach avoiding the complication of size distribution measurements (Dahmann *et al*., 2000; Bukowiecki *et al*., 2002).

Finally, a number of studies have demonstrated the measurement of aerosol surface area by the combination and deconvolution of multiple simultaneous metrics, mainly number and mass (Sverdrup and Whitby, 1977; Woo *et al*., 2001; Maynard, 2003; Ku and Evans, 2012). However due to the large setups involved, such techniques are better suited to controlled laboratory environments rather than *in situ* measurements.

1.4.5. Chemically specific techniques

1.4.5.1. Electron microscopy and X-ray techniques

Determining the chemical nature of aerosols is necessary to provide a proper assessment of potential health or environmental risks. A wide range of approaches have been employed over the years (Mattimaricq, 2007; Chow *et al*., 2008), however the most ubiquitous methods to date have involved offline standard analytical techniques on collected aerosol samples, e.g. on filters (Chow, 1995). For example, electron microscopy systems outfitted with additional detectors can provide valuable chemical data on individually imaged particles (Thölén, 1995; Buffat, 1999; Casuccio *et al*., 2004; Laskin *et al*., 2006; Bzdek *et al*., 2012). Typically this is achieved through the detection of X-rays produced by the decay of excited atomic states stimulated by electron interactions. Measurement of the energy spectrum of these X-rays provides information on the elemental composition of particles, and can also reveal the distribution of elements within more complex particles if the electron beam can be focussed to a spot size small compared to the particle size. This technique is often referred to as energy-dispersive X-ray spectroscopy (EDX – Laskin *et al*., 2002; Krueger *et al*., 2003) due to the use of energy-dispersive spectrometers to measure the spectrum of X-rays produced. Depending on the type of detector used, the lowest atomic number that can be detected by EDX (albeit with low sensitivity), can be 6, 11 or 14, i.e. carbon, sodium or silicon (Maynard, 2000; McMurry, 2000a). However when working with nanoparticles, the sensitivity can be limited to heavier elements (Maynard, 2000). Outside of electron microscopes, characteristic X-rays for aerosols can also be produced and analysed by other techniques such as X-ray fluorescence (XRF – Toyoda *et al*., 2004; Szilágyi and Hartyáni, 2005; Ma and Kim, 2008; Sun *et al*., 2009; Bernardoni *et al*., 2011; Richard, 2011) or proton induced X-ray emission (PIXE – Tomić *et al*., 1987; Chen *et al*., 1988; Winchester *et al*., 1990; Artaxo *et al*., 1992; Wang *et al*., 2000; Lucarelli *et al*., 2011; Díaz *et al*., 2014; Calzolai *et al*., 2014). While XRF is relatively affordable and now available in hand-held systems, PIXE requires an ion accelerator to produce a collimated beam of protons, restricting its use to more specialised applications. Speciation of aerosol samples has also been achieved by analysis of X-ray absorption spectra (Takahashi *et al*., 2006; Higashi and Takahashi, 2009; Sakata *et al*., 2014).

An alternative approach to detecting X-rays in transmission mode electron microscopes is to measure the energy loss of the electrons in the electron beam after they have passed through the sample. This technique is called electron energy-loss spectroscopy (EELS – Maynard, 1995; Egerton, 2011). The energy lost by the transmitted electrons provides information on the inelastic interaction of the electrons within the sample. In this manner, signatures of particular atomic excitations can be detected to yield compositional data similar to that obtained by X-ray analysis. EELS can provide

detection of most elements; however, relative to EDX it is comparatively more sensitive to lighter elements.

Measurement of the diffraction patterns formed by transmitted electrons can also provide crystallographic structural information on individual aerosol particles by such methods as selected area electron diffraction (SAED – Hoflich *et al*., 2005; Li and Shao, 2009; Salma *et al*., 2009; Li *et al*., 2010; Fu *et al*., 2012) and convergent beam electron diffraction (CBED – Brown, 1986; Maynard, 2000; Wang, 2004). However X-ray diffraction (XRD – Thompson *et al*., 1982; Davis, 1984; Tanninen *et al*., 1985) is a more popular approach which does not require an electron microscope. It is generally applied to bulk sample measurements, although correlation to particle size can be provided through a suitable pre-selection or sampling technique such as a cascade impactor (Tani *et al*., 1983; Sturges and Harrison, 1989).

Despite their wide use and single particle analysis strengths, electron microscopy and X-ray techniques have a number of significant disadvantages (Huang and Turpin, 1996). Firstly, the sensitivity of any elemental analysis approach is limited by the choice of substrate which can act as an interfering background signal. The choice of substrate should be carefully considered in light of the desired elemental sensitivity as there is no single choice suitable for the analysis of all aerosol components (McMurry, 2000a; Casuccio *et al*., 2004). Secondly, the vacuum conditions and local heating from the electron beam can cause significant losses of semi-volatile components as well as potential damage or modification to other sample components. Finally, analysis by electron microscopy is a slow process often requiring complex sample pre-treatment. It can take a long time to gather a statistically significant data set, although automated methods can be of great assistance in this regard (Germani and Buseck, 1991; Casuccio *et al*., 2004; Moffet *et al*., 2010).

1.4.5.2. Atomic excitation techniques

Laser-induced breakdown spectroscopy (LIBS – Rusak *et al*., 1997) is a promising technique for measuring the elemental composition of aerosols. LIBS uses a focused high energy laser pulse to form a plasma which vaporises the sample and thermally excites the resulting dissociated atoms. The decay of these excited states produces characteristic photon emission spectra which are detected by a spectrometer. This latter stage is usually referred to as atomic emission spectroscopy (AES) and can provide some determination of the relative abundance of different atomic species. It has been used to measure aerosols collected on filters (Neuhauser *et al*., 1997a; 1999; Panne *et al*., 2001), single isolated aerosol particles (Biswas *et al*., 1987), as well as being used as an online technique for the continuous monitoring of aerosol constituents (Hahn and Lunden, 2000; Carranza *et al*., 2001; Hybl *et al*., 2003; Lithgow *et al*., 2004; Beddows and Telle, 2005). Size measurements of the particles prior to measurement can be carried out for micron sized particles by laser scattering velocimetry (Ottesen *et al*., 1989; 1991), while a DMA can be used to investigate possible size dependent effects for sub-micron or nanoparticles (Hahn, 1998; Amodeo *et al*., 2009). Offline size analysis can also be carried out by microscopy (Radziemski *et al*., 1983). Although there can be issues of larger micron-sized particles not fully vaporising (Carranza and Hahn, 2002), size effects are found to be negligible in the sub-micron regime with a linear response to mass found across different sizes (Amodeo *et al*., 2009), and in general sensitivity is

poor for nanoparticles (< 100 nm, Park *et al*., 2009). AES can also be carried out using inductively-coupled plasmas (ICP) rather than laser breakdown. Menzel *et al*. (2002) showed that elemental analyses of aerosols by PIXE and ICP-AES usually agree within 15%.

Another atomic emission laser based technique which has been applied to aerosols is laser excited atomic fluorescence spectroscopy (LEAFS – Hou *et al*., 1998; Stchur *et al*., 2001). Rather than using thermal energy to excite atoms, LEAFS directly excites gaseous target species with a laser and detects the resulting fluorescence. Vaporisation is required as a first step, and can be carried out for example by passing the sample material through a flame, furnace or plasma. The laser must be tuned to the desired excitation and therefore only one element can be detected at a time. However, the targeted nature of this technique results in less spectral interference (compared to AES based techniques), large dynamic ranges with a linear response, and extremely high sensitivity which has been demonstrated to extend down to the low attogram level for lead (Smith *et al*., 1989). LEAFS has not as yet found widespread usage in aerosol science, presumably due to the limitations imposed by single element detection and the requirement for a tunable laser system. However it has been used to measure levels of lead, thallium, and tin, in samples collected by impaction in a clean room (Liang *et al*., 1990). It has also been used for the online measurement of lead from DMA size-resolved lead nitrate aerosols between 48 and 300 nm in diameter (Neuhauser *et al*., 1997b; 1997c).

Atomic absorption spectroscopy (AAS – Hou and Jones, 2000; Welz and Sperling, 2007) is a much older elemental analysis technique which has also been used for aerosol measurements in the past (e.g. Nottrodt *et al*., 1978). In addition, Fourier transform infrared spectroscopy (FTIR) is often applied to aerosol particles in combination with EDX (Liu *et al*., 2008; Liu and Laskin, 2009; Ryu and Ro, 2009; Song *et al*., 2010; 2013).

1.4.5.3. Mass spectrometry techniques

Mass spectrometry (MS) covers a wide range of technical implementations for evaluating the mass to charge ratio of ions. This identifying fingerprint is ascertained by measuring the flight path or transit time of ions under vacuum conditions in electric (and in some cases also magnetic) fields. The overall approach can be broken down into different stages. First an airborne or deposited sample is broken apart into the required constituents for analysis (e.g. molecules, molecule fragments or atoms), secondly the sample is ionised, and finally the mass to charge ratio (commonly designated as m/z) is measured. The first two of these stages may be carried out as a single step. There may also be a separate pre-stage for creating an airborne sample from a liquid or solid, and this in turn can also be combined with the first dissociation step. In any case, a range of different approaches and technologies have been applied to each of these challenges creating a diverse field of acronyms which can be combined in different manners. Here we will only consider briefly the most commonly encountered MS techniques used for the measurement of aerosol particles (Davis, 1973; Suess and Prather, 1999; Hartonen *et al*., 2011; Nizkorodov *et al*., 2011).

Offline MS techniques (Pratt and Prather, 2012a) refer to the case where the aerosol

particles are first sampled onto a substrate (by e.g. filtration or impaction) before being subsequently analysed by MS. This can bring sensitivity enhancements via accumulation of particles. Here, sample introduction and ionisation stages are often combined as a single step. For example, in laser desorption/ionization (LDI), a pulsed laser beam is applied to the sample surface to remove material which is then ionised in the resultant surrounding hot gas. In secondary ion mass spectrometry (SIMS), a focussed beam of ions is fired at the sample surface resulting in the release of secondary ions from the analyte. While in desorption electrospray ionization (DESI), gaseous ions are produced by directing charged droplets from an electrospray at the sample. Alternatively in electrospray ionisation (ESI), a dissolved sample can be sprayed directly from an electrospray needle such that that airborne ions are formed by evaporation of the resulting charged droplet. In this case, liquid chromatography can also be utilised to provide additional pre-separation of different constituents of the sample.

Online real-time MS techniques (Johnston, 2000; Noble and Prather, 2000; Hunt and Petrucci, 2002; Nash *et al*., 2006; Murphy, 2007; Pratt and Prather, 2012b; Laskin *et al*., 2013) differ from offline techniques mainly at the sample introduction and ionisation stages. Mass spectrometers designed for aerosol studies often incorporate an aerodynamic focusing lens at the inlet to create a narrow beam of aerosol particles within a certain size range. For example, the Aerodyne Aerosol Mass Spectrometer (Jayne *et al*., 2000; Jimenez *et al*., 2003; Canagaratna *et al*., 2007; Robinson *et al*., 2011) is a commercial instrument featuring an aerodynamic selective inlet optimised for the transmission of particles between 70 and 500 nm. The particle aerodynamic diameter is evaluated in a particle time-of-flight (TOF) region by measuring the particle velocity due to gas expansion in low pressure conditions. This is achieved by timing the detection in relation to a mechanical chopper wheel monitored with a photodiode-detector pair which modulates the particle beam. The particles are then vaporised and ionised by impaction onto a heated surface with an incorporated electron impact ioniser in close proximity. Finally, the resultant constituents are analysed in a quadrupole mass analyser, where particular ion paths are selected by a radio frequency quadrupole field between four parallel rods allowing for a wide range of m/z values to be swept quickly.

Another (now discontinued) commercial product was the TSI 3800 ATOFMS (aerosol time-of-flight mass spectrometer – Prather *et al*., 1994; Gard *et al*., 1997; Allen *et al*., 2000; Beddows and Telle, 2005; Giorio *et al*., 2012; Smith *et al*., 2012). Again aerosol particles are focussed in an aerodynamic lens and then sized in a particle TOF region. However, in this case timing is achieved with a laser velocimetry system, comprising two lasers at either end, from which the timing of scattering signals from particles is measured. These signals are also used to time a subsequent high power laser pulse which evaporates and ionises the particle matter. Mass-charge spectra are then determined in a bipolar time-of-flight mass spectrometer. TOF-MS techniques determine m/z values for ions by accelerating them through an electric field and timing how long they take to reach the detector. This dual particle-TOF and ion-TOF approach dates back to the work of Prather, Noble and colleagues in the mid 90s (Nordmeyer and Prather, 1994; Salt *et al*., 1996; Noble and Prather, 1996; 1998), and has seen continued development to make it more transportable (Gard *et al*., 1997; Trimborn *et al*., 2000; Pratt *et al*., 2009) and improve detection efficiency for smaller particles (Su *et al*., 2004). In addition, the Aerodyne AMS instrument discussed above has also been operated in a modified setup utilising TOF-MS (Drewnick *et al*., 2005), with additional

development work on the ion TOF region improving resolution further (DeCarlo *et al*., 2006).

Alternative particle sizing techniques have also been combined with TOF-MS, including optical scattering size measurements (Marijnissen *et al*., 1988; Coggiola *et al*., 2000), pre-size selection in a DMA (Zelenyuk *et al*., 2005), and variable pressure aerodynamic size-selective inlets (Mallina *et al*., 2000).

Aside from the electron and laser ionisation methods mentioned above, additional vaporisation and ionisation techniques which have been used in aerosol studies include inductively coupled plasma (ICP) with collected samples (Mouli *et al*., 2006; Niu *et al*., 2010; Asbach *et al*., 2014), matrix-assisted laser desorption/ionization (MALDI – Harris *et al*., 2005; Müller *et al*., 2007), nanospray desorption/electrospray ionization (O'Brien *et al*., 2013), and chemical ionisation of cloud condensation nuclei with nitric acid (Zhao *et al*., 2010; Jiang *et al*., 2011).

1.4.6. Advanced optical methods for detecting nanoparticles

Standard optical detection systems for particles such as OPCs, utilising simple optical scattering based detection, have traditionally been limited by the wavelength of light used. In the Rayleigh regime, where the size of particles is less than a tenth of the wavelength, the scattering intensity is proportional to the sixth power of the radius resulting in poor sensitivity to small particles. However, a number of approaches have been developed for working around this limitation and extending optical detection systems into the nano-regime.

Developments in microscopy have led to dark field/ultramicroscopy techniques where small particles will appear as fuzzy spots of light against a dark field of view. Usually light is scattered from a sample orthogonal to the incident beam (Braslavsky *et al*., 2001), although total internal reflection off the reverse side of the sample slide has also been used (van Dijk *et al*., 2005). In near-field microscopy (Novotny, 2007; Okamoto and Imura, 2009), an illuminated aperture (or laser irradiated metal tip in tip-enhanced near-field microscopy – Bouhelier *et al*., 2003; 2004; Hartschuh *et al*., 2004; Hartschuh, 2008) is positioned less than one wavelength distance away from the sample. The resolution in this case is only limited by the size or ability to position the aperture/tip. Although the optical power reaching the sample falls off dramatically as the aperture size becomes much less than the wavelength of light. Fluorescence techniques meanwhile utilise molecular transitions to bridge the diffraction limit on resolution (Hell, 2009). It is a large field in its own right but shall not be discussed in any detail here as we are mainly concerned with the detection of non-fluorescent particles. However, it can also be combined with other relevant techniques such as tip-enhanced near-field microscopy (Sánchez *et al*., 1999), and Raman scattering (Hartschuh *et al*., 2003), and is especially useful for biological applications such as Flow Cytometry (Boeck, 2001; Alfonso and Al-Rubeai, 2011; Galanzha and Zharov, 2012).

Since the turn of the century there has been a growing field of research focussed on utilising novel optical approaches to provide online and *in situ* detection systems for nanoparticles in fluids and gases. For example, whispering gallery modes (WGMs) are

resonances tied to a particular morphology of an object which allow for an integral number of wavelengths to circulate. If a nanoparticle now comes into contact with the resonator, some of the light can be lost through it from the resonator disrupting the WGM and causing a shift in the resonance. This can be used as a basis of a detection and sizing technique (Giusto *et al*., 2005; Matsko *et al*., 2005; Mazzei *et al*., 2007; Min *et al*., 2009; Zhu *et al*., 2009; 2011; Kippenberg, 2010; He *et al*., 2011; Lu *et al*., 2011; Shen *et al*., 2012; Shao *et al*., 2013), with a lower size limit of ~10 nm.

The limitations of optical scattering can be avoided altogether by instead utilising an absorption based system which is inherently more sensitive to small particles (Moosmüller *et al*., 2009). Traditional photoacoustic techniques have already been discussed in Section 1.4.1. However in recent years, more advanced photothermal systems have been developed, with greater sensitivity and the potential to measure individual particles online; although currently they are used in offline microscopy systems (Boyer *et al*., 2002; Cognet *et al*., 2003; Zharov and Lapotko, 2005; Adler *et al*., 2008; Kulzer *et al*., 2008; Paulo *et al*., 2009; Gaiduk *et al*., 2010; Selmke *et al*., 2012a; 2012b; 2013; Nedosekin *et al*., 2014). Detection is based on a dual laser system. A pump beam is used to heat particles at or passing through its focus. While a probe beam detects the resulting heat induced change in the refractive index in the surrounding medium by angular deflection or phase/interferometric shifts.

The sixth power dependency of scattering can also be mitigated by use of interference techniques which make use of a reference beam which is coherent with the scattered sample signal. The resultant interference signal will depend on the electric field of the scattered sample signal which is proportional to the third power of particle size providing greater sensitivity to small particles. There is currently a broad range of techniques utilising interference effects in published literature (Ignatovich and Novotny, 2006; Ignatovich *et al*., 2006; van Dijk *et al*., 2006; Sandoghdar *et al*.,2006; Hwang and Moerner, 2007; Plakhotnik, 2007; Deutsch *et al*., 2010; Mitra *et al*., 2010; 2012; Person *et al*., 2011; Wennmalm and Widengren, 2012) using diverse terminology often dependent on the author's background. All of these techniques however share the same fundamental physics defining their effectiveness at detecting nanoparticles.

Optical gradient techniques (Ignatovich and Novotny, 2003; Ignatovich *et al*., 2003; 2006) make use of the momentum of photons in a laser beam to act on the movement of nanoparticles of interest. The force on the particle in this case is proportional to the third power of particle size. Therefore this technique, as with absorption and interferometric approaches, can theoretically provide greater sensitivity to nanoparticles compared to simple scattering mechanisms. Detection can be based on the acceleration or deflection of particles as they pass close to the focus of the laser beam making it inherently suited to an online detection system.

Numerous related online techniques involve the scattering of light from a large number of particles measured over time (Jiang *et al*., 2008). Dynamic Light Scattering (DLS) provides an average diameter of the particle ensemble by measuring an average value of the diffusion coefficient from intensity fluctuations caused by Brownian motion. One advancement on DLS termed Localised Dynamic Light Scattering (LDLS – Bar-Ziv *et al*., 1997) extends the DLS principle to probe single particles. While another called Polarisation Fluctuation Spectroscopy (PFL – Hopcraft *et al*., 2005) measures the change in polarisation in scattered light from the particle ensemble which provides information on how far the particles deviate from a spherical shape. Other optical

techniques for sizing particles larger than the wavelength of light include laser diffraction (de Boer *et al*., 2002; Marriott *et al*., 2006), which can also provide some shape information (Ma *et al*., 2000; 2001; Yamamoto *et al*., 2002; Tinke *et al*., 2008), and transmission fluctuation spectrometry (Shen *et al*., 2008; Xu *et al*., 2008).

1.4.7. Raman spectroscopic identification of aerosol particles

Raman spectroscopy is an effective means of identifying a wide range of compounds relatively quickly and with good sensitivity down to the single particle level. Therefore, it is a promising technique to consider for distinguishing engineered nanoparticles (ENP) from background particles. Raman techniques are not suitable for measuring aerosol samples directly *in situ*, however, they can be used as offline tools if the aerosol can be sampled onto a suitable substrate.

Raman spectroscopic data has been measured from aerosol particles in a variety of schemes before. Straightforward approaches include analysing material collected on a filter (Rosen and Novakov, 1977; Mertes *et al*., 2004) or material impinged by a fluid which is then deposited and dried on a microscopy slide (Kong *et al*. 2011). More complex arrangements have also been used to directly analyse suspended particles (Schweiger, 1990) including; electrodynamic suspension (Buehler *et al*., 1991; Vehring *et al*., 1998; Lee and Chan, 2007), optical trapping (Hoffmann *et al*., 1991; 1995; Ling and Li, 2013), or from a droplet chain arrangement (Vehring, 1998). In recent years Raman spectroscopy has also been utilised to identify particles collected by impaction (Sobanska *et al*., 2006; Batonneau *et al*., 2006; Ivleva *et al*., 2007; Ault *et al*., 2013, Avzianova and Brooks, 2014). In addition, Raman spectroscopy has been combined with other techniques such as scanning electron microscopy (SEM) (Nelson *et al*., 2001), SEM combined with X-ray analysis (Stefaniak *et al*., 2006; Worobiec *et al*., 2010; Sobanska *et al*., 2012), and more recently with atomic force microscopy, electron microscopy and X-ray analysis, and mass spectrometry (Sobanska *et al*., 2014).

The idea of using Raman spectroscopic information to create a chemically resolved spatial surface map has been around for some time (Delhaye and Dhamelincourt, 1975). Raman spatial maps built up from pixels representing discrete sample points have seen some modest applications in recent years in the investigation of both non-biological (Batonneau *et al*., 2001; Sobanska *et al*., 2006; Batonneau *et al*., 2006) as well as biological (Tripathi *et al*., 2009; Schwarzmeier *et al*., 2013) aerosols. The same technique has also been used to study cell mitosis (Matthäus *et al*., 2006), to study the uptake and localization of various nanoparticles in hepatocarcinoma cells (Estrela-Lopis *et al*., 2011), to distinguish carbon nanotubes collected in a personal sampler (Keller *et al*., 2011) and to map solar radiation induced skin damage (Ali *et al*., 2013). In these studies Raman spectroscopy is used to identify particular chemical compounds, or to provide quantification of the relative contributions of different chemical compounds (Ivleva *et al*., 2007).

1.4.8. Summary of existing techniques

For online total mass measurements TEOM provides a strong solution as long as the weaknesses of filter based collection are suitably addressed. However, mass alone is not very useful for evaluating health risk without some further classification. The various electrostatic balance techniques are a promising approach for providing online mass distribution measurements of sub-micron sized particles. Particularly with the ability to combine them with additional classification techniques such as DMA, and the fact that they are non-destructive allowing for any further downstream analysis desired. However, they are not as yet widely available, and do not provide an exposure relevant classification.

The DMA is by far the most established and proven method for the online sizing of nano and sub-micron particles, whereas optical techniques usually take over at larger sizes where multiple charging complicates electrical mobility measurements. The CPC occupies a similarly dominant position for the online counting of particles across the required size range. The combination of these two technologies in the form of SMPS and similar devices is therefore unsurprisingly the preferable approach to measuring online size distributions within the size range provided by the DMA. Such size distributions can provide a reasonable approximation of the exposure scenario neglecting the different equivalent diameters at play. However SMPS devices are typically bulky and restricted to laboratory measurements. Meanwhile, the Nano-ID® Select provides sizing selection with a very good correlation to exposure risk, due to the nature of the sampling methodology mirroring the physical characteristics of the respiratory tract. However, it only provides offline sample collection, although this does allow flexibility in user choice on the manner of analysis or quantification carried out.

For measurements of total surface, BET is well established for the offline characterisation of powder samples, but of uncertain value in aerosol studies. Diffusion charging has emerged as the most popular online total surface measurement technique in recent years. However, there is still much debate on the relevance of the active surface metric it measures, and its reliability for quantifying health risk across the size range. Besides this, there has been much demand from the occupational hygiene community for a direct method of measuring online surface area distributions.

Of the advanced optical techniques discussed, only interferometric and optical gradient force techniques have been previously demonstrated as online detection methods. WGM resonators and photothermal systems may also be suited to online analyses but have not to date been used as such. However none of these approaches have yet been proven as a field-deployable device. Any microscopic type techniques are inherently unsuited to online analyses due to the requirement of comparing different points in a sample by means of scanning across it in a well defined and controllable manner.

In summary; if we wish to make a useful evaluation of the health risk posed by airborne particles, then the approach should reflect the physics of how this risk comes about. Particles must first be inhaled and deposited in a particular region of the respiratory tract dependent on their size. A toxic response must then be stimulated which will be determined by factors such as the mass loading, chemical nature, size, and morphology (e.g. surface area). Approaches that can be considered for the measurement of exposure include the use of an SMPS as an approximate measure of deposition dependent size (requiring quantification of chemical composition), or the use of a Nano-ID® Select type

device requiring further analysis and quantification. While the best metrics for determining the resultant health risk from this exposure might be considered to be either chemical nature (requiring suitable quantification), surface area (requiring suitable interpretation of current methods or new instrumentation), or mass (requiring further classification such as when used in conjunction with chemical nature sensitive techniques). Thus there is no currently available adequate method to quantify the health risk of exposure to nanoparticles.

Chapter 2. Outline of the approach

2.1. Analytical concept

The motivation behind this thesis is to try and address some of the gaps in existing instrumentation required to fully characterise aerosol particle distributions for the purposes of evaluating the resulting exposure and health risks. Ideally measurements should be online or quasi-online and directly relevant to the particle forms as they exist in the air. The method of sampling or measurement should not change any parameters or characteristics of the particles from how they are in the air. In general it is usually not practically achievable to leave particles completely unperturbed during measurements, but some changes can be considered acceptable if they do not modify the particular parameter that is being measured. For example, it is not critical if a sampling system changes the agglomerate state of an aerosol distribution when the measure of choice is total mass. Likewise, a counting system can acceptably change any other parameter such as the size or chemistry of the particles as long as no further analysis is desired downstream. Destructive measurement techniques should always be at the end of a sample line whereas non-destructive measurements may be carried out in series upstream of this.

In particular, it is desirable to develop methods of detecting target nanomaterials in the air. The concentration of these particles could potentially be much lower than the background atmospheric aerosol which is typically ~1,000–10,000 particles/cm^3. Therefore it is necessary to develop a method which can specifically identify these materials, even when they are mixed in with a higher concentration of background aerosol. Ideally, proposed solutions should be economic, robust, and portable – suitable for use in a range of occupational and environmental settings.

Two broadly different routes have been investigated to achieve this over the course of this work. Essentially they differ in the nature of information obtained. The first is to investigate both known and novel aerosol science techniques to investigate different characteristic metrics of the aerosol particles. As the test aerosol is split apart and classified by these different techniques it should be possible to build up an n-dimensional particle space in which different species will occupy distinctly different coordinate positions (i.e. it is a multi-dimensional pattern recognition approach). An example of how this might look is shown in Fig. 2.1–1. Plotting a particular aerosol distribution within this space would allow components to be differentiated and assigned relevant weightings for assessing their potential health impact. The general characteristics are first obtained which then lead to identification. The advantage of this approach is that the techniques involved are possible to implement in an online *in situ* instrument and inherently provide all the characteristic information used (such as size, shape etc.) in addition to the final identification. The disadvantages include potential difficulties in distinguishing similar particles if unique identities cannot be achieved outside of particularly peculiar particles (e.g. carbon nanotubes), as well as complexities inherent in integrating multiple different techniques into a combined method or single instrument.

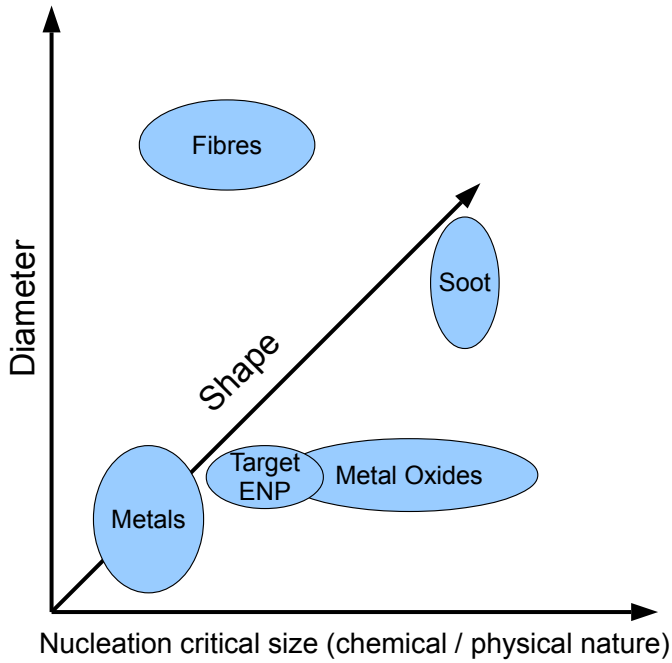

Figure 2.1–1. Example coordinate space for particle characterisation.§

One of the first and most crucial metrics to be determined is particle size. Size will largely determine the mechanical properties of the particle in the air, how far it will travel or move with airstreams, and where in the respiratory tract it is most likely to deposit. The most directly relevant measure of size in this regard is aerodynamic equivalent diameter. However this is usually determined by impaction and/or diffusion sampling, and so does not provide an aerosol outlet to allow further online measurements relating to other metrics (although virtual impactors could be used in the micron range). Such an outlet for the sample is however provided by differential mobility analysers (DMAs), which select for electrical mobility equivalent diameter. Traditional DMAs are large and heavy and so not suitable for field measurements. The first task carried out here was therefore to develop a portable DMA that could provide sizing in a compact package. The output of this DMA could then allow for subsequent measure of additional metrics downstream. Usually the output from a DMA is measured with a condensation particle counter (CPC) which can count nanoparticles. This count can be combined with the sizing information from a DMA to provide a size distribution of the particles present at the input. Such a combined system is usually referred to as a scanning mobility particle sizer (SMPS). Indeed the DMA developed here was incorporated into a commercial SMPS (Nano-ID® NPS500) by Naneum Ltd. Building on this work, further research in heterogeneous nucleation technology is shown to reveal a regime which is sensitive to the surface area of particles. In conjunction with the portable DMA, this new technique allows for the direct online measurement of surface area distributions of nanoparticles.

The second route considered involves direct chemical speciation via Raman spectroscopy. Although not well suited to online characterisation, it is comparably affordable and can now be found in a range of compact forms. Aerodynamically size resolved sampling is here combined with two dimensional Raman spectral mapping,

§ – Adapted from work courtesy of Naneum Ltd.

automated image analysis, and particle counting. In this manner a novel method for quantifying aerosol exposure is established. The advantage of this approach is that Raman spectroscopy provides clear identification of the target materials. The main disadvantage of this method is that it requires separate offline analysis. However in recent years, portable hand-held Raman instruments have emerged on the market, and so a quasi-online method where samples are collected and analysed immediately in the test environment may be envisioned. In addition, clearly there is potential use for a combination of multiple methods including those outlined above in any one measurement. Currently there is no single technique that can provide all the information needed over the entire size range of interest from less than 10 nm to greater than 10 μm.

Further research is needed to understand what methods are best suited for detection and identification of engineered nanoparticles. This is still very much an emerging area of research, along with toxicological studies, which are currently playing catch-up to the proliferation in use of these materials in industry and consumer products. However, by providing practical approaches to their measurement and quantification, further understanding of their potential health risk can be evaluated and used to inform future policy.

2.2. Surface sensitive heterogeneous nucleation

In recent years, it has become increasingly evident that the traditional mass metric for airborne particulates has its limitations for quantifying risk from exposure to aerosols. Due to the complex nature of nanoparticle aerosols it is considered best practice to make measurements of a number of different metrics as are reasonably available (Maynard & Aitken 2007). This approach, as well as allowing better differentiation of different species and forms, also serves to better inform the potential risks that may arise under different conditions. Surface area has increasingly gained traction in recent years as being an important metric in assessing the health impact of nanoparticles once they have been deposited in an organic system. It has been identified in toxicology studies as a key metric in dose response relationships for a number of industry relevant chemical compounds. There is emerging evidence that surface area and surface reactivity plays a significant role in determining the interactions between inhaled particles and biological systems.

Existing methods of measuring particle surface area are either very expensive or measure an auxiliary metric of uncertain correlation to surface area. Most are indirect, offline, and require *a priori* knowledge of the characteristics of the particle. Moreover, all currently available instruments suitable for use in the field only provide a calculated and not a measured surface area as a function of size. A size and morphology-sensitive measurement capability is highly desirable to provide data to inform the assessment of potential exposure to newly developed materials such as engineered nanoparticles.

Here a novel, online, and economical method capable of measuring aerosol particle surface area *in situ* is proposed. This new method is based on fundamental nucleation theory and implemented in an adapted CPC like module which can provide surface area distributions when coupled with a DMA. This forms the basis of a surface area measurement sensor and has been developed and incorporated into a prototype online surface area measurement device. The approach is based on the discovery of a

phenomenon where heterogeneous nucleation is sensitive to surface area under certain specific conditions.

2.3. A novel quantitative exposure assessment technique utilising size selective sampling and Raman spectroscopic mapping analysis

A novel method has been developed for the quantification of airborne particulate matter with chemical speciation, required for health risk assessment. A multi-stage approach is presented whereby the particles are first aerodynamically size segregated from the air in an impaction sampler. These size fractionated samples are subsequently analysed by Raman spectroscopy. Imaging analysis is applied to Raman spatial maps to provide chemically specific quantification of airborne particulate matter for evaluation of exposure against background.

Micro-Raman spectroscopy (Huong and Verma, 1990) provides sensitive detection of chemical traces in a dominant background aerosol matrix. The same technique is also able to distinguish small deposits from a substrate material and has seen increasing application to nanomaterials (Gouadec and Colomban, 2007). Compared to other techniques, Raman spectroscopy offers a relatively economical solution to chemical identification and commercial solutions are now available in compact, portable, packages. The combination of aerodynamic diameter selectivity and Raman characterization may therefore offer a cost-effective and practical technique for the detection of potentially toxic aerosol particle constituents, and the speedy assessment of any associated exposure risks.

The approach is as follows: First, aerosol particles are sampled and size segregated from the atmosphere utilizing a 'Nano-ID® Select' (Gorbunov *et al.*, 2009) to classify particles according to their aerodynamic equivalent diameter. The second stage is to analyse the size ranges of interest with Raman spectroscopy to provide chemically sensitive detection of particles. Finally, with consideration of the sampled volume, a quantitative analysis is carried out which allows for the absolute determination of concentrations of a particular species in the air. This final step is critical for providing a meaningful exposure assessment, and is the key benefit of this approach compared to previous studies.

2.4. Overview

The approaches proposed here can be summarised as follows. The aim is to evaluate the health risk posed by airborne particles (particularly ENP). First we must characterise particles by size to determine the likelihood and locality of deposition in the respiratory tract. At this point we can split apart our requirements into separate nano and micron fractions (with overlap at sub-micron sizes).

For the nano to sub-micron fraction a portable DMA is developed to provide online size evaluation. In conjunction with a CPC this can provide number distributions of

particles. In addition, with surface area controlled nucleation it is also shown to be capable of providing online surface area distributions. This surfacing response also demonstrates sensitivity to chemical nature and therefore it may be possible to extract some measure of chemical identity with this approach with calibration. Both number and surface area metrics are considered important in the nano range. Number provides a simple quantitative measure as an alternative to mass where nano-scale particles are under-represented, while surface area is considered an important health risk metric due to the relatively higher surface areas and reactivity of nanoparticles.

For the sub-micron to micron fraction the cascade impaction stages of the existing Nano-ID® Select instrument are used to provide exposure relevant size resolved sampling. The proposed Raman mapping approach can then provide a chemically resolved quantitative analysis in terms of number. These number fractions could additionally be converted to mass fractions with consideration of the density of each chemical constituent. Mass conversions could also be assisted by comparison of the relative fractions of different chemical constituents and their densities to the total mass from a gravimetric or optical scattering measurement.

In this manner, size resolved number measurements are demonstrated across the entire nano to micron size range. In addition, surface area distributions are demonstrated in the nano to sub-micron range, and combined size and chemical species resolved number measurements are demonstrated in the micron range. Future work is likely to extend the size range of the surface area technique to larger sizes, while there is also potential to extend the range of the Raman approach further down into the sub-micron and nano-range. An alternative approach at smaller sizes may be to better characterise the chemical nature specificity of surface area controlled nucleation.

With further development it may be possible to apply both methods to the same aerosol distribution across an overlapping size-range. In this case the chemical discrimination provided by Raman spectroscopy could be utilised to inform the interpretation of, or serve as a calibration for, chemically sensitive surface area measurements. This presents the possibility of a complete quantification of size, number and chemical nature of a given aerosol distribution.

Chapter 3. Techniques

3.1. Differential mobility analysis

The most common way of sizing nanoparticles in the air is by measuring their electrical mobility (Z) as they travel through an electric field. The standard instrument for doing this is known as a differential mobility analyser (DMA), also known as differential electrical mobility classifier (DEMC) in ISO nomenclature. Coupled with a particle counter (usually condensation particle counters – CPCs), DMAs form a crucial part of scanning mobility particle sizer (SMPS) instruments which measure aerosol particle size distributions (see Section 1.4.3.4).

3.1.1. DMA fundamentals

The basic operational principle of a DMA is shown in Fig. 3.1–1. There are two air flows; a re-circulating sheath air flow (Q_{sh}) and a particle containing aerosol flow (Q_a), which are here shown fed between two parallel plate electrodes. The sheath flow exiting from the right hand side is filtered before being re-introduced into the left hand side. The sheath flow is usually about ten times larger than the aerosol flow. It is important that the flow inside the DMA separation chamber is laminar. Under these conditions, before any consideration or application of charges and fields, it is clear that any particles introduced via the inlet at top left will simply be swept horizontally along the top of the volume and be lost with the rest of the sheath flow exhausted to the right. The same volume of clean sheath flow air will exit through the bottom right aerosol outlet thereby balancing the flows. The important point here is that only clean air reaches the outlet. No particles can traverse the dominant sheath flow to reach the aerosol outlet to be measured (gravitational and inertial effects are negligible for the sizes of particles considered – < 1 μm).

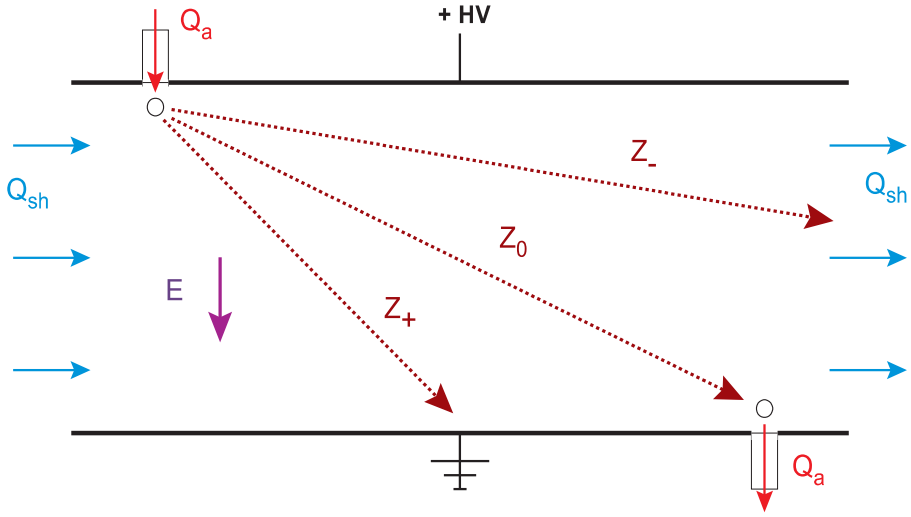

Figure 3.1–1. Operating fundamentals of a differential mobility analyser.

If we now charge the introduced particles (positive in this example), and apply an electric field across the electrodes as shown, the particles will drift in the electric field towards the opposite electrode. The drift velocity (v_{elec}) is determined by the electric mobility Z, such that $v_{elec} = ZE$ and $Z = neB$, where E is the electric field, n is the number of elementary charges on the particle, e is the electron charge and B is the mechanical mobility which is inversely proportional to the particle diameter d:

$$B = \frac{C_C}{3\pi\eta d_p} \tag{2}$$

In Equation 2, η is the dynamic gas viscosity and C_C is the slip correction factor. This factor is also a function of particle size and takes into account the effect of particles being able to "slip" past gas molecules as the size of the particle approaches that of the gas molecules themselves.

Smaller particles with a higher electrical mobility (Z_+) will move quickly in the field and get attached to the opposite electrode, larger particles with a lower electrical mobility (Z_-) will be deflected somewhat by the electric field but will still ultimately be lost to the sheath flow exhaust as in the uncharged case initially considered. Depending on the flows and voltage selected, particles of a particular mobility (Z_0) will move in the field with just the right velocity to reach the aerosol exit. If we assume that all particles are singularly charged, then $Z_0 = eB_0 \propto 1/d_0$ (neglecting C_C). i.e. the particles reaching the outlet will be of a single size – a monodisperse distribution (see Fig. 3.1–2). To change the selected size usually it is simplest just to change the applied voltage. Commercial DMAs generally operate with voltages in the range from 5 V to 10 kV to select particles across the range of 5 – 1000 nm and the flow rates used are typically about 3 l/min for the sheath flow and 0.3 l/min for the aerosol flow.

DMAs can be used in this manner to generate monodisperse aerosols from a polydisperse source, and typically find applications in aerosol research, toxicological studies and instrument calibration. However, they have found wider use as integral components in SMPS systems for measuring aerosol size distributions. When DMAs are

used as part of an SMPS, the voltage is scanned (hence the "scanning" in scanning mobility particle sizer) to give a continuously changing particle size output. The DMA is coupled with a particle counter such as a CPC which can then measure the concentration of particles of each size selected by the DMA in sequence. In this way the particle distribution is built up across the entire size range.

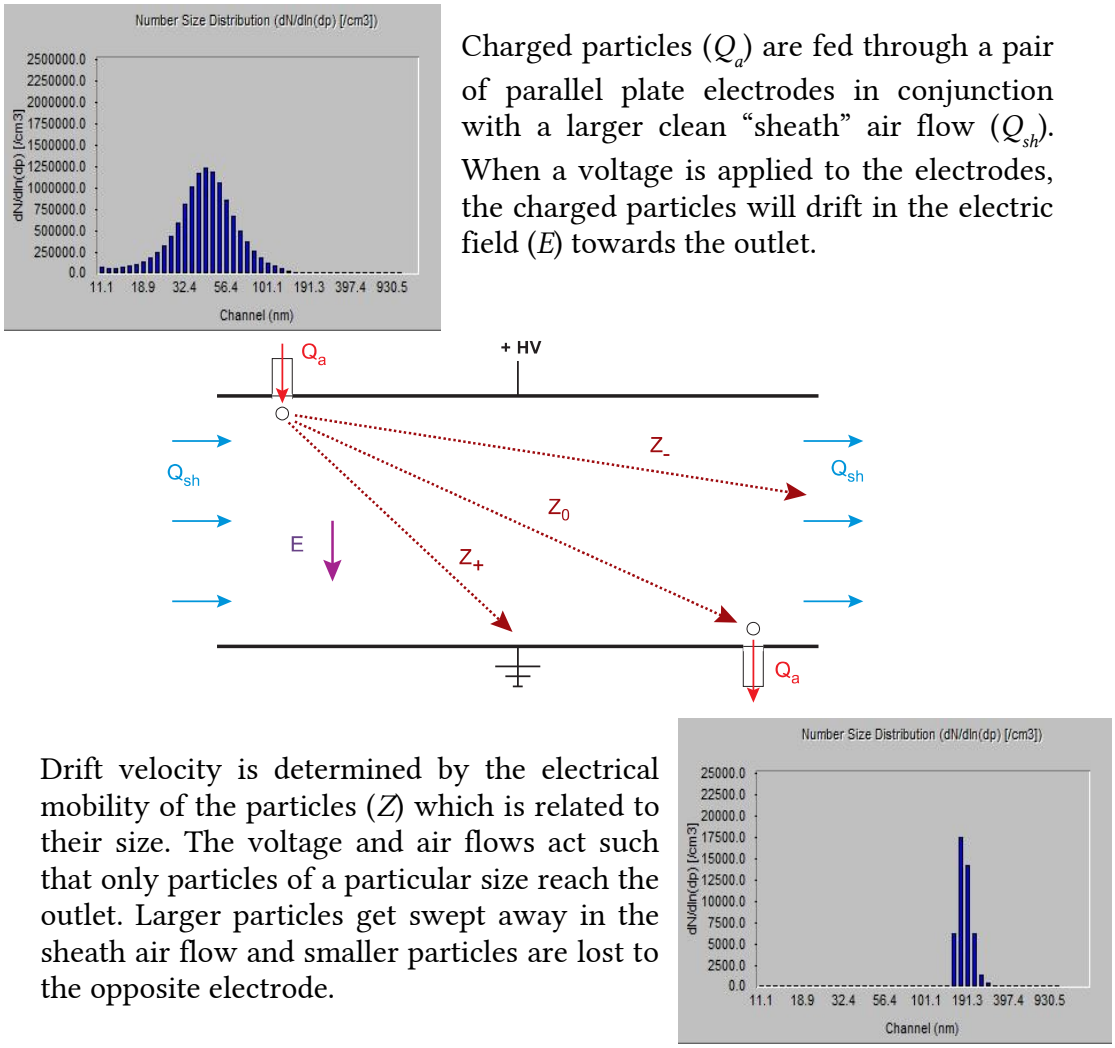

Figure 3.1–2. Overview of the operation of a differential mobility analyser showing an example of how a polydisperse aerosol distribution fed in at the inlet at top left can be converted to a monodisperse distribution at the chosen size to an exit at bottom right.

The width of the distribution selected is mostly determined by the ratio between the two air flow rates – the sheath air flow within the instrument and the aerosol air flow as provided by the user. In general, the larger the sheath air flow is with respect to the aerosol air flow, the narrower or more monodisperse the selected size band will become. However, a larger sheath air flow will reduce the final concentration available at the output port, and too large a sheath flow can result in a broadening of the selected

distribution due to flow instabilities.

The width of an aerosol size distribution is normally indicated with a geometric standard deviation (σ_g). The lower this value, the narrower the distribution, while in physical systems it must always be greater than 1. A full description of σ_g and how it can be calculated from a distribution can be found on p.99 of Baron and Willeke (2001). The exact value of σ_g can depend on the nature of the aerosol selected. Generally σ_g values < 1.2 are considered mono-disperse (single component aerosols), or sometimes a more stringent definition of $\sigma_g < 1.1$ is used. This will roughly correspond to a sheath flow ten times larger than the aerosol flow.

3.1.2. Multiple charging

An important assumption in the above discussion was that the particles are singularly charged ($n = 1$). It is clear from $Z = neB$ that if a particle has two charges ($n = 2$) that it will have twice the mobility and so move twice as fast in an electric field as singularly charged particles. Recall that in a DMA we set a particular voltage and expect a single size of particle to then emerge from the output. However, if there are multiply charged particles present, then larger particles will also get selected at the same voltage. For example, if we set our DMA to select 100 nm singularly charged particles, we will also select 151 nm doubly charged particles, 195 nm triply charged particles and 237 nm quadruple charged particles. These mobility equivalent sizes can be calculated by solving $Z = n_1 eB(d_1) = n_k eB(d_k)$ for d_k where in this example $n_1 = 1$, $d_1 = 100$ nm and $n_k = 2, 3, 4$ respectively.

An example of double and triple charge peaks can be seen in Fig. 3.1–3. Here a polydisperse aerosol has been multiply charged and then selected through a DMA set to ~50 nm. To show the larger multiple charge peaks, the resultant aerosol from the DMA was then passed through a neutraliser to reset the charge distribution. Therefore many of the multiply charged particles return to being singly charged and appear as separate peaks as measured by a Grimm SMPS. If there had been no change to the charge distribution between the DMA and SMPS, and they were both operating with the same polarity, then only the main peak at 50 nm would be apparent. The larger particles would still be multiply charged and measured to be 50 nm by the Grimm SMPS.

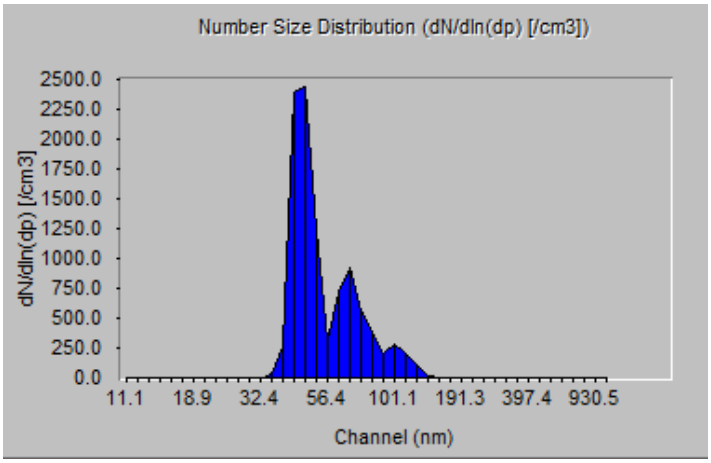

Figure 3.1–3. An example of the particle size distribution output from a DMA set to select 50 nm particles. The larger particles which also get passed through the DMA in conjunction due to multiple charging are shown here by resetting the charge distribution prior to measurement by an SMPS. All of these particles were initially classified as 50 nm by the DMA demonstrating the dangers of using electrical mobility equivalent sizing with highly charged aerosols.

Conversely, we could start with a monodisperse aerosol (e.g. nebulized polystyrene latex particles which are often used for calibration purposes), and then measure it with a scanning DMA (SMPS) with a charger in front. In this case, when some of the particles become multiply charged, they will then appear as *smaller* sized peaks. For example, if we had started with 100 nm PSL particles, then multiply charging them before measurement in front of an SMPS can result in additional secondary peaks at 68, 54 and 46 nm for doubly, triply and quadruple charged particles respectively. Distributions can become even more complicated when there is multiple charging both before the DMA used to select a "monodisperse" distribution and in a charger in front of the SMPS used to measure the result. In this case particles can not only change from being singularly to multiply charged, but can also move between different orders of multiple charging (2→3, 4→2, etc.) between the two systems resulting in further third order peaks. For an example of this see the 150 nm distribution in Fig. 3.1–4.

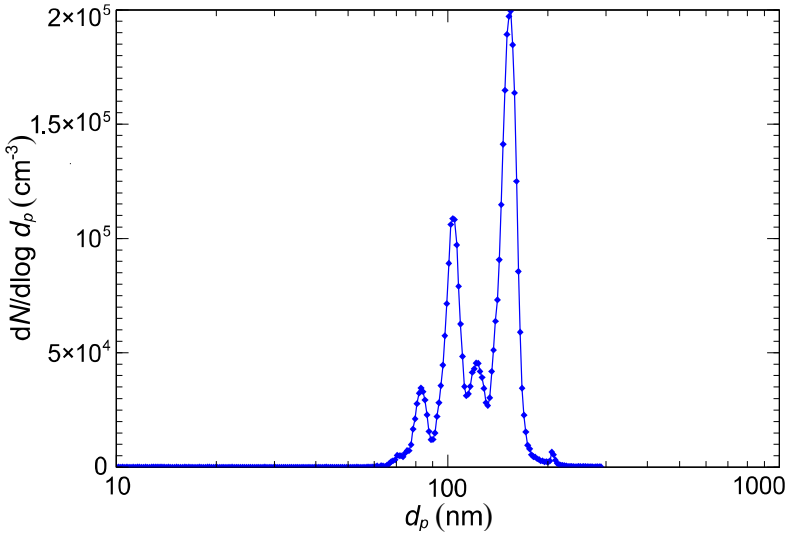

Figure 3.1–4. Example distributions of a complex charged NaCl aerosol. For monodisperse (mobility) aerosol particles selected at 150 nm, many satellites appear representing multiply charged particles. The main peak appears at 154.7 nm. The satellite peaks appearing at 83.0 and 103.4 nm match with the theoretical positions for particles which were singularly charged before entering the DMA and subsequently either triply charged (81.6 nm) or doubly charged (102.9 nm) before measurement by an SMPS. The secondary peaks appearing at 121.7 and 205.7 nm also correspond well with the theoretical positions for particles which were either doubly charged before entering the reference DMA and then subsequently triply charged before the SMPS measurement (121.2 nm), or triply charged before the DMA before becoming doubly charged before measurement by an SMPS (199.9 nm).

3.1.3. Charging mechanisms

DMAs can be setup to measure either positive or negatively charged particles, and some mechanism upstream of the DMA is normally included to charge the incoming particles accordingly.

From the above discussion on multiple charging, it is clear that any particle charging method should preferably result in a single charge being acquired by each particle. Any particles that are not charged will not be measured, while particles that gain more than one charge (multiply charged) will be sized incorrectly.

Particle charging can be split into two main regimes – bipolar charging and unipolar charging. Bipolar charging takes place in the presence of both positive and negative ions and usually the target here is to reach a charge state known as the bipolar equilibrium. This charge state gives a well characterised distribution of charge fractions as a function of particle size and is generally assumed to be the charge state found on mature atmospheric aerosols. A bipolar equilibrium charge distribution is achieved with varying success depending on the neutraliser used, particle size and concentration, and residence time (flow rate) (Covert *et al.*, 1997). Charge based instruments generally measure only one polarity – either positive or negatively charged particles. Therefore, the particles created with the opposing charge in a bipolar charger are not useful for measurement, leading to additional inefficiency. There is existing well developed theoretical groundwork for the correction of multiple charged distributions acquired under bipolar

equilibrium charging conditions (e.g. Wiedensohler, 1988; Hoppel and Frick, 1986). However to achieve this charge distribution, it is usually required to use a radioactive neutraliser; typically using ^{85}Kr, ^{210}Po or ^{241}Am sources. As well as being bulky, radioactive neutralisers can be extremely difficult to move from one location to another, and are unsuitable for *in situ* measurements due to regulatory and safety restrictions. Generally, bipolar neutralisers are considered to be insensitive to the pre-existing charge state of the aerosol as long as the source strength (number of ions produced) and residence time are great enough to compensate.

Unipolar chargers on the other hand charge with a single polarity. Typically, this is achieved with a corona charger where a fine point or wire has a high enough potential applied it to form a corona (Goldman & Sigmond, 1982; Goldman *et al*., 1985; Chang *et al*. 1991; van Veldhuizen and Rutgers 2001). The breakdown of air creates a cascade of electrons and positive ions. A corona charger is designed such that the ions created with the same polarity as the corona source escape to be mixed with the aerosol particles.

Corona chargers avoid the regulatory difficulties associated with radioactive neutralisers, and can generally be made more compact. Although they do require a high voltage source, and connections and can be sensitive to contamination which can drastically reduce their useful lifetime. Corona chargers have been developed with a variety of designs and performance characteristics (e.g. Intra and Tippayawong, 2009; Marquard *et al*., 2006). Unipolar corona chargers can achieve much higher charging fractions compared to neutralisers (e.g. Hernandez-Sierra *et al*., 2006), however this comes at the cost of higher multiple charging (e.g. Alguacil and Alonso, 2006) which makes the data deconvolution significantly more difficult. Generally, higher charge levels from corona chargers are required in the case of measuring numbers of particles with electrometers where high levels of charge are required to be collected in order to produce a measurable current. While there have been some attempts to characterise the charge distributions from unipolar chargers, there is no generic solution to the multiple charge correction issue. Different chargers will have different ion levels and therefore charge fractions produced. Hence, the performance of any particular design must be modelled or measured and suitable corrections calculated. The charge fractions produced can also depend on the pre-existing charge state of the aerosol, mainly if it is of the same polarity as the charger (Qi *et al*., 2009). Additionally, within neutralisers and downstream of both charger types, the particle size distribution can be changed due to charge induced coagulation (Alonso *et al*., 2008).

For this project a DMA has been developed without an in-built charger allowing for user choice and testing of different external corona designs. The DMA was then built and tested.

3.2. Introduction to Raman spectroscopy

An overview of photon scattering processes is shown in Fig. 3.2–1. Vibrational energy levels, v", are shown for the ground electronic state of a molecular system characterised by an anharmonic potential well. The vibrational (and rotational) energy levels depend on the molecular form and on the associated degrees of freedom. Therefore, probing these states can reveal characteristic molecular fingerprints for the purpose of

identifying the material in question. The difference between these energy levels corresponds to infrared (IR) frequencies, and therefore IR absorption spectra can be used to characterise the molecule(s) present. Absorption processes require a change in the dipole moment of the vibrational mode. Hence, only modes that are associated with a change in the dipole moment are visible in an IR spectrum. Raman spectroscopy offers an alternative method of probing vibrational modes of molecules. In contrast to IR techniques, it makes use of photon scattering rather than absorption. Scattering processes involve fluctuations of the electronic cloud, which are normally characterised by intermediate virtual energy states reflecting the energy increase corresponding to the incident photon. Raman scattering is an inelastic process which results in the molecule being left in either a higher energy (Stokes) or lower energy (anti-Stokes) vibrational state. Scattering processes will be more apparent for bonds where the electron cloud is more easily distorted (polarizable). Hence, although both IR and Raman spectroscopy probe vibrational modes, they are each more sensitive to different bonds, and therefore, can yield complementary information. IR is more sensitive to polar bonds with a larger dipole moment, while Raman is more sensitive to non-polar bonds which are comparatively neutral. Indeed the rule of mutual exclusion states that in molecules with a centre of symmetry, no modes can be both IR and Raman active. This does not necessitate that a mode has to be active in either case, and even modes that are theoretically active may not be visible in spectra due to their proximity to more dominant modes or simply having too low a probability of occurring.

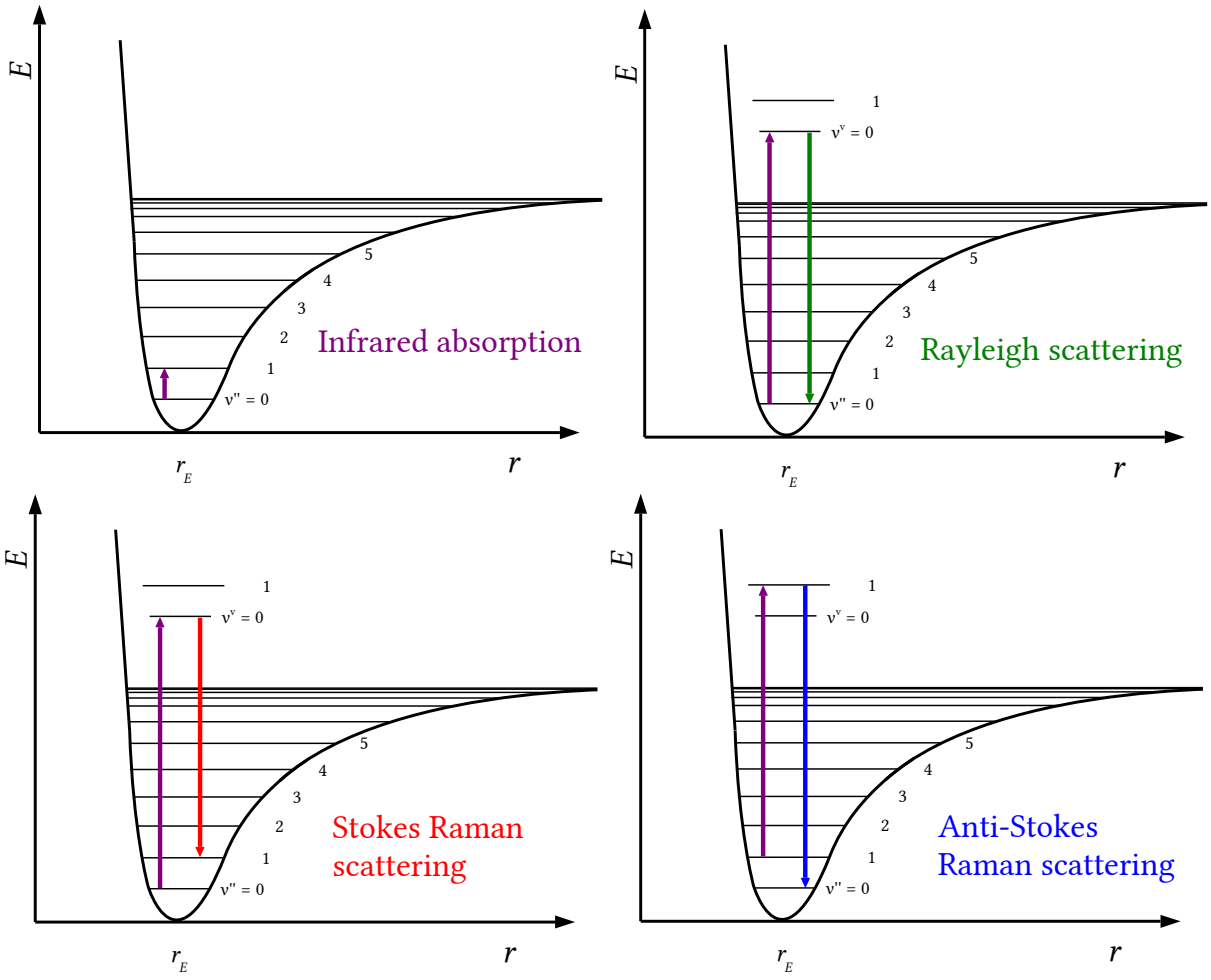

Figure 3.2–1. Energy level diagram showing transitions between vibrational states of the ground electronic state v'', and virtual energy levels v'. *r* is the nuclear coordinate (e.g. atomic separation in a diatomic molecule), r_E is the equilibrium displacement.

3.3. Nucleation technology

3.3.1. Introduction

To understand the principle behind surface sensitive heterogeneous nucleation, we first need to consider the process of nucleation in more detail and some basic theory.

Nucleation refers to the formation of a distinct thermodynamic phase in the form of nuclei within the pre-existing phase. It is characterised by an overall drop in free energy and is usually physical in nature (driven by changes in temperature and pressure) although it can also be chemical (driven by or greatly accelerated by chemical reactions). Nucleation can be divided into two types – homogeneous and heterogeneous (Volmer, 1926; 1939; Abraham, 1974; Fletcher, 1962). Homogeneous nucleation occurs within single component or single phase systems and is rarely found in nature. Heterogeneous nucleation by contrast involves nucleation onto pre-existing seed nuclei of a different material and requires a much lower energy gap compared to homogeneous nucleation (i.e. a smaller divergence from equilibrium is required to form the new state

– Gorbunov, 1999). Seed nuclei can take the form of ionic or molecular clusters (Wilson, 1897; Gamero-Castaño, 2002; Kirkby *et al*. 2011), or the surface of a nanoparticle or other inclusion (Friedlander, 2000). Examples of heterogeneous nucleation in nature include the nucleation of water vapour to form precipitation (Pruppacher and Klett, 1978), the formation of secondary aerosols in the atmosphere (Kulmala, 2000), as well as the solidification of minerals in the Earth's crust (Cantor, 2003). Heterogeneous nucleation is also important in a wide range of human activities, including metallurgy (Kelton and Greer, 2010), microelectronics (Venables, 2000; Minemawari *et al*., 2011), occupational hygiene (Maynard *et al*., 2004), and nanotechnology (Theodore and Kunz, 2005).

Of particular focus here is the utilisation of heterogeneous nucleation in condensation particle counters (CPCs) for the purposes of counting nanoparticles in the air (McMurry, 2000b). CPCs are composed of a condensation unit and an optical particle counter (OPC). The aim is to nucleate liquid droplets onto nanoparticles in the condensation unit such that the resultant droplets are large enough to be counted by optical scattering in the OPC (whereas the nanoparticles themselves are too small to be detected by standard optical techniques). An overview of the operation of a condensation unit is shown in Fig. 3.3–1 below.

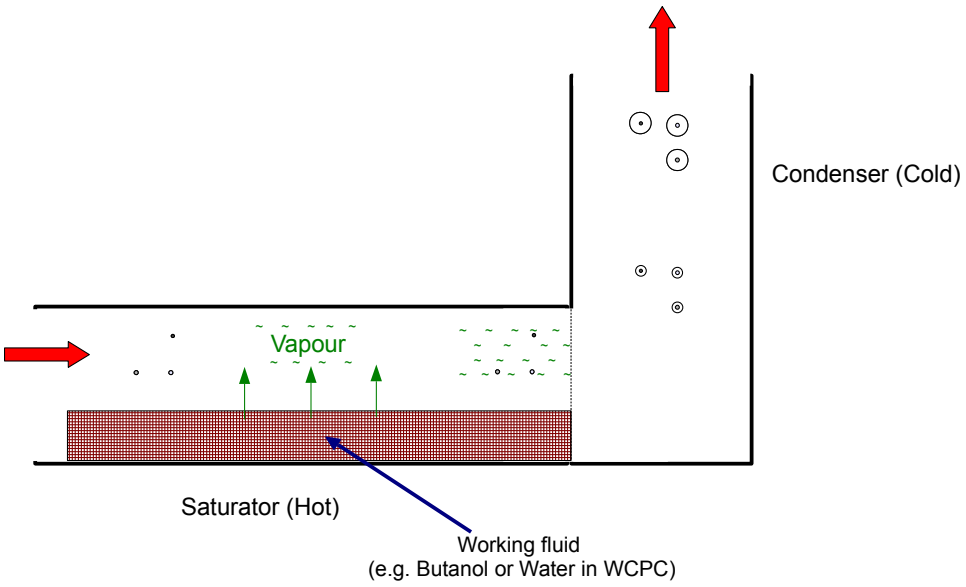

Figure 3.3–1. Operating principle of a condensation unit at the heart of a CPC. Nanoparticles drawn in through the inlet are mixed with a vapour from a heated fluid. The mixture is then cooled to form fluid droplets on the nanoparticles in a condenser. These droplets are then large enough to be counted by optical scattering in an optical particle counter (OPC).

The performance of CPCs is usually characterised by a "d_{50}" cut-off size which refers to the size at which the counting efficiency drops to 50%. That is, at d_{50}, there is a 50% probability of nucleation. The slope of this drop-off in counting efficiency is usually quite steep such that the counting efficiency below d_{50} drops off to < 1% within a few nanometres (e.g. see Fig. 4.5–3). Therefore, we can reasonably approximate to define d_{50} as the minimum detected particles size d_{min}, such that there is no nucleation below

d_{min} and every particle above d_{min} results in the nucleation of a liquid droplet of ~1 μm in size. In this way the number of droplets grown is considered to directly correspond to the number of nanoparticle above d_{min} drawn in through the inlet of the CPC.

3.3.2. Theory

Changes in state are processes driven by a reduction in the Gibbs free energy, G;

$$G = H - T\$ \tag{3}$$

where H, T and $\$$ are respectively the enthalpy, temperature and entropy of the system, and

$$H = U + pV \quad \text{and} \quad \mathrm{d}\$ = \mathrm{d}Q/T \tag{4}$$

where U, p and V are respectively the internal energy, pressure and volume of the system, and $\mathrm{d}Q$ is the transfer of heat to or from the system.

Changes in state in nature are usually driven by changes in temperature. For example, with reference to Fig. 3.3–2, it is energetically favourable for a material to exist as a gas at temperatures above the equilibrium temperature T_E, and as a liquid at temperatures below T_E, i.e. the free energy is minimised.

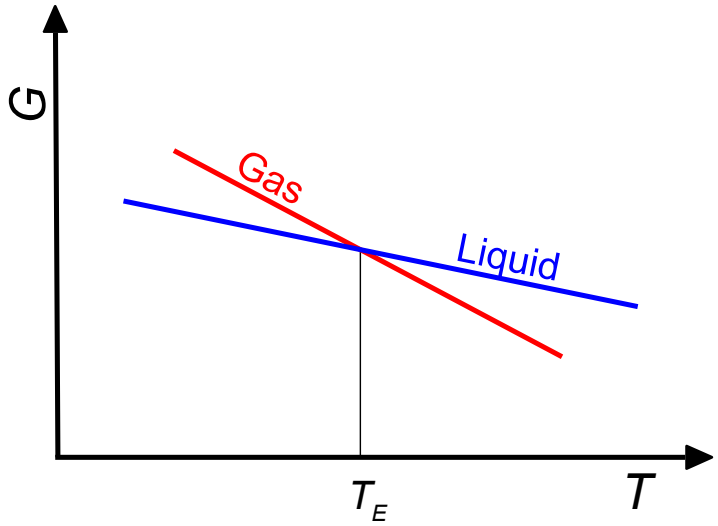

Figure 3.3–2. Phase diagram showing the equilibrium temperature T_E where the two phases are in equilibrium.

This minimisation of free energy provides the impetus for a phase change to occur. However, there is still an energy barrier to overcome associated with the formation of a new structure. For example, considering the homogeneous nucleation of droplets in a vapour, there is an energy barrier associated with the formation of the liquid droplet structures. The change in free energy associated with this barrier is a function of the droplet radius and is the combination of a surface term and a volume term as shown in Fig. 3.3–3.

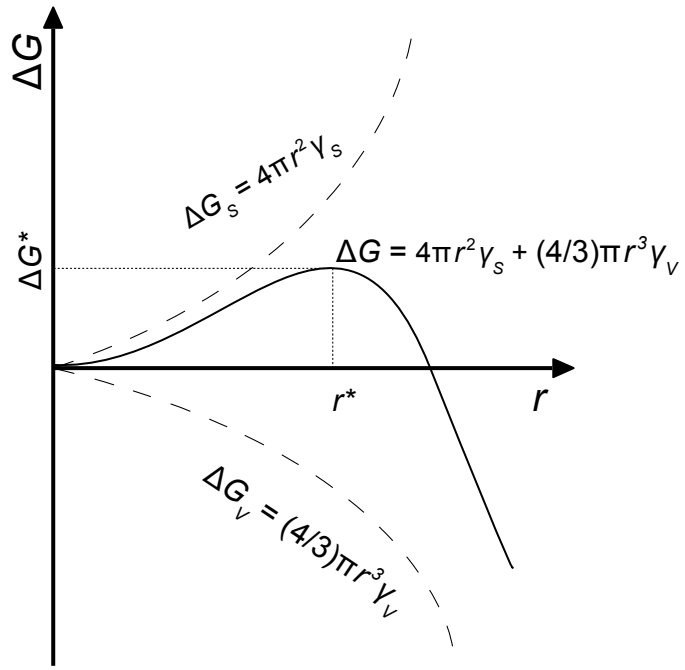

Figure 3.3–3. The change in free energy of a nucleating droplet as a function of its radius is a combination of an increasing surface term and decreasing volume term. The combined total change in free energy exhibits a maximum at a critical radius r^* and associated critical energy barrier ΔG^*. The droplet will grow rapidly once it overcomes this barrier to become larger than r^*. γ_S is the surface energy density and γ_V is the volume energy density.

The surface and volume free energy changes are respectively;

$$\Delta G_S = 4\pi r^2 \gamma_S \qquad \text{and} \qquad \Delta G_V = (4/3)\pi r^3 \gamma_V \tag{5}$$

γ_S is the free energy change per unit surface due to the formation of the nucleation interface between the two phases. In a liquid this is equivalent to the surface tension. γ_V is the free energy change per unit volume due to the change in phase, i.e. it is the difference in free energy associated with the molecules in the newly nucleated phase as compared to the corresponding free energy exhibited in the original phase. This free energy difference is associated with the saturation ratio p/p_E such that:

$$\gamma_V = - n_V kT \ln(p / p_E) \tag{6}$$

where n_V is the number of molecules per unit volume in the nucleated state, k is the Boltzmann constant and T is temperature.

The total change in free energy is the combination of the surface and volume terms:

$$\Delta G = 4\pi r^2 \gamma_S + (4/3)\pi r^3 \gamma_V \tag{7}$$

or

$$\Delta G = 4\pi r^2 \gamma_S - (4/3)\pi r^3 n_V kT \ln(p/p_E) \tag{8}$$

Solving for $d\Delta G / dr = 0$ therefore gives: $$r^* = \frac{-2\gamma_S}{\gamma_V}$$

and substituting this back in to Equation 7 yields: $$\Delta G^* = \frac{16\pi\gamma_S^3}{3\gamma_V^2}$$

Combining these terms with Equation 6 above then gives in full:

$$r^* = \frac{2\gamma_S}{n_V\, kT \ln(p/p_E)} \tag{9}$$

and

$$\Delta G^* = \frac{16\pi\gamma_S^3}{3[n_V\, kT \ln(p/p_E)]^2} \tag{10}$$

Note that the above discussion concerns homogeneous nucleation, that is, nucleation within a single component system forming new phase embryos of the parent material spontaneously within the volume of the prior phase. However, to make this discussion applicable to most real world cases, we must extend it to include the case of heterogeneous nucleation; nucleation which forms on seeds provided by a second material. In this case the energy barrier to nucleation is reduced by a factor *f(θ)*, which is a function of the contact angle θ between the seed material and the associated embryo of the new phase:

$$f(\theta) = \frac{2 - 3\cos\theta + \cos^3\theta}{4} \tag{11}$$

The contact angle is determined by the balance of forces between the interfaces of the three material forms involved: the inclusion (seed material), the nucleus of the newly forming phase, and the surrounding initial phase of the source nucleating material:

$$\sigma_{IS} = \sigma_{IN} + \sigma_{NS}\cos\theta \tag{12}$$

where σ_{IS} is the inclusion-source material interface energy, σ_{IN} is the inclusion-nucleus interface energy, and σ_{NS} is the nucleus-source material interface energy. This system is shown schematically in Fig. 3.3–4 below.

Note that σ_{NS} is the same interfacial energy that we wrote as γ_S above, i.e.:

$$\gamma_S = \sigma_{NS} = \frac{\sigma_{IS} - \sigma_{IN}}{\cos\theta} \tag{13}$$

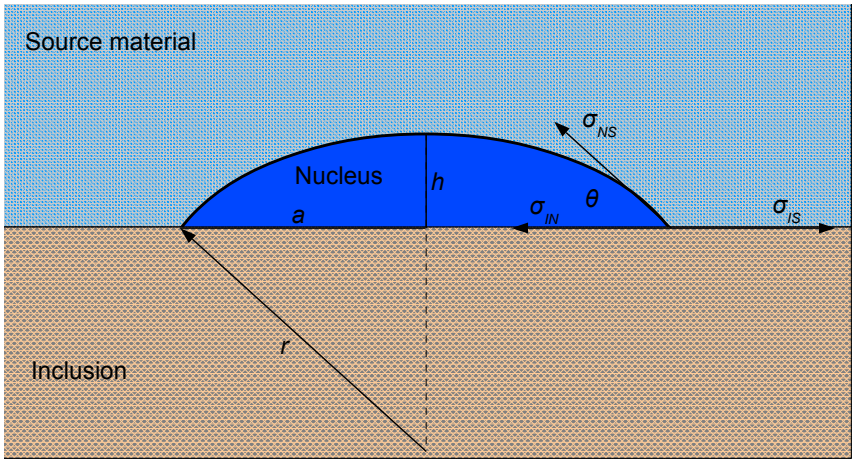

Figure 3.3–4. Heterogeneous nucleation of a new phase nucleus onto an inclusion material with contact angle θ. r is the radius of curvature of the nucleus, h is the nucleus height and a is the radius of the contact area between the nucleus and inclusion. σ_{IS} is the inclusion-source material interface energy, σ_{IN} is the inclusion-nucleus interface energy, and σ_{NS} is the nucleus-source material interface energy.

The probability of heterogeneous nucleation occurring can be described as a function of time as follows:

$$P = 1 - \exp(-JS\Delta t) \tag{14}$$

For a given rate of heterogeneous nucleation J, and an available surface area S of the nucleating inclusion, there is a probability P of nucleation occurring over a time period Δt.

The rate of nucleation, J, is determined by the number of molecules available from the source material, N, the area of the newly formed nucleus available for the molecules to attach to, s*, the attachment rate of the joining molecules, ω, and the energy balance between the nucleation barrier and available thermal energy:

$$J = Ns^*\omega \exp\left(\frac{-\Delta G_{\text{hom}} f(\theta)}{kT}\right) \tag{15}$$

where ΔG_{hom} is the homogeneous nucleation energy barrier, $f(\theta)$ is the correction factor for heterogeneous nucleation mentioned previously, k is the Boltzmann constant and T is temperature.

Note that the formula $1 - \exp(C.x)$ can be expanded as the following converging series:

$$1 - \exp(Cx) \approx -Cx - \frac{C^2x^2}{2} - \frac{C^3x^3}{6} - \frac{C^4x^4}{24} - \ldots \tag{16}$$

and thus Equation 14 can be similarly expanded to:

$$P \approx JS\Delta t - \frac{(JS\Delta t)^2}{2} + \frac{(JS\Delta t)^3}{6} - \frac{(JS\Delta t)^4}{24} + \ldots \tag{17}$$

Therefore for low rates of nucleation (equivalent to a large energy barrier ΔG and a low saturation ratio p/p_E), the probability of nucleation will be linearly dependent on the surface area of the available inclusions S:

$$P \approx J S \Delta t \tag{18}$$

If we now consider the case of nucleating vapour onto nanoparticles as used in CPCs, this means that if we reduce the saturation conditions sufficiently, the nucleation rate will become a function of the surface area of nanoparticles present. That is, the count output by the CPC will no longer be a function of the number of nanoparticles present, but will instead be a measure of their surface area. This is the theoretical basis of the concept of surface controlled nucleation.

Chapter 4. Development and testing

4.1. Development of a portable planar DMA

The design and performance of the first high resolution planar geometry DMA to be commercialised in a stand-alone portable instrument will be described. COMSOL Multiphysics® finite element software has been employed to determine the key parameters that aid to optimize the design characteristics and the performance of the prototype instrument. This design was commercialised by Naneum Ltd. and evaluated by Particle Measuring Systems (USA).

4.1.1. Why choose a planar geometry?

There are three main types of DMAs: cylindrical (see Section 1.4.2.2), planar (Erikson, 1921; Wake *et al*., 1991) and radial (Hurd and Mullins, 1962). The choice of geometry for a portable DMA is not straightforward. On the one hand a planar geometry is easier to manufacture than cylindrical or radial (disk) based (for example, a planar geometry avoids issues of electrode centring). On the other hand, the cylindrical geometry has been used for more than a half a century and one may expect some optimization of the design to have occurred in that period. Indeed, the various manufacturers of commercial (cylindrical) DMAs all use very similar dimensions. Santos *et al.* (2009) have published a description of a high resolution planar DMA with a sheath flow from 200 to 900 l/min. Their DMA was designed for high mobility ions. If the same set of flow rates was used for particle applications it would require long DMA elements and large pumps and therefore would not be suitable for a portable instrument. Potentially the flow rates could be reduced for particle measurements but would likely require some redesign. However, the planar geometry has an advantage. There is no empty space additional to the volumes required for operation. On the contrary, in the cylindrical geometry there is empty space inside the column within the inner electrode which is not generally used. (Although in theory this space could be utilized for example by the electrometers in an FMPS it is rather a challenge in practice due to the high voltage on the inner electrode.) This is not a problem for a desktop instrument but an important issue for a portable device. This makes it difficult and impractical to design a portable DMA with cylindrical electrodes. Another advantage of the planar design is that the parallel-plate electrodes used offer increased resolution for the same sheath to aerosol flow ratios compared to traditional cylindrical designs. The uniform field results in less diffusional broadening of the transfer function (Alonso and Endo, 2001). This effect becomes increasingly significant for particles approximately < 50 nm. Although in theory the flow arrangement in a cylindrical DMA could be reversed to give increased resolution for these smaller particles (Alonso, 2002), this has yet to be demonstrated in practice.

Both planar and radial geometry DMAs can be used for a portable instrument design more effectively than a cylindrical DMA because they have no empty space, as commented above. However it was decided to implement a planar geometry in this work, because of its simplicity and low manufacturing costs.

4.1.2. Prototype design and development

The design of the portable planar DMA is as follows. Two stainless steel plate electrodes are separated by a 5 mm thick PTFE spacer forming the internal space of a separation chamber (Fig. 4.1–1). A sheath flow conditioner is positioned inside the separation chamber across the sheath flow, between the inlet and the internal space of the separation chamber. A second sheath flow conditioner is positioned inside the separation chamber before the sheath flow outlet. The flow conditioners have a double parallel polycarbonate mesh design made up of 54 (3 rows of 18) 1 mm circular apertures in each plane separated by 3 mm. The fraction of open area of the meshes is 0.21.

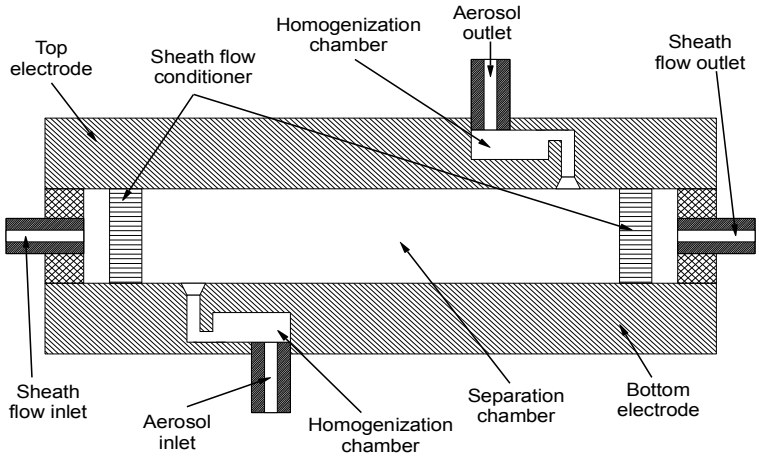

Figure 4.1–1. Schematic cross section of the planar DMA.§

§ Reproduced with permission from Steer et al., 2014. Copyright 2014, Aerosol Science & Technology. Mount Laurel, NJ.

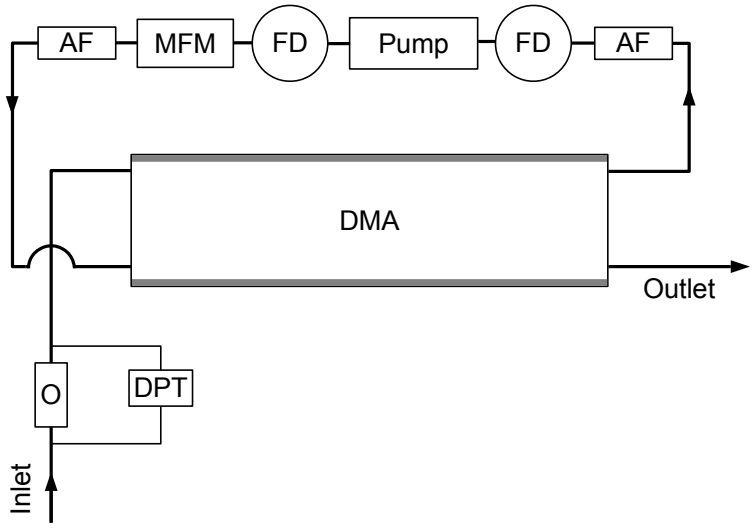

Figure 4.1–2. Schematic of the DMA operating assembly. The DMA is shown with electrodes indicated in grey. O – pressure drop orifice; DPT – differential pressure transducer for measuring the pressure drop across the orifice and thus the flow rate through it; AF - aerosol filter (Mitsubishi); MFM – mass flow meter; FD – flow damper for smoothing the flow output from the pump.

The polydisperse aerosol inlet and the monodisperse aerosol outlet are attached to the separation chamber via homogenization chambers cut into the faces of the planar electrodes. The widths of the aerosol inlet and outlet to and from the separation chamber are 1 mm. The whole DMA assembly is enclosed into an insulating polycarbonate enclosure of 5 mm thickness. The closed loop sheath flow was generated by a rotary vane pump (Gardener Denver), see Fig. 4.1–2. A mass flow meter (Honeywell) and a differential pressure sensor (Honeywell) were used to monitor the flow rates and to control the sheath flow rate. A DC high voltage is applied to the electrodes of the DMA. The assembled DMA and prototype device is shown in Fig. 4.1–3.

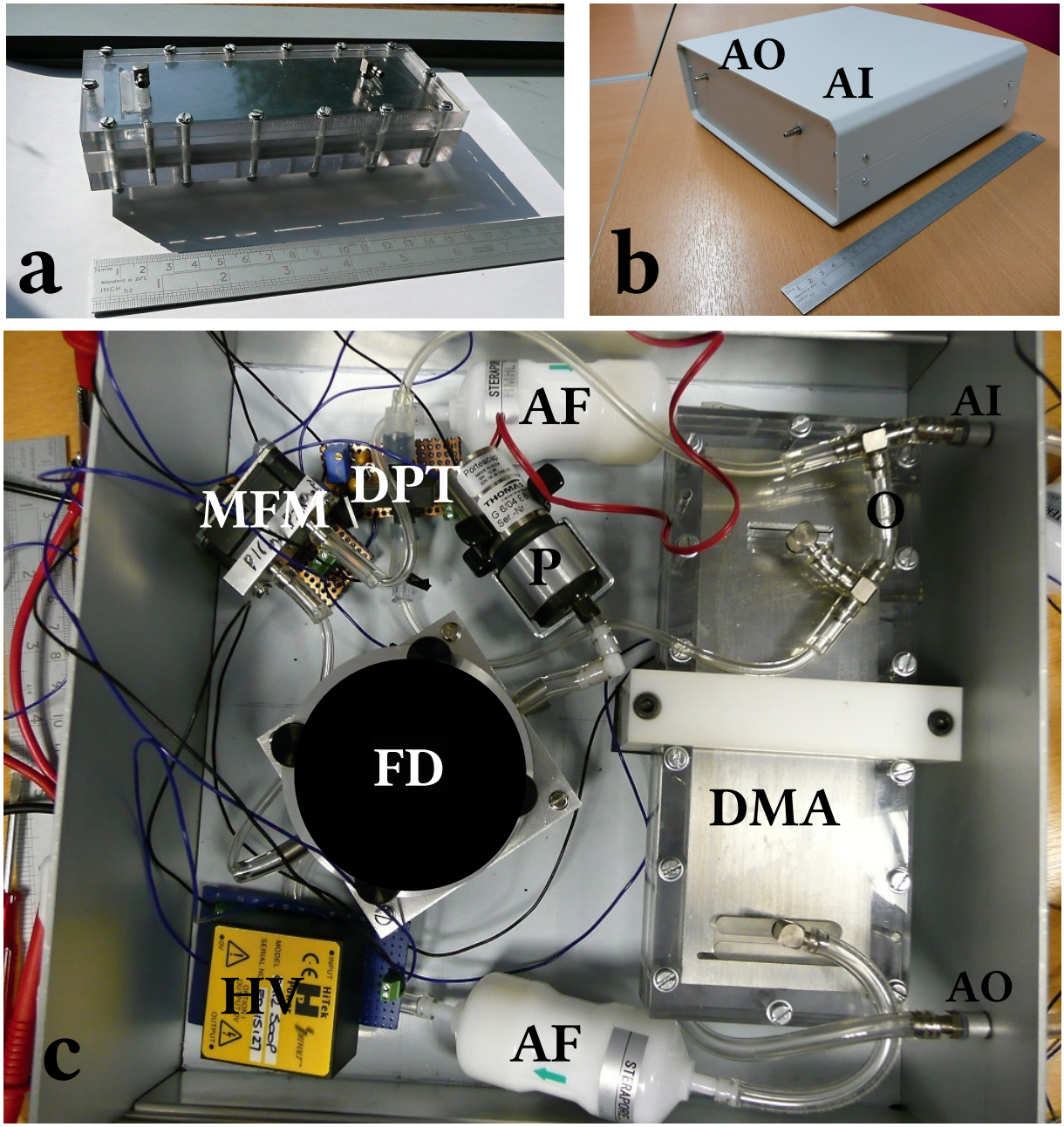

Figure 4.1–3. Prototype DMA construction showing the assembled DMA (a), the assembled prototype (b), and the internal components required for operation (c). AI – aerosol inlet, AO – aerosol outlet, MFM – mass flow meter, DPT – differential pressure transducer, P – 6 volt rotary vane pump (up to 3.5 litres/min), AF – air filter, FD – flow damping components (masked for confidentiality), O – inlet orifice to supply pressure drop for flow measurement by DPT, HV – DC high voltage supply.

To test that the prototype device is operational, some preliminary tests are carried out with atmospheric aerosol from the laboratory air drawn in through the inlet, and the output of the DMA monitored with a CPC. Atmospheric aerosols are considered to typically have a bipolar charge distribution which reaches equilibrium as they mature. Therefore it is possible to carry out some basic operational tests without the requirement

for a charger. It is confirmed that with the voltage supply switched off, the CPC count is zero, and thus there are no particles reaching the outlet of the DMA as expected. Next the voltage is increased in steps, with the CPC counts recorded at each step of the way. In this manner the relative change in the atmospheric concentration as a function of voltage is recorded. When a basic theoretical conversion between DMA voltage and resultant selected particle size is applied to this data, the result is a particle size distribution as shown in Fig. 4.1–4. No calibrations are in place at this stage for either the DMA or CPC used in this test, and so the sizing is quite approximate, and the ordinate scale has not been converted to concentration. The estimated peak size of ~22 nm is smaller than usual for an atmospheric aerosol. However, such distributions can be found on occasion when there has been a recent local particle generation event (e.g. soldering work in the laboratory or truck passing by outside an open window), and there may be higher particle counts at sizes larger than those measured here. In any case, the achievement of a distribution of any kind is an encouraging result, showing that on a basic level the DMA is operating as intended.

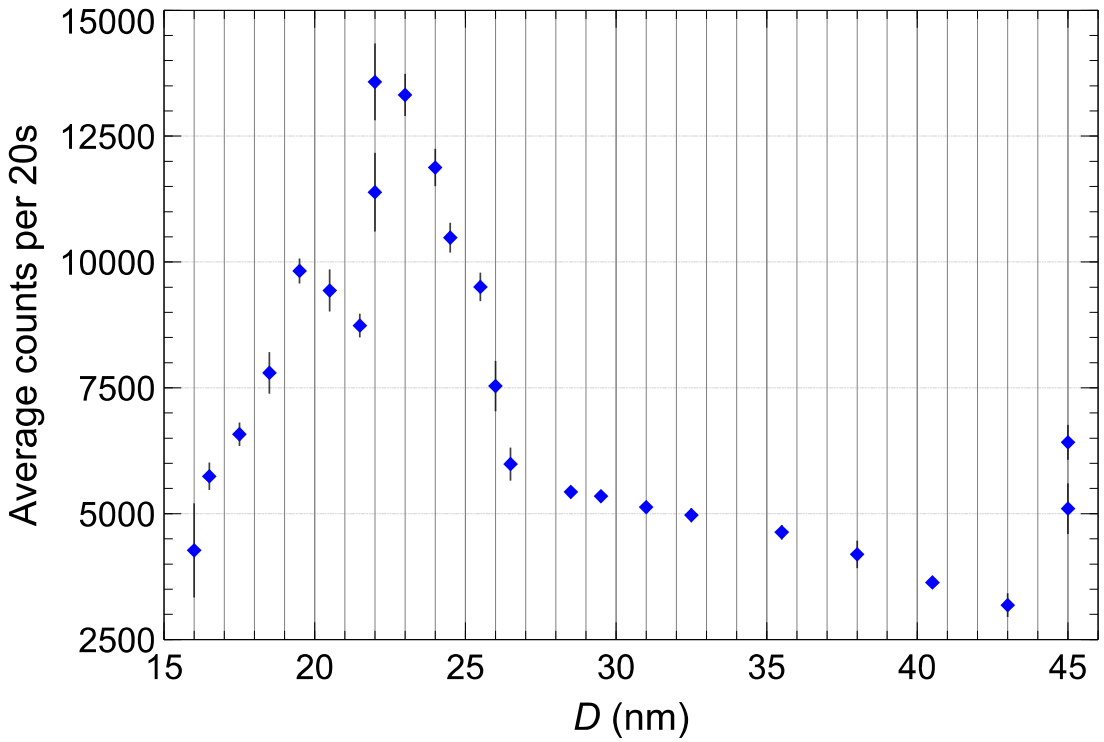

Figure 4.1–4. First atmospheric aerosol size distribution obtained with the DMA and a condensation particle counter. Distribution based on a theoretical data conversion between voltage and size.

4.1.3. Calibration

4.1.3.1. Introduction and apparatus

The basic approach taken to calibrate the planar DMA involves first creating source particles using a "soot" generator (carbonaceous particles), charging them, selecting a size band with the DMA to be calibrated, and then analysing the resultant distribution using a Grimm SMPS which consists of a DMA connected to a CPC. The arrangement is shown in Fig. 4.1–5 below.

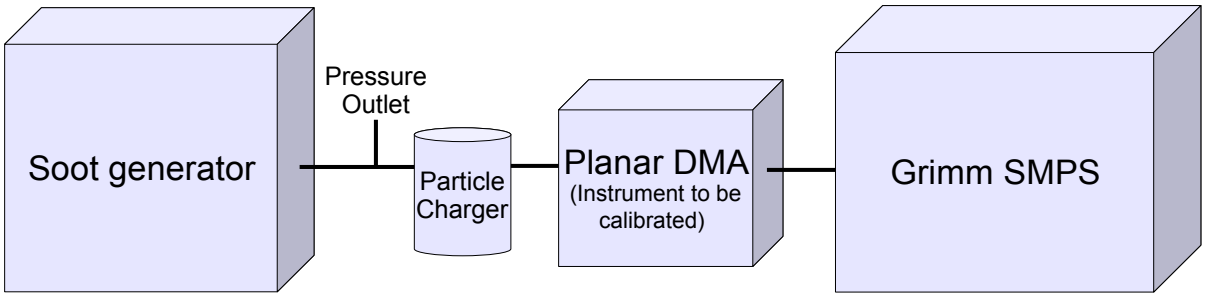

Figure 4.1–5. Setup for calibration of the planar DMA.

Atmospheric aerosol has also been tested in place of the soot but generally the soot generator is preferred as it gives a more consistent output with a higher concentration. The Grimm SMPS supplies an aerosol flow rate of 0.3 l/min. If a lower aerosol flow rate through the DMA is required, then an additional valve controlled filtered input can simply be added between the test DMA and the Grimm DMA. If a higher aerosol flow rate through the DMA is required, then a bypass is added in the same position but this time connected to the vacuum side of a pump set as necessary. A filter is used in front of the pump to stop particles damaging it, and the pressure side of the pump is fed back to an extraction hood for extraction of gases associated with the soot.

4.1.3.2. Soot generator

Nitrogen from a pressurised cylinder is driven through two flasks of acetone with the airflow measured by a flow meter and controlled by a valve. The acetone laden air is then heated in an oven to form soot nanoparticles the size of which is determined by the oven temperature and flow rate. Flow rates generally range between 50 and 250 ml/min and typical temperatures are between 600 and 750 °C.

4.1.3.3. Charger

An Americium-241 unipolar charger is used to charge the particles similar to that described by Adachi, *et al*. (1996). The charger design is shown in Fig. 4.1–6.

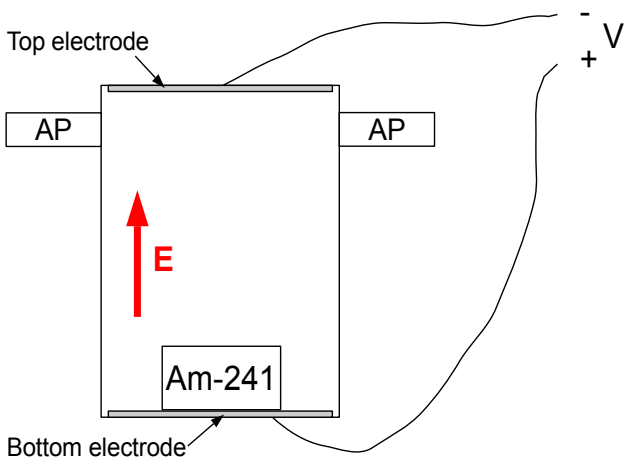

Figure 4.1–6. Am-241 particle charger design. Aerosol ports (AP) allow an air flow of particles to be charged through the volume of the device. Americium-241 is used as an ionisation sources. To preferentially select a particular polarity, electrodes at either end of the device are connected to a voltage supply. The resultant electric field (E) drives ions of each polarity to opposing ends of the device. With the field as chosen above, negative ions are quickly lost to the bottom electrode whereas positive ions travel up through the volume of the device where they can collide with aerosol particles. This action drives a preferential positive charging of the aerosol particles whereas switching the polarity of the applied field will similarly achieve a preferential negative charging of the particles.

A voltage is applied to increase the percentage of charged particles and to select a polarity (negative used in this calibration as the Grimm SMPS measures negative particles). The ion output from the charger is shown in Fig. 4.1–7.

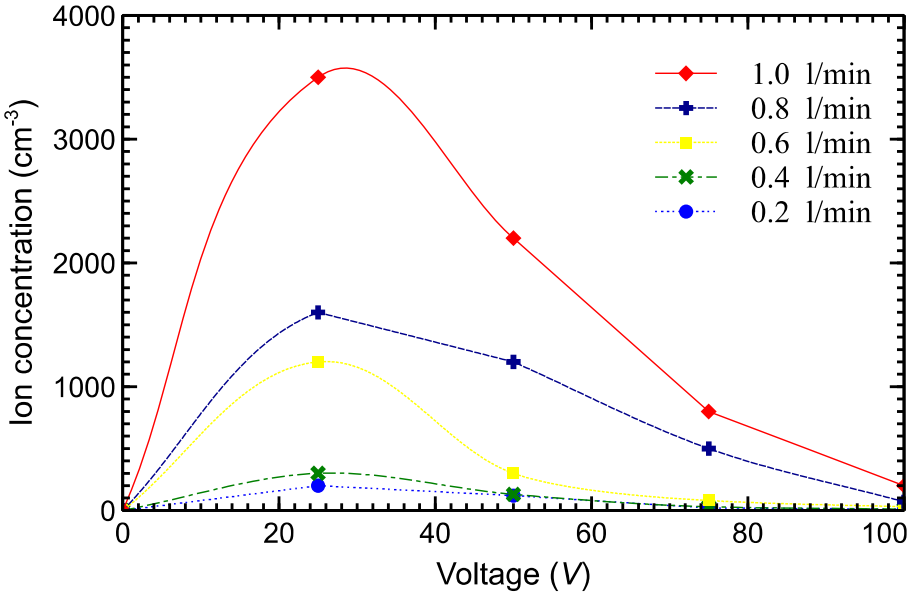

Figure 4.1–7. Particle charger performance as measured by an ion counter at the outlet of the device as a function of the voltage applied for flow rates between 0.2 and 1 litre/min.

As would be expected, increasing the flow rate significantly increases the amount of ions extracted from the charger. An initial voltage is required to pull ions of the selected mobility into the flow path. However, it can be noted that increasing the voltage further then decreases the ion output, as ions are pulled out of the flow and lost to the top electrode. Note that these measurements are not a direct measure of charging performance, and as such are only indicative of the dynamics of the system. Also consider that in some situations it may be preferable to reduce the charger performance to reduce the degree of multiple charging.

4.1.3.4. Mini-DMA

A schematic representation of the DMA is shown in Fig. 4.1–2 above. The selector houses a pair of parallel electrodes through which the air flow passes. When a voltage is applied to these electrodes at a particular flow rate the corresponding particles of the respective mobility will be drifted to the aerosol outlet. If all the particles have the same charge (e.g. all singularly charged) then this mobility will correspond to a particular particle size (neglecting shape effects). All other particles will be swept into the sheath flow system made up of the top row of elements in Fig. 4.1–2 Above.

4.1.3.5. Grimm SMPS+C 5.401

Figure 4.1–8. Grimm SMPS. Aerosol input can be seen at upper left. For this calibration the neutraliser attached to the top of the DMA (displaying the radioactive symbol) is removed.

The main components of the Grimm SMPS shown in Fig. 4.1–8 are the neutraliser (Am241 with "Radioactive" sign above), the DMA (centred) and the CPC (bottom right). It operates by applying a bipolar charge distribution to the incoming particles with the neutraliser, scanning the voltage on the DMA in steps from 10 kV to 5.8 V, and recording the output using the CPC. The resultant particle size distribution is then output as a visual plot and numerical data via software.

For this calibration the neutraliser is removed from the Grimm SMPS and the charge distribution is not changed from that applied by the charger before the planar DMA. In effect this means that we are calibrating the planar DMA to particle mobility rather than size. If we leave the Grimm neutraliser in place, then any multiply charged particles that have passed through the mini-DMA are likely to lose their extra charge in the bipolar charge distribution in the neutraliser. In this case they appear in larger size channels in the Grimm DMA resulting in additional peaks at larger sizes in the final data. We wish to avoid these additional peaks for the analysis of the data, and so the Grimm neutraliser is removed from the apparatus. This has the disadvantage that the charge distribution is not as would usually be created by the Grimm neutraliser before the SMPS, and so the charge distribution correction applied by the software may not be quite correct. By comparison with the raw data, it can be seen that any errors this may introduce do not manifest themselves in a shift of the distribution peak. Therefore it is not a concern for the current calibration. However, there remains uncertainty in terms of defining the width of the distribution (σ_g).

4.1.3.6. Typical particle number size distribution graphs

The soot generator produces broad distributions in high concentrations in the order of 10^6 particles/cm^3 as shown in Fig. 4.1–9. These are useful characteristics for calibrating the DMA as it allows us to cover a wide range of particle sizes without having to re-adjust the generator settings such as temperature which can take a long time to settle. In addition it is preferable to start off with quite high concentrations such as to provide good count statistics to the SMPS downstream despite high losses as will usually occur in a DMA.

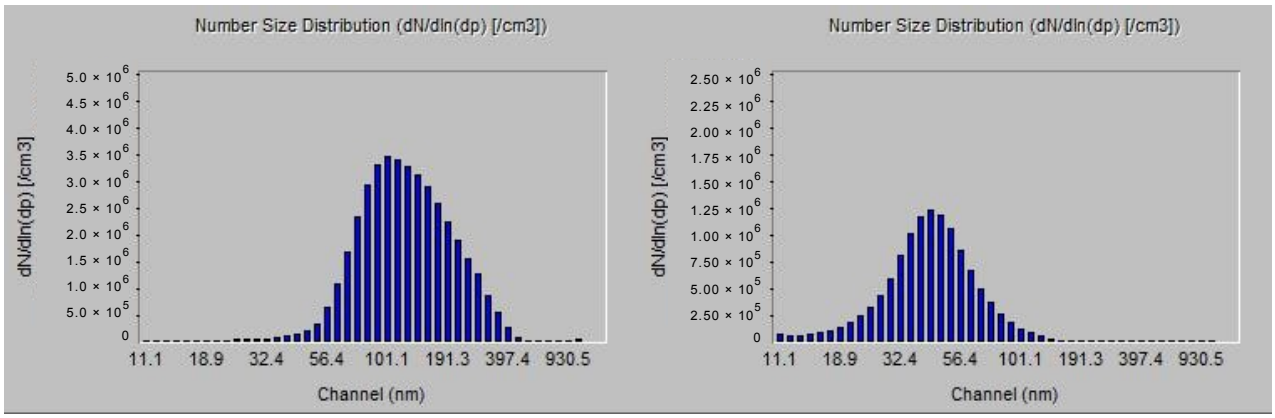

Figure 4.1–9. Examples of larger and smaller sized particle size distributions obtained from the soot generator. These have been measured directly from the generator with the SMPS without the test DMA in line.

Once the generator is providing the requisite particle distribution, the planar DMA can be connected in line before the SMPS. Some example particle size distributions as selected by the planar DMA and measured by the Grimm SMPS are shown in Figs. 4.1–10 to 4.1–13 below. In all cases voltages and flow rates (Q_{sh} – sheath flow, Q_a – aerosol flow) indicate that the distribution was selected by the planar DMA with those respective parameters.

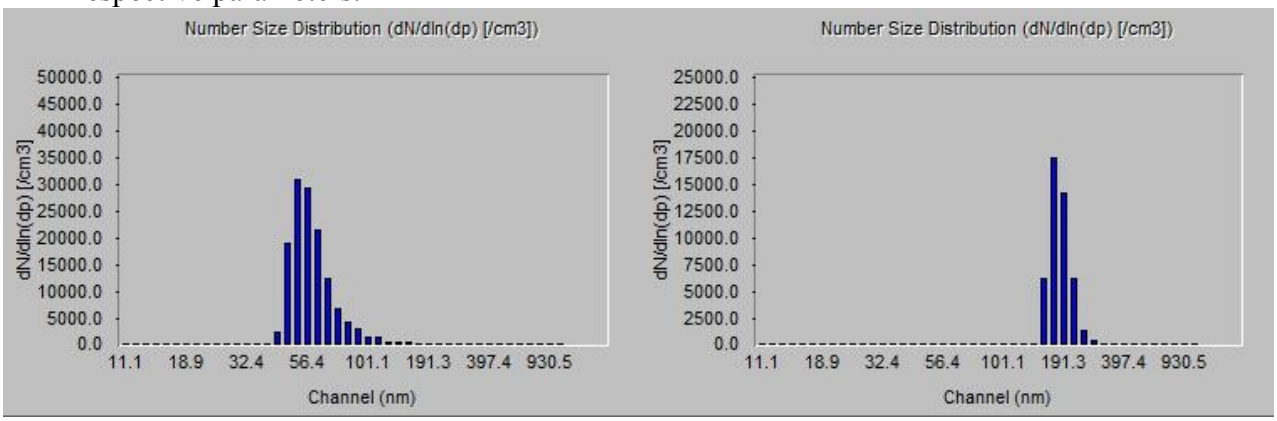

Figure 4.1–10. DMA cut soot distributions selected with the following parameters: Q_{sh} = 3.5 l/min, Q_a = 0.15 l/min, V_{DMA} = 500 V and 6 kV respectively.

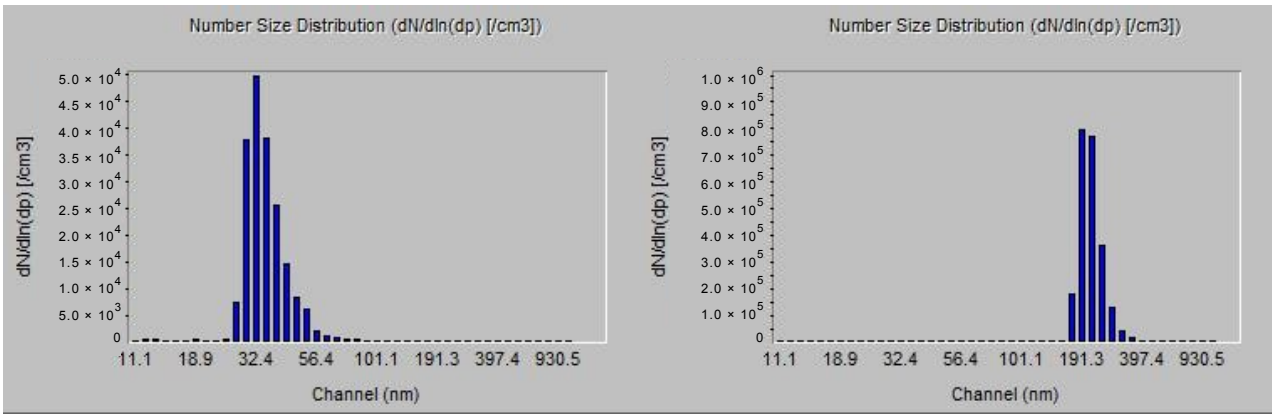

Figure 4.1–11. DMA cut soot distributions selected with the following parameters: Q_{sh} = 3 l/min, Q_a = 0.3 l/min, V_{DMA} = 200 V and 7.4 kV respectively.

With high sheath to aerosol flow ratios (Q_{sh}/Q_a) the planar DMA selects a narrow size cut of particles. Increasing the voltage applied to the planar DMA electrodes selects particles of a larger size (lower mobility).

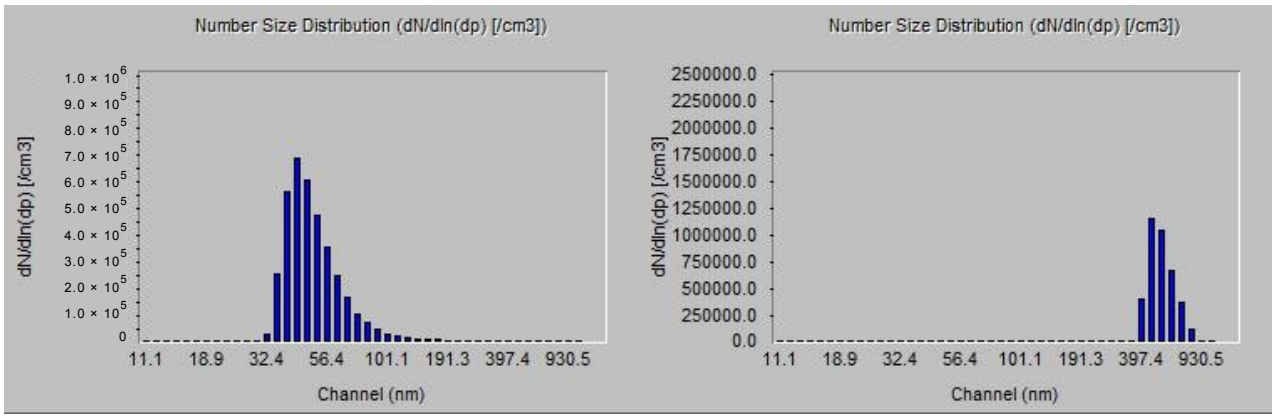

Figure 4.1–12. DMA cut soot distributions selected with the following parameters: Q_{sh} = 0.95 l/min, Q_a = 0.3 l/min, V_{DMA} = 100 V and 7.4 kV respectively.

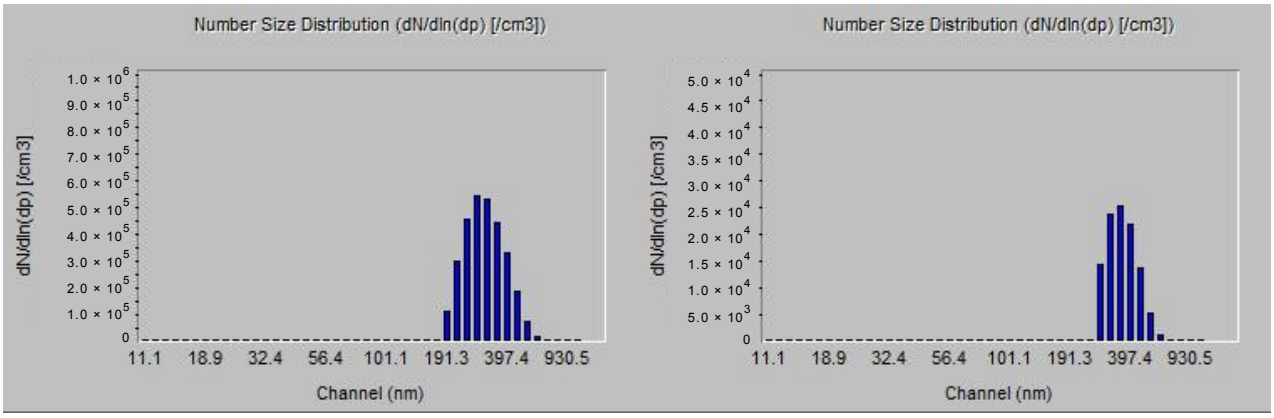

Figure 4.1–13. DMA cut soot distributions selected with the following parameters: Q_{sh} = 0.95 l/min, Q_a = 0.95 l/min, V_{DMA} = 3 kV and 7 kV respectively.

With lower sheath to aerosol flow ratios (Q_{sh}/Q_a), the distributions selected by the DMA are broader. In addition lower flow rates correspond to lower voltage requirements to select a particular size band. For example, compare the 500 V selection in Fig. 4.1–10 to the 100 V selection in Fig. 4.1–12, or the 7.4 kV selection in Fig. 4.1–11 to the 7.4 kV selection in Fig. 4.1–12 or Fig. 4.1–13. This means that within the voltage confines of any particular DMA, the largest particle size that can be selected can be increased by reducing the flow rates used and thus sacrificing resolution.

4.1.4. Modelling of the DMA performance: mobility vs. voltage

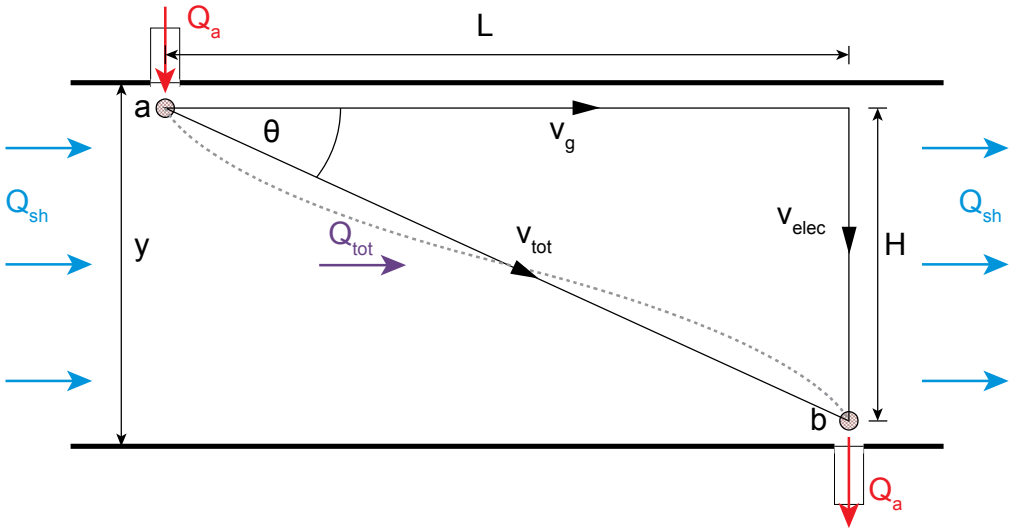

Figure 4.1–14. Side view of the mini-DMA separator unit showing the selected aerosol path. Q_{sh} - sheath flow; Q_a – aerosol flow; Q_{tot} – total (combined) flow; L – length of selection region; y – height of selection region; H – vertical distance travelled by selected particles; v_{tot} – selected particle velocity vector; v_g – component of the particle velocity due to the air flow rate (gas velocity); v_{elec} – component of the particle velocity due to the electric field (assuming a charged particle).

To reach the aerosol outlet a particle must travel from point *a* to point *b* as shown in Fig. 4.1–14. The expected trajectory shape is shown in grey dash but it can be shown that the straight line trajectory will give the same result (Gorbunov, 2009). The resultant trajectory from a model in COMSOL Multiphysics® software in fact gave quite a linear path (see Fig. 4.1–18). The total velocity of a charged particle along this path will be v_{tot}, consisting of the component due to the gas velocity v_g, and the component due the applied electric field v_{elec}.

If the voltage between the top and bottom electrodes (separated by a distance y, and for the moment we assume $y = H$) required to select the particle size in question is ΔV, the electric field is E, and the electrical mobility of the particle is Z, then:

$$\Delta V = EH \qquad \text{and} \qquad E = \frac{v_{elec}}{Z}$$

$$\therefore \Delta V = \left(\frac{v_{elec}}{Z} \right) H \tag{19}$$

Simple geometry gives:

$$v_{elec} = v_{tot} \sin\theta \qquad \text{and} \qquad v_{tot} = \frac{v_g}{\cos\theta}$$

$$\therefore v_{elec} = v_g \tan\theta = v_g (H / L) \tag{20}$$

Where τ is the residence time of the particle in the system in seconds. This can be calculated from $\tau = Vol^* / Q_{tot}$, where Q_{tot} is the total flow rate and Vol^* is the total volume which that flow occupies, i.e.

$$\tau = \frac{Vol*}{Q_{tot}} = \frac{W\,L\,H}{Q_a + Q_{sh}} \tag{21}$$

Where W is the total width of the channel (see Fig. 4.1–15 below).

As $v_g = L / \tau$ and $v_{elec} = H / \tau$ giving:

$$\Delta V = \frac{H^2}{\tau Z} \tag{22}$$

The electrical mobility is given by the mechanical mobility times the total charge:

$Z = neB$ where n is the number of charges on the particles (n set to 1 here), e is the elementary unit of charge and B is the mechanical mobility given by:

$$B = \frac{C_C}{3\pi\eta d_p} \tag{23}$$

Where C_C is the Cunningham slip correction factor, η is the air viscosity (nominally 1.8203×10^{-5} kg/m s) and d_p is the particle diameter.

The final equation is now:

$$\Delta V = \frac{3\pi\,\eta\,d_p\,H^2}{\tau\,n\,e\,C_C} \tag{24}$$

There now only remains to calculate C_C and H.

An empirical fit to air data for solid particles (Allen and Raabe, 1985) gives:

$$C_C = 1 + Kn\left[1.142 + 0.558\exp\left(-0.999/Kn\right)\right] \tag{25}$$

Where the Knudsen number $Kn = 2\lambda / d_p$.

At 293 K and atmospheric pressure the mean free path λ_r = 0.0664 μm, while at other temperatures and pressures one can use (Willeke, 1976):

$$\lambda = \lambda_r \left(\frac{101}{P}\right)\left(\frac{T}{293}\right)\left(\frac{1+110/293}{1+110/T}\right) \tag{26}$$

where P is in kPa and T in K.

We can also directly adjust C_C for pressure changes (Hinds, 1999) using:

$$C_C = 1 + \frac{1}{P d_p}\left[15.60 + 7.00\exp\left(-0.059 P d_p\right)\right] \tag{27}$$

Where P is in kPa and d_p is in μm.

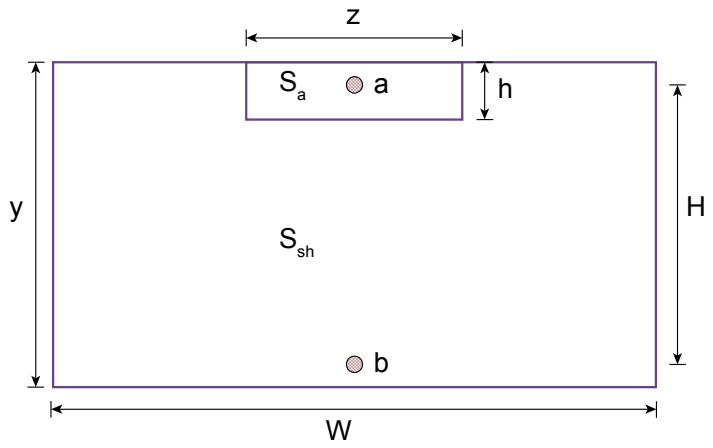

Figure 4.1–15. A cross-sectional view of the mini-DMA separator unit flow showing simplified initial areas occupied by the sheath and aerosol flows at the aerosol point of entry (S_{sh} and S_a respectively).

To calculate H we consider the end on view in Fig. 4.1–15, and the initial areas occupied by the aerosol and sheath flows (S_a and S_{sh} respectively). We assume the system is symmetric, and that at the outlet the centre of the selected distribution will come from point *b* at a distance $h/2$ from the bottom edge, just as the centre of the distribution at the inlet (point *a*) is a distance $h/2$ from the top edge. Therefore the average vertical distance travelled by the particles in our resultant distribution is given by: $H = y - h$.

z is the width of the inlet slot. Although we would expect the initial aerosol width to be $> z$ this should be a smaller perturbation compared to the vertical spread h and so we approximate that $S_a = z.h$ or $h = S_a / z$

The initial areas of the aerosol and sheath flows should be found to be proportionally the same as their respective flows such that $S_a / S_{sh} = Q_a / Q_{sh}$. Also, clearly $S_a + S_{sh} = y.W$

Combining the above gives:

$$H = y - \left(\frac{Q_a}{Q_a + Q_{sh}}\right)\frac{y\,w}{z} \tag{28}$$

The above calculations of C_C and H can now be used to calculate from Equation 24 the required voltage (ΔV) to select a particular particle diameter d_p.

4.1.5. Finite element modelling

COMSOL Multiphysics® finite element software was employed to model the flow velocity profile and particle trajectories in the planar DMA. An example of velocity field calculations is shown in Fig. 4.1–16 below.

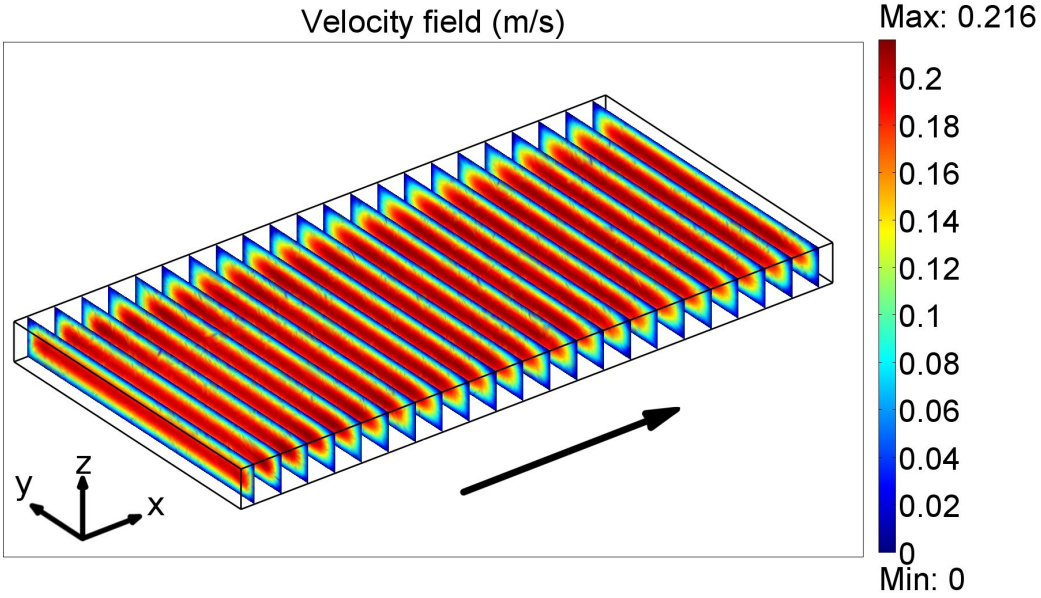

Figure 4.1–16. Air velocity field in the planar DMA at P = 101 kPa and T = 20 °C. The separation height between the electrodes in the z direction is 5 mm and the width in the y direction is 40 mm. The total flow rate in the DMA was 2 l/min. The velocity is coded according to the scale bar on the right in (m/s). The arrow indicates the direction of flow.§

Cross sections of the flow profile are shown in Fig. 4.1–17. The flow is laminar and a stable Poiseuille profile is established throughout the volume, decreasing to 0 at the boundaries. Of note here is the uniform flow in the y direction across the majority of the width of the separation region. The deviation is less than 1% across the central region of 0.006 m < y < 0.034 m. This is important such that particles of the same mobility stay together as they traverse the length of the DMA and thus maintain good resolution at the output. By contrast, the steeper flow profile in the z direction does not affect resolution as particles are travelling between the electrodes in the z direction and therefore are all affected by this profile equally.

§ Reproduced with permission from Steer et al., 2014.
Copyright 2014, Aerosol Science & Technology. Mount Laurel, NJ.

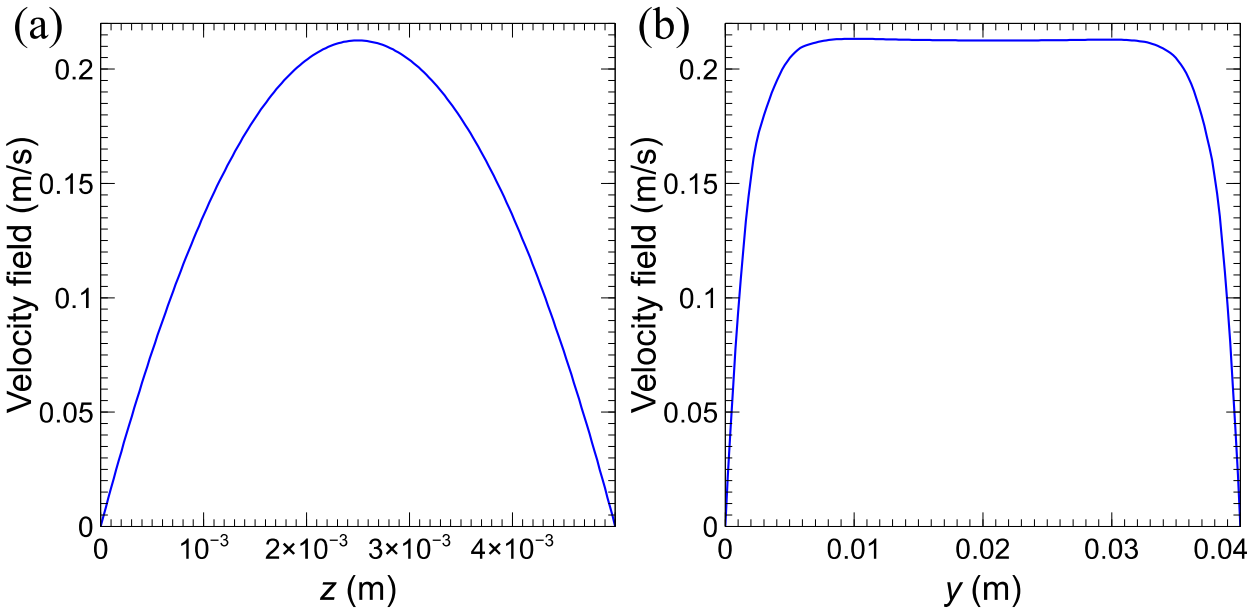

Figure 4.1–17. Velocity profile in the x direction at (a) x = 0.04 m and y = 0.02 m and (b) x = 0.04 m and z = 0.0025 m.[§]

Fig. 4.1–17 (b) illustrates a potential disadvantage of using a planar geometry compared to a traditional cylindrical one: the presence of side walls that do not exist in the cylindrical design. The flow profile resulting from the boundary condition of zero flow at the side walls can cause broadening of the transfer function (reduction in resolution) as a range of selected mobilities will result from the range of particle velocities found across the profile. To eliminate this problem, the aerosol flow in this design is constrained such that it does not come in contact with the side walls and is kept at a uniform velocity. To achieve this, the aerosol entrance and exit slits to the DMA are restricted to being a narrower 25 mm in width (y direction) compared to the 40 mm full width of the classification zone. It was found that the 25 mm in width of aerosol flow compared to the 40 mm full width of the classification zone enables the disadvantage of the planar geometry to be eliminated. This ensures that the aerosol flow is kept away from the walls and the region where the flow velocity is reduced due to boundary effects (see Fig. 4.1–17 (b)). The flow profile in the z direction (Fig. 4.1–17 (a)) is less important as by the nature of the DMA operation different z positions correspond to different particle mobilities such that there is no detriment to the uniqueness of the mobility of particles reaching the outlet.

Another concern which must be addressed is achievement of uniform flows across the rectangular cross section. To ensure this, flow conditioners are placed in the sheath flow at either end of the classification zone such that the aerosol flow is always contained between them. Once the sheath flow is uniform the aerosol flow is introduced and extracted through homogenization chambers cut into the electrodes. These chambers ensure that the aerosol flow is uniformly spread along the full width of the interface slots following the interface for tubing interconnects. The aerosol slot length (x direction) is 1 mm and was chosen mainly on the basis of experience and tests. The choice of slot dimensions can also impact on the resolution. While the results presented here show that the current choice is sufficient to achieve the design goals this is

§ Reproduced with permission from Steer et al., 2014.
Copyright 2014, Aerosol Science & Technology. Mount Laurel, NJ.

potentially an area where additional small improvement could be made with further optimization studies as for example carried out by Martínez-Lozano and Labowsky (2009).

Example charged particle trajectories for a given applied electric field are shown in Fig. 4.1–18. Particles of the selected mobility do not follow a linear path between the inlet and outlet. In particular at the inlet and outlet the trajectories are distorted by the steep flow curvatures in these regions as shown in Fig. 4.1–19.

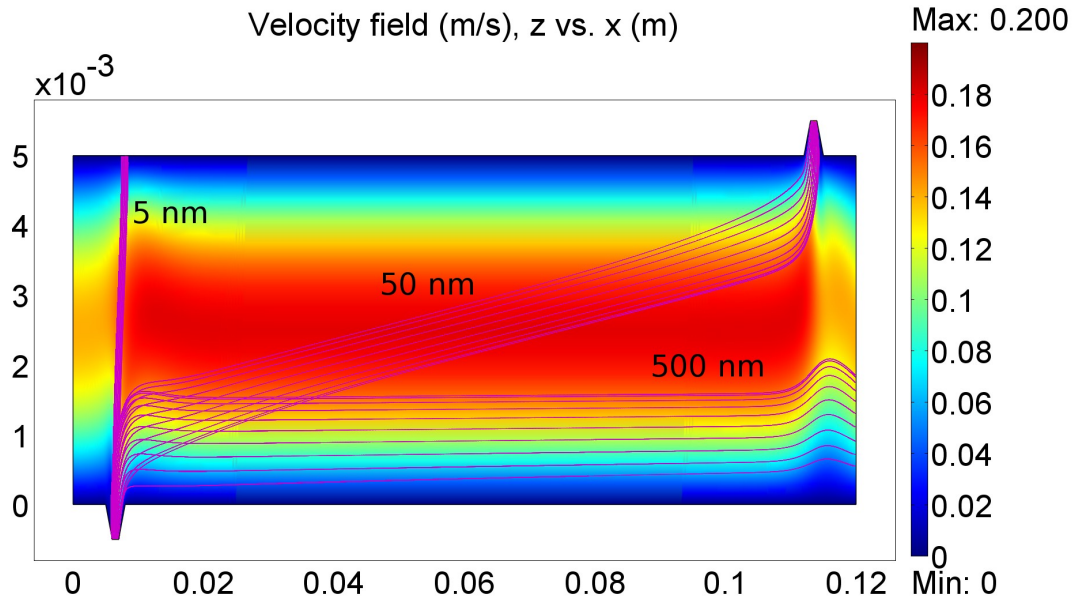

Figure 4.1–18. Trajectories are shown for 5, 50 and 500 nm singularly charged aerosol particles in the air velocity field of the planar DMA at 220 V (P = 101 kPa, T = 20 °C). The separation zone is 5 × 40 × 108 mm. The cross-section at y = 0.02 m is shown. The sheath flow rate Q_{sh} is 1.8 l/min, the aerosol flow rate Q_a is 0.2 l/min, and the voltage difference across the DMA electrodes is 220 V. Particles are introduced from the bottom left. Under these conditions it can be seen that the 50 nm particles are selected and sent to the outlet while particles smaller or larger are lost to the opposite electrode or sheath flow respectively. The velocity is coded according to the scale bar on the right in (m/s). The vertical scale (z) and the horizontal scale (x) are in metres.[§]

§ Reproduced with permission from Steer et al., 2014.
Copyright 2014, Aerosol Science & Technology. Mount Laurel, NJ.

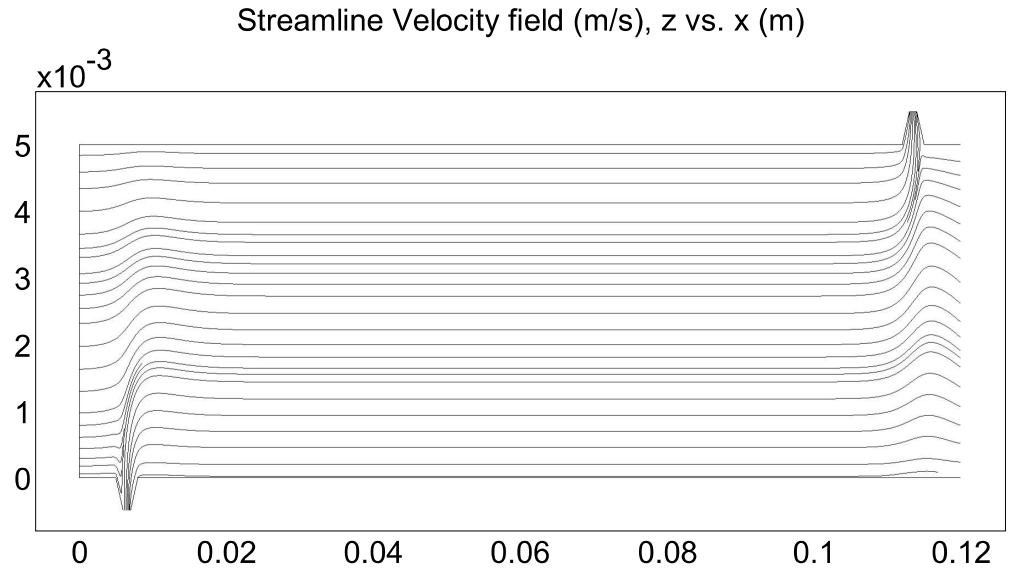

Figure 4.1–19. Air molecule streamlines in the DMA.§

By modelling the proportion of particles that reach the output as a function of particle size (assuming singularly charged), apparatus functions for the DMA performance can be mapped out. These functions demonstrate the theoretical limitations on the resolving performance of the DMA (Flagan, 1999). Some examples are shown below in Fig. 4.1–20.

§ Reproduced with permission from Steer et al., 2014.
Copyright 2014, Aerosol Science & Technology. Mount Laurel, NJ.

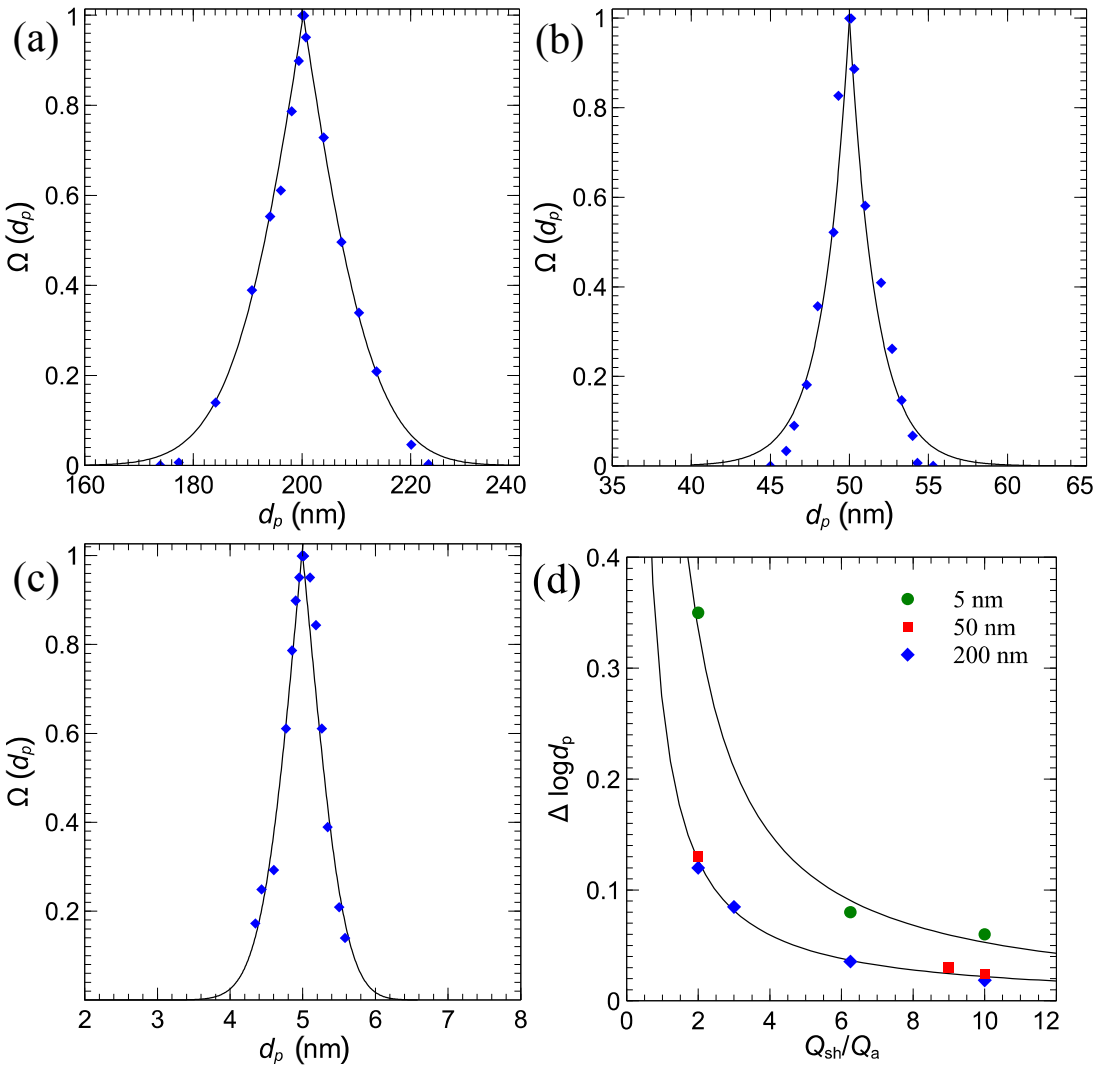

Figure 4.1–20. An example of an apparatus function for the planar DMA $\Omega(d_p)$ for monodisperse particles of (a) – 200 nm, (b) – 50 nm, and (c) – 5 nm, with sheath flow Q_{sh} = 1.8 l/min and aerosol flow Q_a = 0.2 l/min. The markers show numerical calculations based on particle trajectories used in the model, while the solid curve shows an exponential parameterised fit function for each branch of the transfer function. (d) – An example of the change in DMA resolution $\Delta \log d_p = \log(d_2/d_1)$ as a function of flow rate ratio. Data points show the results of calculations for the current geometry. Q_{sh} is the sheath flow rate and Q_a is the aerosol flow rate. d_1 and d_2 are the sizes corresponding to 50% of the transfer function height such that $\log(d_2/d_1)$ is the full width half maximum in logarithmic scale. Green circles – 5 nm; red squares – 50 nm and blue diamonds – 200 nm.[§]

The apparatus functions display sharp maxima with exponential decays on either side. The widths of these functions in terms of geometric standard deviation (σ_g) from a lognormal approximation are 1.03, 1.02, and 1.052 for the 200, 50 and 5 nm distributions respectively – Fig. 4.1–20 (a) – (c). Usually distributions with $\sigma_g < 1.1$ are considered to be "monodisperse", i.e. of single size, and therefore these results demonstrate good resolving potential. The difference between the 200 and 50 nm results

§ Reproduced with permission from Steer et al., 2014.
Copyright 2014, Aerosol Science & Technology. Mount Laurel, NJ.

is not significant and is only caused by a change in slope of the relationship between particle size and electrical mobility at ~100 nm (see e.g. Fig. 18–1 in Baron and Willeke, 2001). They are the same width in mobility space. The greater width at 5 nm is to be expected due to diffusion broadening. It is difficult to keep such small particles well contained in time and space due to their relatively high diffusion constants.

Fig. 4.1–20 (d) shows the relationship between the width of the apparatus function and the sheath to aerosol flow ratio Q_{sh}/Q_a as given by the modelling results. A steep improvement in resolution is evident at lower flow ratios while at higher flow ratios diminishing returns are encountered for further flow rate ratio increases. Again, a significant drop in resolution is observed for the smallest particles considered (5 nm) due to diffusion broadening. However this is only significant at the very smallest sizes considered (< 20 nm). In general, the ratio of the sheath and aerosol flows is the most significant parameter in determining the resolution of a DMA.

4.1.6. Test results of the planar DMA in a commercialised system

The planar DMA was implemented by Naneum Ltd. in a commercial standalone portable DMA (Nano-ID® PMC500) and in a portable SMPS (Nano-ID® NPS500).

An example monodisperse particle distribution at 100 nm as selected by the PMC500 and measured with a Grimm SMPS (5.400) is shown in Fig. 4.1–22 (a). Testing of the combined NPS500 SMPS system (which includes a corona particle charger and miniature CPC) was carried out at Particle Measuring Systems Inc., Boulder, Colorado, USA. The test setup is shown in Fig. 4.1–21. Test aerosols of NaCl and PSL (polystyrene latex) were generated in a sub-micrometer monodisperse aerosol generator (3940, TSI, USA), and neutralised in a bipolar charging environment (Krypton-85 Aerosol Neutralizer 3012; TSI, USA), before being sent to the reference DMA (Electrostatic Classifier 3080, TSI). The reference monodisperse distributions were then sent to the NPS500 where the particles are charged with a corona charger before the distribution is finally measured with the combined planar DMA and miniature CPC. The results are shown in Fig. 4.1–22 (b) – (d).

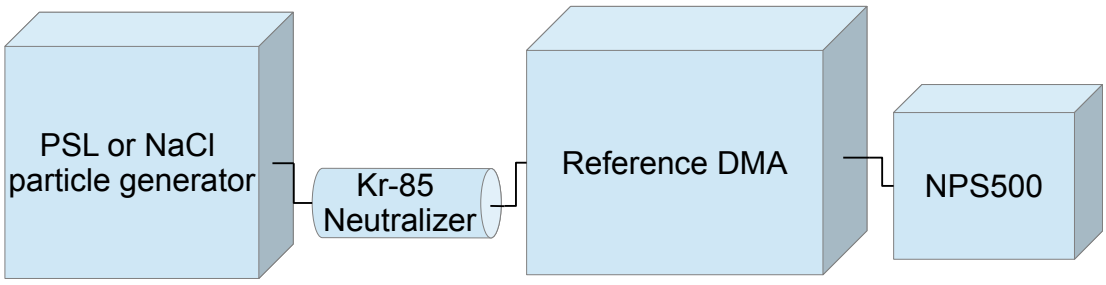

Figure 4.1–21. Test setup. The NPS500 SMPS includes a corona particle charger, the planar DMA and a miniature CPC.§

§ Reproduced with permission from Steer et al., 2014.
Copyright 2014, Aerosol Science & Technology. Mount Laurel, NJ.

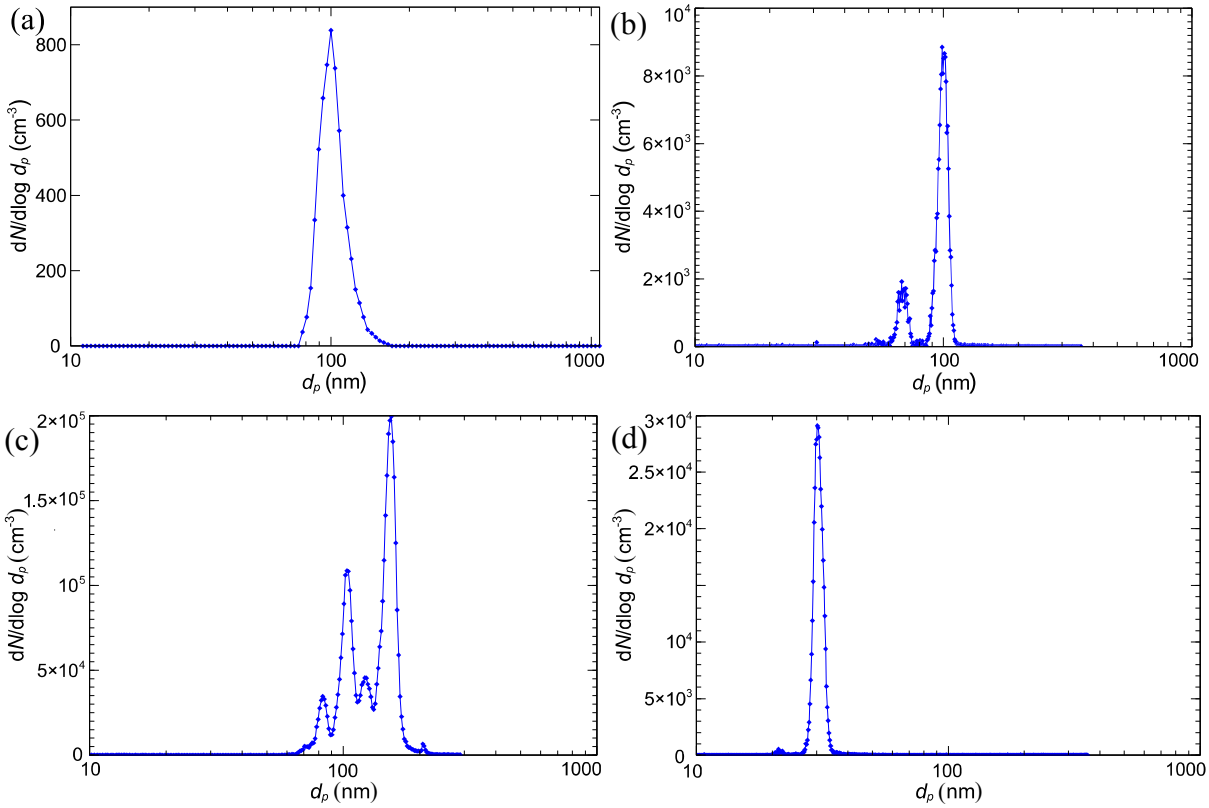

Figure 4.1–22. (a) – An example 100 nm monodisperse selection of atmospheric aerosol selected by the PMC500 and measured by a Grimm SMPS. The aerosol and sheath flow were 0.3 and 3 l/min respectively both in the PMC500 DMA and in the Grimm SMPS. (b) – A typical size distribution measured by the NPS500 with PSL particles of 100 nm selected with a 100 nm cut in the reference DMA. (c) – A typical size distribution measured by the NPS500 with NaCl particles selected with a 150 nm and (d) – 30 nm cut and in the reference DMA. The planar DMA flow rates used in the NPS500 were Q_{sh} = 1.8 l/min and Q_a = 0.2 l/min.[§]

An example size distribution of 100 nm PSL is shown in Fig. 4.1–22 (b). The reference DMA is set to 100 nm to ensure and narrow monodisperse selection and accurate mobility based sizing. The measured distribution from the NPS500 utilising the planar DMA displays a main peak at 98.8 nm and a secondary peak at 67.9 nm. The secondary peak position match well with the theoretical expectation for particles doubly charged in the corona (66.7 nm). A lognormal fit to the main peak yields a geometric standard deviation (σ_g) of 1.04. This is close to the theoretical apparatus function derived from modelling which yielded σ_g = 1.03.

NaCl distributions as generated are broader and allow for a wider selection of sizes to be selected by the reference DMA. At 150 nm many additional peaks due to multiple charging effects are apparent – Fig. 4.1–22 (c). The main peak is measured by the NPS500 at 154.7 nm with secondary peaks apparent at 83.0, 103.4, 121.7 and 205.7 nm. The first two are a good match to the expected positions for particles singularly charged in the neutraliser before the reference DMA and subsequently doubly or triply charged by the corona before measurement by the NPS500 (102.9 and 81.6 nm respectively). The third peak is a good match to the expected position for particles doubly charged in

§ Reproduced with permission from Steer et al., 2014.
Copyright 2014, Aerosol Science & Technology. Mount Laurel, NJ.

the neutraliser before the reference DMA and subsequently triply charged in the corona before measurement by the NPS500 (121.2 nm). While the last peak corresponds reasonably well with the expected position for particles initially triply charged in the neutraliser before selection by the reference DMA and which then lose a charge to become only doubly charged in the corona before measurement by the NPS500 (199.9 nm).

Multiple charging effects are much less significant at smaller sizes. This is evident from the NaCl reference DMA selection at 30 nm – Fig. 4.1–22 (d). The main peak as measured by the NPS500 is measured at 30.2 nm. Here there is only a single small secondary peak just about visible at 21.2 nm. This is a good fit to the expected position for particles doubly charged in the corona (20.6 nm).

In general the positions of all the multiply charged peaks are in good accordance with theory (Hoppel and Frick, 1986) and show the expected trend of increased multiple charging at larger sizes. In addition, it is also as expected for this size range (Wiedensohler, 1988) that the higher the order of the multiply charged peaks, the less prominent they are. The average sizing accuracy for the positions of the NPS500 peaks as compared to the chosen size in the reference DMA was 4.2 %.

4.2. Formation of Zn and ZnO nanoparticles by homogeneous nucleation

4.2.1. Introduction

To study ENP aerosols effectively it is necessary to first be able to produce them in some manner. It is possible to directly aerosolise powder samples (as will be used in Section 4.3). However it is difficult to pull apart the particle agglomerates fully, and hence the resultant aerosol distribution created can have quite a large modal size (e.g. 200 – 300 nm), and be rather broad. For examples see Figs. 4.3–5 – 4.3–6. This particle size exhibits low deposition in the human respiratory system (ref. Fig. 1.4–1) and is therefore of less toxicological interest. In addition the distribution created by the aerosoliser was quite similar across the different CeO_2 and ZnO powder samples. Therefore it may be considered to be a reflection of the aerosol generation method, and may not fully indicate the range of aerosol sizes generated at source in ENP manufacturing plants or in workplaces. To tackle these shortcomings, it was decided to develop a ZnO furnace generator where Zn is first nucleated from Zn vapour and then oxidised in a second stage. The aim was to cheaply produce a ZnO aerosol with more controllable characteristics (mainly size) which could be used for toxicological studies, instrument testing and development.

4.2.2. Zn particle generator

The first step is to develop and test the initial Zn stage of the generator. The setup is shown in Fig. 4.2–1. A filtered nitrogen gas supply is fed through a furnace with an adjustable bypass. The total flow is measured after the filter with a rotameter and the

bypass flow is measured with a mass flow meter. In this text the total flow used was 0.3 l/min while the bypass was 0.2 l/min giving a sample flow through the furnace of 0.1 l/min. Zn powder is placed in a ceramic boat within the furnace (see Fig. 5.2–5). As the furnace temperature is adjusted the output is monitored with a Grimm 5.400 SMPS.

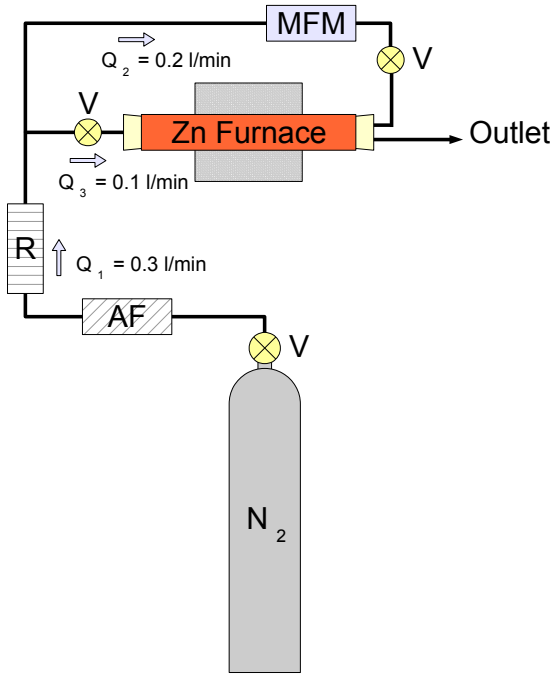

Figure 4.2–1. Zn generator setup. All nitrogen flow rates are indicated in litres/minute. The total flow is measured by a rotameter (R) between an air filter (AF) and the furnace. A bypass flow is measured with a mass flow meter (MFM) with the balance of flows controlled by valves (V).

4.2.3. ZnO particle generator

Next the oxidation stage is added to the setup as shown in Fig 4.2–2. Filtered ambient air is pumped into the system and the total flow is then fed through a second furnace to facilitate oxidation of the Zn. The total flow at the output is measured using a differential pressure flow meter (a mass flow meter is not suitable in this position due to their sensitivity to contamination). As before the output is monitored with a Grimm 5.400 SMPS system. The prototype generator is shown in Figs. 4.2–3 and 4.2–4.

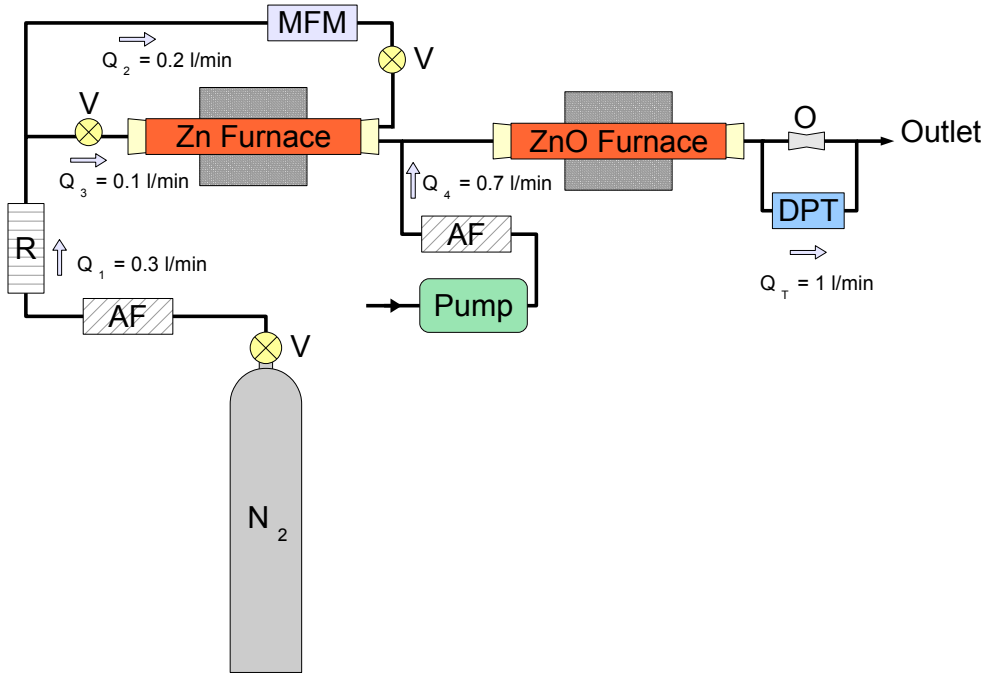

Figure 4.2–2. ZnO generator setup. All flow rates are indicated in litres/minute and all inputs are filtered through HEPA air filters (AF). The nitrogen input flow is measured by a rotameter (R) and the Zn bypass flow is measured with a mass flow meter (MFM) and controlled with valves (V) as before. Added to this is a filtered ambient air input to supply oxygen for the ZnO furnace while a differential pressure transducer (DPT) measures the total output flow.

Figure 4.2–3. ZnO Generator front panel.

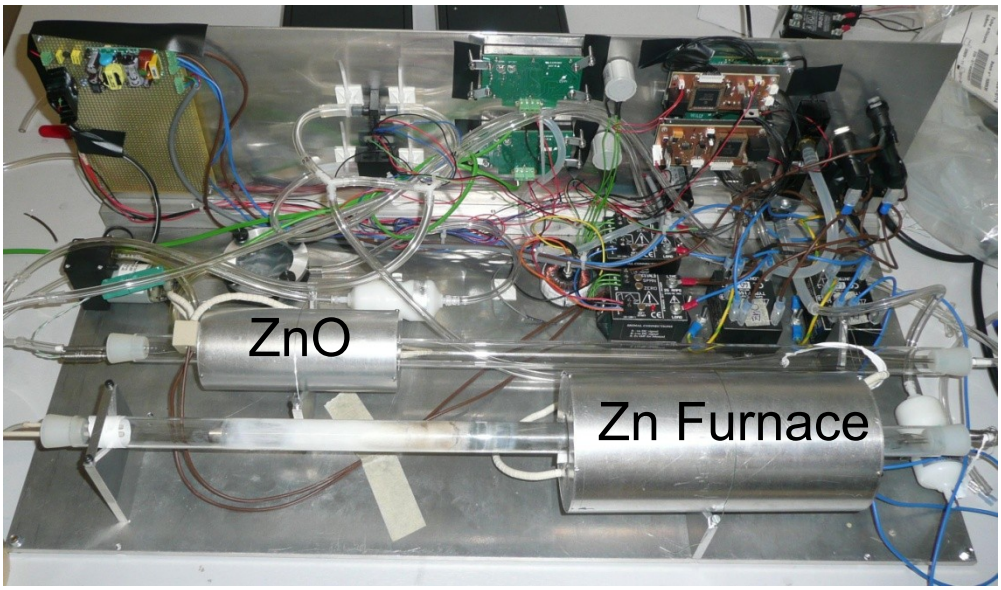

Figure 4.2–4. Inner workings of the ZnO generator.

4.3. SMPS measurements of ZnO and CeO_2 aerosols at NPL

4.3.1. Introduction

As part of the PROSPEcT project the seven ENP samples were aerosolised to allow the measurement of aerosol size distributions. This work was carried out in conjunction with the consortium member NPL (National Physical Laboratory, Teddington, UK) in their aerosol lab utilising the Naneum PA100 aerosoliser and NPS500 SMPS along with the NPL standard reference TSI SMPS and CPC.

The samples measured are detailed in Table I in Section 1.3.3.

4.3.2. Setup

The setup is shown in Fig. 4.3–1.

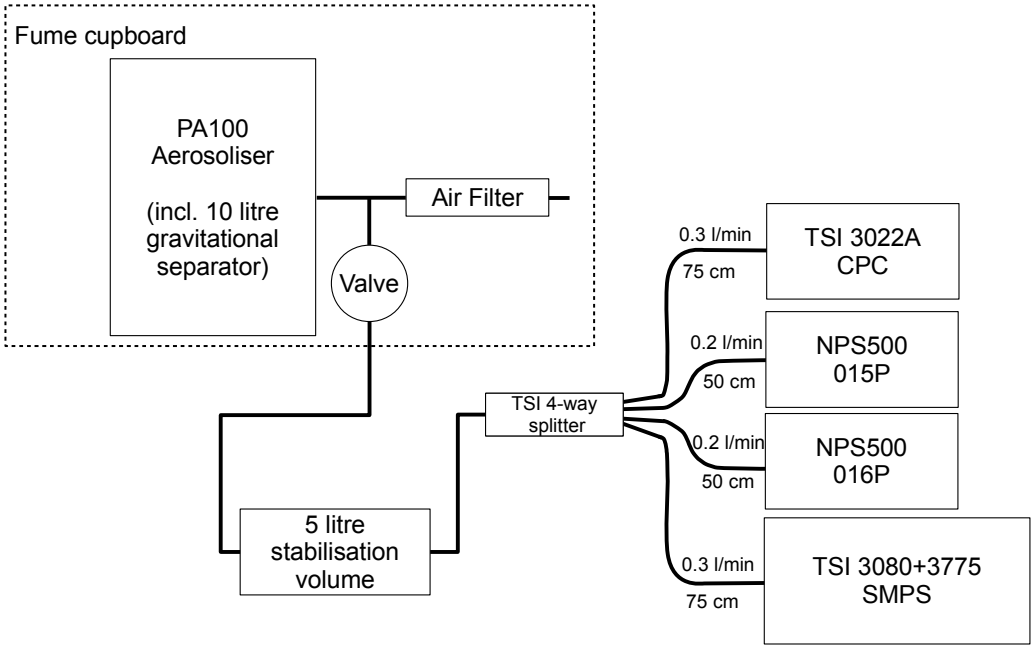

Figure 4.3–1. Setup for measuring airborne ENP samples. Powder samples are aerosolised in a PA100 aerosoliser from Naneum Ltd. An additional 5 litre stabilisation volume was added to the line to provide a more stable aerosol distribution. The sample is then split into 4 measurement lines by a TSI splitter. Tubing lengths and flow rates are shown to each of the measurement instruments.

The samples are loaded into a powder aerosoliser (PA100), Fig. 4.3–2, which creates an aerosol from the powder by directing a compressed clean gas supply through an array of small holes in a nozzle positioned an adjustable distance above the powder. The nozzle is designed to create strong vortices and shear forces in the gas flow which are effective at pulling apart particle agglomerates. The resultant aerosol is fed through a 10 litre internal stabilisation chamber and gravitational separator before being fed out of the PA100. From there the sample flow is split between a valve to switch on/off the sample flow to the measurement instruments and a filter to allow excess flow bleed off. The sample flow after the valve was directed to a second 5 litre stabilisation chamber before going to a four way splitter which distributes the sample evenly to the four measurement instruments (two NPS500, TSI CPC, TSI SMPS), Fig. 4.3–3. The tubing lengths to the different instruments were adjusted to compensate for the different flow rates in the instruments (0.2 l/min in the NPS500, 0.3 l/min in the reference instruments) so that particle losses would be equal in each case.

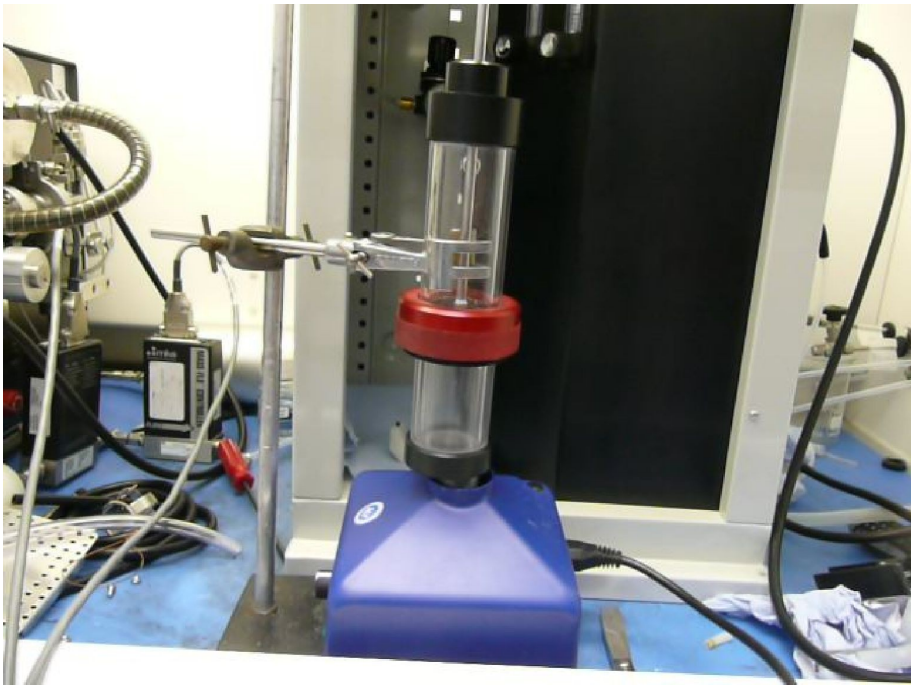

Figure 4.3–2. Modified PA100 aerosoliser setup. The sample chamber is placed on a shaker and lightly supported by a clamp.

During initial setup testing it was found that particles would build up on the internal walls of the aerosoliser chamber (see Fig. 4.3–4) and thereafter at irregular intervals these build-ups would collapse back into the aerosolisation zone causing bursts in the aerosol concentration output. To try and alleviate this issue and gain a more stable output a shaker was added to the setup underneath the aerosolisation chamber to act as an agitator. The shaker was set to perturb the chamber to reduce the amount of particle build-up on the chamber walls.

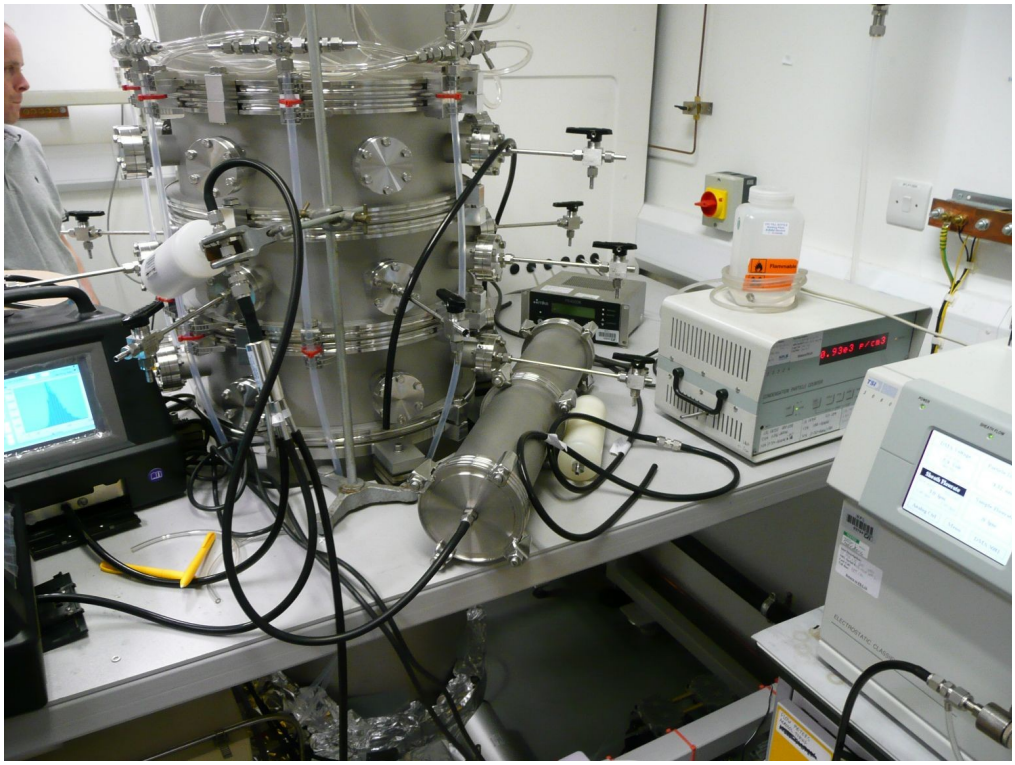

Figure 4.3–3. ENP aerosol measurement setup. The long cylindrical 5 litre stabilisation volume is shown centre leading to the 4-way splitter held aloft in a clamp to its left. The two NPS500s are shown in black cases on the far left hand side. The TSI SMPS is shown on the on the far right foreground while the TSI CPC is shown behind it to the right of the stabilisation volume.

While the addition of a shaker improved the output stability, the concentration still tended to exhibit increasing or decreasing trends. It was therefore difficult to pick out intervals of stable concentration for measurement. As the SMPS scans were set to be between 3 and 5 minutes in total length, it is important to have periods of stability to allow for a representative measure of the distribution. Both the NPS500 and TSI SMPS measure from small to large sizes. Therefore, if the particle concentration is increasing/decreasing during a scan then the distribution will be artificially shifted towards the larger/smaller sized particles.

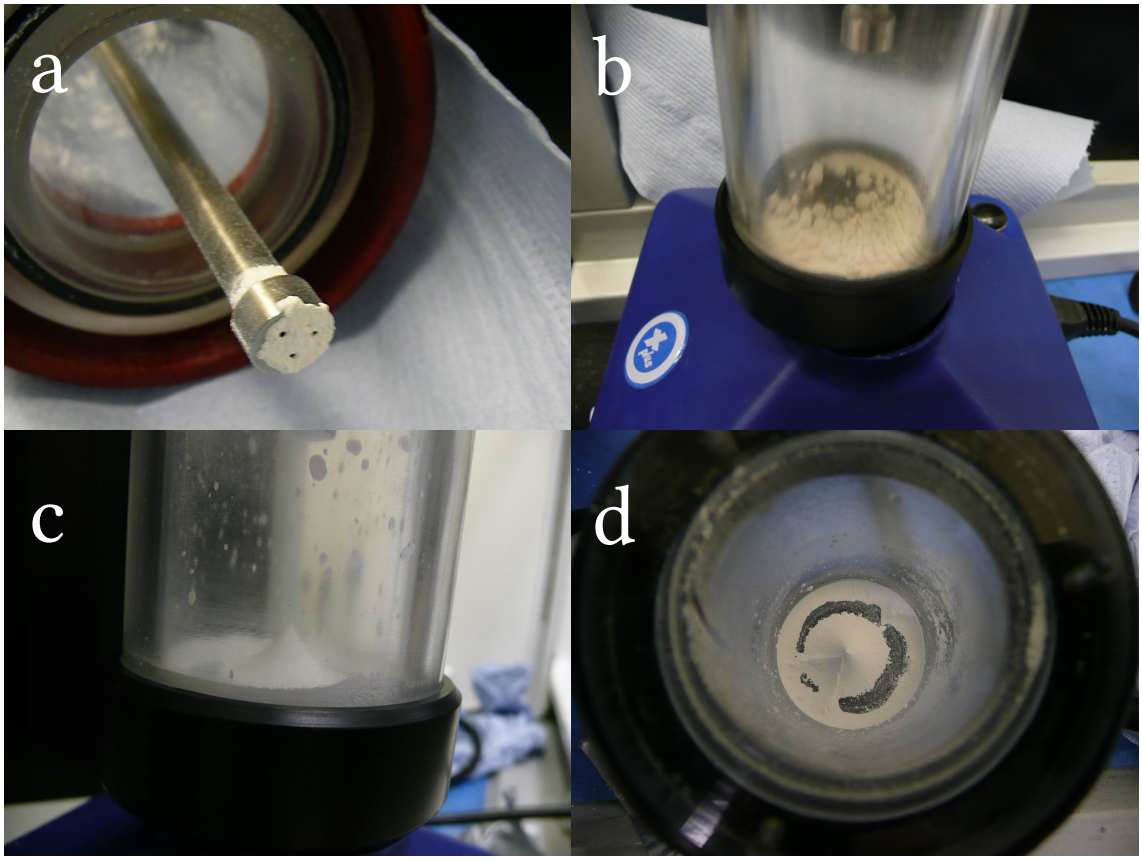

Figure 4.3–4. Operational points of interest when aerosolising ENP samples. (a) – powder build-up can be significant, even as far as coating the nozzle where the high pressure air vortices are emerging. (b) – some samples form large aggregated balls when jostled around by the shaker inside the sample chamber. (c) and (d) – during aerosolisation, some samples formed rigid conical structures at the base of the sample chamber.

4.3.3. Results

An example ZnO measurement is shown in Fig. 4.3–5 from sample NM-112. The TSI SMPS exhibits a peak in the 200 – 300 nm range and measures a much higher concentration than the NPS500s and over an order of magnitude higher than measured by the TSI CPC. Therefore the TSI SMPS results have also been corrected to give a matching concentration to that obtained from the TSI CPC, and denoted "TSI SMPS Corrected". The peaks measured by the NPS500s are found at a smaller size between 100 – 200 nm and measure a concentration somewhere between those from the TSI CPC and SMPS measurements.

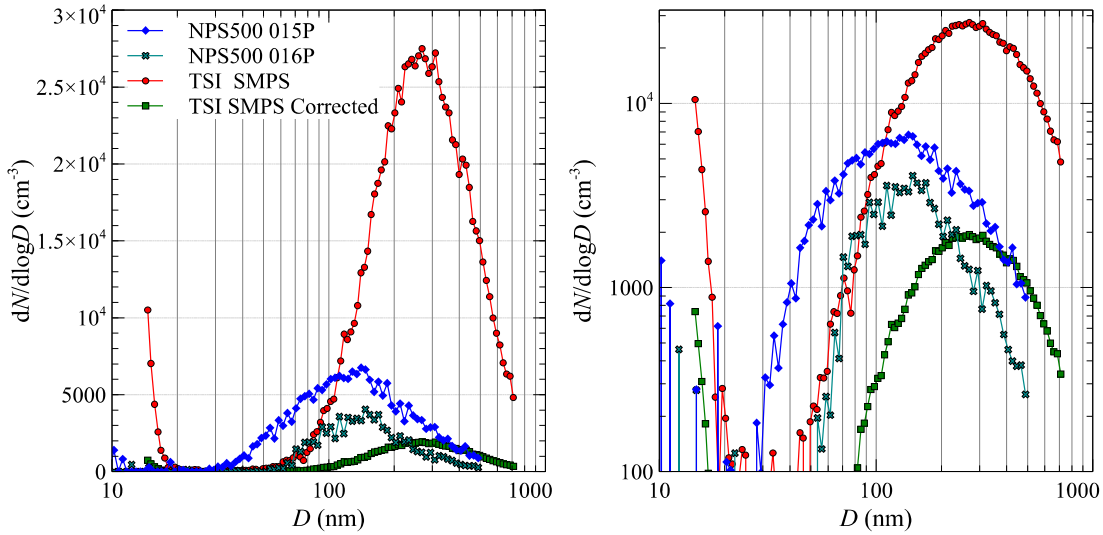

Figure 4.3–5. ZnO sample NM-112 as measured by two different NPS500s, a TSI SMPS and the same TSI SMPS with its concentration corrected to a reference CPC. The displayed distributions are an average from three sequential scans. Data is shown on a linear-log scale on the left and a log-log scale on the right.

An example CeO_2 measurement is shown in Fig. 4.3–6 from sample NM-211. The TSI SMPS shows a peak slightly above 200 nm and again measures a much higher concentration than the TSI CPC prompting the inclusion of data corrected to the CPC concentration for comparison. The distributions measured by the two NPS500 instruments in this case show quite different results. NPS500 015P exhibits a very broad distribution with a main peak around 70 – 80 nm and an additional peak around 15 nm with a total concentration slightly larger than that measured by the uncorrected TSI SMPS. NPS500 016P on the other hand shows some level of reasonable agreement to the corrected TSI SMPS results with a peak around 200 nm and a concentration about 50% higher than measured by the TSI CPC.

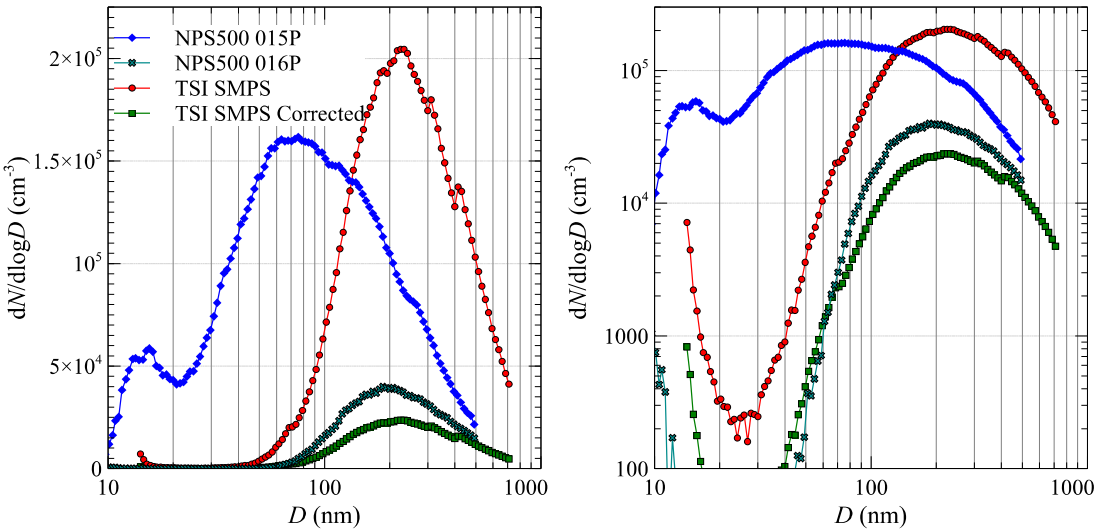

Figure 4.3–6. CeO_2 sample NM-211 as measured by two different NPS500s, a TSI SMPS and the same TSI SMPS with its concentration corrected to a reference CPC. The displayed distributions are an average from 15 sequential scans. Data is shown on a linear-log scale on the left and a log-log scale on the right.

The full set of results as measured by the TSI SMPS are shown in Fig. 4.3–7 and Fig. 4.3–8 below. The data has been fitted with a lognormal peak in each case and the resulting geometric mean sizes and geometric standard deviations (σ_g) are shown in Table II.

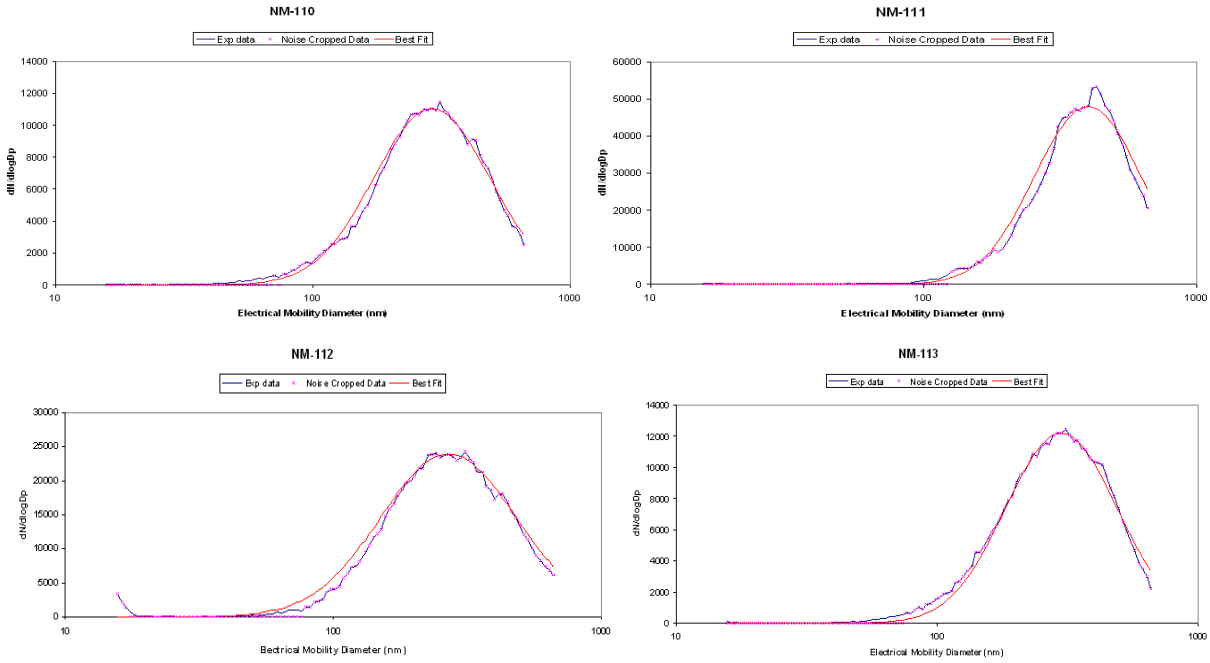

Figure 4.3–7. ZnO samples as measured by the TSI SMPS and lognormal peak fits.

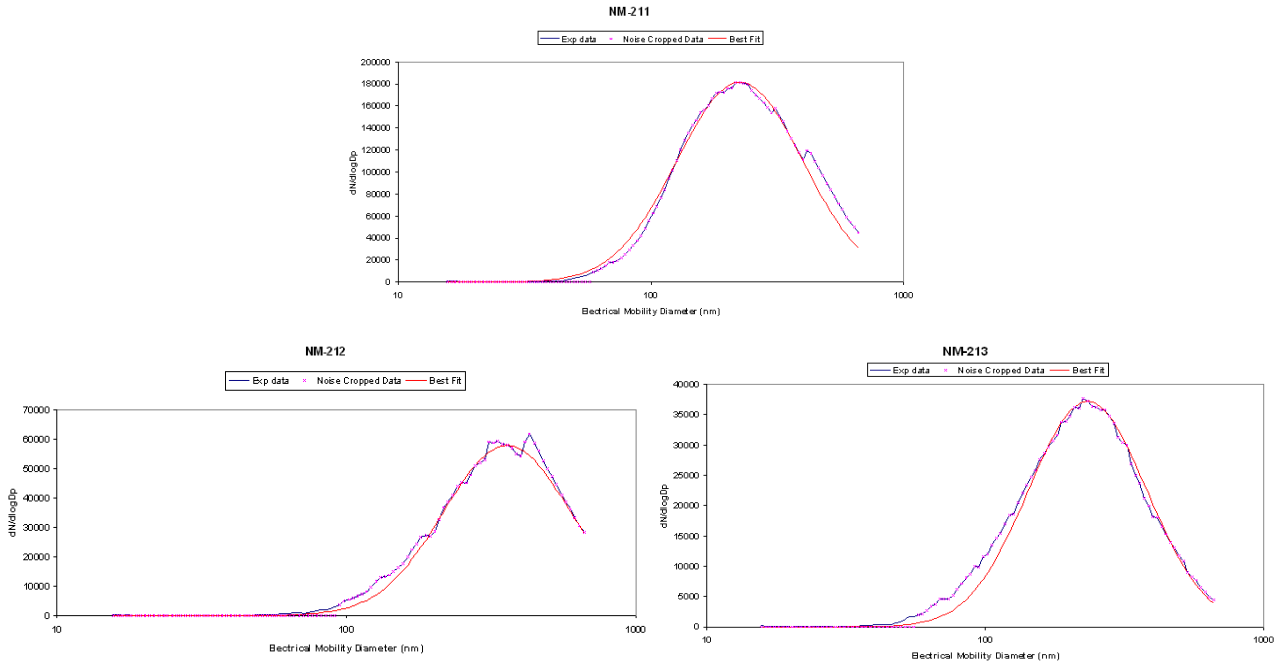

Figure 4.3–8. CeO_2 samples as measured by the TSI SMPS and lognormal peak fits.

	Sample	Geometric Mean Particle Size	Geometric Standard Deviation of log-normal fit
ZnO	NM-110	289 nm	1.68
	NM-111	400 nm	1.57
	NM-112	269 nm	1.80
	NM-113	300 nm	1.63
CeO_2	NM-211	225 nm	1.77
	NM-212	359 nm	1.66
	NM-213	233 nm	1.63

Table II. Geometric mean particle size of the different aerosolised PROSPEcT powders as measured by lognormal peak fits to the data from a TSI SMPS 3936.

4.3.4. Discussion

Despite there being seven different samples of ZnO and CeO_2 the measured aerosol distributions were all somewhat similar with broad peaks centred around 200 – 400 nm as measured by the TSI SMPS. This suggests that it is difficult to break these particles apart down to their constituent primary particle size (in the nano range for most of these samples). It may therefore be considered that these results are more significantly a reflection of the aerosol generation method. However, the sizing result is in line with other methods used on these powder samples in the PROSPEcT consortium, suggesting

that there is some generality to this result, and that the particles are likely to exist in this size range in different conditions and states. It is interesting, and perhaps not surprising, that the largest sized aerosol is given by the coated sample Z-COTE HP1 (NM-111).

The shift in the size distributions measured by the NPS500 instruments is expected due to them not having a multiple charge correction algorithm as is carried out in the TSI SMPS. However, the widely varying concentrations as measured across all four instruments used here is more surprising. It is not clear what might have caused this, although the comparatively large size and high concentration of these particles may have resulted in issues such as build-up in sampling or internal aerosol lines or saturation of the optical particle counters in the CPCs of the instruments.

4.3.5. Conclusion

The PROSPEcT ENP samples have been successfully aerosolised, with the resulting aerosol distributions measured in synchrony by three SMPS type instruments and a stand-alone CPC. The size distributions as measured by the TSI SMPS are considered more reliable compared to those from the NPS500s due to the multiple charge algorithm in the TSI instrument and its long established history compared to the marginally developmental NPS500. The large differences seen in the concentrations measured, especially between the TSI SMPS and TSI CPC, reinforces the view that SMPS instruments cannot always be considered to be a reliable measure of concentration. However, the main purpose of this work was to measure the size of particles generated to understand how they might be encountered in occupational or environmental exposure scenarios. As such the results shown in Table II are a successful outcome and can be used to inform future studies or risk criteria.

4.4. Raman analysis

4.4.1. Raman characterization of PROSPEcT samples

As a first step to realizing a Raman approach to ENP detection, the Raman spectra of all the PROSPEcT ZnO and CeO_2 samples were measured with two different available Raman systems: the University of Kent's Dilor Remote Raman Microscope, and an Ocean Optics QE Raman spectrometer on loan from a distributor. The Ocean Optics device is interesting in that it is a small bench top unit which is extremely portable and easy to use. It could therefore be considered for use in site testing and workplaces to provide quasi-online characterisation of aerosol samples collected e.g. by personal samplers worn by workers.

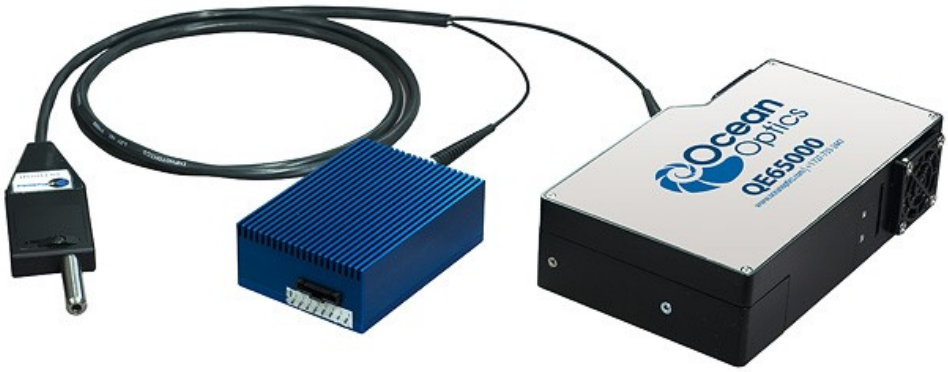

Figure 4.4–1. Ocean Optics miniature desktop Raman system which incorporates a probe, 785 nm laser source and QE65000 spectrometer.

The two Raman systems investigated for their potential in identifying CeO_2 and ZnO samples – a Dilor Remote Raman Microscope and an Ocean Optics miniature desktop Raman system (QEB0306 – Fig. 4.4–1) utilise source wavelengths of 632.8 nm and 785 nm respectively.

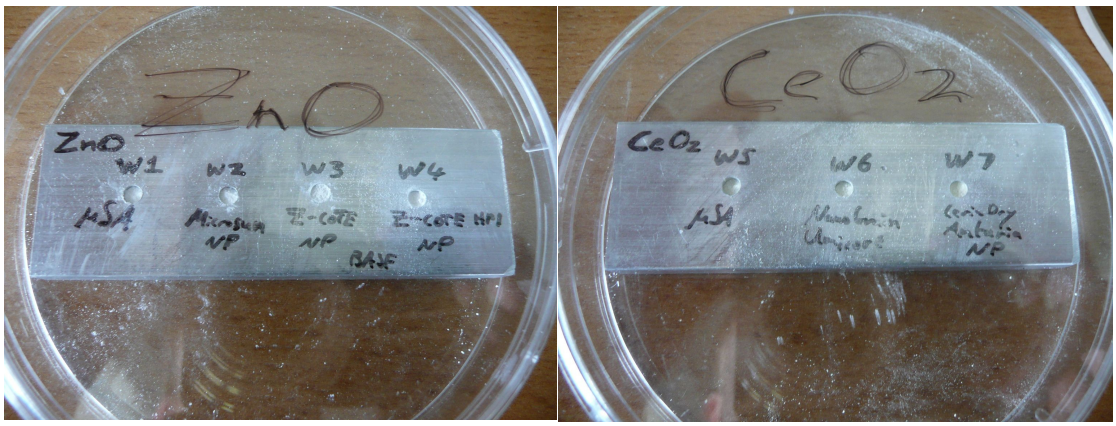

Figure 4.4–2. Aluminium blocks with powder sample wells for Raman analysis.

Aluminium test blocks where made for holding the powder samples for Raman analysis as shown in Fig. 4.4–2. All samples were analysed by both Raman systems available to compare their performance. Example spectra from the first sample (micron sized ZnO from Sigma Aldrich) are shown in Fig. 4.4–3.

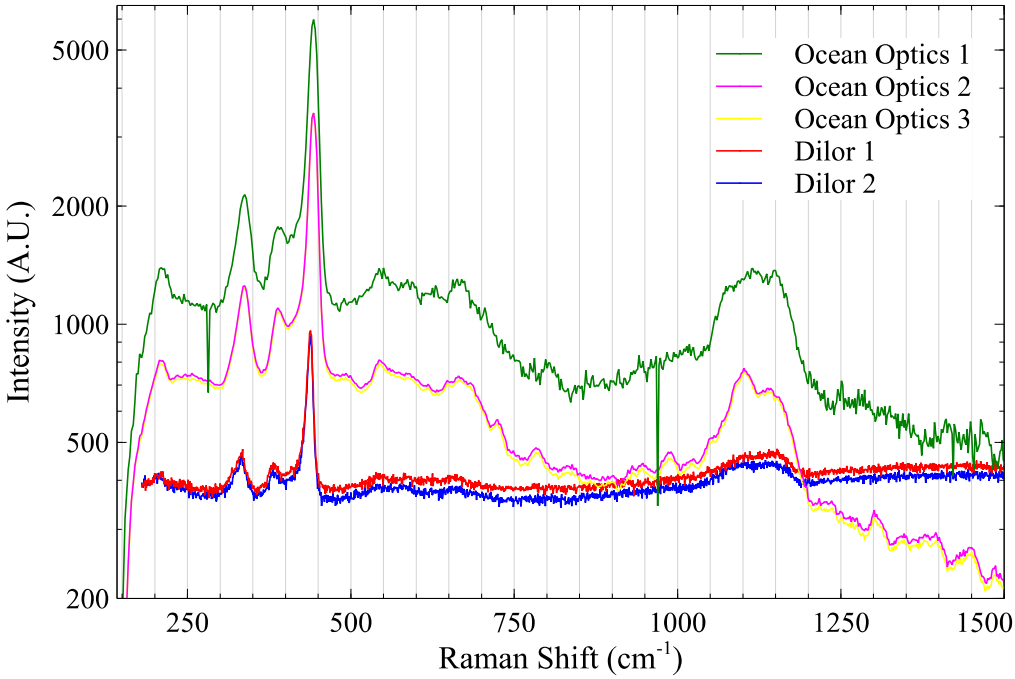

Figure 4.4–3. Example of ZnO spectra from the Sigma Aldrich sample achieved with a Dilor Remote Raman Microscope (UKC) compared to those achieved with an Ocean Optics QE Raman spectrometer.

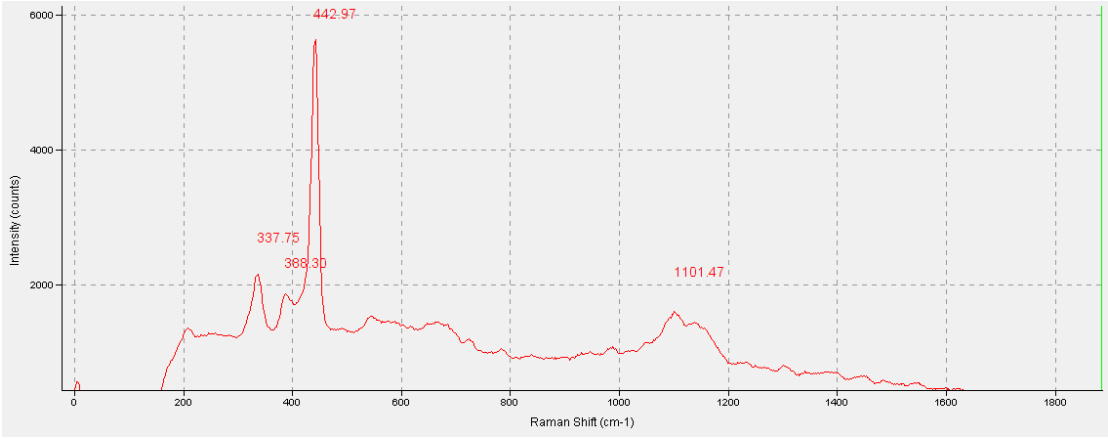

Figure 4.4–4. Detail of one of the ZnO spectra achieved with the Ocean Optics QEB0306 with peak positions marked.

Although the Ocean Optics spectrometers exhibited 3 – 4 times lower resolution, the higher signal to noise ratio yielded much clearer spectra compared to those achieved with the Dilor system (e.g. Fig. 4.4–4). In addition, the Ocean Optics device was easier to use and quicker to run due to its compact nature. However, the integrated microscope on the Dilor system can be a significant advantage.

4.4.2. Raman spectroscopic mapping analysis of aerodynamically size selected samples

Image analysis is applied to Raman spatial maps to quantify the number of particles and particle sizes present. By consideration of the sampling system and measurement time, these data can then be related back to what was originally present in the air. Glass slides are used as a sampling substrate, which give a complex Raman background spectrum to test the discrimination efficacy. In addition, in combination with a choice of larger agglomerates for analysis, the use of glass slides allows for validation of the approach by utilising optical microscopy as a reference method for discriminating the particles of interest. Immediately prior to collection of the Raman data, equivalent analysis is also applied to the optical microscopy images acquired from the same sample area. The results for the particle counts and sizes from the Raman maps are then compared to those obtained with optical microscopy. This provides a proof of concept study for the presented technique. However, in principle optical measurements are not required, and hence their use does not represent a restriction on the applicability of this approach in general.

Here ZnO particles (considered as agglomerated nanoparticles or nano-structured microparticles) are used as a test case material.

4.4.2.1. Methods

The sampling setup is shown in Fig. 4.4–5. The test aerosol is generated from ZnO powder (NM-113–Sigma-Aldrich 205532) using a modified Naneum PA100 aerosoliser. In the above measurements with an SMPS, the aerosolised powder is found to form an airborne state with a geometric mean particle size of 300 nm and geometric standard deviation of 1.63 (see Table II). However, the underlying size distribution is not considered to be important for this proof of concept study. The setup is designed to provide a stabilized ZnO aerosol flow to two measurement instruments: (i) a ‘TSI 3007 CPC’, which is used to monitor the total concentration and (ii) a ‘Nano-ID® Select’, which provides size segregated samples. The size bins available on the ‘Nano-ID® Select’ are detailed in Table III. The impaction stages collect narrow bands of aerosol particles deposited along the centre of the chosen substrate (here standard glass microscopy slides), as shown in Fig. 4.4–6. A number of sampling runs provided a range of deposited concentrations.

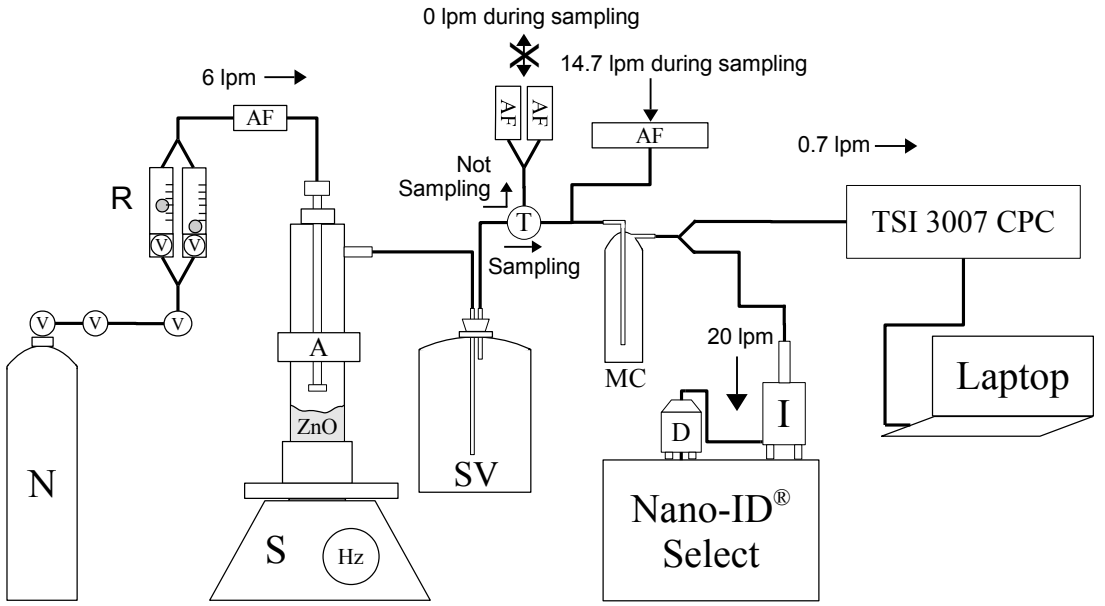

Figure 4.4–5. Sampling setup. N – Nitrogen tank; V – valve; R – rotameter; AF – air filter; A – aerosoliser; S – shaker, run at 15 - 20 Hz; SV – Stabilization Volume of 18.9 litres; T – three-way switching valve; MC – Mixing Chamber. I – impactor stages on Nano-ID® Select; D – diffusion net stages on Nano-ID® Select (not used apart from final filter stage).

Size Stage #	**1**	**2**	**3**	**4**	**5**	**6**	**7**	**8**	**9**	**10**	**11**	**12**
Min. cut-off diameter	20	8.1	4.0	2.0	1.0	0.5	0.25	60	15	5	1.5	1
Max. cut-off diameter	~35	20	8.1	4.0	2.0	1.0	0.5	250	60	15	5	1.5
	Impaction stages (size in µm)							Diffusion stages (size in nm)				

Table III. Aerodynamic diameter ranges of the Nano-ID® Select sampling channels. The impaction stages show the lower d_{50} size cut-off with the upper size limit being set by the preceding stage or by the inlet geometry for the first stage. The diffusion stages are ordered in the reverse pattern in the flow path with the smaller particles being removed first.

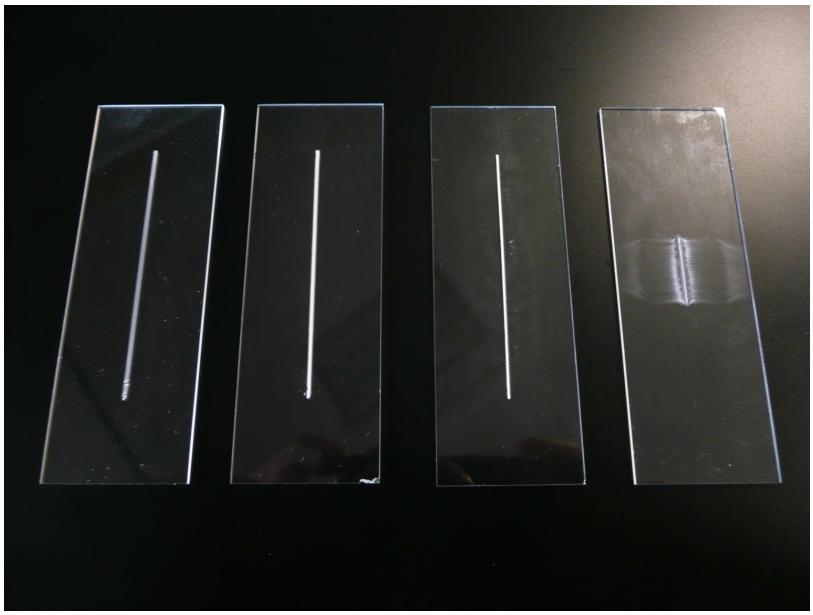

Figure 4.4–6. Example sample set from run H (detailed in Table IV in Section 5.4.1) showing impactor stages 4 – 7 from left to right which correspond to aerodynamic equivalent diameter ranges 2 – 4 μm, 1 – 2 μm, 0.5 – 1 μm and 0.25 – 0.5 μm respectively. The smearing evident in stage 7 is as a result of overloading of the stage causing particle bouncing and should be avoided.

Raman data is collected using a Horiba LabRam-HR with an external 473 nm excitation laser and ×50 objective lens. Simple line scans were first carried out to verify that particles could be distinguished from background from the resulting Raman spectra. An example is shown in Fig. 4.4–7. Raman spectra are collected from a series of points along a line which crosses over different regions of either ZnO or glass. By plotting the resulting spectral data as a contour map as shown in Fig. 4.4–8, it can be seen that there is potential to distinguish ZnO particles from background by their characteristic spectral signatures. In this example, ZnO is most simply characterised by its 435 cm^{-1} feature (Fig. 4.4–8 (a)) while glass is most easily distinguished from its 1100 cm^{-1} feature (Fig. 4.4–8 (b)).

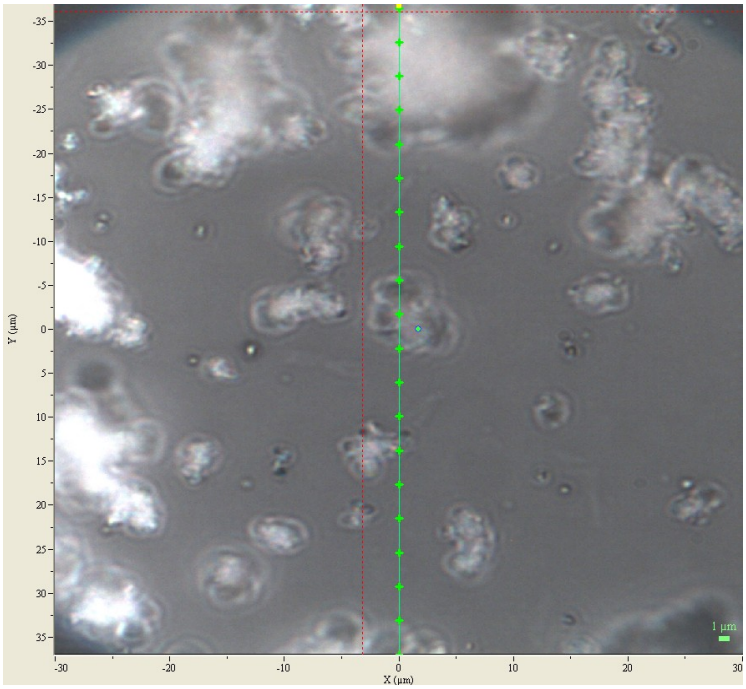

Figure 4.4–7. Example Raman line scan across ZnO particles on a glass slide. A Raman spectrum is collected from each of the points marked with a cross.

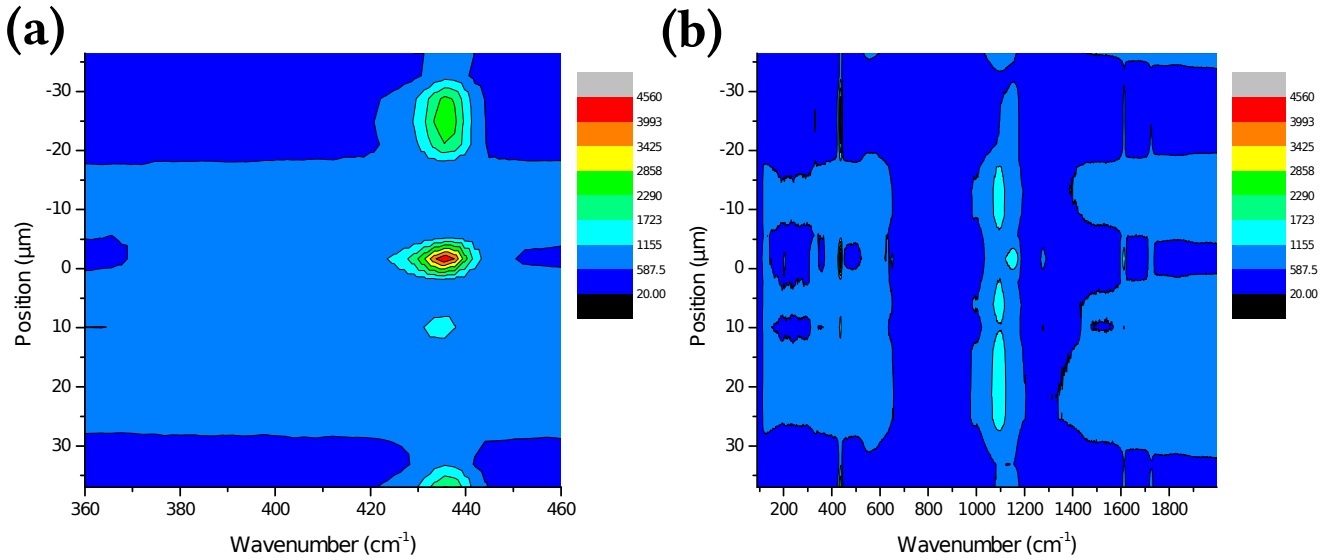

Figure 4.4–8. Contour maps of the resulting Raman spectra collected from the line scan shown in Fig. 4.4–7. The Raman signal intensity is colour coded from blue (low signal) to red (high signal). The data is magnified in (a) around the region of the main ZnO Raman peak at ~435 cm^{-1}, while the entire range is shown in (b).

Next, Raman data was collected from 31 × 31 point grids with a 2 μm spacing between each point. Particular spectral features indicative of ZnO were chosen, and their intensity mapped to either a greyscale or colour (with different component contributions) pixel value for each measurement point on the grid. Combining these pixels into a single image yields a resulting Raman map, showing the distribution of the chosen spectral features (and hence compound of interest) in the chosen grid area. Sample slides were positioned and focussed using an integrated computer controlled stage. Starting from a lengthwise central point on the edge of the slide, where the xyz stage coordinates were zeroed, the total width of the slide ('y-value') was measured using the xyz microscopy stage readout. This y-value was then divided by 2 and then input into the stage positioning software to give a centrally chosen point without any preview, avoiding any researcher bias. Sample areas were imaged using an optical microscope and an integrated white light source in transmission mode. Horiba's 'Lab-Spec 5' software was used for data acquisition and generation of contour maps to identify ZnO particles based on their 435, 1613 and 1724 cm^{-1} Raman peaks (see Fig. 4.4–10) in the ZnO Raman spectrum (Alim *et al.*, 2005).

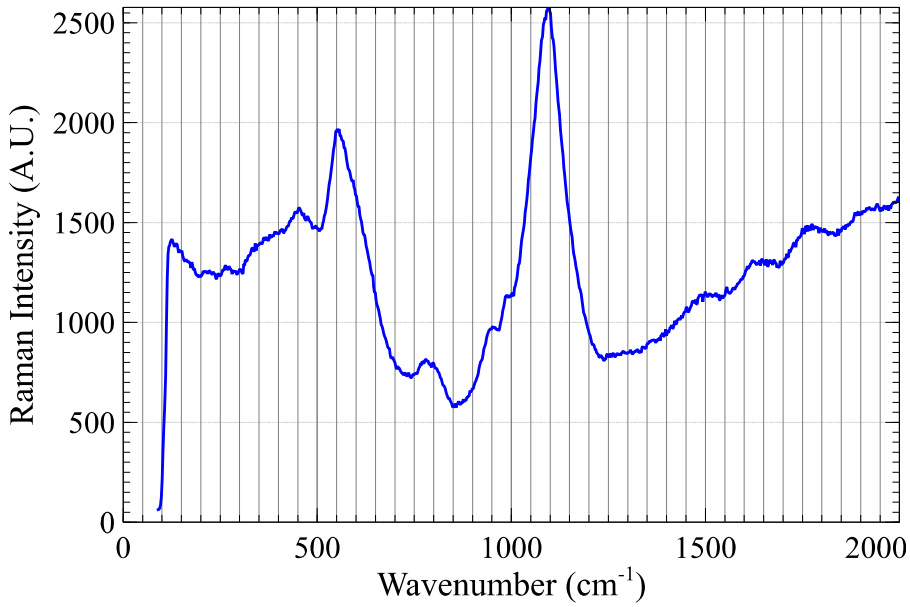

Figure 4.4–9. Example background Raman spectrum measured from a clean glass slide. The SiO_2 line is dominant at 1100 cm^{-1} and is still clearly apparent when measuring ZnO particles on the slide as seen in Fig. 4.4–8 (b).

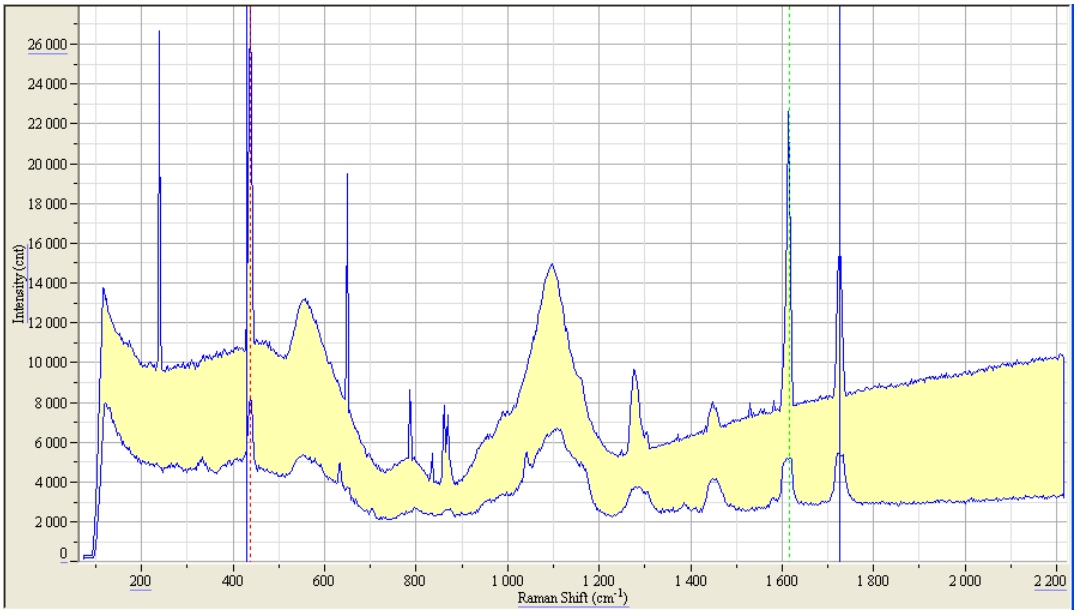

Figure 4.4–10. Example range of ZnO Raman spectra obtained from the measurement grid used on sample C4 (ref. Fig. 5.4–1). The plot shows the limits from all of the 961 individual spectra measured from the grid positions. The Stokes peaks used to distinguish ZnO particles from background in the resulting data maps are marked at 435, 1613 and 1724 cm^{-1} respectively. Note that these latter two peaks are found to be associated with the ZnO particles only in these impaction samples, and did not appear in the spectra from powder well samples. Therefore they may be related to some surface contaminant on the ZnO particles picked up during the sample aerosolisation, impaction or subsequent handling of the sample.

The image processing package 'Fiji' (distribution of 'ImageJ' – Abràmoff *et al.*, 2007) was used to process the microscope images, to produce Raman contour maps, and to carry out counting and sizing analyses. Counts were also performed by eye with the aid of a cell counter plug-in to mark particles and keep track of counts. The results of this manual count were compared to those obtained with the semi automated process. Software analysis involved processing and thresholding the images to allow a particle analysis algorithm to distinguish and demarcate particles from background. Firstly the scale is measured off the image and applied to the image such as to provide the software with a conversion from pixel values to distance in micrometres. The full field of view of the particles is then selected, and a 4 pixel median filter is applied to smooth out noise and artefacts while retaining the edge sharpness of the particles. The contrast and brightness of the image is optimised before converting it to 8-bit greyscale. A threshold is then applied to create a binary distinction on the image between "particles" and "background". The resulting image is then selected again and Fiji's "Analyze Particles" routine can then be run with the necessary restrictive parameters on acceptable limits of particle size (e.g. 0.35 – infinity μm^2) and circularity (defined as $4\pi\{area/perimeter^2\}$ – e.g. 0.1 – 1). The output can then be set to display the measured outlines of particles as well as measured counts, sizes and other parameters. For the purposes of this study it was decided to use the measured area and convert it to a single, circular equivalent size parameter "d_{equiv}". Counts and sizing were compared between the Raman and microscopy data. In the case of optical microscopy results, this routine will characterize

any and all particles visible on the substrate. However, when the same routine is utilized on Raman maps, it can be used to measure only the particles of interest from the relevant Raman peak(s). An overview of the entire process is presented in Fig. 4.4–11.

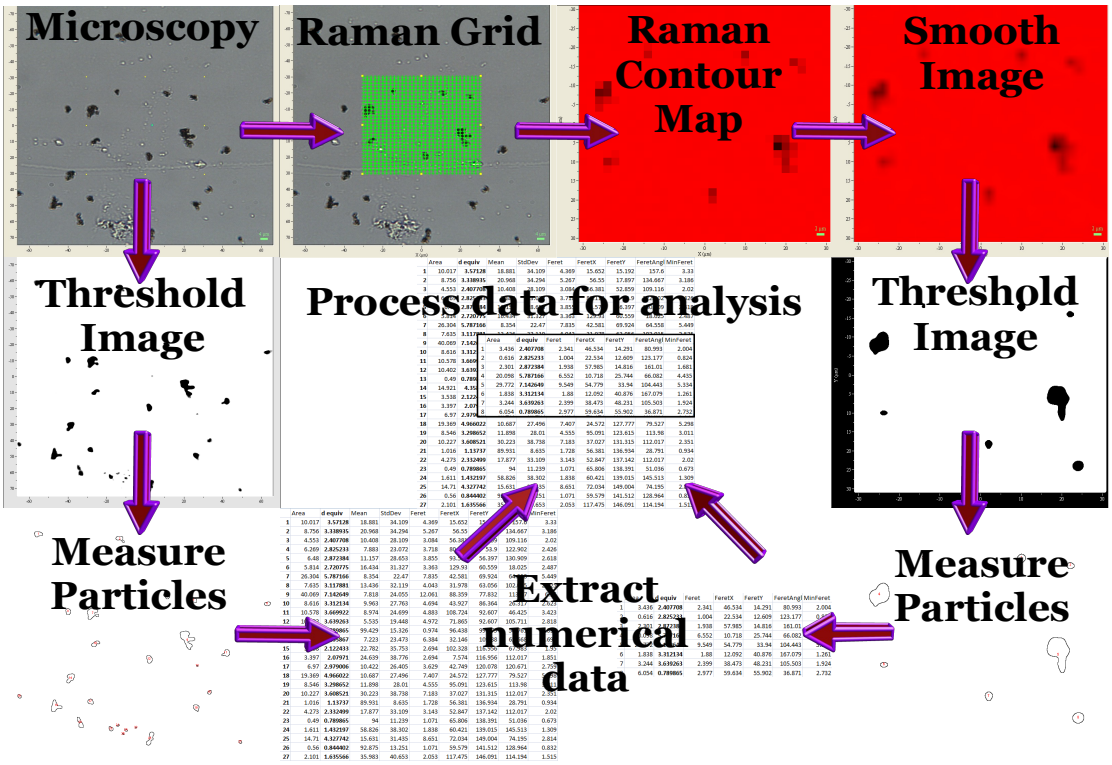

Figure 4.4–11. Overview of the routine used to process microscopy and Raman images starting from the top left. The same example data set is shown to illustrate each step.

In this proof of concept study, we examine ZnO particles on a glass substrate that gives a significant Raman background (see Fig. 4.4–9), on which the ZnO signal has to be positively identified. This allows us to assess the effectiveness of the Raman data in measuring the size and number of particles present by direct comparison to the optical microscopy results. The validation approach employed for this study requires the case where the compound of interest is optically distinct from the background, such that the data can be correctly correlated between the Raman and optical microscopy data. However the optical microscopy data is not in general required and therefore is not a limitation on the applicability of the overall approach.

4.5. Surface sensitive heterogeneous nucleation

4.5.1. Surface sensitivity

The different regimes of nucleation discussed in Section 3.3 are summarised in Fig. 4.5–1 below. In supersaturated conditions the new phase can form spontaneously within a single component system (homogeneous nucleation). At lower saturation levels nucleation can still form on a seed material due to the reduction in the free energy barrier by a factor $f(\theta)$ (heterogeneous nucleation). In highly saturated conditions, as usually used in CPCs, the probability of heterogeneous nucleation will be close to 1 and will be independent of the seed particle size above a certain cut-off size (d_{min}). However here we also consider the case of much lower saturation conditions, close to the onset of heterogeneous nucleation. In this case the probability of nucleation will now exhibit a square dependency on particle size – i.e. it is surface area sensitive.

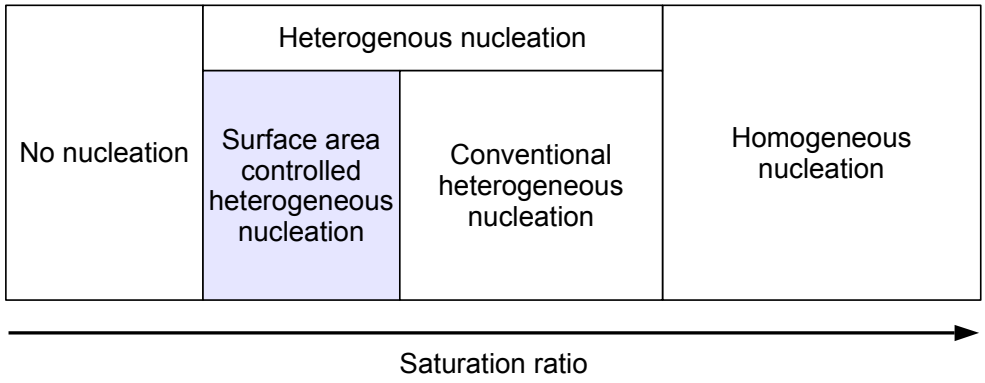

Figure 4.5–1. Schematic of nucleation zones at various deviations from equilibrium.[§]

To experimentally test for the surface area controlled nucleation regime, a surface area sensor was developed to allow fine control over the saturation conditions. The sensor consists of a saturator to create a fluid vapour from dimethyl benzene-1,2-dicarboxylate (DBD), a condenser to form the saturation conditions, and an optical particle counter to count the DBD droplets formed on seed aerosol particles fed in at the inlet. The condenser was made of a 150 mm long stainless steel tube, with a 6.7 mm ID, with the temperature controlled either with a fan (initially), or with a Peltier thermoelectric cooler for finer control. Porous silica (pore diameter 2.5 μm) soaked with DBD was heated in the saturator by an electrical heater. The finer details cannot be revealed here due to their commercial sensitivity.

The sensor can be operated as a normal CPC at higher saturation conditions. However, here it is used at much lower saturation conditions to probe for a surfacing response. The level of saturation of DBD was controlled by varying the temperature of the saturator.

To test the response of the surface area sensor, monodisperse fractions of a generated aerosol selected by the planar DMA are fed to both the surface area sensor and a reference CPC as shown in Fig. 4.5–2.

§ Reproduced with permission from Steer *et al*., 2012.
Copyright 2012, AIP Publishing LLC.

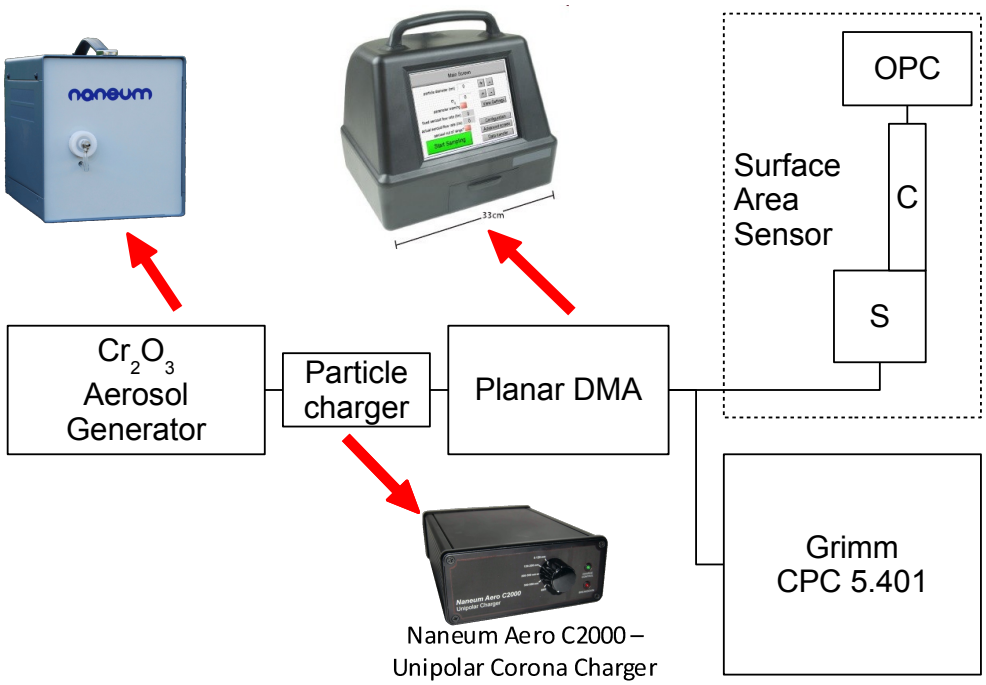

Figure 4.5–2. Schematic used for testing the response as a function of size of the surface area sensor compared to a reference CPC. S – saturator, C – condenser, OPC – optical particle counter. The particle charger can be either a radioactive source such as Am-241 or a corona charger as shown here. The working fluid used in the saturator is dimethyl benzene-1,2-dicarboxylate (DBD), and the OPC is an off-the-shelf device (RNet, Particle Measuring Systems Inc.).

The probability of heterogeneous nucleation was calculated as the ratio of the counts measured by the surface sensor to the number measured with the Grimm CPC. The saturation ratio was calculated using the finite element software COMSOL Multiphysics®. The physical properties of DBD were taken from Berger *et al*. (2002).

4.5.2. Testing the principle

Examples of the change in nucleation response with reduced saturation ratios are shown in Fig. 4.5–3. Conventional heterogeneous nucleation shows little dependency on the seed particle size above a sharp cut-off. However, reducing the saturation conditions reveals a square response against particle size. The position of this response can be seen to depend both on the saturation ratio chosen and on the type of aerosol particle measured. This is due to the surface chemistry of the different components which influence $f(\theta)$.

§ Reproduced with permission from Steer *et al*., 2012. Copyright 2012, AIP Publishing LLC.

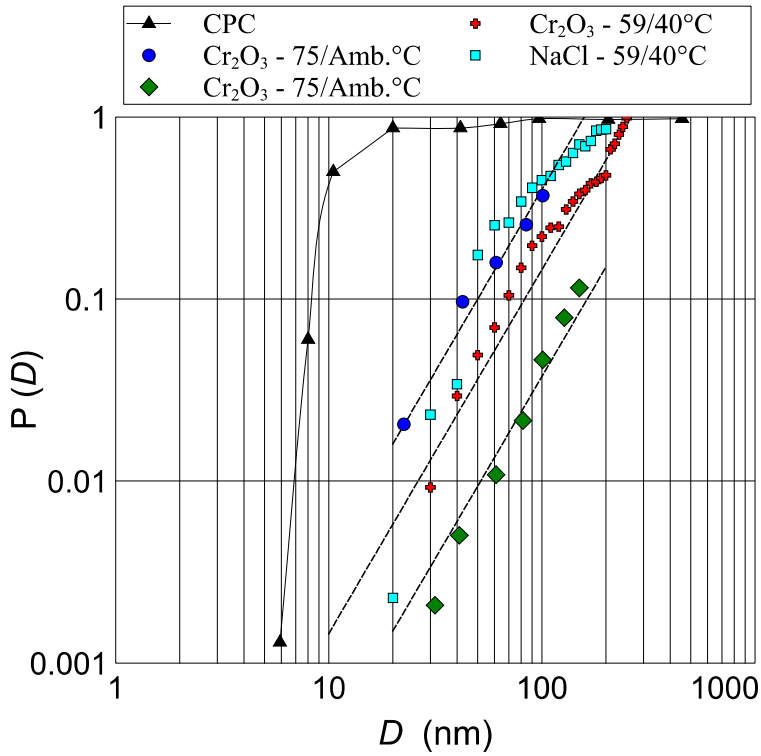

Figure 4.5–3. The probability of heterogeneous nucleation vs. aerosol particle size. Fully developed heterogeneous nucleation with a high saturation ratio as used in CPCs is shown for reference with black triangles and a solid line. The surface controlled regime using a much lower saturation ratio as measured with DBD working fluid is shown for Cr_2O_3 and NaCl particles under different conditions of saturator/condenser temperatures. "Amb." indicates a condenser temperature held at instrument ambient with a fan. The lower set in this case (green diamonds) have been measured after a longer period of operation and therefore with a higher instrumental ambient temperature. The 40°C condenser temperature data have been controlled with Peltier thermoelectric heaters/coolers. Square response fits are shown with dashed lines.

It is therefore a requirement of this technique to first make measurements of the nucleation probability for the aerosol that is to be tested, and thus find the requisite saturation conditions necessary to produce a surface sensitive response. This can be done by comparing the counting efficiency as a function of size for the surface sensitive device to that given by a CPC (assumed to have a counting efficiency of 1 above the cut-off size). It is also evident that both the condenser and saturator temperatures need to be well controlled in order to provide a repeatable response.

4.5.3. Surface area prototype

Following successful demonstration of the surfacing principle, the surface area sensor was incorporated into a prototype device. This utilises a corona particle charger as well as the planar DMA as a sizing front end to provide a complete package for measuring the surface area distribution of nanoparticle aerosols. The final prototype device is shown in Fig. 4.5–4.

Figure 4.5–4. Surface area prototype instrument during testing. The y-splitter visible at the inlet is providing an equal aerosol split between the prototype instrument and in this case a Grimm CPC at the edge of the field of view to the right. The condenser temperature is controlled by the temperature controllers to the left of the main screen whereas the saturator temperature is controlled via the main software interface operated through the touch panel.

4.5.4. Calibrating the surface area prototype

One of the biggest challenges in developing an online aerosol surface area sensor is the lack of a reliable reference technique. Due to the different particle loss mechanisms associated with DMA/SMPS-like systems they are difficult to calibrate from first principles. Also, as there is no prior technology considered reliable for the measurement of aerosol surface area distributions *in situ*, it creates a problem for finding a reference method or instrument for this technique. At larger sizes, spherical particles (e.g. polysterence-latex or liquid droplets) could be used and referenced to SMPS measurements from which the surface area distribution can be correctly calculated based on the spherical particle assumption. However, as both techniques rely on electrical mobility (DMA) techniques for sizing, they both suffer complications of multiple charging at these sizes. At smaller sizes however (e.g. < 100 nm), it is more difficult to generate a source of reliably spherical particles.

Therefore a first step / approximate calibration has been employed here. This interim approach adjusts the overall surface area concentration (distribution height / total area) with a linear correction and was undertaken as follows. A calibrated SMPS was used as a reference device. Particle size distributions were generated, stabilised, and split

equally between the surface area device (surface area sensor plus DMA) and the reference SMPS. The distributions from the reference SMPS were converted to calculated surface area distributions assuming spherical particles. A correction factor is then calculated to adjust the measured total surface area (integrated distribution) to be the same as the reference calculated total surface area. It is a simple linear correction to the overall height of the distribution, to approximately account for the losses in the system, but has no effect on the shape of the distribution. Clearly this is of limited validity if the particles are not spherical, as other particle shapes, especially fractal structures, could have considerably higher surface areas. However, this correction will still go some way towards correcting for losses in the system (e.g. charging efficiency and particle losses to tubing walls due to diffusion or inertial effects). These need to be taken into account as in an SMPS system and will set a lower boundary limit on what the true surface area is.

Chapter 5. Results and discussion

5.1. Differential mobility analyser

5.1.1. Comparison of theory to data

Experimental results (data points) are compared to theoretical curves (lines) at five different flow rates in Fig. 5.1–1 below. Theoretical data were calculated according to Equation 24 with NTP (normal temperature and pressure, 20 °C and 101.325 kPa) system parameters.

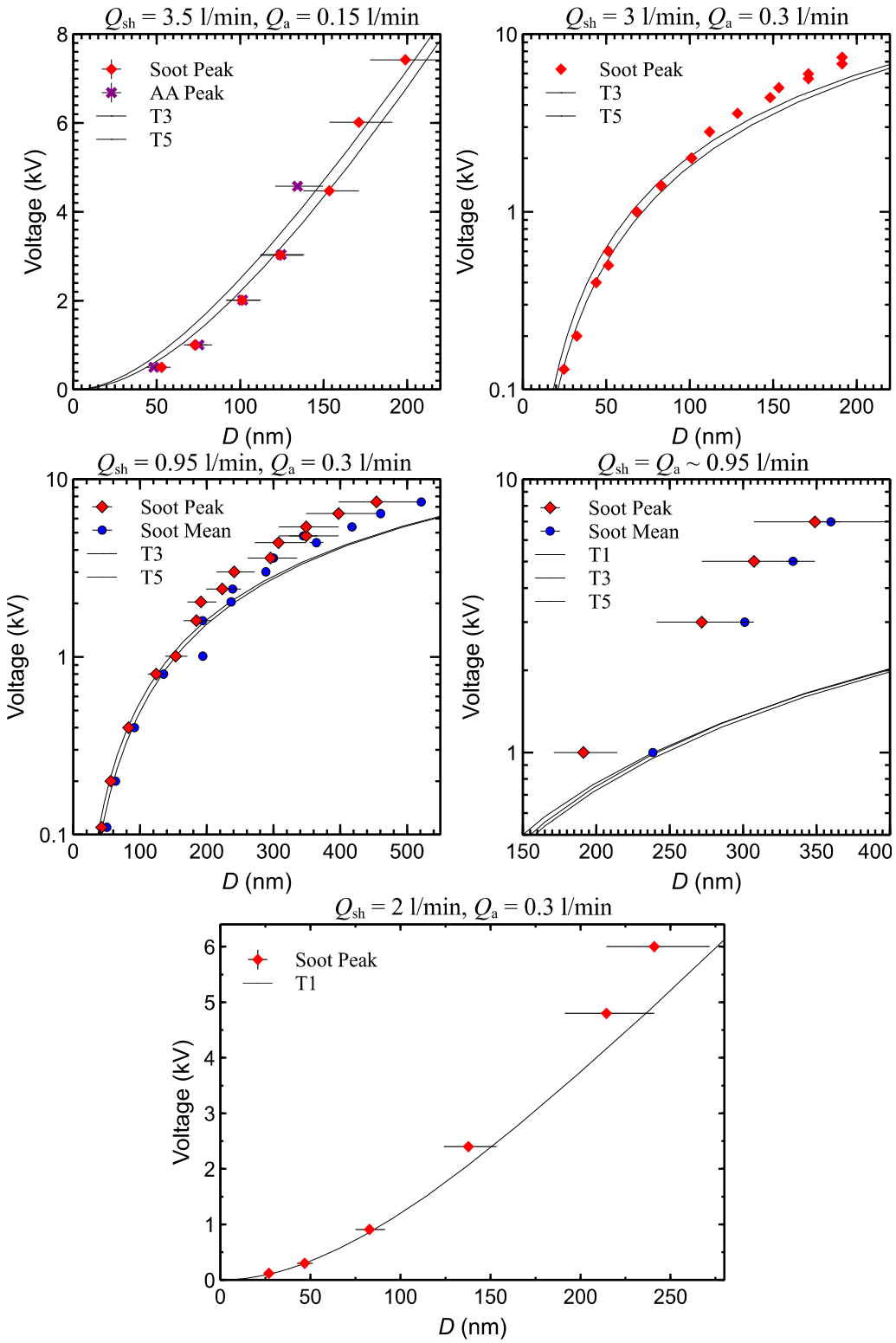

Figure 5.1–1. Theory (lines) compared to experiment (data points) for different values of sheath (Q_{sh}) and aerosol flow (Q_a). Experimental data is shown for peak positions of the selected distributions both for generated soot and atmospheric aerosol (AA). Mean positions (d_{50} size value) are also shown for some of the soot data in cases of wider distributions (lower Q_{sh}, larger σ_g). Example theoretical curves are shown based on different values in the literature for the slip correction factor coefficients (Eq. 25). T1 from Allen and Raabe, (1985), T3 from da Roza (1982), and T5 from Rader, (1990).

5.1.1.1. Discussion

The data shown in Fig. 5.1–1 appear to be somewhat similar to theory at all flow rates, apart from the case where the two flow rates are equal at ~0.95 l/min. However in all cases, at higher voltages and particle sizes, the experimental data increasingly diverges away from theory towards higher voltages or lower particle sizes.

Possible reasons for this divergence could include:

- Spreading of the aerosol flow immediately after the entrance slot along the width of the separation chamber is not taken into account (see Fig. 4.1–15). This would reduce *h* to keep the relative areas between the sheath and aerosol flows the same as was initially considered. This effect can be modelled and it is planned to improve the theory with the results of this in the future.
- The details of what happens when the sheath and aerosol flows meet at the aerosol inlet and diverge at the aerosol exit, and how this influences the particle trajectory across the DMA. It may also be possible to improve our understanding of this using modelling techniques. It has already been discovered through modelling that the aerosol flow is initially "shot" further into the separator at the inlet and "sucked" out from a greater distance at the outlet effectively decreasing the vertical distance that the particles are drifted through (see Fig. 4.1–18).
- The possible creation of ions in the DMA at high voltages leading to charging and de-charging of particles (e.g. singly charged becoming doubly charged and doubly charged becoming singly charged). This could be investigated by connecting an ion counter to the outlet of the DMA and monitoring the counts in relation to DMA voltage with an ion free air flow into the DMA.
- Changes in the flow meter calibrations due to pressure, temperature, and carrier gas type. The pressure response of the aerosol flow meter (differential pressure transducer) has been investigated. Further investigation of both types of flow meter response may be required in the future.
- Problems with the reference Grimm SMPS instrumentation. Concerns include incorrect charge distribution correction due to not using the Grimm neutraliser, whether the high particle size cut-off impactor at the DMA entrance is effective for our low density soot agglomerate particles, and inconsistencies in data obtained with different wait times between scans. Investigation of the data from this instrument is ongoing.
- Broader (higher σ_g) DMA cuts being overly affected by the soot source distribution shape. This effect can be diminished by using a wider source and/or changing the source appropriately for each data point.
- It has been assumed that the reference method provides correct sizing data.

5.1.2. Parameterised fit

5.1.2.1. Introduction

Due to the difficulties encountered in defining the precise form that the theoretical equation should take in order to give a good fit across a broad range of flows, it was decided to create a parameterised fit to experimental data. Good results were attained with a power law fit with voltage as a function of particle diameter, with the coefficient and power of this equation taking the form of quadratic functions of the sheath flow rate.

The current form of this expression is as follows:

$$V\,(\mathrm{kV}) = C.d_p(\mathrm{nm})^P \tag{29}$$

For each set of flow rates a power fit is made to the resulting V vs. d_p data. The set of constants (C) and powers (P) corresponding to a set of flow rates is then analysed to look for a correlation between these parameters and the chosen flow rate values. The best correlation was found to relate to the sheath flow with the following polynomial fit equations:

$$C = 1.5907\text{E-}04x^3 - 1.4998\text{E-}03x^2 + 3.8620\text{E-}03x - 1.7429\text{E-}03 \tag{30}$$

$$P = 0.10883\mathrm{x}^2 - 0.32083\mathrm{x} + 1.71621 \tag{31}$$

(where $x = Q_{\mathrm{sh}}$ in l/min)

5.1.2.2. Fits

In the below graphs (Fig. 5.1–2), the power fit is compared to experimental data and R^2 values have been calculated. In Fig. 5.1–3 an example comparison is shown between theoretical and parameterised curves along with experimental data. The data indicates peak positions from atmospheric aerosol.

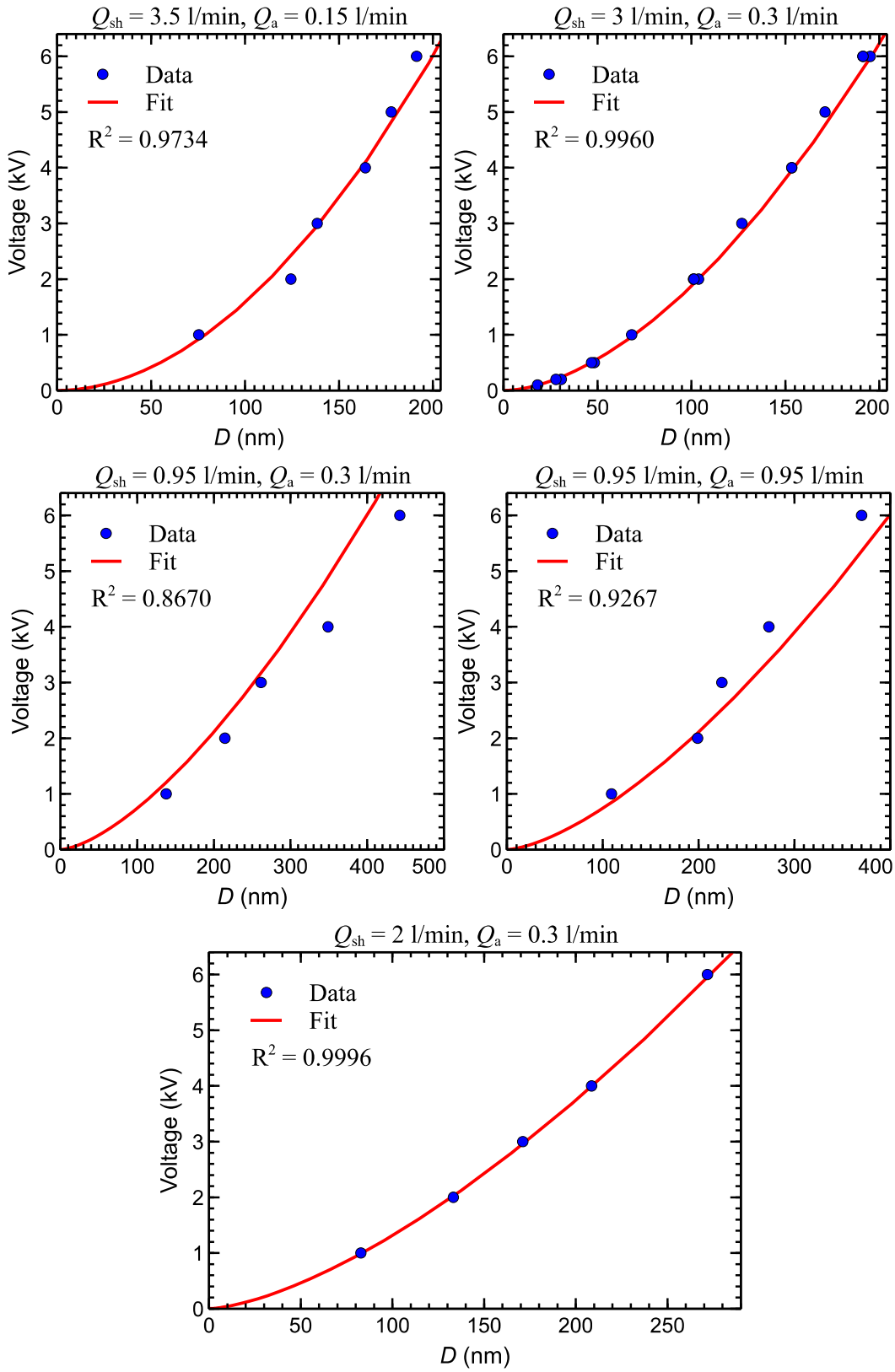

Figure 5.1–2. Parameterised fit (lines) compared to experiment (data points) for a range of sheath (Q_{sh}) and aerosol (Q_a) flows.

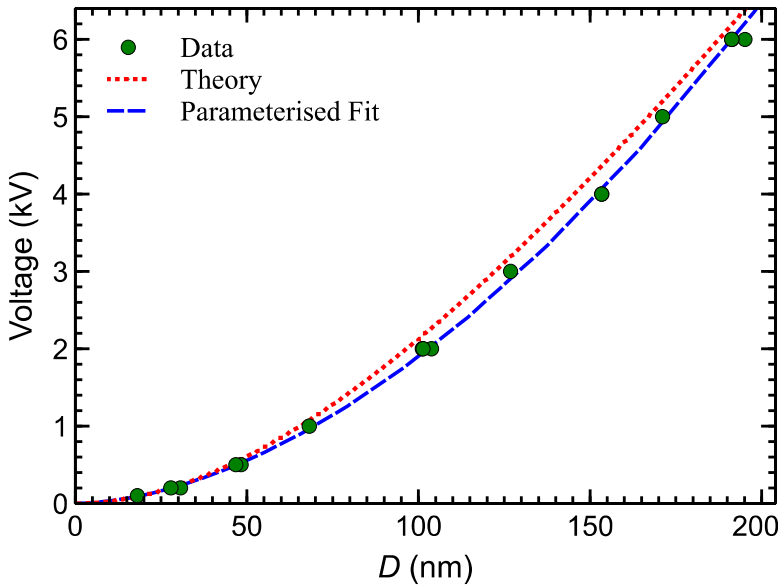

Figure 5.1–3. Comparison between experimental data, theory, and parameterised fits at Q_{sh} = 3 l/min and Q_a = 0.3 l/min.

5.1.2.3. Discussion

The fits are all quite good as expected as the fit formula was generated from this data. However the universality of this formula is highly doubtful, and such it will likely be more limited in its applicability compared to a theoretical fit. To check how well behaved the fit function is, it has been plotted against a range of sheath flow values in Fig. 5.1–4 below.

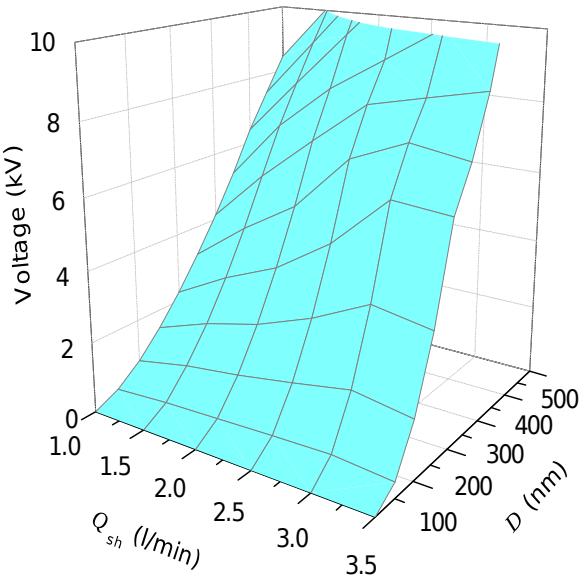

Figure 5.1–4. Parameterised fit function plotted against a range of sheath flow values.

It is apparent that this fit function is very smooth across the majority of the range of parameters considered. There is a "crinkle" in the surface function at the top right of the figure towards the highest flow rates and particle sizes considered. However in practice, this DMA has been developed to work with a 6 kV high voltage supply, and therefore this region is not attainable (and hence lower flow rates are required to reach particle sizes above ~300 nm). Another issue is the dependence of the performance of the DMA on the charge distribution which will depend on the charging device used. The charge distribution should not have much effect on the sizing of a DMA at smaller sizes (<< 100 nm). However as the particle size increases, multiple charging effects can become more significant, which can start to distort the shape and mean size of the selected distribution. Ideally, at least at higher sizes, the calibration will have to be defined with a particular charging device. Alternatively, multiple charge corrections can be calculated to deconvolute the data, but again, these corrections would have to be defined for a particular charge distribution (e.g. usually these corrections are applied assuming an equilibrium bipolar charge distribution as attained from a radioactive neutraliser).

5.1.2.4. Final Expression

The above expression can be seen to work quite well across a limited set of flow rates. However, as it exhibits no dependency on the aerosol flow rate, it is not likely to work well across a broader range of cases where the aerosol flow makes up a significant proportion of the total flow rate. Ideally an instrument calibration should work reasonably well across the full range of flow rates available and all points in between, not just those that have been tested and calibrated to. As the number of different flow rates increases, it becomes increasingly difficult to find a parameterised fit that still gives reasonable accuracy across the range. Ignoring one of the flow rates (e.g. keeping Q_a fixed) would allow for a reasonable approach to fitting the remaining three parameters (e.g. fitting software can be used to determine a three dimensional surface fit). However, given the complexity involved in fitting all four parameters at once, refinement of theoretical expressions is considered more likely to successfully yield a general solution.

Courtesy of consultations with another aerosol scientist; Ajaya Ghimire of Particle Measuring Systems Inc., a theoretical model was found which gave broadly acceptable results and particularly in the main flow range of the planar DMA considered to be most useful (Q_a from 0.1 to 0.3 l/min and Q_{sh} from 1 to 3 l/min). Upon analysis the important distinctions this model had from that given above were as follows:

- Simpler geometrical model with no height corrections for initial flow boundaries as were calculated in Equation (28). i.e. H is simply taken to be $H = y$.
- The result of Equation (24) can be quite sensitive to the particular choice of some constants (mean free path λ and air viscosity η) which can vary slightly depending on the source material referenced. This can be seen to some extent in the different theoretical lines presented in Fig. 5.1–1. The final parameters found to work best were taken from Hinds (1999).

5.1.3. Comparative performance measurements

5.1.3.1. Introduction

The planar DMA presented here was further developed and commercialised by Naneum Ltd. as the Nano-ID® PMC500 Particle Mobility Classifier. This formed the foundation of the first portable SMPS system – the Nano-ID® NPS500 Nanoparticle Spectrometer.

The main components of the NPS500 include the planar DMA, a miniature CPC and a unipolar corona particle charger. Typically SMPS systems utilise a radioactive source as a particle charger. However these sources carry many legal restrictions with them and are difficult to re-locate under typical regulatory frameworks. Therefore it is important for a portable instrument to use an alternative means of charging particles, avoiding any radioactive elements and X-Ray sources. A corona charger also allows for much greater charging efficiencies compared to a radioactive neutraliser, however, this will generally come at the expense of higher multiple charging rates. The incorporated mini-CPC is also a proprietary Naneum design utilising an organic fluid as the working fluid for nucleation. Traditional CPCs utilise alcohol (usually isopropanol or butanol) as a working fluid and are notorious for creating associated fumes in the laboratory environment. The working fluid used in the NPS500 by comparison, DBD (dimethyl benzene-1,2-dicarboxylate), is odourless and has a much lower fluid consumption rate which is useful for extended and untended field campaigns.

The performance of the NPS500 was evaluated in comparison tests at the National Physical Laboratory (NPL), Teddington, UK. The underlying sizing and resolution performance of this device is defined by the DMA at its heart. Therefore these tests are hereby presented as a demonstration of the effectiveness of the planar DMA's design and performance.

Four different aerosol challenges across different size and concentration ranges were generated. The resulting distributions as measured by two NPS500 instruments were compared to those measured in parallel by a reference SMPS, and to the total concentration as measured by a reference CPC.

5.1.3.2. Setup

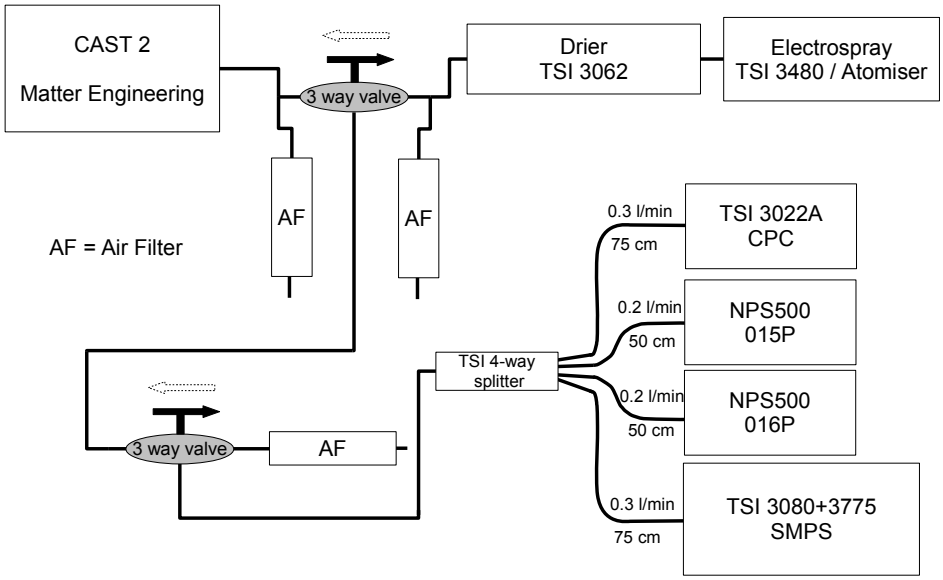

Figure 5.1–5. A four way comparison experimental setup between three SMPS instruments and a reference CPC. One three way valve allowed for fast selection between two different test aerosol sources once the generators were stabilised. The aerosols used were soot from a CAST 2, sucrose from an electrospray and NaCl or PSL from an atomiser in place of the electrospray. A second three way valve allowed for either the test aerosol or filtered air to be sent to the splitter and measurement instruments. Extra exhaust filters were located at the outlet of each generator to allow venting of any extra pressure. The flow rates and tubing lengths to each of the test instruments are indicated.

The test set up comprises three aerosol generators in total and a flow maintenance system enabling the aerosol to be split and delivered to the reference instruments and NPS500 (Fig. 5.1–5). Four different aerosol challenges were generated in all (Fig. 5.1–6 (a)). Soot aerosols from a CAST 2, sucrose aerosols from an electrospray, and NaCl or PSL (polystyrene latex) aerosols from an atomiser. A three way valve is used to select the source aerosol and excess or make-up airflow is provided as necessary through filters. A second three way valve allows the sample flow to be switched to a filtered output to allow setup changes at the sampling point without destabilising the generator flows. The sample flow is split four ways to two test NPS500s, a reference SMPS and a reference CPC (Fig. 5.1–6 (b)). A four way splitter branched the test aerosol into four flows for the four measurement instruments that were part of the test. Two NPS500 instruments were compared to the NPL reference SMPS – TSI 3936 consisting of a TSI 3080 electrostatic classifier and 3775 CPC. A reference total concentration was also monitored with a TSI 3022A CPC. Two different DMAs were used on the TSI classifier to cover the size range required – a nano DMA 3085 (4.4 – 165 nm), and a long DMA 3081 (14 – 673 nm). The NPS500 range is 5 – 500 nm. All the SMPS systems were set to a 4 minute total scan time which included a 30 second reverse scan in the NPS500 / down scan in the 3936 to clear out particles between scans. To compensate for the different flow rates of the instruments involved (0.2 l/min in the NPS500, 0.3 l/min in the reference instruments) the tubing lengths to each instrument were adjusted to the

same ratios as per ISO (ISO 27891) guidelines such that particle losses would be equal in each case. Before each new measurement, the air source was switched to filtered air to check that all the particles from the preceding measurement had been cleared away, and that every instrument read zero correctly.

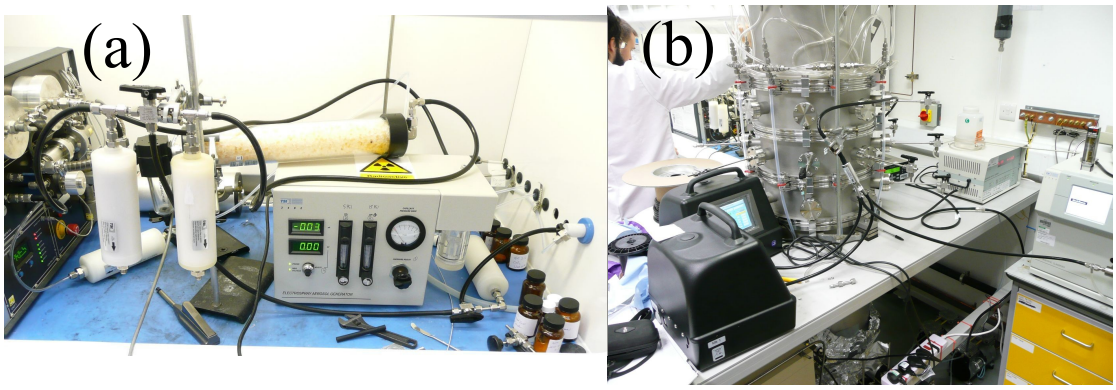

Figure 5.1–6. (a) Generators setup with the CAST 2 soot generator on the left and the sucrose electrospray on the right. The filter assembly and aerosol selection valve is shown in between them held up by clamps. (b) Measurement setup with 4-way splitter shown at centre leading to the two NPS500s – black cases on left, a reference CPC – centre right, and a reference SMPS –far right.

5.1.3.3. Results

First the total concentrations measured by each instrument are compared across the different aerosol types (see Fig. 5.1–7 and 5.1–8 below). For the SMPS instruments, the measured distributions are integrated to provide a total concentration figure. The CPC on the other hand is measuring total concentration directly every second, and therefore this data is simply averaged over each scan to provide a single figure.

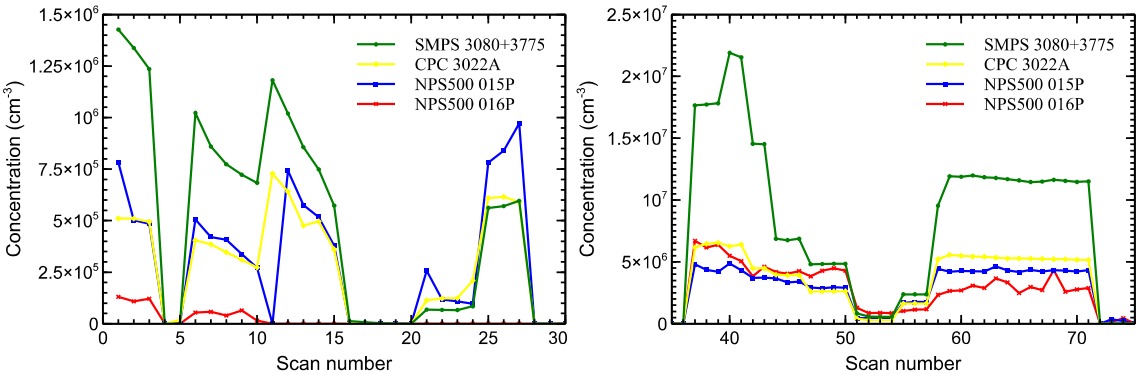

Figure 5.1–7. Total concentration measured by each instrument for each scan taken with sucrose aerosol from the electrospray (left) and soot aerosol from the CAST 2 (right).

One of the NPS500 instruments (016P) gave faulty readings which were manifested in a large cut in the data and/or excessive noise levels below ~50 nm. This is evident in Fig. 5.1–7 above in the very low concentration readings given for the sucrose aerosol from

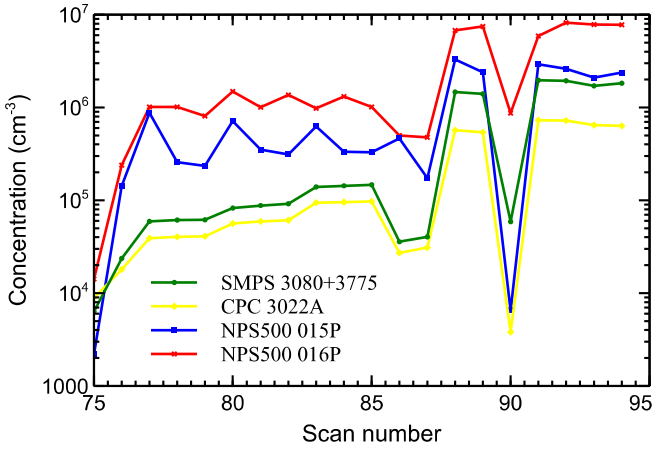

Figure 5.1–8. Total concentration measured by each instrument for scans 75 – 95. The aerosol in this case is polystyrene latex (PSL) beads for scans 75 – 85 and NaCl for scans 86 – 95.

this instrument. Therefore the data from this instrument has been omitted from some of the figures below where it is not considered to provide any meaningful information. In addition, the TSI SMPS was found to often measure concentrations significantly higher than those provide by the TSI CPC for the same aerosol. CPCs provide a far more direct, and therefore reliable, measurement of concentration. Hence it was decided to correct the output of the TSI SMPS, such as to give the same overall concentration as measured by the TSI CPC, and thus provide what is considered to be a more reliable reference measurement of the distribution. This correction shall be indicated in the data as "TSI SMPS corrected".

Comparison data are shown below in Figs. 5.1–9 – 5.1–17 for sucrose, soot, PSL and NaCl aerosols.

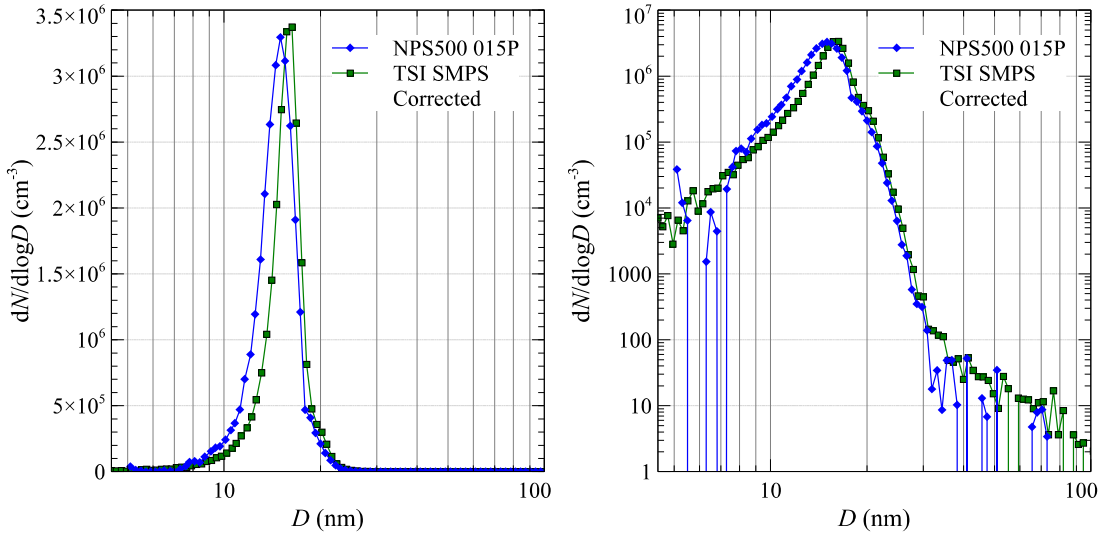

Sucrose aerosol from electrospray				
	Peak size (nm)	Median diameter (nm)	Geometric mean diameter (nm)	Concentration (cm^{-3})
NPS500	15.0	14.5	14.3	444,791
Reference	16.3	15.6	15.1	378,530
% deviation	8%	7.1%	5.3%	17.5%

Figure 5.1–9. Comparison data for a 15 nm sucrose aerosol comparing NPS500 performance to a reference TSI SMPS averaged over three sequential scans. Data is shown on a linear-log scale on the left and a log-log scale on the right. Associated sizing and total measured concentration data is shown in the table with the percentage deviation of the NPS500 value from the reference value.

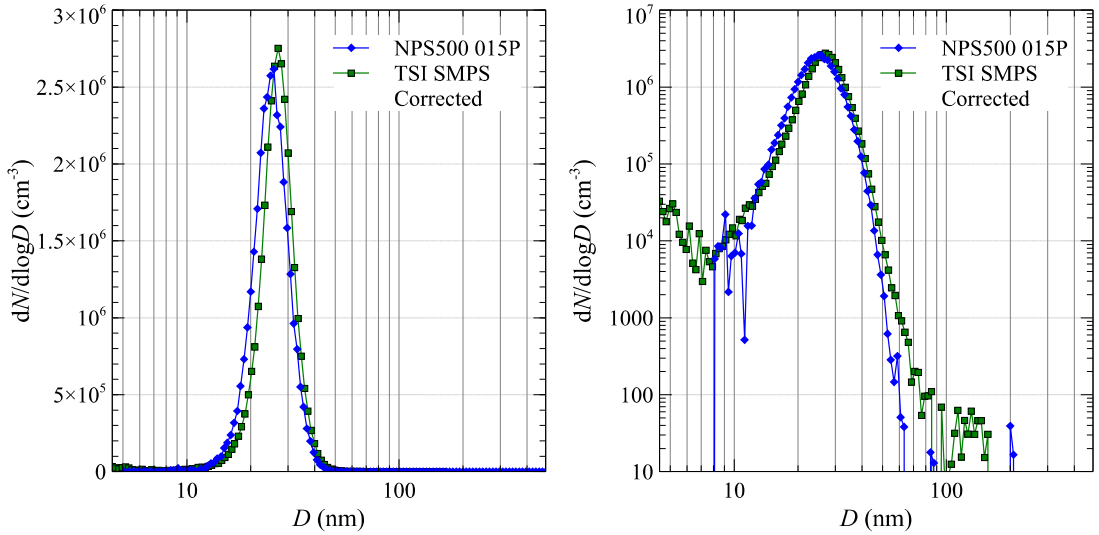

Sucrose aerosol from electrospray				
	Peak size (nm)	Median diameter (nm)	Geometric mean diameter (nm)	Concentration (cm^{-3})
NPS500	25.7	24.5	24.6	517,989
Reference	26.9	26.6	25.9	496,678
% deviation	4.5%	7.9%	5.0%	4.3%

Figure 5.1–10. Comparison data for a 25 nm sucrose aerosol comparing NPS500 performance to a reference TSI SMPS over a single scan. Data is shown on a linear-log scale on the left and a log-log scale on the right. Associated sizing and total measured concentration data is shown in the table below with the percentage deviation of the NPS500 value from the reference value.

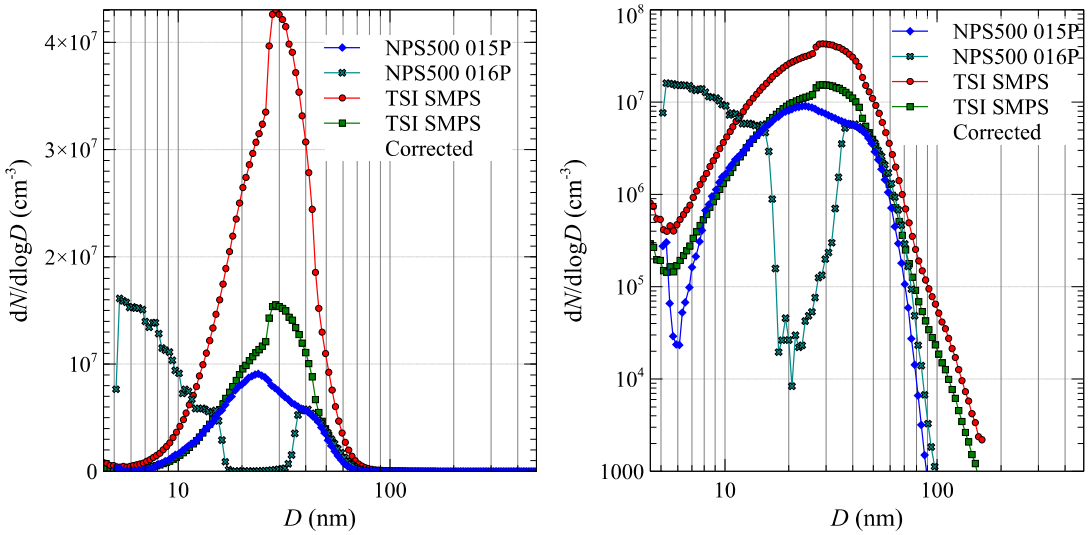

Figure 5.1–11. Comparison data with a soot distribution of peak size ~35 nm from the CAST 2 generator averaged over three sequential scans. All data is shown as an example of some of the instrumental errors encountered and shown on a linear-log

scale on the left and a log-log scale on the right. The curious error demonstrated by NPS500 016P is seen in the cut in data below 40 nm and excess noise below 20 nm. The significant over-counting of concentration is evident in the uncorrected TSI SMPS data. Also, the step response seen near the peak in the TSI data is due to the TSI CPC in the SMPS switching between single particle counting and photometric mode for higher concentrations. The concentration of the source aerosol was reduced to avoid this discontinuity in the following measurement runs.

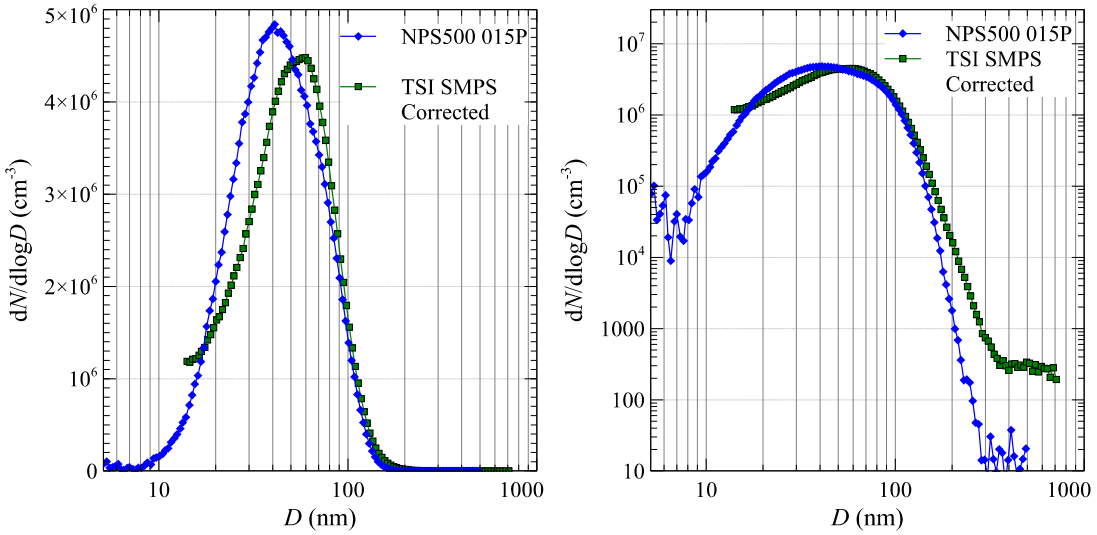

Soot aerosol from CAST 2				
	Peak size (nm)	Median diameter (nm)	Geometric mean diameter (nm)	Concentration (cm^{-3})
NPS500	41.0	41	41.1	2.91×10^6
Reference	59.4	47.9	45.7	2.62×10^6
% deviation	31%	14.4%	10.1%	11.1%

Figure 5.1–12. Comparison data for a ~50 nm soot aerosol comparing NPS500 performance to a reference TSI SMPS averaged over four sequential scans. Data is shown on a linear-log scale on the left and a log-log scale on the right. Associated sizing and total measured concentration data is shown in the table below with the percentage deviation of the NPS500 value from the reference value.

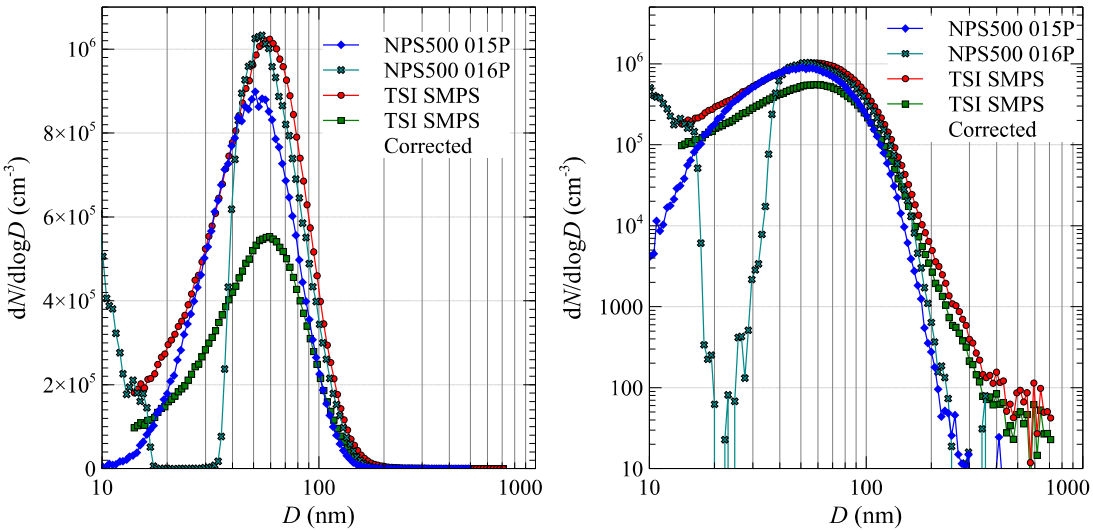

Figure 5.1–13. Comparison data for a lower concentration ~50 nm soot aerosol comparing NPS500 performance to a reference TSI SMPS averaged over three sequential scans. Data is shown on a linear-log scale on the left and a log-log scale on the right. In this case both NPS500 readings appear to match better with the uncorrected TSI reading.

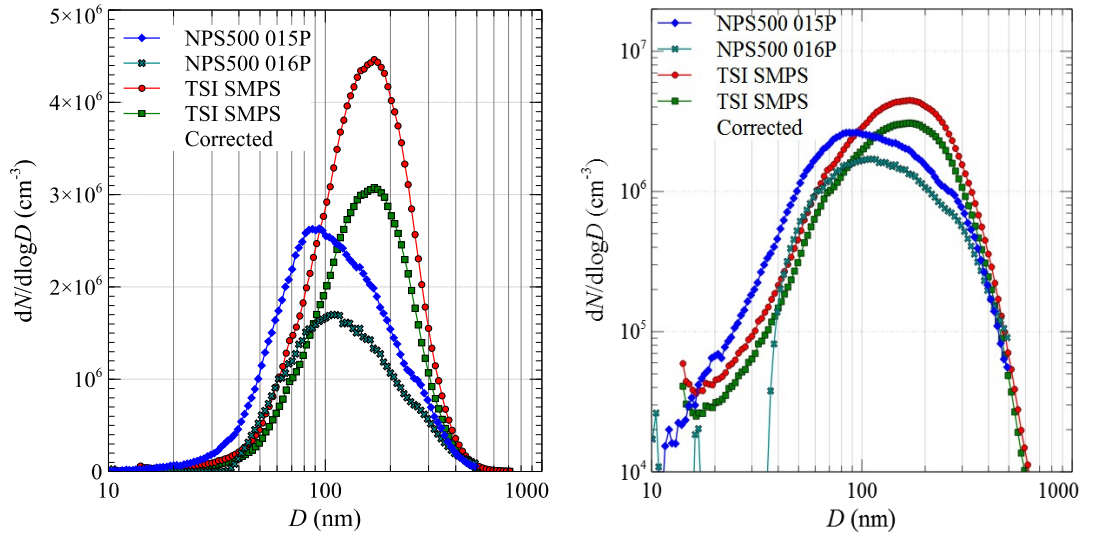

Figure 5.1–14. Comparison data for a larger sized soot aerosol comparing NPS500 performance to a reference TSI SMPS averaged over three sequential scans. Data is shown on a linear-log scale on the left and a log-log scale on the right. NPS500 016P appears to be operating without fault above 50 nm.

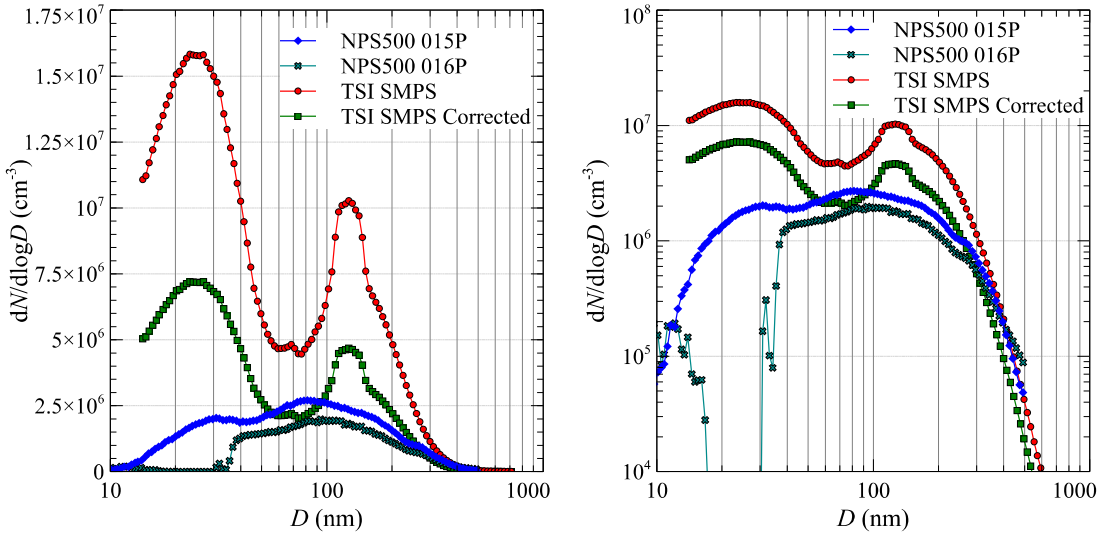

Figure 5.1–15. Comparison data for a bimodal soot aerosol comparing NPS500 performance to a reference TSI SMPS averaged over 13 sequential scans. Data is shown on a linear-log scale on the left and a log-log scale on the right.

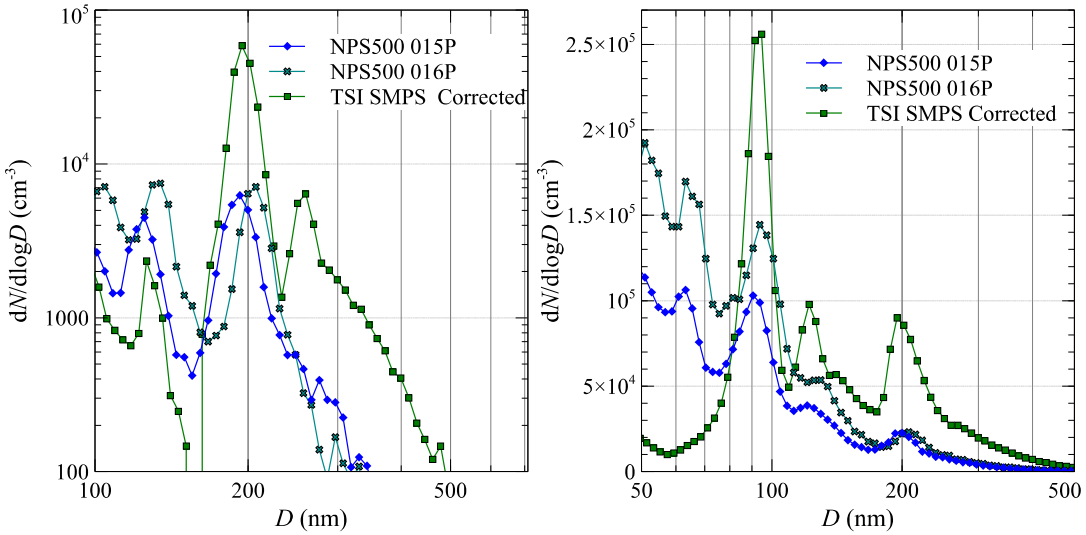

PSL aerosol from atomiser				
	Peak size (nm) 200 nm		Peak size (nm) 90 nm	Peak size (nm) 200 nm
NPS500 015P	192.7	NPS500 015P	90.5	199.8
% deviation **015P**	**3.7%**	% deviation **015P**	**0.6%**	**0.1%**
NPS500 016P	207.1	NPS500 016P	93.8	207.1
% deviation **016P**	**3.6%**	% deviation **016P**	**4.2%**	**3.6%**
TSI Reference	194.6	TSI Reference	94.7	194.6
% deviation **TSI**	**2.7%**	% deviation **TSI**	**5.2%**	**2.7%**

Figure 5.1–16. Comparison data for PSL aerosols comparing NPS500 performance to a reference TSI SMPS. On the left is shown a measurement of 200 nm PSL while on the right is shown a measurement of a mixture of 90 nm and 200 nm PSL. Each measurement is the result of averaging three sequential scans. Positions of the main peaks are compared in the table. In this case all instruments are compared to the expected PSL positions of 200 and 90 nm respectively.

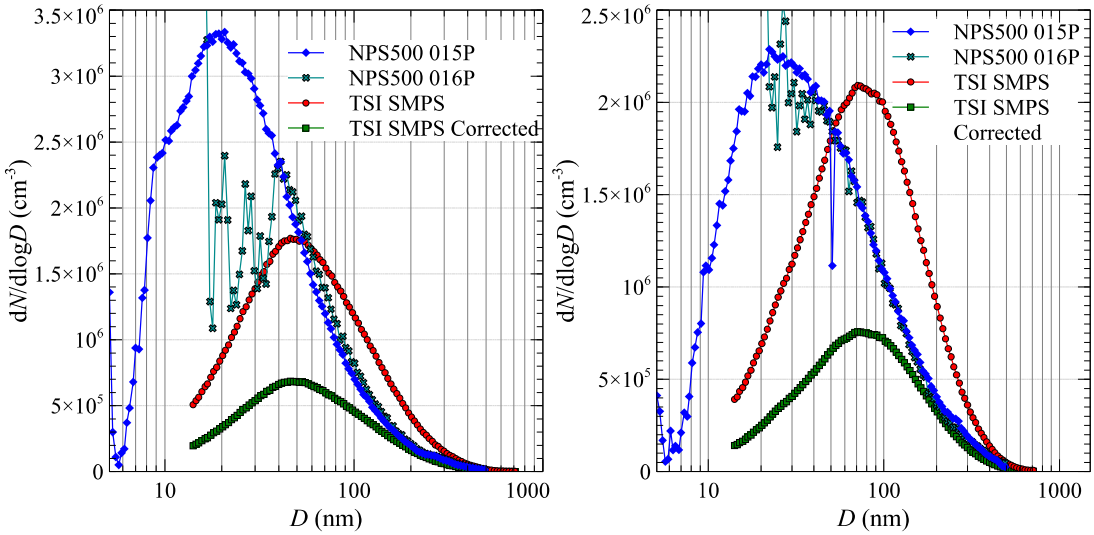

Figure 5.1–17. Comparison data for NaCl aerosols comparing NPS500 performance to a reference TSI SMPS. Two example measurements are shown, each the average of two sequential scans.

5.1.3.4. Discussion

Comparisons were carried out with a reference SMPS and CPC. Sucrose, soot, PSL and NaCl aerosols were generated in the size range from 5 nm to 500 nm and the concentration range from 10^3 to 10^6 cm^{-3}. The stability of the measurement instruments was investigated in a series of scans of the same aerosol and was found to be sufficiently stable to enable reliable data on size distributions to be obtained. For each size, several scans (normally 3 to 5) have been recorded for the NPS500 and the reference SMPS. The repeatability of the data on size distributions was good and variation of distribution parameters was less than or equal to the difference between the reference and the NPS500.

Clearly there is a significant issue with NPS500 016P in the lower size range below 50 nm. Such small charged particles are particularly sensitive to electric fields, and therefore likely explanations for the error include a contaminant / charge build-up in a part of the flow system or a faulty corona charger. The additional noise at the smallest sizes is perhaps more suggestive of the latter as breakdown in the corona can lead to particle generation in the few nm size region. It is also apparent that the reference SMPS is not a reliable measure of total concentration as compared to the reference CPC. This is not particularly surprising as it is widely accepted by aerosol scientists that SMPS instruments are rarely very accurate as a measure of concentration (e.g. Asbach *et al.*, 2009), although possibly the magnitude of the offset seen in some cases here is larger than would be expected. However, the approach taken here of correcting the reference concentration to that obtained from the CPC is considered acceptable and provides independent measures of size and concentration. Note that as the CPC will count all particles above its lower size cut-off, this correction is only valid in the case when the entire distribution is contained within the size range of the SMPS (i.e. there are no particles that cannot be measured in the SMPS but are still counted in the CPC). This appears to be a safe assumption in most cases. Although in some of the soot

distributions (Figs. 5.1–12 – 5.1–15), the tail to smaller sizes is cut-off in the reference data due to the use of the TSI long DMA with a lower size limit of 14 nm. Therefore, in these cases the adjustment to CPC may be slightly under-correcting the data.

An extremely good agreement is seen between NPS500 015P and the reference data in both the sucrose aerosol examples, both in sizing and concentration. Therefore a fully functional NPS500 is clearly capable of providing reliable data in this range.

Data from the soot aerosol provide slightly more mixed results. At the lower size range there is generally reasonable agreement between NPS500 015P and the corrected SMPS results. Although at the lowest concentration measured here (Fig. 5.1–13) the NPS500 measures significantly higher concentrations more in line with the uncorrected reference SMPS results than those from the CPC. However at larger sizes (Fig. 5.1–14), there is a noticeable offset between the distributions measured by the NPS500 compared to the reference. This is likely due to a combination of multiple charging and instrument saturation effects. Multiple charging will shift the apparent size distribution to smaller sizes compared to the singularly charged case and is significant for these larger particles > 100 nm. The TSI reference instrument includes a correction algorithm for this phenomenon to shift the distribution back to larger sizes to reflect an idealised singularly charged measurement. The NPS500 does not make such an adjustment and therefore some offset at larger sizes will always be expected. In addition, at these larger sizes, the concentration measured here is close to the saturation level of the optical particle counter used in the NPS500 (which does not have a photometric mode). Due to the much higher diffusion losses and lower charging efficiency for smaller nanoparticles, the saturation level in SMPS instruments is higher at smaller sizes < 100 nm than at larger sizes, and increases sharply at the lower end of the scale < 20 nm. Therefore a saturated distribution will appear to be shifted towards smaller sizes. The bimodal distribution (Fig. 5.1–15) is much less clearly resolved in the NPS500 compared to the reference data. Again this is likely due to a combination of multiple charging and saturation effects as discussed above. It is evident that the smaller sized peaks are in reasonable agreement whereas the larger sized peak is shifted to smaller sizes in the NPS500 compared to the reference. This result in the peaks appearing closer together and are therefore less clearly distinguished.

The PSL data (Fig. 5.1–16) is particularly revealing due to its monodisperse nature. The sizing from all instruments is quite impressive with just a small offset between the two NPS500 instruments falling either side of the TSI SMPS data. In this case the sizes taken from the PSL particles serve as a better reference for all the sizing instruments as this is commonly how such instruments are calibrated. The average sizing offset of the NPS500 data is 2.6% and for the TSI SMPS it is 3.5%. Multiple charging is less of an issue for comparison of sizing here as it manifests itself as clearly distinguished secondary peaks due to the monodisperse aerosol rather than a shift in the distribution as seen for polydisperse aerosols. Multiple charging is more evident to the left of the main peaks as would be expected, whereas the additional larger sized peaks in the reference data may be artefacts as a result of the multiple charge correction assuming that some portion of the main peak is a multiple charged contribution from larger sized particles which do not exist here. The NPS500 measured considerably lower PSL peaks compared to the reference data. The consistency of this result is suggestive of a lower sensitivity of the DBD working fluid used in the NPS500 to PSL particles. This is a problematic issue with using DBD due to the widespread acceptance of PSL as a

calibration particle in the aerosol science industry. However it is of little practical concern in the field, as it is not a material ever likely to be encountered in any occupational or environmental measurements.

Although it is not shown in the PSL data, both the PSL and NaCl data (Fig. 5.1–17), and indeed any measurements from an atomiser using water based suspensions or solutions, show much higher counts at the lower size range compared to the reference instrument. It is considered that this may be due to higher sensitivity of the DBD working fluid to ultra-fine contaminants in the deionised water used compared to the isopropanol working fluid in the TSI instruments. It is very difficult to remove all contaminants in this size range even in the highest grade water available. Indeed, the reference measurement for PSL also showed a broadly increasing distribution towards small sizes, which was of a similar or larger magnitude to the main PSL peaks by the time it was cut-off at the lower size limit of the long DMA at 14 nm. Although it was not as significant as the NPS500 data which is measuring down to 5 nm, it is suggestive that there is some true contaminant being measured here.

In the NaCl data (Fig. 5.1–17) there still appears to be an offset at larger sizes that cannot be explained by any small contaminants. Possibly this is due to changes in the aerosol structure occurring in the different charging mechanisms used in front of the DMAs (bipolar radiation based neutraliser in the reference line compared to unipolar corona based charger in the NPS500), or due to a remaining water layer on the NaCl after the drier being affected by the different temperature/humidity conditions in the different instruments.

5.1.3.5. Conclusions

The first portable SMPS-type instrument, the Nano-ID® NPS500, has been tested and compared with a traditional reference SMPS using various aerosols within a range of sizes and concentrations.

In general distributions measured with the NPS500 are roughly in accord with those from the concentration corrected reference SMPS, with a very good match obtained in some cases at smaller sizes. SMPS instruments, which involve a complex pre-stage to a CPC, are generally not as reliable measures of total concentration as CPCs themselves, while CPCs are considered to be accurate within about 20% when calibrated. Therefore, to get two SMPS instruments of completely different design agreeing well within 20% can be quite challenging. Especially in this case where the working fluids used by the underlying CPCs are quite different. This is perhaps one reason why the aerosol science industry has traditionally been conservative in its choice of working fluid materials, mainly sticking to isopropanol, butanol and water.

The sizing agreement between the NPS500 and reference instrument is exceptionally good for the sucrose distributions. For larger sized polydisperse aerosols, the agreement between the NPS500 and reference instrument is not so good due to the different particle charging characteristics.

In particular it is worth highlighting, as evident from the PSL data, that the underlying sizing performance of the NPS500 matches very closely with the reference

DMA/SMPS. This demonstrates that the offsets seen at larger sizes are mostly due to a lack of a multiple charge correction algorithm in the NPS500, as well as some influence of saturation effects at higher concentrations. The good sizing accuracy and resolution performance confirms the success of the developed portable planar DMA at its heart. This is testament to the sizing performance and reliability of the planar DMA as a nanoparticle sizing device.

5.2. Zn and ZnO nanoparticle generation

5.2.1. Zn generation

5.2.1.1. Results

The first stage of the ZnO generator was initially tested independently to confirm successful generation of Zn particles, and to study the trend in the size distribution with increasing furnace temperatures. Example distributions as measured with a Grimm SMPS are shown in Fig. 5.2–1.

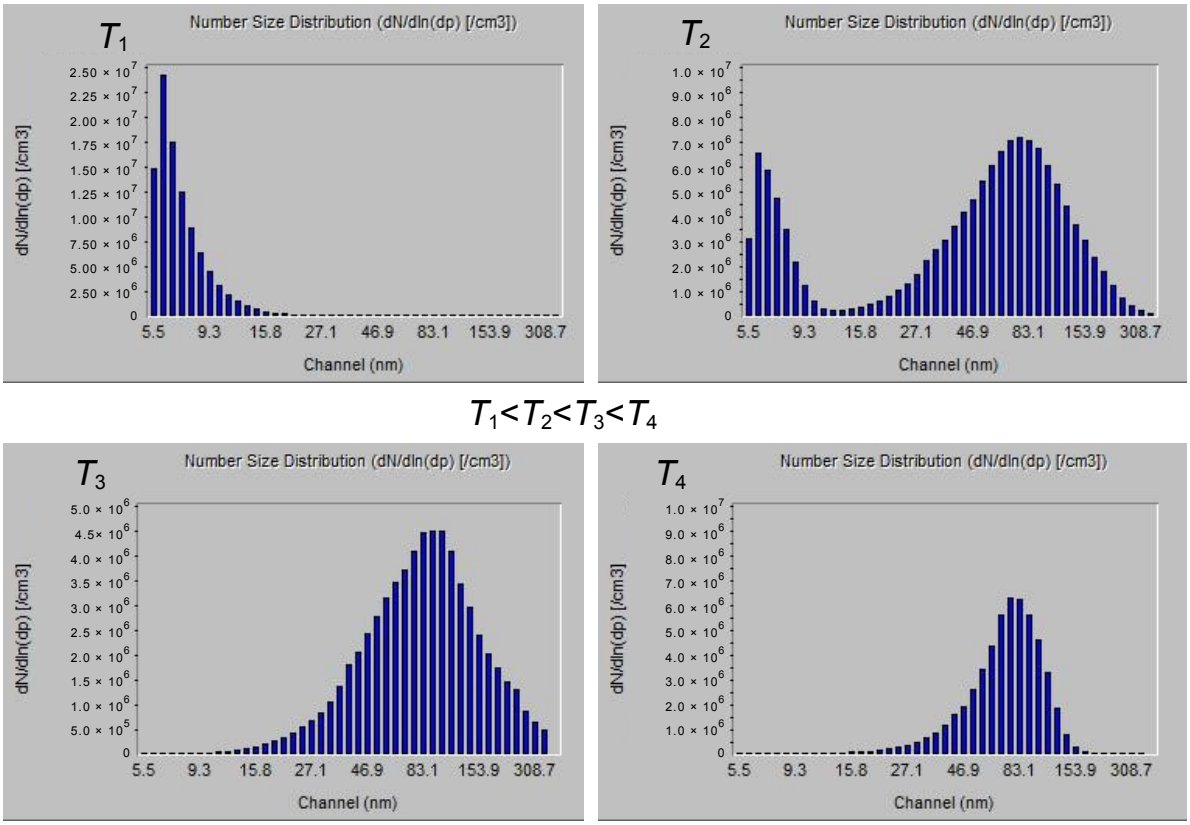

Figure 5.2–1. Change in generated Zn aerosol with increasing furnace temperature. T_1, T_2, T_3 and T_4 are approximately 540, 575, 580 and 595 °C respectively.

At lower temperatures a small size mode at ~6 nm first appears. It should be noted that this SMPS system is not considered to be reliable in this size range (e.g. the 5.5 nm channel is always lower than the 6 nm channel) and so the modal size may be even

smaller than this. As the furnace temperature is increased, a second mode at ~80 nm appears, and, as the temperature is increased further, the smaller sized mode dies away completely leaving only the 80 nm mode.

This behaviour is rather curious. There are two distinct modes. Increasing the temperature of the generator decreases the small particle mode and increases the large particle mode. We would usually expect the size of particles to gradually increase with temperature as more vapour is produced.

In addition to the SMPS measurements, Zn deposits were collected and analysed by TEM at the Natural History Museum, London, in conjunction with collaborators at Imperial College London. This allows us to also consider the morphology of the generated particles and the results are shown in Figs. 5.2–2 – 5.2–4.

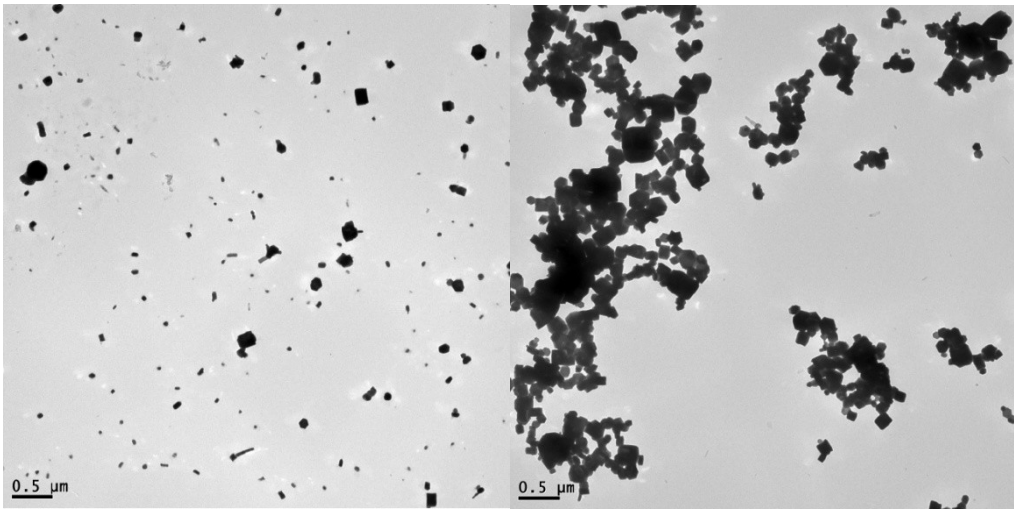

Figure 5.2–2. TEM images of generated Zn particles showing a broad range of sizes and morphologies with many smaller particles visible in the left hand image while those on the right are mostly larger and in a more agglomerated state.

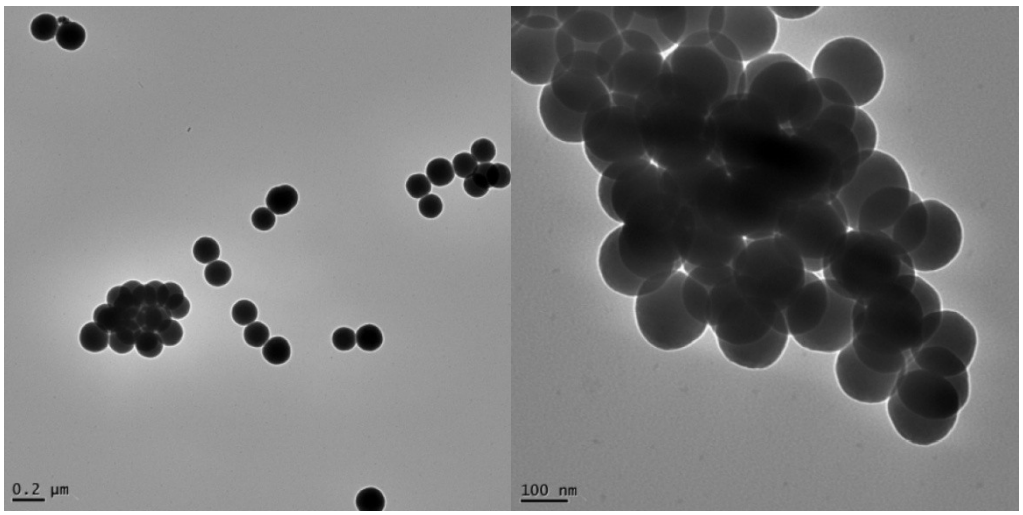

Figure 5.2–3. Also seen are highly regular spherical Zn particles of ~100 nm. A detailed view of a larger agglomerate is shown on the right.

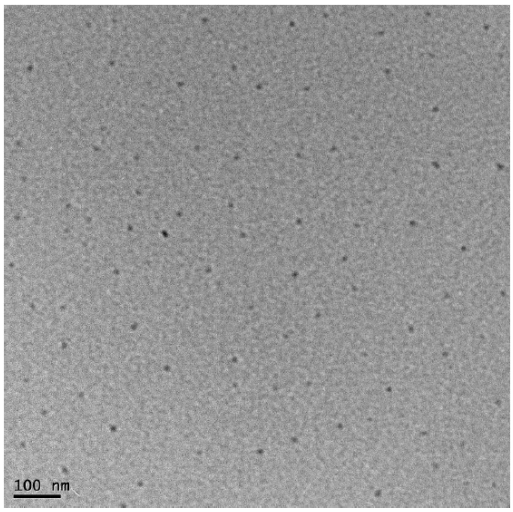

Figure 5.2–4. At higher TEM magnifications numerous smaller particles of 10 nm or less are just about visible.

5.2.1.2. Zn TEM discussion

In the TEM images two groups of particle morphologies and two groups of dominant sizes are evident. There are particles of mixed morphology and size in Figs. 5.2–2, many roughly spherical particles close to 100 nm in Fig. 5.2–3, and particles < 10 nm just visible in the background of Fig. 5.2–4. The two distinct morphology groups suggest two different mechanisms of particle formation are at play. From homogeneous nucleation theory (e.g. Fletcher, 1962), the free energy of embryo formation of spherical and crystalline particles are different. This also suggests different underlying physics at work. To gain a better understanding of this, COMSOL Multiphysics® finite element software was employed to model the Zn vapour supersaturation in the generator oven (Fig. 5.2–5).

Nucleation from a gas phase is controlled by the ratio of the partial vapour pressure of the nucleating material p to its equilibrium pressure p_e and is known as the saturation ratio ($S = p/p_e$). The saturation ratio, or similarly the supersaturation ($S - 1$), are measures of the degree of deviation from the equilibrium condition ($p = p_e$).

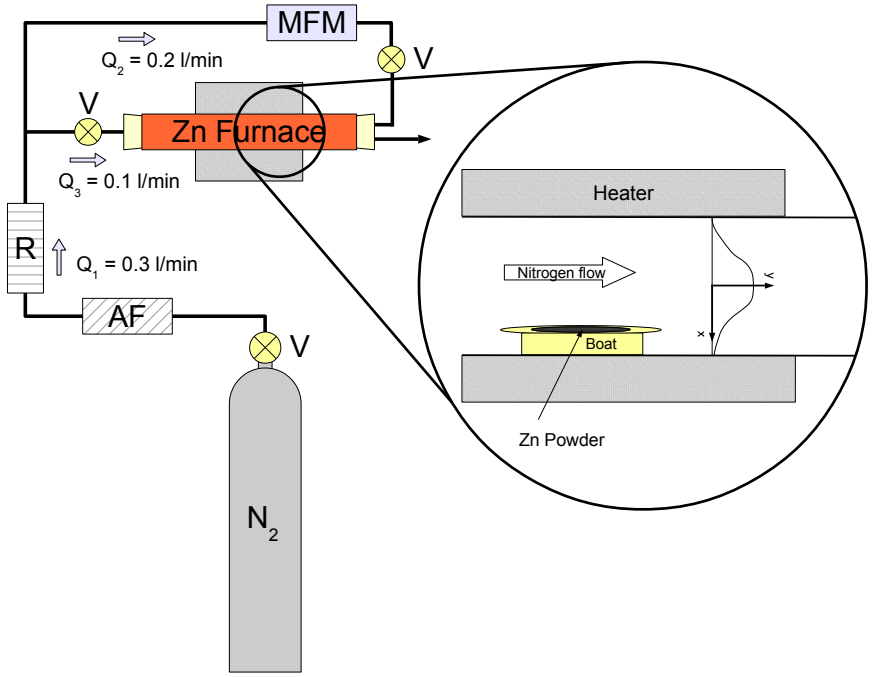

Figure 5.2–5. Internals of the Zn generator furnace and coordinate setup for modelling.

The calculated saturation ratio around the region of the Zn powder and extended downstream in the oven is shown in Fig. 5.2–6. In Fig. 5.2–7 a sectioned line plot from the marked position in Fig. 5.2–6 shows the profile of the saturation ratio going from the centre out to the wall of the furnace tube.

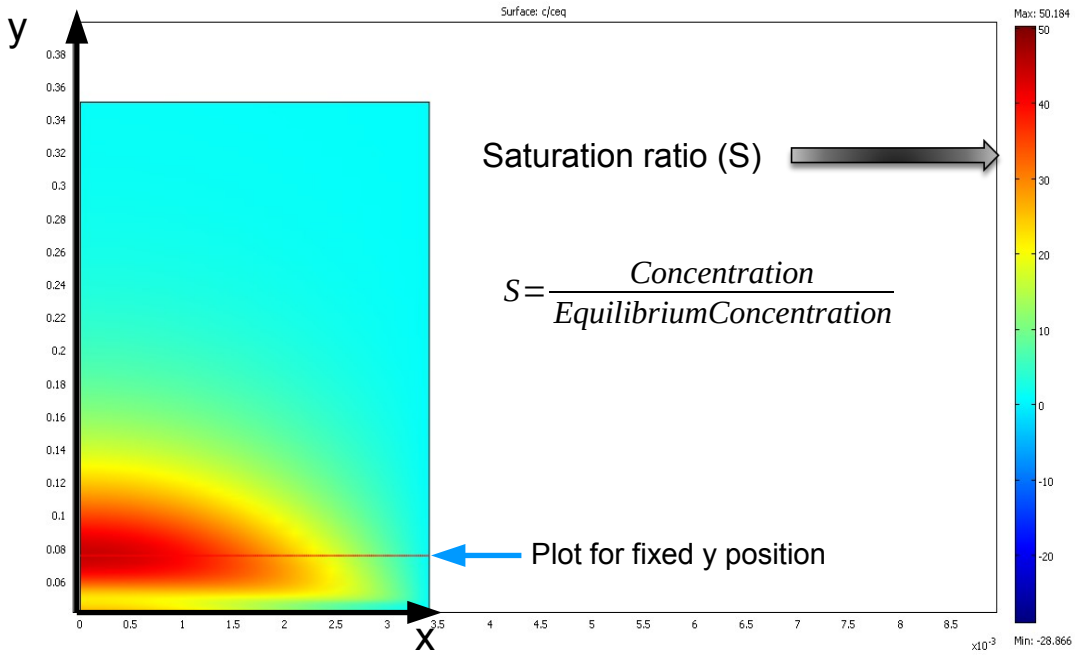

Figure 5.2–6. Saturation distribution within the Zn furnace as modelled using COMSOL Multiphysics® finite element software.

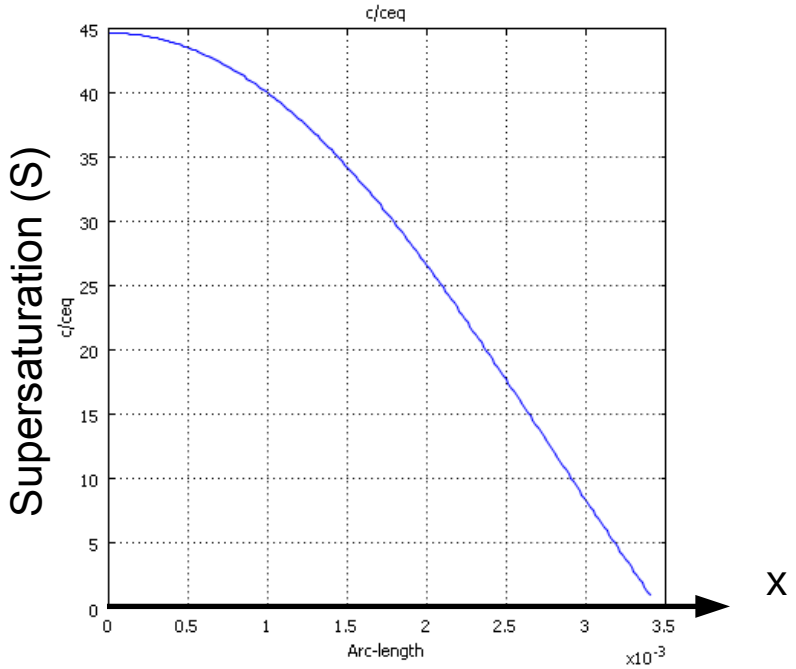

Figure 5.2–7. Plot of saturation distribution within the Zn furnace at the y-position marked in Fig. 5.2–6.

5.2.1.3. Zn summary

In summary; Zn nanoparticle aerosols were successfully produced and analysed by SMPS and TEM. A range of sizes and morphologies were observed showing a dichotomy of aerosol distribution modes produced and two divergent morphology groups. It is hypothesised that a range of saturation conditions leading to different nucleation pathways is the cause of these observations and modelling of the saturation within the furnace supports this idea. This work could be extended to better correlate particular TEM images with the modes seen in the SMPS. However this would be a divergence from our main task, which is to build a ZnO generator. The first step of which has now been shown to be operational.

5.2.2. ZnO generation

5.2.2.1. Results

Following the successful operation of the Zn stage of the generator, the complete system was tested for its ability to generate ZnO particles. Again the output of the generator was measured with a Grimm SMPS, and some example distributions are shown in Fig. 5.2–8.

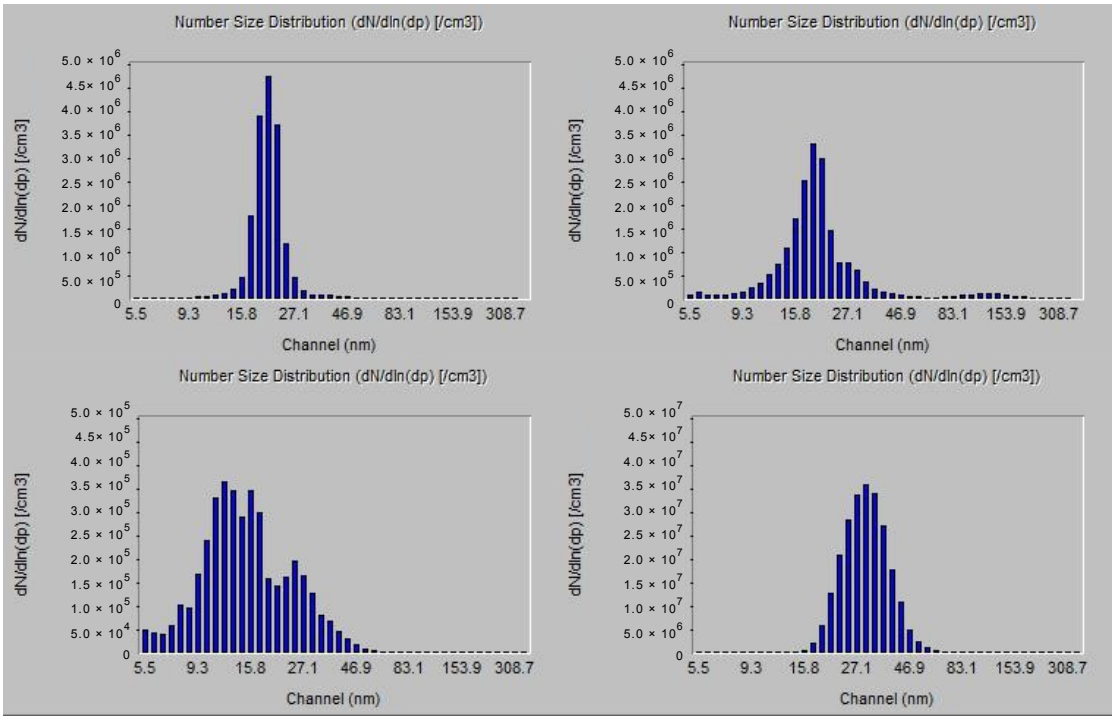

Figure 5.2–8. Example aerosol distributions measured from the ZnO generator with a Zn furnace temperature of 450 °C and a ZnO furnace temperature of 300 °C.

With the oxidation stage, distributions of ~20 – 30 nm are produced which are quite distinct from the Zn distributions seen previously. Apart from the clear size difference, the distributions are much narrower than those seen for Zn. The appearance of these distributions coincides with increasing the oxidation temperature (second furnace stage), and it was not possible to reproduce these distributions without the air (oxygen) intake. In addition, the particles produced following the oxidation stage, mainly visible as build-up in the generator and downstream tubing, were white. This is very much indicative of ZnO compared to the black/grey colouration of Zn.

5.2.2.2. Discussion

The correlation of different aerosol distributions produced with the oxidation parameters, and visible "white" build-up in the generator, provides good evidence that ZnO is successfully being produced. It was envisioned that TEM and further verification of the ZnO would be carried out in collaboration with Imperial College London. In addition, it was hoped to employ the isotopic labelling expertise of Imperial in conjunction with this generator to allow the nucleation of labelled particles of a variety of sizes. This would then be an extremely useful aerosol source for investigating ENP aerosols, especially for toxicological studies where ZnO particles could be extracted from various organic tissues, and the source and pathways could be tracked by the inscribed Zn isotope ratios. Unfortunately due to personnel changes at Imperial this collaborative work is still outstanding.

5.3. Raman spectroscopic characterisation of ZnO and CeO_2 nanoparticles

5.3.1. Results

All seven PROSPEcT ENP powder samples (see Table I) were analysed by both a Dilor Remote Raman Microscope and an Ocean Optics QE miniature desktop Raman spectrometer. Only data from the Ocean Optics system are presented here for clarity with the ZnO samples shown in Fig. 5.3–1 and the CeO_2 samples shown in Fig. 5.3–2.

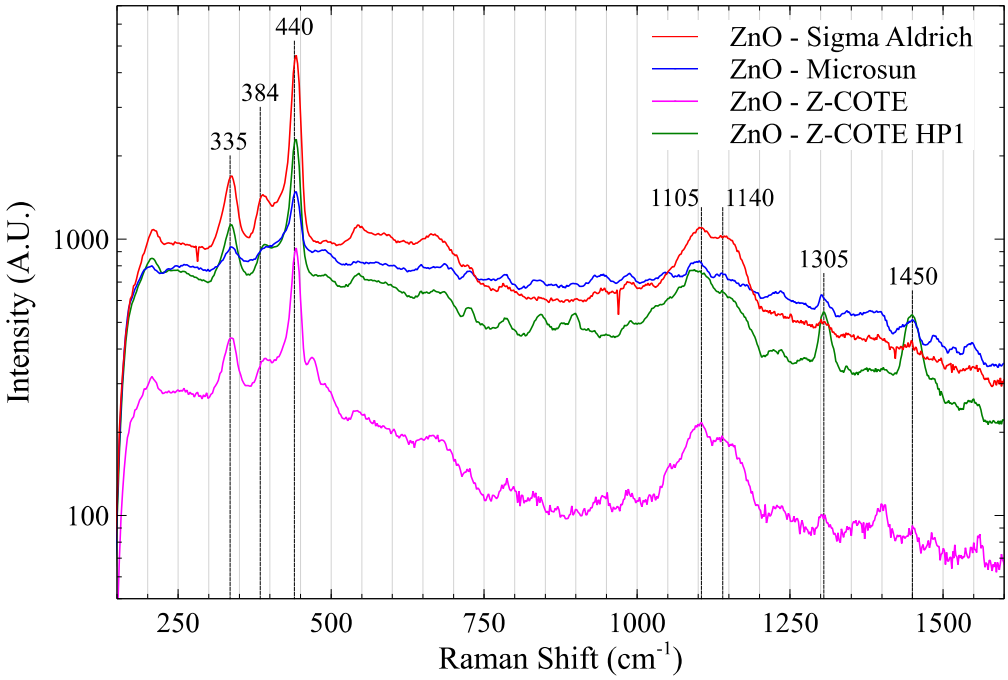

Figure 5.3–1. Comparison of Raman spectra for the different ZnO samples analysed. Each spectrum is an average of 2 – 4 measurement runs.

All of the ZnO spectra are rather similar with the well known characteristic peak at 440 cm^{-1} most clearly significant. Apart from small changes in peak height ratios, the stand-out individual characteristics are strong peaks at 1305 and 1450 cm^{-1} in the hydrophobic coated Z-COTE HP1 sample. In addition, the peaks are less prominent in the Microsun ZnO sample which also exhibits a much reduced broad feature in the 1100s cm^{-1} range compared to the other samples.

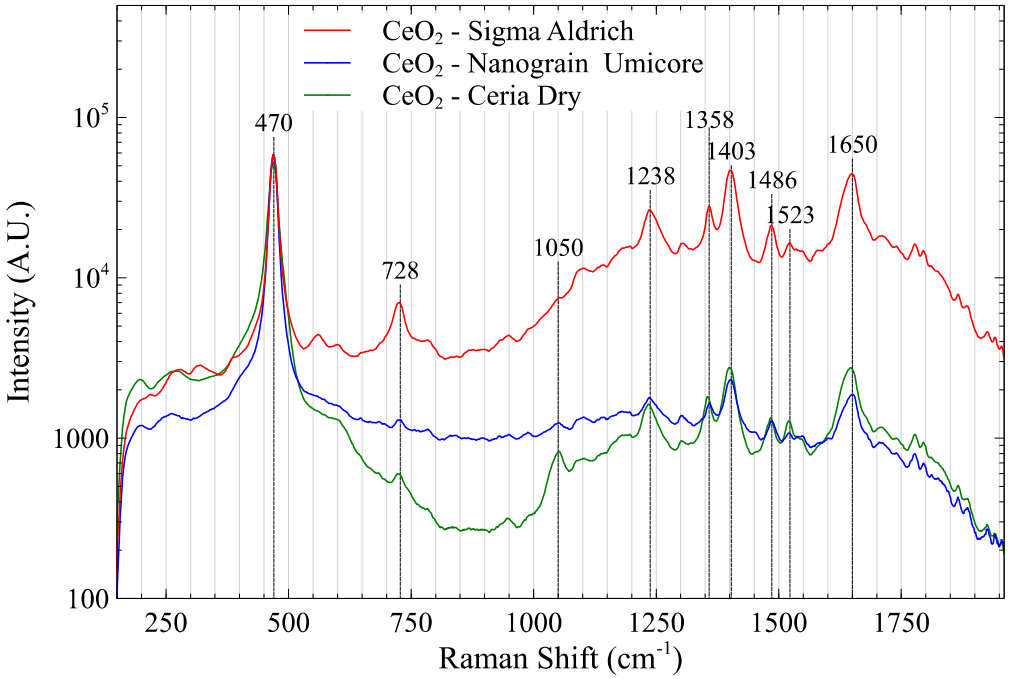

Figure 5.3–2. Comparison of Raman spectra for the different CeO_2 samples analysed. Each spectrum is an average of 2 – 3 measurement runs.

In the CeO_2 results, the main 470 cm^{-1} peak is particularly dominant across all samples. The prominence of some of the peaks changes across the different samples, most notably for the 728 cm^{-1} peak. There is potentially also a peak at 1050 cm^{-1} which is only clearly distinguishable in the Ceria Dry sample.

5.3.2. Discussion

The main ZnO peaks seen at ~330, 380 and 440 cm^{-1} are in line with expectations for ZnO from the literature (e.g. Khan *et al.*, 2005; Dong *et al.*, 2006). Although they are on average a few cm^{-1} higher suggesting that the Ocean Optics system may have benefited from a calibration routine before the measurements (the Dilor system is routinely calibrated to a silicon peak position and indeed the measured peak positions it reported were slightly lower). There may also be potential to distinguish different forms of ZnO ENP, especially those that include additional components or coatings.

The main peak seen for the CeO_2 samples at 470 cm^{-1} is also clearly indicative of CeO_2, although again this is slightly higher than expected from the literature (~464 cm^{-1}, e.g. Spanier *et al.*, 2001; Wang, 2001; Zhang *et al.*, 2002; Kostić *et al.*, 2007; Li *et al.*, 2010). There may be some possibility to distinguish different sample sources here, however, any differences such as the strength of the 728 cm^{-1} peak or possible 1050 cm^{-1} peak, are subtle, and would be difficult to reliably detect. Clearly any change would have to relate to some underlying physical restriction on the vibrational modes, for example relative peak height changes could relate to the structure being more crystalline or disordered in nature. Changes in structure can also start to reveal themselves when nanoparticles are made very small. For example, the main CeO_2 peak has been shown to broaden with decreasing particle size (Wang, 2001; Zhang *et al.*, 2002). However, the

sizes below which such effects start to become noticeable (~20 nm) are not commonly encountered.

5.3.3. Conclusions

Raman spectroscopy has been demonstrated to be effective at identifying ENP samples even with compact and easy to use miniature desktop systems. Spectral differences between the different sample sources of each compound are found to be minimal. This is not surprising given that there is no difference expected in the underlying molecular structure. However, additional peaks are visible in the case of the coated ZnO sample Z-COTE HP1. Although perhaps unsurprising, this is interesting and stimulates further consideration of the possibilities presented by molecular tagging of ENP. The use of additional inactive compounds as additives could be used as a means to track and regulate the passage of ENP through industry, applications and as end-of-life pollutants. Although suitable tagging compounds would need to be developed to be clearly identifiable in spectra, resistant to breakdown in application, and having minimal effect on the desired ENP properties. It is for these reasons that the elsewhere considered isotopic labelling of ENP (Larner *et al.*, 2012) can be considered advantageous, although requiring more expensive techniques to detect.

5.4. Quantitative Raman spectroscopic mapping of aerodynamically size selected samples

5.4.1. Results

An experiment was conducted in four stages. First, aerosols were generated from a ZnO powder; see Fig. 4.4–5. Second, airborne particles of ZnO were collected onto glass slides. After that, Raman spectra of slides containing ZnO particles were recorded. And finally, data were analysed.

Sampling periods were adjusted to achieve different concentrations. Table IV shows the measured total number of particles which passed through the Nano-ID® Select during each sampling interval. This was calculated from the number concentration measured by the CPC (representing all the particle sizes), the sampling time, and the sampling flow rate. Sampling intervals ranged from 15 seconds to 10 minutes, with the target of collecting a range of concentrations within the constraints of having sufficient numbers for representative statistics whilst avoiding overlap of neighbouring particles. Clearly separated particles are necessary to provide a correct count, and therefore, if higher concentrations or longer sampling times are needed, either a diluter or multiple shorter samples may be required.

Sample	A	B	C	D
Total throughput: (No. of Particles)	9.19×10^6	2.46×10^7	4.05×10^7	1.06×10^8
Sample	**E**	**F**	**G**	**H**
Total throughput: (No. of Particles)	2.34×10^8	3.33×10^8	8.28×10^8	1.54×10^9

Table IV. Total sampling throughput for each of the eight sampling runs.

Samples were collected from size stages 4 – 7, covering a total size range of 0.25 – 4 μm (see Table III in Section 4.4.2.1). The relative differences between the total sampling concentrations are the same as the relative differences across any particular size channel only if the shape of the size distribution remains the same throughout.

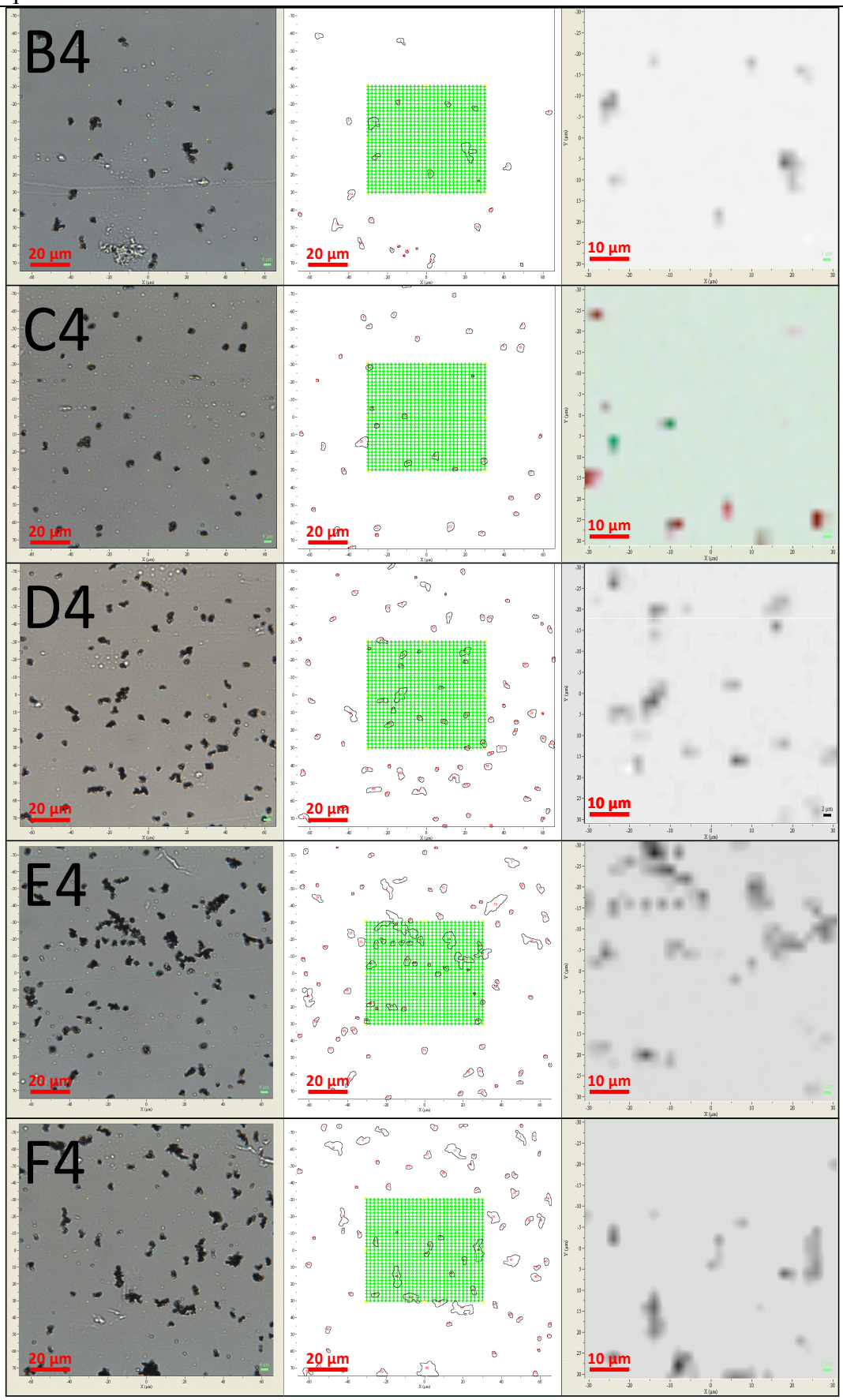

Figure 5.4–1. Overview of images acquired for samples B4 – F4. The full microscopy field of view is shown on the left column. The 31 × 31 grid arrangement for Raman measurements is shown in the centre column, and is overlaid on top of a post-processed version of the microscopy images showing the measured outlines of particles. The right column shows the resulting smoothed Raman data as output from Lab Spec 5 utilizing the 435, 1613, and 1724 cm^{-1} ZnO peaks.

Each individual sample is designated with the letter from Table IV, indicating the sample run concentration, and the channel number (size stage) from Table III, indicating the channel size range. Stage 4 samples in the concentration range B – F were chosen for this Raman study (the specific samples from stage 4 for each concentration shall henceforth be designated B4 – F4). The larger particle size allows for the requisite comparison to microscopy results, while the concentration range chosen gave reasonable count statistics and particle overlap without needing to adjust the analysis process. An overview of the optical and sub-area Raman results achieved for the selected samples B4 – F4 are presented in Fig. 5.4–1. This shows the microscopy images of the chosen sample areas (left column), positioning of the Raman grid relative to each sample (middle column), and resultant smoothed Raman data generated from signal intensity in ZnO Raman peaks (right column) for five different sample concentrations deposited on stage number 4 of the Nano-ID® Select. The sampled areas were systematically chosen from the central region of the particle deposit as described in Section 4.4.2.1.

As well as providing a reference for the Raman data, the optical microscopy images are also useful for testing the efficacy of the automated particle sizing and counting procedure. The accuracy of automated counting is compared to that obtained manually by eye (with assistance of the "Cell Counter" Fiji plug-in) for the microscopy and Raman data in Fig. 5.4–2.

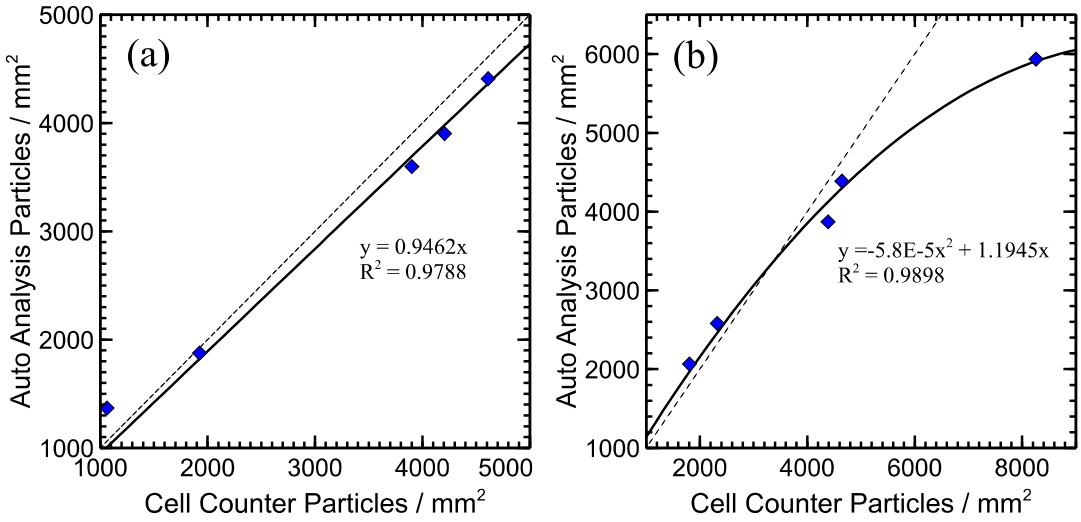

Figure 5.4–2. Comparison of counts per unit area achieved with automatic image analysis / thresholding (Auto Analysis) compared to counting by eye and marking particles (Cell Counter) for the microscopy (a) and Raman (b) images from samples B4 – F4. Dashed lines show a perfect y=x correlation while solid lines show fits to the data with associated fitting parameters.

The counts obtained from the automated counting of Raman and microscopy data from the same samples (B4 – F4) are compared in Fig. 5.4–3. The auto analysis routine provides a measured projected area (A) of the particle in units of μm², once the

appropriate scale has been set in the software. This has been converted to a circular equivalent diameter d_{equiv} (µm) such that $d_{equiv} = 2\sqrt{A/\pi}$.

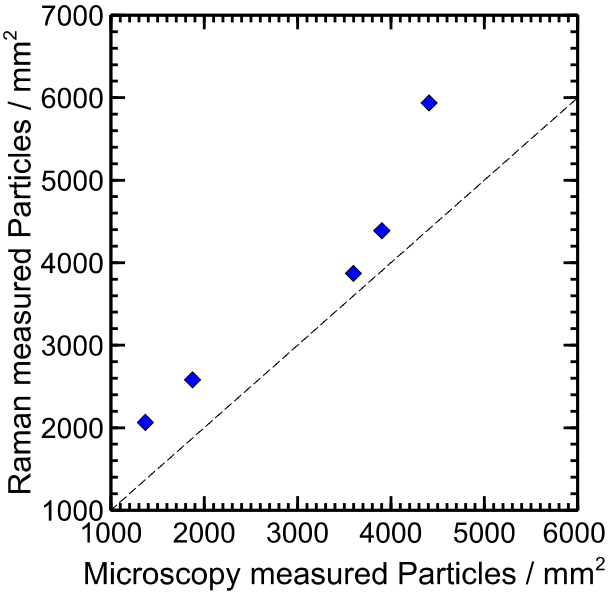

Figure 5.4–3. Comparison of particle concentration measured from the Raman data to that measured from the optical microscopy data. A perfect correlation is shown by the dashed (y=x) line.

Number density distributions for d_{equiv} are shown in Fig. 5.4–4 in order to provide a direct comparison of the sizing between the microscopy and Raman data.

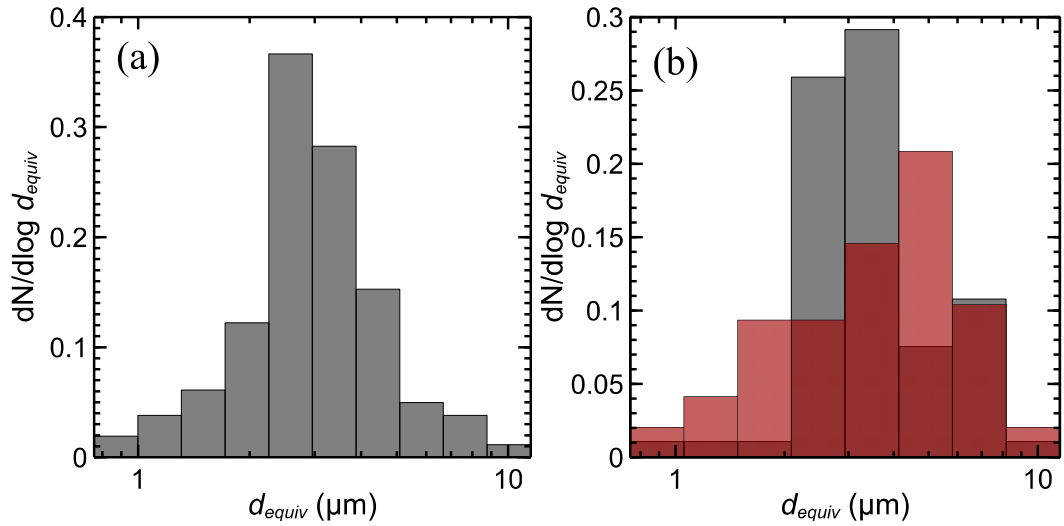

Figure 5.4–4. (a) Size distribution of all particles measured from size stage number 4 microscopy images. (b) Comparison of size distribution from Raman measurements (red, overlaid semi-transparent) compared to the same set of particles measured with microscopy (grey). The y-axis shows the number (*N*) density per log unit size.

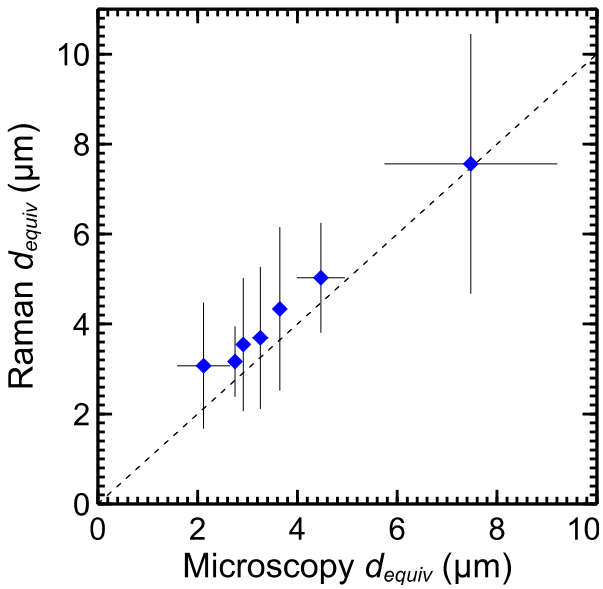

Figure 5.4–5. Particle size measurement comparison between the Raman and microscopy images. Each marker represents a 15 point data cluster with error bars showing the standard deviation of each cluster.

5.4.2. Discussion

Obtaining correct information from Raman maps requires some careful consideration. Many parameters need to be optimized and verified to characterize ENP correctly. These include: the spot size and intensity of the Raman laser source, transversal resolution from the grid density, sampling time, and statistical characterizations of the particle ensemble. With the correct choice of Raman spectroscopy parameters it can be seen (Fig. 5.4–1) that ZnO particles can be reliably resolved, even when using a sampling resolution (here 2 microns) comparable to the particle size. Fig. 5.4–2 (a) demonstrates that particles distinguishable by eye in the image can be accurately counted with automatic image analysis. Accurate counting and sizing is also demonstrated in Fig. 5.4–1 by comparison of the measured particle outlines in the middle column to the raw optical images in the left column. This technique has been successfully carried over for processing the Raman data.

The critical step in the image processing procedure is the thresholding step, where each pixel is limited to a binary distinction between “particle” and “background”. Setting the threshold level too high will result in the merging of neighbouring particles, whilst setting the level too low results in smaller particles or those with a lower contrast to the background not being measured. Due to the constant light levels in the microscopy images, it was possible to use the same level adjustment across all of the optical images. Therefore, in theory the analysis could have been fully automated for the microscopy images. However for the Raman map images, there was some adjustment of contrast/brightness and thresholding steps from image to image, and so additional work would be required here to fully automate this process. Further study may allow the entire process to be made fully autonomous, with tighter controls on the Raman

mapping parameters, or by developing an effective thresholding algorithm.

The correlation to manual counts in Fig. 5.4–2 (b) tails off at higher concentrations, which can be attributed to the comparatively low transversal resolution of the Raman data obtained using a 2 μm grid spacing. This results in an increased overlap of adjacent particles at higher concentrations, causing the analysis routine to measure multiple particles as one. This leads to under-counting and over-sizing. The over-sizing can be seen in the shift in the Raman distribution in Fig. 5.4–4 (b), as well as the greater abundance of data points above the 1:1 dashed line shown in Fig. 5.4–5. The grid resolution was deliberately kept low in this study to allow for a large enough area to be measured to generate useful statistics within reasonable measurement times (~70 minutes for each of the 961 point Raman maps acquired in this study). For a given sampling period, higher concentrations of particles in the air would lead to a higher deposited concentration, and hence increased particle overlap. However, this situation can be avoided for higher concentration aerosols, by either reducing the sampling time and volume of air sampled, diluting the aerosol by a known ratio prior to sampling, or by taking multiple shorter samples over the course of the desired total sampling period. The sampling approach should be optimised for any given exposure scenario. For example, longer sampling periods may be required to provide a representative exposure assessment over a working shift, while the relevance of the chosen sampling point to personal exposure should also be taken into account.

A higher grid resolution (down to 500 nm) could also be used to more clearly distinguish particles. The limits on resolution will ultimately be set by the spot size of the laser. Spot sizes with a full-width at half-maximum of < 1 μm have been achieved utilizing a 100× objective lens. Here we focussed on particles in the micron size range as a first proof of principle allowing for the required comparison to optical microscopy results. In addition, the 473 nm laser used in this study should offer improved transversal resolution compared to the more commonly employed 633 nm laser.

As the ZnO particles were well resolved they could be counted reliably in the Raman data. Any offset from the microscopy data in counts as seen in Fig. 5.4–3 can be attributed to the reduced statistical significance of the Raman data due to the reduced sample areas measured compared to the optical images.

The size distributions given in Fig. 5.4–4 demonstrate that the d_{equiv} size parameter chosen correlates reasonably well to the aerodynamic particle size (expected to be 2 – 4 μm in this sampling stage). This may be expected for samples without complicated structural or fractal properties. The reduced resolution used for the Raman sampling can be seen to cause broadening of the size distribution and a slight shift to larger sizes due to neighbouring particles becoming merged. The limited transversal resolution, and difficulty in choosing a correct threshold in the software analysis, causes significant uncertainty in the particle sizes measured from the Raman data as seen in Fig. 5.4–5. The critical point to bear in mind is that the aerodynamic particle size obtained from the sampling method is the size parameter of importance when considering particle deposition in the lung and associated health risks. However, it is interesting to note the potential for sizing information to be obtained from the Raman data alone. This could allow some approximate size information to be assigned to polydisperse particles obtained from a simpler sampling system, or provide more detailed characterization information when combined with the aerodynamic particle size obtained from the Nano-ID® Select.

The glass substrate used in this study (without ZnO particles) gives a complicated Raman spectrum: comprising amorphous SiO_2, other unidentified lines (Fig. 4.4–9), a fluorescent background Raman signal and additionally, some contaminating particles (visible as white particles in the microscopy images in the left column of Fig. 5.4–1). This generates a background signal that must be filtered out to identify the (ZnO) particles of interest. Therefore, the clear, unambiguous detection of ZnO particles observed here, demonstrates the ability to resolve a specific chemical species against a contaminating background Raman signal. It is worth considering that the influence of interfering substances is likely to be scenario specific and under certain conditions such as mixed species agglomerates, the discrimination power of Raman will potentially be reduced. In addition, the Raman spectrum could be complicated by additional lines if multiple species inhabit the region covered by the laser spot size. However, these are standard challenges in the field, and, as long as a signal can be detected for a given species, the number of such signatures can be quantified and correlated to the aerodynamic size as defined by the sampling method.

This study has focussed on the micron size range to allow for proof-of-concept by comparison to microscopy images. The size range can be extended to sub-micron by changing the objective lens in the setup to a 100×. Although reliable sizing information may not be achievable into the nanometre range from the Raman data alone, detection and some quantification should still be achievable. Particles which are smaller than the laser beam diameter still contribute to the Raman signal, but their size will be unresolvable by Raman alone. Here the segregated sampling could be of advantage to provide size-resolved information. The sensitivity of the approach can be further improved by considering more advanced Raman techniques such as Surface Enhanced Raman Spectroscopy (SERS), or Coherent Anti-Stokes Raman Spectroscopy (CARS), although the latter requires prior knowledge of the target material.

Although the Raman spectrometer system used in this study is certainly not compact, the approach should be equally possible utilising a small bench-top spectrometer coupled with an automated miniature translation stage.

Due to the large number of parameters in this study, it is difficult to assess the lower detection limit of this approach. However we can make a rough estimation by considering the detection of a single particle in one grid area measurement. A high detection rate is considered to be justified by the good correlation between the optical microscopy and Raman results shown in Fig. 5.4–1. The Raman map grid area used (as shown in the centre column of Fig. 5.4–1) is 3,600 μm^2 and a total deposit area on the slide is 50 mm^2. If we assume uniform deposition across the deposit area, a single detected particle in a grid would correspond to a total of ~14,000 particles deposited on the slide. If we conservatively estimate that only particles in the diameter range (d_{equiv}) of 2 – 4 μm will be reliably detected by our 2 μm grid spacing, this leads to a deposited mass sensitivity of ~200 ng (assuming spherical particles of density 1,000 kg/m^3). While considering the detection of one of the smallest particles seen above (~0.7 – 0.8 μm) gives a total deposited mass of ~3 ng. These values are approximate estimates, especially in the latter case where the measured size from the image is smaller than can be properly resolved, and there starts to be significant probability of being missed by the sampling grid due to undersampling. However, the values obtained can be taken as indicative of the order of mass sensitivity available, even without optimization of the system. Clearly this could be improved on simply by measuring a larger area of the

deposit, or by adjusting the Raman setup for better sensitivity to smaller particles, or by increasing the density of the deposit with better particle focussing in the sampling system.

These estimates can be used to evaluate the number concentration and the mass concentration of airborne particles. For 2 – 4 μm particles, the lowest number concentration is 14,000/*V*, where *V* is the sampling volume. The Nano-ID® Select sampling flow rate is 20 litres/min. If we consider a typical sampling time of 100 minutes, the sampled volume *V* is therefore 2,000 litres or 2 m^3. The lower detection limit of the number concentration of particles is then 7,000 per m^3 or 7×10^{-3} particles per cm^3.

From the above, the lower mass concentration limit of 2 – 4 μm particles is 200 ng / 2 m^3 equal to 100 ng/m^3. This is considerably lower than the majority of exposure limits for toxic substances. Thus, Raman chemical speciation, quantified in the manner described above, is practically suitable for the majority of occupational hygiene applications to evaluate potential health risks at working places.

Importantly, it is known that nanoparticles will generally agglomerate resulting in sub-micron or micrometer sized clusters. The aerosols obtained in this study were generated from typical commercial samples currently in use in the nanotechnology industry.

5.5. Surface sensitive heterogeneous nucleation

5.5.1. Results

A stabilised test aerosol of NaCl was generated with a nebuliser from Particle Measuring Systems Inc. and recorded by the surface area prototype. The prototype was adjusted to measure either surface area distributions, or alternatively, number distributions by increasing the saturation conditions such that it is operating as an SMPS. Example data from an NaCl aerosol is shown below in Figs. 5.5–1 and 5.5–2. The measured surface area distribution is also compared to that calculated from the number distribution assuming spherical particles as is often presented as an option in SMPS instruments.

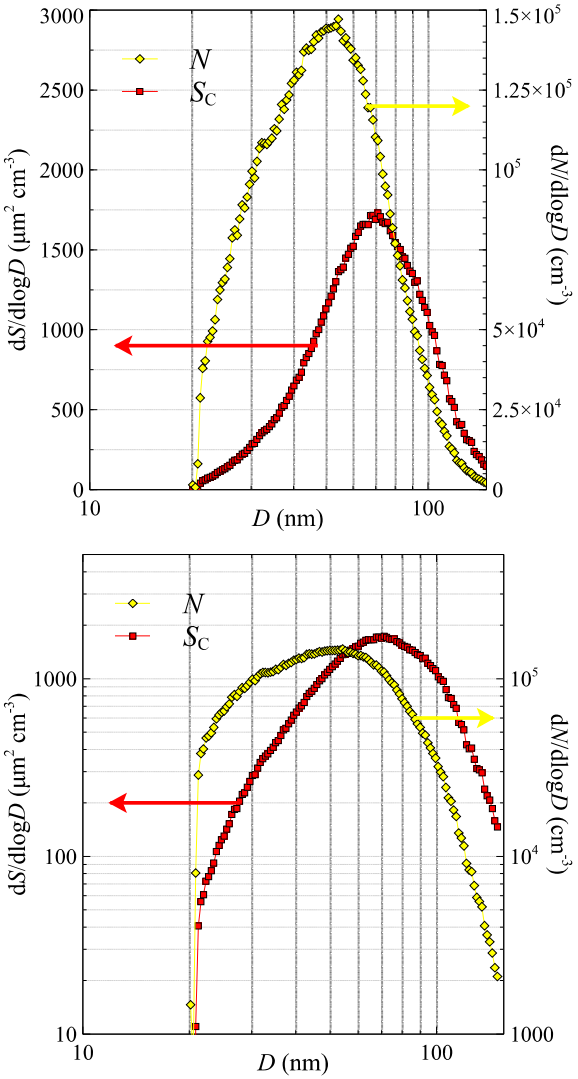

Figure 5.5–1. Number particle distribution (N, right side ordinate) of a NaCl aerosol. Also shown is the traditional calculated surface distribution assuming spherical particles (S_C, left side ordinate). Linear scale ordinate in top figure, logarithmic scale ordinate in bottom figure.

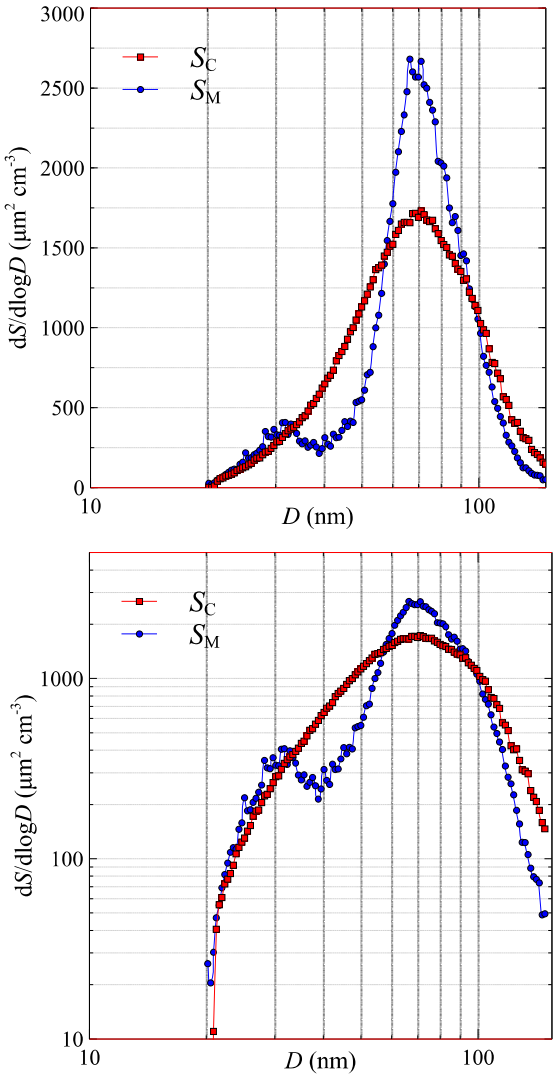

Figure 5.5–2. The calculated surface distribution from Fig. 5.5–1 is shown again – S_C, this time compared to the surface area distribution as measured with the surface sensor – S_M. Linear scale ordinate in top figure, logarithmic scale ordinate in bottom figure.

5.5.2. Discussion

In Fig. 5.5–1 we can see the standard approach to calculating a surface area distribution assuming spherical particles, as used for example in traditional SMPS instruments. The number distribution has been measured using a standard DMA and CPC (SMPS) setup. The calculated surface area distribution is shifted to the right of the number distribution as expected from the d^2 dependency of surface area, but there is no meaningful change to the distribution as it is just a change to the displayed scaling. There is no new information. In Fig. 5.5–2 we compare the calculated surface area distribution from the previous figure to the surface area distribution as measured directly with the modified CPC / surface sensor setup. First, it is worth noting that the main characteristics of the calculated and measured surface area distributions are similar. The distributions are of a similar overall shape and the total (integrated) surface area is similar in both cases (as expected from the calibration approach in Section 4.5.4). The similarity in overall shape and position is a good demonstration that the theory is working correctly, and that we are measuring surface area as expected. In addition, a second feature is seen in the measured surface area distribution which is not visible in the calculated distribution. This suggests a potential bimodality of morphologies across this size range. This is new information about the aerosol that is not present in the number distribution (or the surface area distribution calculated from it). For more complex materials the differences between the calculated and measured surface area distributions are expected to be more significant.

Although these initial results with this new technology are promising; there is still much work needed to understand it fully. For example, heterogeneous nucleation is also sensitive to the chemical nature of both the nucleus surface and the working fluid material used to form the nucleated droplets. This can be seen in Fig. 4.5–3 where square relation slopes for Cr_2O_3 and NaCl aerosols are offset from each other under identical saturation conditions. Therefore, the operating parameters of the surface sensor need to be optimised depending on the aerosol to be measured. This also creates an uncertainty in interpreting results in the case of unknown or mixed aerosols. These circumstances are much more realistic in real-world toxicology/exposure scenarios compared to the lab generated single component aerosols used here. Also, the validity of interpreting the distribution shape as being a surface area distribution is defined by the related counting efficiency curve (as shown in Fig. 4.5–3), showing a square response over the particle size range of interest. In practise it is found that the size range over which a square fit is valid is in general more limited than the total size range of an SMPS system for measuring size. However, the size range of the surfacing response can be adjusted by changing the operating parameters of the surface sensor device. Therefore, in operation, it is preferable to have some *a priori* knowledge of both the size range and material that one is interested in measuring. It may be possible to mitigate the difficulty in this somewhat by either running the device multiple times with different settings, or, by having a larger device with parallel detectors measuring under different conditions simultaneously.

5.6. Outstanding questions

There are inevitably a number of outstanding questions related to the new approaches presented here. The most important are considered to be as follows for each of the two main avenues of research:

Surface sensitive nucleation

Q1. How does the response vary for a broader range of materials?

Q2. How to interpret or calibrate the response in the case of an unknown or mixed aerosol?

Q3. How far can the applicable size range be extended and does the size response power (d^x) maintain a value of 2 for larger sized particles?

Quantitative size-resolved Raman spectroscopic analysis

Q4. How is the sensitivity impacted for different target materials across a range of mixed aerosol backgrounds?

Q5. Can the image analysis be fully automated for controlled laboratory experiments or even in the field?

Q6. How far can advanced Raman techniques push the limits of size sensitivity and resolution?

The surface area prototype device has been sent to the Institute of Occupational Medicine in Edinburgh to undergo further laboratory testing and field trials. It is hoped that these trials will generate data which will improve our understanding of how this technology performs in a wider range of conditions and begin to answer Q1 – Q3. A proper understanding of the relevant chemical nature and size dependency of surface sensitive nucleation would be a great step forward from both a theoretical and practical standpoint. When considering nucleation on a particle, one may be tempted to consider the nucleation rate to be controlled by the rate of attachment of vapour molecules, and therefore that the surface area dependency might be the same "Fuchs" or "active" surface area as relevant to ion attachment rates. However, with respect to equations (14) and (15) in Section 3.3.2, it can be seen that the situation is complicated by the fact that the nucleation rate is governed by the attachment rate of molecules to the newly formed phase embryo surface, which is independent of the particle (inclusion) surface. A larger particle surface area will result in more sites for these embryos to form, and hence a higher probability of nucleation. In any case, a more detailed analysis and further testing are required to gain a better understanding of the details of this process and verify a distinct advantage over existing techniques.

To confirm the general applicability of the Raman methodology, Q4 needs to be addressed with a broad range of mixed aerosols of varying relative proportions. Only once its usefulness can be demonstrated in real world scenarios can it then be considered to try to push the boundaries of speed and sensitivity in Q5 – Q6. However, to date the basic principle of both approaches has been successfully demonstrated, and so further investigation and development can be warranted. Looking further ahead, it could be envisioned to carry out parallel measurements with both techniques on the same aerosol source. This has great potential to provide complete and direct characterisation of size, number, surface area, and chemical nature of aerosol distributions relevant to occupational hygiene or environmental monitoring.

Chapter 6. Conclusions

6.1. Quantitative exposure assessment from size selective sampling and Raman spectroscopic mapping analysis

A new approach has been developed and demonstrated for the quantification of exposure, and potential toxicological response, to airborne particles and nanomaterials. Size resolved sampling is combined with Raman spectroscopic spatial mapping analysis to provide chemically distinguished quantification of ZnO particles. This combination considerably reduces or eliminates uncertainties related to the sensitivity of the Raman signal to particle size. Therefore, in this way a quantitative evaluation of ZnO particle number and mass with Raman spectroscopy becomes possible. In principle this technique can be extended to any aerosol below 100 nm with a detectable Raman signature. The test case particles are shown to be reliably detected in the Raman data, and can be counted and sized in a manner which is at least comparable to what is achievable with optical microscopy imaging. The most significant advantage of using a Raman mapping approach is the crucial chemical information acquired, allowing different species to be discriminated, enabling a determination of the concentration of benign and toxic particles in a sample. Although this comes with a time penalty compared to optical imaging, it adds significantly to the value of the data.

There is still some debate as to what the most significant metric is for determining the toxicity of airborne pollutants (e.g. number, mass, surface area, etc.), but it is generally recommended to gather as much chemically selective and other distinguishing information as possible. The aerodynamically selected first stage used here is critical in determining aerosol deposition in the respiratory tract. Combined with Raman quantification, a specific measure of exposure can be obtained. Ongoing progress in the development of miniature Raman systems, and miniature translation stages as required for mapping, opens the possibility of using this technique as a tool for *in situ* occupational hygiene health risk assessment.

The lower detection limit of the described approach is conservatively estimated at 200 ng in a sample. Given a sampling time of 100 minutes this would correspond to a number concentration sensitivity of 7×10^{-3} cm^{-3} or a mass concentration sensitivity of 100 ng/m^3. The sensitivity of this technique is therefore more than sufficient to cover the majority of occupational hygiene exposure risk requirements.

6.2. Surface sensitive heterogeneous nucleation

A prototype device has been developed for the online measurement of nanoparticle surface area distributions in aerosols. The approach is based on a newly discovered type of heterogeneous nucleation operating at much lower saturation conditions than normally used in nucleation techniques. Under these conditions, the probability of nucleation is found to be proportional to the surface area of the nuclei. Thus, the number of droplets formed, and therefore the number of counts measured, is proportional to the surface area of nanoparticles present rather than their number. This is a truly ground-breaking and novel way of quantifying one of the most important health related metrics – the surface area of nanoparticles. It has great potential for many applications and currently the Institute of Occupational Medicine in Edinburgh is testing the prototype instrument in the field. It is also interesting to consider what impact the consideration of low saturation nucleation conditions may have in other fields. Any dynamic system transitioning from one phase to another must at some stage experience low saturation conditions before the onset of fully developed nucleation. It is therefore likely that the first embryos of the new phase formed, which are likely to direct the rest of the phase change process, will be characterised by the surface area of nuclei present.

6.3. Main results achieved

In this thesis the following major results have been achieved:

- A portable planar differential mobility analyser (DMA) has been developed and built, and demonstrated successful and accurate operation across a useful range of flow rates and nanoparticle sizes.
- Zn and ZnO aerosols have been successfully generated allowing for the use of any Zn source to be used as desired (e.g. for calibration of instruments and toxicological studies).
- Industrial standard ZnO and CeO_2 samples from the PROSPEcT project have been characterised by Raman spectroscopy and by SMPS analysis of aerosol size distributions from an aerosoliser.
- Discrimination of sampled ZnO aerosols against a background material is demonstrated with Raman spectroscopy.
- Raman spectroscopic mapping and image analysis is combined with aerodynamically size resolved sampling to demonstrate a novel methodology for the chemical nature and size resolved quantitative assessment of aerosol exposure.
- A novel surface sensitive nucleation technology is presented and demonstrated as a proof of principle.
- A surface area prototype device, incorporating the portable DMA and nucleation based surface sensor, has been built, tested, and is undergoing further laboratory tests and field trials at the Institute of Occupational Medicine in Edinburgh.

Acknowledgements

Sofia Billet[1] and Gillian Carse[1]

Contribution of data presented in Fig. 4.5–3.

Agnieszka Dybowska[2] and Eva Valsami-Jones[2]

TEM images of Zn particles from generator shown in Figs. 5.2–2 – 5.2–4.

Ajaya Ghimire[3]

DMA testing at Particle Measuring Systems Inc. (data in Fig. 4.1–22 (b) – (d)).

Harald Gnewuch[4]

ZnO generator manufacture and development. Assistance with electronics development for DMA prototype.

Boris Gorbunov[4]

All COMSOL Multiphysics® modelling.

David Green[4]

Assistance with setting up the PA100 aerosoliser at NPL.

Fiona Larner[5]

Additional testing of Zn/ZnO generator. Cooperation and organisation with Imperial College London.

Alexander Meadway[6], Chris Costa[6] and Adrian Bradu[6]

Assistance with various optical experiments at UKC.

Robert Muir[4]

Review of material, assistance with collaborations and coordination within PROSEPEcT consortium.

Mark Price[6]

Assistance with the UKC Raman spectrometer systems.

Vinay Ranganathan[4]

Particle charger performance measurements for the data shown in Fig. 4.1–7. Additional testing of Zn/ZnO generator.

Mark Rehkamper[5]

Cooperation and organisation with Imperial College London.

Jonathan Rowles[4]

Contribution of data presented in Figs. 4.5–3, 5.5–1 and 5.5–2.

Dimitris Sarantaridis[7]

General assistance at NPL and with electrospray sucrose generator.

Jordan Tompkins[7]

General assistance at NPL. Figs. 4.3–7 – 4.3–8 and the data shown in Table II.

[1] – Institute of Occupational Medicine, Edinburgh, UK.

[2] – Natural History Museum, London, UK.

[3] – Particle Measuring Systems Inc., Boulder, Colorado, USA.

[4] – Naneum Ltd., Canterbury, UK.

[5] – Imperial College London, London, UK.

[6] – University of Kent, Canterbury, UK.

[7] – National Physical Laboratory, Teddington, UK.

(Affiliations relate to period when work was carried out and may in some cases be outdated).

This work was conducted as part of PROSPEcT, which is a public-private partnership between DEFRA, EPSRC and TSB and the Nanotechnology Industries Association (NIA Ltd.) and its members, and was administered by the DEFRA LINK Programme.

References

Abraham, F. F. (1974). *Homogeneous Nucleation Theory: The Pretransition Theory of Vapor Condensation* (pp. 2–62). Academic Press, New York.

Abràmoff, M. D., Magalhães, P. J., & Ram, S. J. (2004). "Image processing with ImageJ". *Biophotonics International*, *11*(7), 36–42. Retrieved from http://webeye.ophth.uiowa.edu/dept/BIOGRAPH/ABRAMOFF/ImageJ.pdf

Adachi, M., Okuyama, K., Kim, T., Kadono, H., & Cho, S. J. (1996). "Experimental evaluation of ion-induced nucleation in nanometer-aerosol formation by α-ray radiolysis of $SO_2/H_2O/N_2$ mixtures". *Colloids and Surfaces A: Physicochemical and Engineering Aspects*, *109* (20 April), 39–48. doi:10.1016/0927-7757(95)03472-2

Adams, K. M. (1988). "Real-time in situ measurements of atmospheric optical absorption in the visible via photoacoustic spectroscopy. 1: Evaluation of photoacoustic cells." *Applied Optics*, *27*(19), 4052–6. doi:10.1364/AO.27.004052

Adams, K. M., Davis, L. I., Japar, S. M., & Pierson, W. R. (1989). "Real-time, in situ measurements of atmospheric optical absorption in the visible via photoacoustic spectroscopy—II. Validation for atmospheric elemental carbon aerosol". *Atmospheric Environment*, *23*(3), 693–700. doi:10.1016/0004-6981(89)90017-6

Adler, D. C., Huang, S.-W., Huber, R., & Fujimoto, J. G. (2008). "Photothermal detection of gold nanoparticles using phase-sensitive optical coherence tomography." *Optics Express*, *16*(7), 4376–93. doi:10.1364/OE.16.004376

Agarwal, J., & Sem, G. (1980). "Continuous flow, single-particle-counting condensation nucleus counter". *Journal of Aerosol Science*, *11*(4), 343–357. doi:10.1016/0021-8502(80)90042-7

Ahlquist, N. C., & Charlson, R. J. (1967). "A New Instrument for Evaluating the Visual Quality of Air". *Journal of the Air Pollution Control Association*, *17*(7), 467–469. doi:10.1080/00022470.1967.10469006

Ahn, K.-H., & Chung, H. (2010). "Aerosol electrical mobility spectrum analyzer". *Journal of Aerosol Science*, *41*(4), 344–351. doi:10.1016/j.jaerosci.2010.01.005

Aizenberg, V., Grinshpun, S. A., Willeke, K., Smith, J., & Baron, P. A. (2000). "Measurement of the Sampling Efficiency of Personal Inhalable Aerosol Samplers Using a Simplified Protocol". *Journal of Aerosol Science*, *31*(2), 169–179. doi:10.1016/S0021-8502(99)00037-3

Aizenberg, V., Choe, K., Grinshpun, S. A., Willeke, K., & Baron, P. A. (2001). "Evaluation of personal aerosol samplers challenged with large particles". *Journal of Aerosol Science*, *32*(6), 779–793. doi:10.1016/S0021-8502(00)00119-1

Alfonso, B.-F., & Al-Rubeai, M. (2011). "Flow Cytometry". In M. Moo-Young (Ed.), *Comprehensive Biotechnology* (Second Edition, pp. 559–578). Academic Press, New York, San Francisco, London. doi:10.1016/B978-0-08-088504-9.00065-9

Alguacil, F. J., & Alonso, M. (2006). "Multiple charging of ultrafine particles in a corona charger". *Journal of Aerosol Science*, *37*(7), 875–884. doi:10.1016/j.jaerosci.2005.08.007

Ali, S. M., Bonnier, F., Ptasinski, K., Lambkin, H., Flynn, K., Lyng, F. M., & Byrne, H. J. (2013). "Raman spectroscopic mapping for the analysis of solar radiation induced skin damage". *The Analyst*, *138*, 3946–3956. doi:10.1039/c3an36617k

Alim, K. A., Fonoberov, V. A., Shamsa, M., & Balandin, A. A. (2005). "Micro-Raman investigation of optical phonons in ZnO nanocrystals". *Journal of Applied Physics*, *97*(12), 124313. doi:10.1063/1.1944222

Allen, G., Sioutas, C., Koutrakis, P., Reiss, R., Lurmann, F. W., & Roberts, P. T. (1997). "Evaluation of the TEOM® Method for Measurement of Ambient Particulate Mass in Urban Areas". *Journal of the Air & Waste Management Association*, *47*(6), 682–689. doi:10.1080/10473289.1997.10463923

Allen, J. O., Fergenson, D. P., Gard, E. E., Hughes, L. S., Morrical, B. D., Kleeman, M. J., Gross, D. S., Gälli, M. E., Prather, K. A., Cass, G. R. (2000). "Particle Detection Efficiencies of Aerosol Time of Flight Mass Spectrometers under Ambient Sampling Conditions". *Environmental Science & Technology*, *34*(1), 211–217. doi:10.1021/es9904179

Allen, M. D., & Raabe, O. G. (1985). "Slip correction measurements of spherical solid aerosol particles in an improved Millikan apparatus". *Aerosol Science and Technology*, *4*(3), 269–286. doi:10.1080/02786828508959055

Alonso, M., & Endo, Y. (2001). "Dispersion of aerosol particles undergoing Brownian motion". *Journal of Physics A: Mathematical and General*, *34*(49), 10745–10755. doi:10.1088/0305-4470/34/49/301

Alonso, M. (2002). "Reducing the diffusional spreading rate of a Brownian particle by an appropriate non-uniform external force field". *Journal of Aerosol Science*, *33*(3), 439–450. doi:10.1016/S0021-8502(01)00190-2

Alonso, M., & Alguacil, F. J. (2008). "Particle Size Distribution Modification During and After Electrical Charging : Comparison between a Corona Ionizer and a Radioactive Neutralizer". *Aerosol and Air Quality Research*, *8*(4), 366–380. doi:10.4209/aaqr.2008.07.0029

Alvarez-Román, R., Naik, a, Kalia, Y. N., Guy, R. H., & Fessi, H. (2004). "Skin penetration and distribution of polymeric nanoparticles." *Journal of Controlled Release : Official Journal of the Controlled Release Society*, *99*(1), 53–62. doi:10.1016/j.jconrel.2004.06.015

Amodeo, T., Dutouquet, C., Le Bihan, O., Attoui, M., & Frejafon, E. (2009). "On-line determination of nanometric and sub-micrometric particle physicochemical characteristics using spectral imaging-aided Laser-Induced Breakdown Spectroscopy coupled with a Scanning Mobility Particle Sizer". *Spectrochimica Acta Part B: Atomic Spectroscopy*, *64*(10), 1141–1152. doi:10.1016/j.sab.2009.07.031

Anastasio, C., & Martin, S. T. (2001). "Atmospheric Nanoparticles". *Reviews in Mineralogy and Geochemistry*, *44*(1), 293–349. doi:10.2138/rmg.2001.44.08

Andreae, M. O., & Rosenfeld, D. (2008). "Aerosol–cloud–precipitation interactions. Part 1. The nature and sources of cloud-active aerosols". *Earth-Science Reviews*, *89*(1-2), 13–41. doi:10.1016/j.earscirev.2008.03.001

Annibaldi, A., Truzzi, C., Illuminati, S., & Scarponi, G. (2011). "Direct gravimetric determination of aerosol mass concentration in central antarctica." *Analytical Chemistry*, *83*(1), 143–51. doi:10.1021/ac102026w

Ardelean, H., Frateur, I., & Marcus, P. (2008). "Corrosion protection of magnesium alloys by cerium, zirconium and niobium-based conversion coatings". *Corrosion Science*, *50*(7), 1907–1918. doi:10.1016/j.corsci.2008.03.015

Armendariz, A., & Leith, D. (2002). "Concentration measurement and counting efficiency for the aerodynamic particle sizer 3320". *Journal of Aerosol Science*, *33*(1), 133–148. doi:10.1016/S0021-8502(01)00152-5

Arnold, M. S., Avouris, P., Pan, Z. W., & Wang, Z. L. (2003). "Field-Effect Transistors Based on Single Semiconducting Oxide Nanobelts". *The Journal of Physical Chemistry B*, *107*(3), 659–663. doi:10.1021/jp0271054

Arnott, W. P., Moosmüller, H., Rogers, C. F., Jin, T., & Bruch, R. (1999). "Photoacoustic spectrometer for measuring light absorption by aerosol: instrument description". *Atmospheric Environment*, *33*(17), 2845–2852. doi:10.1016/S1352-2310(98)00361-6

Arnott, W. P., Moosmüller, H., & Walker, J. W. (2000). "Nitrogen dioxide and kerosene-flame soot calibration of photoacoustic instruments for measurement of light absorption by aerosols". *Review of Scientific Instruments*, *71*(12), 4545. doi:10.1063/1.1322585

Arnott, W. P., Hamasha, K., Moosmüller, H., Sheridan, P. J., & Ogren, J. A. (2005). "Towards Aerosol Light-Absorption Measurements with a 7-Wavelength Aethalometer: Evaluation with a Photoacoustic Instrument and 3-Wavelength Nephelometer". *Aerosol Science and Technology*, *39*(1), 17–29. doi:10.1080/027868290901972

Artaxo, P., Rabello, M., Maenhaut, W., & van Grieken, R. (1992). "Trace elements and individual particle analysis of atmospheric aerosols from the Antarctic peninsula". *Tellus*, *44B*(4), 318–334. doi:10.1034/j.1600-0889.1992.00010.x

Asbach, C., Fissan, H., Stahlmecke, B., Kuhlbusch, T. A. J., & Pui, D. Y. H. (2008). "Conceptual limitations and extensions of lung-deposited Nanoparticle Surface Area Monitor (NSAM)". *Journal of Nanoparticle Research*, *11*(1), 101–109. doi:10.1007/s11051-008-9479-8

Asbach, C., Kaminski, H., Fissan, H., Monz, C., Dahmann, D., Mülhopt, S., Paur, H. R., Kiesling, H. J., Herrmann, F., Voetz, M., Kuhlbusch, T. A. J. (2009). "Comparison of four mobility particle sizers with different time resolution for stationary exposure measurements". *Journal of Nanoparticle Research*, *11*(7), 1593–1609. doi:10.1007/s11051-009-9679-x

Asbach, C., Aguerre, O., Bressot, C., Brouwer, D. H., Gommel, U., Gorbunov, B., Le Bihan, O., Jensen, K. A., Kaminski, H., Keller, M., Koponen, I. K., Kuhlbusch, T. A. J., Lecloux, A.,

Morgeneyer, M., Muir, R., Shandilya, N., Stahlmecke, B., Todea, A. M. (2014). "Chapter 7 – Examples and Case Studies". In *Handbook of Nanosafety Measurement - Exposure and Toxicology* (pp. 223–278). Elsevier Inc. doi:10.1016/B978-0-12-416604-2.00007-X

Ault, A. P., Zhao, D., Ebben, C. J., Tauber, M. J., Geiger, F. M., Prather, K. A., & Grassian, V. H. (2013). "Raman microspectroscopy and vibrational sum frequency generation spectroscopy as probes of the bulk and surface compositions of size-resolved sea spray aerosol particles". *Physical Chemistry Chemical Physics : PCCP*, *15*(17), 6206–14. doi:10.1039/c3cp43899f

Avzianova, E., & Brooks, S. D. (2014). "Analysis of nickel (II) in particulate matter by Raman microspectroscopy". *Journal of Aerosol Science*, *67* (January), 207–214. doi:10.1016/j.jaerosci.2013.10.003

Babich, P., Wang, P.-Y., Allen, G., Sioutas, C., & Koutrakis, P. (2000). "Development and Evaluation of a Continuous Ambient PM 2.5 Mass Monitor". *Aerosol Science and Technology*, *32*(4), 309–324. doi:10.1080/027868200303641

Babis, J. S., Sperline, R. P., Knight, A. K., Jones, D. A., Gresham, C. A., & Denton, M. B. (2009). "Performance evaluation of a miniature ion mobility spectrometer drift cell for application in hand-held explosives detection ion mobility spectrometers". *Analytical and Bioanalytical Chemistry*, *395*(2), 411–9. doi:10.1007/s00216-009-2818-5

Baltensperger, U., Gäggeler, H. W., & Jost, D. T. (1988). "The epiphaniometer, a new device for continuous aerosol monitoring". *Journal of Aerosol Science*, *19*(7), 931–934. doi:10.1016/0021-8502(89)90101-8

Bamwenda, G. R., & Arakawa, H. (2000). "Cerium dioxide as a photocatalyst for water decomposition to O2 in the presence of Ce_{aq}^{4+} and Fe_{aq}^{3+} species". *Journal of Molecular Catalysis A: Chemical*, *161*(1-2), 105–113. doi:10.1016/S1381-1169(00)00270-3

Bamwenda, G. R., Uesigi, T., Abe, Y., Sayama, K., & Arakawa, H. (2001). "The photocatalytic oxidation of water to O_2 over pure CeO_2, WO_3, and TiO_2 using Fe^{3+} and Ce^{4+} as electron acceptors". *Applied Catalysis A: General*, *205*(1-2), 117–128. doi:10.1016/S0926-860X(00)00549-4

Bar-Ziv, R., Meller, A., Tlusty, T., Moses, E., Stavans, J., & Safran, S. (1997). "Localized Dynamic Light Scattering: Probing Single Particle Dynamics at the Nanoscale". *Physical Review Letters*, *78*(1), 154–157. doi:10.1103/PhysRevLett.78.154

Baron, P. A. (1986). "Calibration and Use of the Aerodynamic Particle Sizer (APS 3300)". *Aerosol Science and Technology*, *5*(1), 55–67. doi:10.1080/02786828608959076

Baron, P. A. (1998). "Personal Aerosol Sampler Design: A Review". *Applied Occupational and Environmental Hygiene*, *13*(5), 313–320. doi:10.1080/1047322X.1998.10390088

Baron, P.A. & Willeke, K. (2001). *Aerosol Measurement; Principles, Techniques and Applications*. John Wiley & Sons.: New York, Chichester, Weinheim, Brisbane, Singapore, Toronto.

Batonneau, Y., Laureyns, J., Merlin, J.-C., & Brémard, C. (2001). "Self-modeling mixture analysis of Raman microspectrometric investigations of dust emitted by lead and zinc smelters". *Analytica Chimica Acta*, *446*(1-2), 23–37. doi:10.1016/S0003-2670(01)00909-6

Batonneau, Y., Sobanska, S., Laureyns, J., & Bremard, C. (2006). "Confocal microprobe Raman imaging of urban tropospheric aerosol particles". *Environmental Science & Technology*, *40*(4), 1300–6. doi:10.1021/es051294x

Bau, S., Witschger, O., Gensdarmes, F., Rastoix, O., & Thomas, D. (2010). "A TEM-based method as an alternative to the BET method for measuring off-line the specific surface area of nanoaerosols". *Powder Technology*, *200*(3), 190–201. doi:10.1016/j.powtec.2010.02.023

Baxter, J. B., & Aydil, E. S. (2005). "Nanowire-based dye-sensitized solar cells". *Applied Physics Letters*, *86*(5), 053114. doi:10.1063/1.1861510

Beddows, D. C. S., & Telle, H. H. (2005). "Prospects of real-time single-particle biological aerosol analysis: A comparison between laser-induced breakdown spectroscopy and aerosol time-of-flight mass spectrometry". *Spectrochimica Acta Part B: Atomic Spectroscopy*, *60*(7-8), 1040–1059. doi:10.1016/j.sab.2005.05.018

Berger, L. I., Covington, A. K., Fox, R. B., Frederikse, H. P. R., Fuhr, J. R., Goldberg, R. N., Gschneidner, K. A., Hammond, C. R., Hampson, R. F., Holden, N. E., Jenkins, H. D. B., Kehiaian, H. V., Kerr, J. A., Kishore, N., Lennen, R., Lovas, F. J., Martin, W. C., Miller, J. S., Miller, T. M., Reader, J., Snyder, L. E., Stocker, D. W., Taylor, B. N., Trippe, T. G., Vanýsek, P., Wiese, W. L., Wilks, E. S., Wohlfarth, C. (2002). *Handbook of Chemistry and Physics*. (D. R. Lide, Ed.) (83rd edition). CRC, Boca Raton, FL. ISBN: 978-084930483-5

Bernardoni, V., Cuccia, E., Calzolai, G., Chiari, M., Lucarelli, F., Massabò, D., Nava, S., Prati, P., Valli, G., Vecchi, R. (2011). "ED-XRF set-up for size-segregated aerosol samples analysis". *X-Ray Spectrometry*, *40*(2), 79–87. doi:10.1002/xrs.1299

Biskos, G., Reavell, K., Hands, T., & Collings, N. (2003). "Fast measurements of aerosol spectra". *Journal of Aerosol Science*, *34* (Supplement 1), S67–S68. doi:10.1016/S0021-8502(03)00126-5

Biskos, G., Reavell, K., & Collings, N. (2005). "Description and Theoretical Analysis of a Differential Mobility Spectrometer". *Aerosol Science and Technology*, *39*(6), 527–541. doi:10.1080/027868291004832

Biswas, A., Latifi, H., Shah, P., Radziemski, L. J., & Armstrong, R. L. (1987). "Time-resolved spectroscopy of plasmas initiated on single, levitated aerosol droplets." *Optics Letters*, *12*(5), 313–5. doi:10.1364/OL.12.000313

Boccuzzi, F., Chiorino, A., Tsubota, S., & Haruta, M. (1995). "An IR study of CO-sensing mechanism on Au/ZnO". *Sensors and Actuators B: Chemical*, *25*(1-3), 540–543. doi:10.1016/0925-4005(95)85117-8

Boeck, G. (2001). "Current status of flow cytometry in cell and molecular biology." *International Review of Cytology*, *204*, 239–98. doi:10.1016/S0074-7696(01)04006-2

Bond, T. C., Anderson, T. L., & Campbell, D. (1999). "Calibration and Intercomparison of Filter-Based Measurements of Visible Light Absorption by Aerosols". *Aerosol Science and Technology*, *30*(6), 582–600. doi:10.1080/027868299304435

Bond, T. C., & Bergstrom, R. W. (2006). "Light Absorption by Carbonaceous Particles: An Investigative Review". *Aerosol Science and Technology*, *40*(1), 27–67. doi:10.1080/02786820500421521

Bouhelier, A., Renger, J., Beversluis, M. R., & Novotny, L. (2003). "Plasmon-coupled tip-enhanced near-field optical microscopy." *Journal of Microscopy*, *210*(3), 220–224. doi:10.1046/j.1365-2818.2003.01108.x

Bouhelier, A., Beversluis, M. R., & Novotny, L. (2004). "Applications of field-enhanced near-field optical microscopy." *Ultramicroscopy*, *100*(3-4), 413–9. doi:10.1016/j.ultramic.2003.10.007

Boyer, D., Tamarat, P., Maali, A., Lounis, B., & Orrit, M. (2002). "Photothermal imaging of nanometer-sized metal particles among scatterers." *Science*, *297*(5584), 1160–3. doi:10.1126/science.1073765

Braslavsky, I., Amit, R., Jaffar Ali, B. M., Gileadi, O., Oppenheim, A., & Stavans, J. (2001). "Objective-Type Dark-Field Illumination for Scattering from Microbeads". *Applied Optics*, *40*(31), 5650. doi:10.1364/AO.40.005650

Bricard, J., Delattre, P., Madelaine, G., & Pourprix, M. (1976). "Detection of ultrafine particles by means of a continuous flux condensation nuclei counter". In B. Y. H. Liu (Ed.), *Fine Particles – Aerosol Generation, Measurement, Sampling, and Analysis* (pp. 565–580). Academic Press, Academic Press, New York, San Francisco, London.

Brown, L. (1986). "Recent applications of STEM to small particles". *Ultramicroscopy*, *20*, 39–41. doi:10.1016/0304-3991(86)90166-X

Brown, D. M., Wilson, M. R., MacNee, W., Stone, V., & Donaldson, K. (2001). "Size-dependent proinflammatory effects of ultrafine polystyrene particles: a role for surface area and oxidative stress in the enhanced activity of ultrafines." *Toxicology and Applied Pharmacology*, *175*(3), 191–9. doi:10.1006/taap.2001.9240

Bruce, C., & Pinnick, R. (1977). "In-situ measurements of aerosol absorption with a resonant CW laser spectrophone". *Applied Optics*, *17*(7), 1762–1765. Retrieved from http://www.opticsinfobase.org/ao/fulltext.cfm?uri=ao-16-7-1762

Brunauer, S., Emmett, P., & Teller, E. (1938). "Adsorption of gases in multimolecular layers". *Journal of the American Chemical Society*, *60*(2), 309–319. doi:10.1021/ja01269a023

Buehler, M. F., Allen, T. M., & Davis, E. J. (1991). "Microparticle Raman Spectroscopy of Multicomponent Aerosols". *Journal of Colloid and Interface Science*, *146*(1), 79–89. doi:10.1016/0021-9797(91)90008-V

Buffat, P. (1999). "Electron microscopy for the characterisation of atmospheric particles". *Analusis*, *27*(4), 340 – 346. doi:10.1051/analusis:1999270340

Bukowiecki, N., Kittelson, D. B., Watts, W. F., Burtscher, H., Weingartner, E., & Baltensperger, U. (2002). "Real-time characterization of ultrafine and accumulation mode particles in ambient combustion aerosols". *Journal of Aerosol Science*, *33*(8), 1139–1154. doi:10.1016/S0021-8502(02)00063-0

Burtscher, H., Scherrer, L., Siegmann, H. C., Schmidt-Ott, A., & Federer, B. (1982). "Probing aerosols by photoelectric charging". *Journal of Applied Physics*, *53*(5), 3787. doi:10.1063/1.331120

Burtscher, H. (1992). "Measurement and characteristics of combustion aerosols with special consideration of photoelectric charging and charging by flame ions". *Journal of Aerosol Science*, *23*(6), 549–595. doi:10.1016/0021-8502(92)90026-R

Bzdek, B. R., Pennington, M. R., & Johnston, M. V. (2012). "Single particle chemical analysis of ambient ultrafine aerosol: A review". *Journal of Aerosol Science*, *52*, 109–120. doi:10.1016/j.jaerosci.2012.05.001

Calzolai, G., Chiari, M., Lucarelli, F., Nava, S., Taccetti, F., Becagli, S., Frosini, D., Traversi, R., Udisti, R. (2014). "PIXE–PIGE analysis of size-segregated aerosol samples from remote areas". *Nuclear Instruments and Methods in Physics Research Section B: Beam Interactions with Materials and Atoms*, *318*(A), 125–129. doi:10.1016/j.nimb.2013.05.097

Canagaratna, M. R., Jayne, J. T., Jimenez, J. L., Allan, J. D., Alfarra, M. R., Zhang, Q., Zhang, Q., Onasch, T. B., Drewnick, F., Coe, H., Middlebrook, A., Delia, A., Williams, L. R., Trimborn, A. M., Northway, M. J., Decarlo, P. F., Kolb, C. E., Davidovits, P., Worsnop, D. R. (2007). "Chemical and microphysical characterization of ambient aerosols with the aerodyne aerosol mass spectrometer". *Mass SpectrometrReviews*, *26*(2), 185–222. doi:10.1002/mas.20115

Cantor, B. (2003). "Heterogeneous nucleation and adsorption". *Philosophical Transactions of the Royal Society A: Mathematical, Physical and Engineering Sciences*, *361*(1804), 409–417. doi:10.1098/rsta.2002.1137

Carranza, J., Fisher, B., Yoder, G., & Hahn, D. (2001). "On-line analysis of ambient air aerosols using laser-induced breakdown spectroscopy". *Spectrochimica Acta Part B: Atomic Spectroscopy*, *56*(6), 851–864. doi:10.1016/S0584-8547(01)00183-5

Carranza, J. E., & Hahn, D. W. (2002). "Assessment of the upper particle size limit for quantitative analysis of aerosols using laser-induced breakdown spectroscopy." *Analytical Chemistry*, *74*(21), 5450–4. doi:10.1021/ac020261m

Cartwright, J. (1954). "The electron microscopy of airborne dusts". *British Journal of Applied Physics*, *5*(S3), S109–S117. doi:10.1088/0508-3443/5/S3/339

Cartwright, J., Nagelschmidt, G., & Skidmore, J. W. (1956). "The study of air pollution with the electron microscope". *Quarterly Journal of the Royal Meteorological Society*, *82*(351), 82–86. doi:10.1002/qj.49708235108

Cass, G. R., Hughes, L. a., Bhave, P., Kleeman, M. J., Allen, J. O., & Salmon, L. G. (2000). "The chemical composition of atmospheric ultrafine particles". *Philosophical Transactions of the Royal Society A: Mathematical, Physical and Engineering Sciences*, *358*(1775), 2581–2592. doi:10.1098/rsta.2000.0670

Casuccio, G. S., Schlaegle, S. F., Lersch, T. L., Huffman, G. P., Chen, Y., & Shah, N. (2004). "Measurement of fine particulate matter using electron microscopy techniques". *Fuel Processing Technology*, *85*(6-7), 763–779. doi:10.1016/j.fuproc.2003.11.026

Chang, C. (2010). "The immune effects of naturally occurring and synthetic nanoparticles." *Journal of Autoimmunity*, *34*(3), J234–46. doi:10.1016/j.jaut.2009.11.009

Chang, J.-S., Lawless, P. A., & Yamamoto, T. (1991). "Corona discharge processes". *IEEE Transactions on Plasma Science*, *19*(6), 1152–1166. doi:10.1109/27.125038

Chang, M., Kim, S., & Sioutas, C. (1999). "Experimental studies on particle impaction and bounce: effects of substrate design and material". *Atmospheric Environment*, *33*(15), 2313–2322. doi:10.1016/S1352-2310(99)00082-5

Charlson, R. J., Ahlquist, N. C., & Horvath, H. (1968). "On the generality of correlation of atmospheric aerosol mass concentration and light scatter". *Atmospheric Environment*, *2*(5), 455–464. doi:10.1016/0004-6981(68)90039-5

Charlson, R. (1969). "Atmospheric visibility related to aerosol mass concentration: A review". *Environmental Science & Technology*, *3*(10), 913–918. doi:10.1021/es60033a002

Chen, B., Cheng, Y., & Yeh, H. (1989). "An experimental approach to studying particle density effects in the TSI aerodynamic particle sizer (3300)". *Journal of Aerosol Science*, *20*(8), 1489–1492. doi:10.1016/0021-8502(89)90869-0

Chen, D., Pui, D. Y. H., Hummes, D., Fissan, H., Quant, F. R., & Sem, G. J. (1996). "Nanometer differential mobility analyzer (Nano-DMA): Design and numerical modeling". *Journal of Aerosol Science*, *27*(1986), S137–S138. doi:10.1016/0021-8502(96)00141-3

Chen, D.-R., Pui, D. Y. H., Hummes, D., Fissan, H., Quant, F. R., & Sem, G. J. (1998). "Design and evaluation of a nanometer aerosol differential mobility analyzer (Nano-DMA)". *Journal of Aerosol Science*, *29*(5-6), 497–509. doi:10.1016/S0021-8502(97)10018-0

Chen, J. X., Che, J. M., Sun, C. N., Zeng, X. Z., Tang, G. H., Ren, C. G., Yao, H. Y., Huang, F. Y., Wang, X. D., Tang, J. Y. (1988). "Analysis of atmospheric aerosol compositions by PIXE". *Physica Scripta*, *37*(2), 291. doi:10.1088/0031-8949/37/2/017

Cheng, H.-M., Chiu, W.-H., Lee, C.-H., Tsai, S.-Y., & Hsieh, W.-F. (2008). "Formation of Branched ZnO Nanowires from Solvothermal Method and Dye-Sensitized Solar Cells Applications". *The Journal of Physical Chemistry C*, *112*(42), 16359–16364. doi:10.1021/jp805239k

Cheng, Y. S., Keating, J., & Kanapilly, G. (1980). "Theory and calibration of a screen-type diffusion battery". *Journal of Aerosol Science*, *11*(5-6), 549–556. doi:10.1016/0021-8502(80)90127-5

Cheng, Y. S., & Yeh, H. C. (1980). "Theory of a screen-type diffusion battery". *Journal of Aerosol Science*, *11*(3), 313–320. doi:10.1016/0021-8502(80)90105-6

Chow, J. C. (1995). "Measurement methods to determine compliance with ambient air quality standards for suspended particles". *Journal of the Air & Waste Management Association*, *45*(5), 37–41. doi:10.1080/10473289.1995.10467369

Chow, J. C., Doraiswamy, P., Watson, J. G., Chen, L.-W. A., Ho, S. S. H., & Sodeman, D. A. (2008). "Advances in integrated and continuous measurements for particle mass and

chemical composition". *Journal of the Air & Waste Management Association*, *58*(2), 141–163. doi:10.3155/1047-3289.58.2.141

Chung, K., & Park, D. (1996). "Water photolysis reaction on cerium oxide photocatalysts". *Catalysis Today*, *30*(1-3), 157–162. doi:10.1016/0920-5861(96)00006-5

Clarke, A. D., Noone, K. J., Heintzenberg, J., Warren, S. G., & Covert, D. S. (1987). "Aerosol light absorption measurement techniques: Analysis and intercomparisons". *Atmospheric Environment*, *21*(6), 1455–1465. doi:10.1016/0004-6981(67)90093-5

Coggiola, M. J., Shi, Z., & Young, S. E. (2000). "Airborne Deployment of an Instrument for the Real-Time Analysis of Single Aerosol Particles". *Aerosol Science and Technology*, *33*(1-2), 20–29. doi:10.1080/027868200410822

Cognet, L., Tardin, C., Boyer, D., Choquet, D., Tamarat, P., & Lounis, B. (2003). "Single metallic nanoparticle imaging for protein detection in cells." *Proceedings of the National Academy of Sciences of the United States of America*, *100*(20), 11350–5. doi:10.1073/pnas.1534635100

Cohen, B. S., Li, W., Xiong, J. Q., & Lippmann, M. (2000). "Detecting H+ in ultrafine ambient aerosol using iron nano-film detectors and scanning probe microscopy." *Applied Occupational and Environmental Hygiene*, *15*(1), 80–9. doi:10.1080/104732200301881

Cohen, J., Deloid, G., Pyrgiotakis, G., & Demokritou, P. (2013). "Interactions of engineered nanomaterials in physiological media and implications for in vitro dosimetry." *Nanotoxicology*, *7*(4), 417–31. doi:10.3109/17435390.2012.666576

Cohen, J. M., Derk, R., Wang, L., Godleski, J., Kobzik, L., Brain, J., & Demokritou, P. (2014). "Tracking translocation of industrially relevant engineered nanomaterials (ENMs) across alveolar epithelial monolayers in vitro." *Nanotoxicology*, *5390*(January), 1–10. doi:10.3109/17435390.2013.879612

Colles, M. J., Geddes, N. R., & Mehdizadeh, E. (1979). "The optoacoustic effect". *Contemporary Physics*, *20*(1), 11–36. doi:10.1080/00107517908227800

Corma, A., Atienzar, P., García, H., & Chane-Ching, J.-Y. (2004). "Hierarchically mesostructured doped CeO2 with potential for solar-cell use." *Nature Materials*, *3*(6), 394–7. doi:10.1038/nmat1129

Covert, D., Wiedensohler, A., & Russell, L. (1997). "Particle Charging and Transmission Efficiencies of Aerosol Charge Neutralizes". *Aerosol Science and Technology*, *27*(2), 206–214. doi:10.1080/02786829708965467

Cunningham, D. D. (1873). “Microscopic Examination of the Air”. Superintendent of Government Printing, Calcutta, India

da Roza, R. A. (1982). “Particle Size for Greatest Penetration of HEPA Filters—and Their True Efficiency”. *DOE report, UCRL-53311*. doi:10.2172/6241348

Dahmann, D., Mosimann, T., & Matter, U. (2000). "Validation of online sensors for monitoring occupational exposures from diesel engines". *Journal of Aerosol Science*, *31* (Supplement 1), S21–S22. doi:10.1016/S0021-8502(00)90027-2

Davis, W. D. (1973). "Abstract: Surface Ionization Mass Spectroscopy of Airborne Particulates". *Journal of Vacuum Science and Technology*, *10*(1), 278. doi:10.1116/1.1317991

Davis, B. (1984). "X-ray diffraction analysis and source apportionment of Denver aerosol". *Atmospheric Environment*, *18*(10), 2197–2208. doi:10.1016/0004-6981(84)90207-5

de Boer, A. H., Gjaltema, D., Hagedoorn, P., & Frijlink, H. W. (2002). "Characterization of inhalation aerosols: a critical evaluation of cascade impactor analysis and laser diffraction technique." *International Journal of Pharmaceutics*, *249*(1-2), 219–31. doi:10.1016/S0378-5173(02)00526-4

de la Mora, J. F., Hering, S. V., Rao, N., & McMurry, P. H. (1990). "Hypersonic impaction of ultrafine particles". *Journal of Aerosol Science*, *21*(2), 169–187. doi:10.1016/0021-8502(90)90002-F

de la Mora, J. F., & Kozlowski, J. (2013). "Hand-held differential mobility analyzers of high resolution for 1–30nm particles: Design and fabrication considerations". *Journal of Aerosol Science*, *57*(March), 45–53. doi:10.1016/j.jaerosci.2012.10.009

de Lima, J. F., Martins, R. F., Neri, C. R., & Serra, O. A. (2009). "ZnO:CeO2-based nanopowders with low catalytic activity as UV absorbers". *Applied Surface Science*, *255*(22), 9006–9009. doi:10.1016/j.apsusc.2009.06.071

DeCarlo, P. F., Kimmel, J. R., Trimborn, A., Northway, M. J., Jayne, J. T., Aiken, A. C., Gonin, M., Fuhrer, K., Horvath, T., Docherty, K. S., Worsnop, D. R., Jimenez, J. L. (2006). "Field-deployable, high-resolution, time-of-flight aerosol mass spectrometer". *Analytical Chemistry*, *78*(24), 8281–8289. doi:8410.1029/2001JD001213.Analytical

Delhaye, M., & Dhamelincourt, P. (1975). "Raman microprobe and microscope with laser excitation". *Journal of Raman Spectroscopy*, *3*, 33–43. doi:10.1002/jrs.1250030105

Deutsch, B., Beams, R., & Novotny, L. (2010). "Nanoparticle detection using dual-phase interferometry." *Applied Optics*, *49*(26), 4921–5. doi:10.1364/AO.49.004921

Díaz, R. V., López-Monroy, J., Miranda, J., & Espinosa, A. A. (2014). "PIXE and XRF analysis of atmospheric aerosols from a site in the West area of Mexico City". *Nuclear Instruments and Methods in Physics Research Section B: Beam Interactions with Materials and Atoms*, *318*(A), 135–138. doi:10.1016/j.nimb.2013.05.095

Dimoulas, A., Panayiotatos, Y., Sotiropoulos, A., Tsipas, P., Brunco, D. P., Nicholas, G., Van Steenbergen, J., Bellenger, F., Houssa, M., Caymax, M., Meuris, M. (2007). "Germanium FETs and capacitors with rare earth CeO2/HfO2 gates". *Solid-State Electronics*, *51*(11-12), 1508–1514. doi:10.1016/j.sse.2007.09.029

Donaldson, K., Li, X., & MacNee, W. (1998). "Ultrafine (nanometre) particle mediated lung injury". *Journal of Aerosol Science*, *29*(5-6), 553–560. doi:10.1016/S0021-8502(97)00464-3

Donaldson, K., Stone, V., Gilmour, P. S., Brown, D. M., & MacNee, W. (2000). "Ultrafine particles: mechanisms of lung injury". *Philosophical Transactions: Mathematical, Physical and Engineering Sciences*, *358*(1775), 2741–2749. doi:10.1098/rsta.2000.0681

Donaldson, K., & Poland, C. A. (2012). "Inhaled nanoparticles and lung cancer - what we can learn from conventional particle toxicology." *Swiss Medical Weekly*, *142*(June 2012), w13547. doi:10.4414/smw.2012.13547

Dong, Z. W., Zhang, C. F., Deng, H., You, G. J., & Qian, S. X. (2006). "Raman spectra of single micrometer-sized tubular ZnO". *Materials Chemistry and Physics*, *99*(1), 160–163. doi:10.1016/j.matchemphys.2005.10.005

Dresselhaus, M. S., & Thomas, I. L. (2001). "Alternative energy technologies". *Nature*, *414*(6861), 332–7. doi:10.1038/35104599

Drewnick, F., Hings, S. S., DeCarlo, P., Jayne, J. T., Gonin, M., Fuhrer, K., Weimer, S., Jimenez, J. L., Demerjian, K. L., Borrmann, S. Worsnop, D. R. (2005). "A New Time-of-Flight Aerosol Mass Spectrometer (TOF-AMS)—Instrument Description and First Field Deployment". *Aerosol Science and Technology*, *39*(7), 637–658. doi:10.1080/02786820500182040

Eatough, D. J., Obeidi, F., Pang, Y., Ding, Y., Eatough, N. L., & Wilson, W. E. (1999). "Integrated and real-time diffusion denuder sample for PM 2.5". *Atmospheric Environment*, *33*(17), 2835–2844. doi:10.1016/S1352-2310(98)00326-4

Eatough, D. J., Eatough, N. L., Obeidi, F., Pang, Y., Modey, W., & Long, R. (2001). "Continuous Determination of PM 2.5 Mass, Including Semi-Volatile Species". *Aerosol Science and Technology*, *34*(1), 1–8. doi:10.1080/02786820121229

Eatough, D. J., Long, R. W., Modey, W. K., & Eatough, N. L. (2003). "Semi-volatile secondary organic aerosol in urban atmospheres: meeting a measurement challenge". *Atmospheric Environment*, *37*(9-10), 1277–1292. doi:10.1016/S1352-2310(02)01020-8

Egerton, R. F. (2011). *Electron Energy-Loss Spectroscopy in the Electron Microscope* (Third Edit.). Springer - New York, Dordrecht, Heidelberg, London. ISBN: 978-1-4419-9583-4

Eggersdorfer, M. L., & Pratsinis, S. E. (2014). "Agglomerates and aggregates of nanoparticles made in the gas phase". *Advanced Powder Technology*, *25*(1), 71–90. doi:10.1016/j.apt.2013.10.010

Ehara, K., Hagwood, C., & Coakley, K. J. (1996). "Novel method to classify aerosol particles according to their mass-to-charge ratio—aerosol particle mass analyser". *Journal of Aerosol Science*, *27*(2), 217–234. doi:10.1016/0021-8502(95)00562-5

Ehara, K., Takahata, K., & Koike, M. (2006a). "Absolute Mass and Size Measurement of Monodisperse Particles Using a Modified Millikan's Method: Part I—Theoretical Framework of the Electro-Gravitational Aerosol Balance". *Aerosol Science and Technology*, *40*(7), 514–520. doi:10.1080/02786820600714379

Ehara, K., Takahata, K., & Koike, M. (2006b). "Absolute Mass and Size Measurement of Monodisperse Particles Using a Modified Millikan's Method: Part II—Application of Electro-Gravitational Aerosol Balance to Polystyrene Latex Particles of 100 nm to 1 μm in Average Diameter". *Aerosol Science and Technology*, *40*(7), 521–535. doi:10.1080/02786820600714387

ENRHES Project, (2009). *ENRHES Final Report - Engineered Nanoparticles: Review of Health and Environmental Safety*. Retrieved from http://ihcp.jrc.ec.europa.eu/whats-new/enhres-final-report

EPA. (2005). *Toxicological review of zinc and compounds* (EPA/635/R–05/002). U.S. Environmental Protection Agency, Washington, D.C. Retrieved from www.epa.gov/iris/toxreviews/0426tr.pdf

Erikson, H.A. (1921). The Change of Mobility of the Positive Ions in Air with Age. *Phys. Rev.* 18: 100.

Estrela-Lopis, I., Romero, G., Rojas, E., Moya, S. E., & Donath, E. (2011). "Nanoparticle uptake and their co-localization with cell compartments – a confocal Raman microscopy study at single cell level". *Journal of Physics: Conference Series*, *304*, 012017. doi:10.1088/1742-6596/304/1/012017

Ettinger, H. J., & Royer, G. W. (1972). "Visibility and Mass Concentration in a Nonurban Environment". *Journal of the Air Pollution Control Association*, *22*(2), 108–111. doi:10.1080/00022470.1972.10469613

Faraday, M. (1857). "The Bakerian Lecture: Experimental Relations of Gold (and Other Metals) to Light". *Philosophical Transactions of the Royal Society of London*, *147* (January), 145–181. doi:10.1098/rstl.1857.0011

Feldpausch, P., Fiebig, M., Fritzsche, L., & Petzold, A. (2006). "Measurement of ultrafine aerosol size distributions by a combination of diffusion screen separators and condensation particle counters". *Journal of Aerosol Science*, *37*(5), 577–597. doi:10.1016/j.jaerosci.2005.04.009

Ferin, J., Oberdörster, G., & Penney, D. P. (1992). "Pulmonary retention of ultrafine and fine particles in rats." *American Journal of Respiratory Cell and Molecular Biology*, *6*(5), 535–42. doi:10.1165/ajrcmb/6.5.535

Fierz, M., Scherrer, L., & Burtscher, H. (2002). "Real-time measurement of aerosol size distributions with an electrical diffusion battery". *Journal of Aerosol Science*, *33*(7), 1049–1060. doi:10.1016/S0021-8502(02)00057-5

Fierz, M., Weimer, S., & Burtscher, H. (2009). "Design and performance of an optimized electrical diffusion battery". *Journal of Aerosol Science*, *40*(2), 152–163. doi:10.1016/j.jaerosci.2008.09.007

Fissan, H., Neumann, S., Trampe, A., Pui, D. Y. H., & Shin, W. G. (2006). "Rationale and principle of an instrument measuring lung deposited nanoparticle surface area". *Journal of Nanoparticle Research*, *9*(1), 53–59. doi:10.1007/s11051-006-9156-8

Flagan, R. C. (1998). "History of Electrical Aerosol Measurements". *Aerosol Science and Technology*, *28*(4), 301–380. doi:10.1080/02786829808965530

Flagan, R. C. (1999). "On differential mobility analyzer resolution". *Aerosol Science & Technology*, *30*(6), 556–570. doi:10.1080/027868299304417

Fletcher, N. H. (1962). *The Physics of Rainclouds* (pp. 64–282). Cambridge University Press, Cambridge, England. ISBN: 9780521154796 (2011 reissue)

Friedlander, S. K. (2000). *Smoke, Dust, and Haze: Fundamentals of Aerosol Dynamics* (Second Edition). Oxford University Press. ISBN: 978-0-19-512999-1

Fu, H., Zhang, M., Li, W., Chen, J., Wang, L., Quan, X., & Wang, W. (2012). "Morphology, composition and mixing state of individual carbonaceous aerosol in urban Shanghai". *Atmospheric Chemistry and Physics*, *12*(2), 693–707. doi:10.5194/acp-12-693-2012

Fuchs, N. A., Stechkina, I. B., & Starosselskii, V. I. (1962). "On the determination of particle size distribution in polydisperse aerosols by the diffusion method". *British Journal of Applied Physics*, *13*(6), 280–281. doi:10.1088/0508-3443/13/6/307

Fuchs, N. A. (1964). "The Mechanics of Aerosols", Translated by R. E. Daisley and Marina Fuchs; Edited by C. N. Davies. Pergamon Press, London.

Fujitani, Y., Hasegawa, S., Fushimi, A., Kondo, Y., Tanabe, K., Kobayashi, S., & Kobayashi, T. (2006). "Collection characteristics of low-pressure impactors with various impaction substrate materials". *Atmospheric Environment*, *40*(18), 3221–3229. doi:10.1016/j.atmosenv.2006.02.001

Gäggeler, H. W., Baltensperger, U., Emmenegger, M., Jost, D. T., Schmidt-Ott, A., Haller, P., & Hofmann, M. (1989). "The epiphaniometer, a new device for continuous aerosol monitoring". *Journal of Aerosol Science*, *20*(5), 557–564. doi:10.1016/0021-8502(89)90101-8

Gaiduk, A., Ruijgrok, P. V., Yorulmaz, M., & Orrit, M. (2010). "Detection limits in photothermal microscopy". *Chemical Science*, *1*(3), 343. doi:10.1039/c0sc00210k

Galanzha, E. I., & Zharov, V. P. (2012). "Photoacoustic flow cytometry." *Methods*, *57*(3), 280–96. doi:10.1016/j.ymeth.2012.06.009

Galata, S. F., Evangelou, E. K., Panayiotatos, Y., Sotiropoulos, A., & Dimoulas, A. (2007). "Post deposition annealing studies of lanthanum aluminate and ceria high-k dielectrics on germanium". *Microelectronics Reliability*, *47*(4-5), 532–535. doi:10.1016/j.microrel.2007.01.023

Gamer, A. O., Leibold, E., & van Ravenzwaay, B. (2006). "The in vitro absorption of microfine zinc oxide and titanium dioxide through porcine skin." *Toxicology in Vitro : An International Journal Published in Association with BIBRA*, *20*(3), 301–7. doi:10.1016/j.tiv.2005.08.008

Gamero-Castaño, M., & de la Mora, J. F. (2002). "Ion-induced nucleation: Measurement of the effect of embryo's size and charge state on the critical supersaturation". *The Journal of Chemical Physics*, *117*(7), 3345. doi:10.1063/1.1492279

Gard, E., Mayer, J. E., Morrical, B. D., Dienes, T., Fergenson, D. P., & Prather, K. A. (1997). "Real-Time Analysis of Individual Atmospheric Aerosol Particles: Design and Performance of a Portable ATOFMS". *Analytical Chemistry*, *69*(20), 4083–4091. doi:10.1021/ac970540n

Gebhart, J., Heyder, J., Roth, C., Stahlhofen, W. (1976). Optical Aerosol Size Spectrometry Below And Above The Wavelength Of Light - A Comparison. *Fine Particles - Aerosol Generation, Measurement, Sampling, and Analysis*, Academic Press, 793–815.

Gehr, P., Mühlfeld, C., Rothen-Rutishauser, B., & Blank, F. (Eds.). (2010). *Particle-lung interactions* (Second Edition). Informa Healthcare, New York, London. ISBN: 9781420072563

Germani, M., & Buseck, P. (1991). "Automated scanning electron microscopy for atmospheric particle analysis". *Analytical Chemistry*, *63*(20), 2232–2237. doi:10.1021/ac00020a008

Giechaskiel, B., Maricq, M., Ntziachristos, L., Dardiotis, C., Wang, X., Axmann, H., Bergmann, A., Schindler, W. (2014). "Review of motor vehicle particulate emissions sampling and measurement: From smoke and filter mass to particle number". *Journal of Aerosol Science*, *67*(January), 48–86. doi:10.1016/j.jaerosci.2013.09.003

Giorio, C., Tapparo, A., Dall'Osto, M., Harrison, R. M., Beddows, D. C. S., Di Marco, C., & Nemitz, E. (2012). "Comparison of three techniques for analysis of data from an Aerosol Time-of-Flight Mass Spectrometer". *Atmospheric Environment*, *61*, 316–326. doi:10.1016/j.atmosenv.2012.07.054

Giusto, A., Savasta, S., & Saija, R. (2005). "Interaction of a microresonator with a nanoscatterer". *Journal of Physics: Conference Series*, *6*(1), 103–108. doi:10.1088/1742-6596/6/1/008

Goharshadi, E. K., Samiee, S., & Nancarrow, P. (2011). "Fabrication of cerium oxide nanoparticles: characterization and optical properties." *Journal of Colloid and Interface Science*, *356*(2), 473–80. doi:10.1016/j.jcis.2011.01.063

Gojova, A., Lee, J.-T., Jung, H. S., Guo, B., Barakat, A. I., & Kennedy, I. M. (2009). "Effect of cerium oxide nanoparticles on inflammation in vascular endothelial cells." *Inhalation Toxicology*, *21* (Supplement 1), 123–30. doi:10.1080/08958370902942582

Goldberger, J., Sirbuly, D. J., Law, M., & Yang, P. (2005). "ZnO nanowire transistors". *The Journal of Physical Chemistry B*, *109*(1), 9–14. doi:10.1021/jp0452599

Goldman, M., & Sigmond, R. S. (1982). "Corona and Insulation". *IEEE Transactions on Electrical Insulation*, *EI-17*(2), 90–105. doi:10.1109/TEI.1982.298543

Goldman, M., Goldman, A., & Sigmond, R. S. (1985). "The corona discharge, its properties and specific uses". *Pure and Applied Chemistry*, *57*(9), 1353–1362. doi:10.1351/pac198557091353

Gorbunov, B. (1999). "Free energy of embryo formation for heterogeneous multicomponent nucleation". *Chemical Physics*, *110*(20), 10035–10045. doi:10.1063/1.478877

Gorbunov, B., Priest, N. D., Muir, R. B., Jackson, P. R., & Gnewuch, H. (2009). "A novel size-selective airborne particle size fractionating instrument for health risk evaluation." *The Annals of Occupational Hygiene*, *53*(3), 225–37. doi:10.1093/annhyg/mep002

Gorbunov, B. (2009). Private communication. August, 2009.

Gouadec, G., & Colomban, P. (2007). "Raman Spectroscopy of nanomaterials: How spectra relate to disorder, particle size and mechanical properties". *Progress in Crystal Growth and Characterization of Materials*, *53*(1), 1–56. doi:10.1016/j.pcrysgrow.2007.01.001

Gregg, S. J. and Sing, K. S. W. (1982). “Adsorption, Surface Area and Porosity”, Second Edition. Academic Press, London.

Griffiths, W. D., & Vaughan, N. P. (1986). "The aerodynamic behaviour of cylindrical and spheroidal particles when settling under gravity". *Journal of Aerosol Science*, *17*(3), 431. doi:10.1016/0021-8502(86)90123-0

Griffiths, W., Iles, P., & Vaughan, N. (1986). "The behaviour of liquid droplet aerosols in an APS 3300". *Journal of Aerosol Science*, *17*(6), 921–930. doi:10.1016/0021-8502(86)90018-2

Grimm: http://www.grimm-aerosol.com/en/component/phocadownload/category/5-datasheets.html?download=119:scanning-mobility-particle-sizer-and-condensation-particle-counter-smps-c (Visited December 2013)

Gulson, B., McCall, M. J., Korsch, M., Gomez, L., Casey, P., Oytam, Y., Taylor, A., McCulloch, M., Trotter, J., Kinsley, L., Greenoak, G. (2010). "Small amounts of zinc from zinc oxide particles in sunscreens applied outdoors are absorbed through human skin." *Toxicological Sciences: An Official Journal of the Society of Toxicology*, *118*(1), 140–9. doi:10.1093/toxsci/kfq243

Gulson, B., Wong, H., Korsch, M., Gomez, L., Casey, P., McCall, M. J., McCulloch, M., Trotter, J., Stauber, J., Greenoak, G. (2012). "Comparison of dermal absorption of zinc from different sunscreen formulations and differing UV exposure based on stable isotope tracing." *The Science of the Total Environment*, *420*(15 March), 313–8. doi:10.1016/j.scitotenv.2011.12.046

Hahn, D. W. (1998). "Laser-induced breakdown spectroscopy for sizing and elemental analysis of discrete aerosol particles". *Applied Physics Letters*, *72*(23), 2960. doi:10.1063/1.121507

Hahn, D. W., & Lunden, M. M. (2000). "Detection and Analysis of Aerosol Particles by Laser-Induced Breakdown Spectroscopy". *Aerosol Science and Technology*, *33*(1-2), 30–48. doi:10.1080/027868200410831

Hansen, A., Rosen, H., & Novakov, T. (1982). "Real-time measurement of the absorption coefficient of aerosol particles". *Applied Optics*, *21*(17), 3060–3062. Retrieved from http://www.opticsinfobase.org/ao/fulltext.cfm?uri=ao-21-17-3060&id=26066

Hansen, A., Rosen, H., & Novakov, T. (1984). "The aethalometer—an instrument for the real-time measurement of optical absorption by aerosol particles". *The Science of the Total Environment*, *36* (1 July), 191–196. doi:10.1016/0048-9697(84)90265-1

Hansen, A. D. A., & Novakov, T. (1990). "Real-Time Measurement of Aerosol Black Carbon During the Carbonaceous Species Methods Comparison Study". *Aerosol Science and Technology*, *12*(1), 194–199. doi:10.1080/02786829008959339

Harris, W. A, Reilly, P. T. A, & Whitten, W. B. (2005). "MALDI of individual biomolecule-containing airborne particles in an ion trap mass spectrometer." *Analytical Chemistry*, *77*(13), 4042–50. doi:10.1021/ac050187i

Harrison, R. M., Jones, M., & Collins, G. (1999). "Measurements of the physical properties of particles in the urban atmosphere". *Atmospheric Environment*, *33*(2), 309–321. doi:10.1016/S1352-2310(98)00164-2

Harrison, R. M., & Yin, J. (2000). "Particulate matter in the atmosphere: which particle properties are important for its effects on health?" *The Science of the Total Environment*, *249*(1-3), 85–101. doi:10.1016/S0048-9697(99)00513-6

Hartonen, K., Laitinen, T., & Riekkola, M.-L. (2011). "Current instrumentation for aerosol mass spectrometry". *Trends in Analytical Chemistry*, *30*(9), 1486–1496. doi:10.1016/j.trac.2011.06.007

Hartschuh, A., Pedrosa, H. N., Novotny, L., & Krauss, T. D. (2003). "Simultaneous fluorescence and Raman scattering from single carbon nanotubes." *Science*, *301*(5638), 1354–6. doi:10.1126/science.1087118

Hartschuh, A., Beversluis, M. R., Bouhelier, A., & Novotny, L. (2004). "Tip-enhanced optical spectroscopy." *Philosophical Transactions. Series A, Mathematical, Physical, and Engineering Sciences*, *362*(1817), 807–19. doi:10.1098/rsta.2003.1348

Hartschuh, A. (2008). "Tip-enhanced near-field optical microscopy." *Angewandte Chemie (International Ed. in English)*, *47*(43), 8178–91. doi:10.1002/anie.200801605

Hauck, H., Berner, A., Gomiscek, B., Stopper, S., Puxbaum, H., Kundi, M., & Preining, O. (2004). "On the equivalence of gravimetric PM data with TEOM and beta-attenuation measurements". *Journal of Aerosol Science*, *35*(9), 1135–1149. doi:10.1016/j.jaerosci.2004.04.004

He, L., Ozdemir, S. K., Zhu, J., Kim, W., & Yang, L. (2011). "Detecting single viruses and nanoparticles using whispering gallery microlasers." *Nature Nanotechnology*, *6*(7), 428–32. doi:10.1038/nnano.2011.99

Hell, S. W. (2009). "Far-field optical nanoscopy." In A. Gräslund, R. Rigler, & J. Widengren (Eds.), *Single Molecule Spectroscopy in Chemistry, Physics and Biology* (Vol. 316, pp. 365–398). Springer.

Hernandez-Sierra, A., Alguacil, F. C., & Alonso, M. (2003). "Unipolar charging of nanometer aerosol particles in a corona ionizer". *Journal of Aerosol Science*, *34*(6), 733–745. doi:10.1016/S0021-8502(03)00033-8

Hewitt, G. (1957). "The Charging of Small Particles for Electrostatic Precipitation". *American Institute of Electrical Engineers, Part I: Communication and Electronics, Transactions of the*, *76*(3), 300–306. doi:10.1109/TCE.1957.6372672

Higashi, M., & Takahashi, Y. (2009). "Detection of S(IV) species in aerosol particles using XANES spectroscopy." *Environmental Science & Technology*, *43*(19), 7357–63. doi:10.1021/es900163y

Hinds, W.C. (1999). *Aerosol Technology: Properties, Behavior, and Measurement of Airborne Particles, 2nd Edition.* New York: John Wiley & Sons. ISBN: 978-0-471-19410-1

Hoet, P. H., Brüske-Hohlfeld, I., & Salata, O. V. (2004). "Nanoparticles - known and unknown health risks." *Journal of Nanobiotechnology*, *2*(1), 12. doi:10.1186/1477-3155-2-12

Hoffmann, G. G., Oelichmann, B., & Schrader, B. (1991). "Raman spectroscopy of optically trapped single aerosol particles". *Journal of Aerosol Science*, *22*(Supplement 1), S427–S430. doi:10.1016/S0021-8502(05)80129-6

Hoffmann, G. G., Lübben, J. F., & Schrader, B. (1995). "Composition analysis of optically levitated aerosol single particles". *Journal of Molecular Structure*, *349*(95), 145–147. doi:10.1016/0022-2860(95)08730-J

Hoflich, B. L. W., Weinbruch, S., Theissmann, R., Gorzawski, H., Ebert, M., Ortner, H. M., Skogstad, A., Ellingsen, D. G., Drablos, P. A., Thomassen, Y. (2005). "Characterization of individual aerosol particles in workroom air of aluminium smelter potrooms." *Journal of Environmental Monitoring : JEM*, *7*(5), 419–24. doi:10.1039/b418275h

Hofmann, W. (2011). "Modelling inhaled particle deposition in the human lung—A review". *Journal of Aerosol Science*, *42*(10), 693–724. doi:10.1016/j.jaerosci.2011.05.007

Hopcraft, K. I., Chang, P. C. Y., Jakeman, E., & Walker, J. G. (2005). "Polarization fluctuation spectroscopy". In G. Videen, Y. Yatskiv, & M. Mishchenko (Eds.), *Photopolarimetry in Remote Sensing* (pp. 137–174). Springer Netherlands. doi:10.1007/1-4020-2368-5_6

Hoppel, W. A., & Frick, G. M. (1986). "Ion-Aerosol Attachment Coefficients and the Steady-State Charge Distribution on Aerosols in a Bipolar Ion Environment". *Aerosol Science and Technology*, *5*(1), 1–21. doi:10.1080/02786828608959073

Hou, X., Stchur, P., Yang, K., & Michel, R. (1998). "Progress in laser excited atomic fluorescence spectrometry". *Trends in Analytical Chemistry*, *17*(8-9), 532–542. doi:10.1016/S0165-9936(98)00057-0

Hou, X., & Jones, B. T. (2000). "Field instrumentation in atomic spectroscopy". *Microchemical Journal*, *66*(1-3), 115–145. doi:10.1016/S0026-265X(00)00058-8

Huang, M. H., Mao, S., Feick, H., Yan, H., Wu, Y., Kind, H., Weber, E., Russo, R., Yang, P. (2001). "Room-temperature ultraviolet nanowire nanolasers." *Science*, *292*(5523), 1897–9. doi:10.1126/science.1060367

Huang, P., & Turpin, B. (1996). "Reduction of sampling and analytical errors for electron microscopic analysis of atmospheric aerosols". *Atmospheric Environment*, *30*(24), 4137–4148. doi:10.1016/1352-2310(96)00150-1

Hunt, A., & Petrucci, G. (2002). "Analysis of ultrafine and organic particles by aerosol mass spectrometry". *Trends in Analytical Chemistry*, *21*(2), 74–81. doi:10.1016/S0165-9936(01)00138-8

Huong, P. V., & Verma, A. L. (1990). "Characterization of materials by micro-Raman spectroscopy". *Materials Science and Engineering: B*, *5*(2), 255–260. doi:10.1016/0921-5107(90)90064-I

Hurd, F., & Mullins, J. (1962). "Aerosol size distribution from ion mobility". *Journal of Colloid Science*, *17*(2), 91–100. doi:10.1016/0095-8522(62)90001-6

Hwang, J., & Moerner, W. (2007). "Interferometry of a single nanoparticle using the Gouy phase of a focused laser beam". *Optics Communications*, *280*(2), 487–491. doi:10.1016/j.optcom.2007.08.032

Hybl, J. D., Lithgow, G. A., & Buckley, S. G. (2003). "Laser-induced breakdown spectroscopy detection and classification of biological aerosols". *Applied Spectroscopy*, *57*(10), 1207–1215. Retrieved from http://www.opticsinfobase.org/abstract.cfm?uri=as-57-10-1207

Ibald-Mulli, A., Wichmann, H.-E., Kreyling, W., & Peters, A. (2002). "Epidemiological evidence on health effects of ultrafine particles". *Journal of Aerosol Medicine : The Official Journal of the International Society for Aerosols in Medicine*, *15*(2), 189–201. doi:10.1089/089426802320282310

ICRP. (1994). "Human Respiratory Tract Model for Radiological Protection". *ICRP Publication 66. Annals of the ICRP*, *24*(1-3), 1–8. doi:10.1016/0146-6453(94)90029-9

Ignatovich, F. V., & Novotny, L. (2003). "Experimental study of nanoparticle detection by optical gradient forces". *Review of Scientific Instruments*, *74*(12), 5231. doi:10.1063/1.1628823

Ignatovich, F. V., & Novotny, L. (2006). "Real-time and background-free detection of nanoscale particles". *Physical Review Letters*, *96*(January), 013901. doi:10.1103/PhysRevLett.96.013901

Ignatovich, F. V., Hartschuh, A., & Novotny, L. (2003). "Detection of nanoparticles using optical gradient forces". *Journal of Modern Optics*, *50*(10), 1509–1520. doi:10.1080/0950034031000064924

Ignatovich, F. V., Topham, D., & Novotny, L. (2006). "Optical Detection of Single Nanoparticles and Viruses". *IEEE Journal of Selected Topics in Quantum Electronics*, *12*(6), 1292–1300. doi:10.1109/JSTQE.2006.885086

Intra, P., & Tippayawong, N. (2009). "Progress in unipolar corona discharger designs for airborne particle charging: A literature review". *Journal of Electrostatics*, *67*(4), 605–615. doi:10.1016/j.elstat.2008.12.018

ISO 15900 (2009). "Determination of particle size distribution - Differential electrical mobility analysis for aerosol particles." http://www.iso.org/iso/catalogue_detail.htm?csnumber=39573 (Visited November 2012)

ISO 27891 (Under development). "Aerosol particle number concentration - Calibration of condensation particle counters." http://www.iso.org/iso/catalogue_detail.htm?csnumber=44414 (Visited May 2014)

Ivleva, N. P., McKeon, U., Niessner, R., & Pöschl, U. (2007). "Raman Microspectroscopic Analysis of Size-Resolved Atmospheric Aerosol Particle Samples Collected with an ELPI: Soot, Humic-Like Substances, and Inorganic Compounds". *Aerosol Science and Technology*, *41*(7), 655–671. doi:10.1080/02786820701376391

Izu, N., Shin, W., Murayama, N., & Kanzaki, S. (2002). "Resistive oxygen gas sensors based on CeO_2 fine powder prepared using mist pyrolysis". *Sensors and Actuators B: Chemical*, *87*(1), 95–98. doi:10.1016/S0925-4005(02)00224-1

Jaklevic, J. M., Gatti, R. C., Goulding, F. S., & Loo, B. W. (1981). "A β-Gauge Method Applied to Aerosol Samples". *Environmental Science & Technology*, *15*(6), 680–6. doi:10.1021/es00088a006

Japar, S., & Killenger, D. (1979). "Photoacoustic and absorption spectrum of airborne carbon particulate using a tunable dye laser". *Chemical Physics Letters*, *66*(1), 207–209. doi:10.1016/0009-2614(79)80397-8

Järvinen, A., Aitomaa, M., Rostedt, A., Keskinen, J., & Yli-Ojanperä, J. (2014). "Calibration of the new electrical low pressure impactor (ELPI+)". *Journal of Aerosol Science*, *69*(March), 150–159. doi:10.1016/j.jaerosci.2013.12.006

Jaworek, A., Krupa, A., & Czech, T. (2007). "Modern electrostatic devices and methods for exhaust gas cleaning: A brief review". *Journal of Electrostatics*, *65*(3), 133–155. doi:10.1016/j.elstat.2006.07.012

Jayne, J. T., Leard, D. C., Zhang, X., Davidovits, P., Smith, K. A., Kolb, C. E., & Worsnop, D. R. (2000). "Development of an Aerosol Mass Spectrometer for Size and Composition Analysis of Submicron Particles". *Aerosol Science and Technology*, *33*(1-2), 49–70. doi:10.1080/027868200410840

Jiang, J., Oberdörster, G., & Biswas, P. (2008). "Characterization of size, surface charge, and agglomeration state of nanoparticle dispersions for toxicological studies". *Journal of Nanoparticle Research*, *11*(1), 77–89. doi:10.1007/s11051-008-9446-4

Jiang, J., Zhao, J., Chen, M., Eisele, F. L., Scheckman, J., Williams, B. J., Kuang, C., McMurry, P. H. (2011). "First Measurements of Neutral Atmospheric Cluster and 1–2 nm Particle Number Size Distributions During Nucleation Events". *Aerosol Science and Technology*, *45*(4), ii–v. doi:10.1080/02786826.2010.546817

Jimenez, J., Jayne, J., Shi, Q., Kolb, C., Worsnop, D., Yourshaw, I., Seinfeld, J. H., Flagan, R. C., Zhang, X., Smith, K.A., Morris, J.W., Davidovits, P. (2003). "Ambient aerosol sampling using the aerodyne aerosol mass spectrometer". *Journal of Geophysical Research*, *108*(D7), 8425. doi:10.1029/2001JD001213

Johnston, M. (2000). "Sampling and analysis of individual particles by aerosol mass spectrometry". *Journal of Mass Spectrometry*, *595*(January), 585–595. doi:10.1002/(SICI)1096-9888(200005)35:5<585::AID-JMS992>3.0.CO;2-K

Jung, H., & Kittelson, D. B. (2005). "Characterization of Aerosol Surface Instruments in Transition Regime". *Aerosol Science and Technology*, *39*(9), 902–911. doi:10.1080/02786820500295701

Jung, H., Kittelson, D. B., & Zachariah, M. R. (2005). "The influence of a cerium additive on ultrafine diesel particle emissions and kinetics of oxidation". *Combustion and Flame*, *142*(3), 276–288. doi:10.1016/j.combustflame.2004.11.015

Keady, P.B., Quant, F.R., Sem, G.J. (1984). "Automated Differential Mobility Particle Sizer". In B. Y. H. Liu, D. Y. H. Pui and H. Fissan (Eds.), *Proceedings of the 1st International Aerosol Conference* (pp. 71-74). Elsevier, New York.

Keller, A., Fierz, M., Siegmann, K., Siegmann, H. C., & Filippov, A. (2001). "Surface science with nanosized particles in a carrier gas". *Journal of Vacuum Science & Technology A: Vacuum, Surfaces, and Films*, *19*(1), 1. doi:10.1116/1.1339832

Keller, M., Kreck, G., Holzapfel, Y., Neubauer, N., & Seipenbusch, M. (2011). "Monitoring Method for Carbon Nanotubes (CNT): Personal Sampler and Corresponding Reading Device". *Proceedings of the 8th International Conference on Multi-Material Micro Manufacture*, 149–155. doi:10.3850/978-981-07-0319-6_212

Kelton, K. F., & Greer, A. L. (2010). *Nucleation in Condensed Matter* (pp. 1–743). Pergamon. ISBN: 978-0-08-042147-6

Kenny, L., & Lidén, G. (1991). "A technique for assessing size-selective dust samplers using the APS and polydisperse test aerosols". *Journal of Aerosol Science*, *22*(1), 91–100. doi:10.1016/0021-8502(91)90095-Y

Keskinen, J., Pietarinen, K., & Lehtimäki, M. (1992). "Electrical low pressure impactor". *Journal of Aerosol Science*, *23*(4), 353–360. doi:10.1016/0021-8502(92)90004-F

Khan, F. R., Laycock, A., Dybowska, A., Larner, F., Smith, B. D., Rainbow, P. S., Luoma, S. N., Rehkämper, M., Valsami-Jones, E. (2013). "Stable isotope tracer to determine uptake and efflux dynamics of ZnO Nano- and bulk particles and dissolved Zn to an estuarine snail." *Environmental Science & Technology*, *47*(15), 8532–9. doi:10.1021/es4011465

Kippenberg, T. J. (2010). "Microresonators: Particle sizing by mode splitting". *Nature Photonics*, *4*(1), 9–10. doi:10.1038/nphoton.2009.246

Kirkby, J., Curtius, J., Almeida, J., Dunne, E., Duplissy, J., Ehrhart, S., Franchin, A., Gagné, S., Ickes, L., Kürten, A., Kupc, A., Metzger, A., Riccobono, F., Rondo, L., Schobesberger, S., Tsagkogeorgas, G., Wimmer, D., Amorim, A., Bianchi, F., Breitenlechner, M., David, A., Dommen, J., Downard, A., Ehn, M., Flagan, R. C., Haider, S., Hansel, A., Hauser, D., Jud, W., Junninen, H., Kreissl, F., Kvashin, A., Laaksonen, A., Lehtipalo, K., Lima, J., Lovejoy, E. R., Makhmutov, V., Mathot, S., Mikkilä, J., Minginette, P., Mogo, S., Nieminen, T., Onnela, A., Pereira, P., Petäjä, T., Schnitzhofer, R., Seinfeld, J. H., Sipilä, M., Stozhkov, Y., Stratmann, F., Tomé, A., Vanhanen, J., Viisanen, Y., Vrtala, A., Wagner, P. E., Walther, H., Weingartner, E., Wex, H., Winkler, P. M., Carslaw, K. S., Worsnop, D. R., Baltensperger, U., Kulmala, M. (2011). "Role of sulphuric acid, ammonia and galactic cosmic rays in atmospheric aerosol nucleation". *Nature*, *476*(7361), 429–33. doi:10.1038/nature10343

Klaine, S. J., Alvarez, P. J. J., Batley, G. E., Fernandes, T. F., Handy, R. D., Lyon, D. Y., Mahendra, S., McLaughlin, M.J., Lead, J. R. (2008). "Nanomaterials in the environment: Behavior, fate, bioavailability, and effects". *Environmental Toxicology and Chemistry*, *27*(9), 1825–1851. doi:10.1897/08-090.1

Klein, F., Ranty, C., & Sowa, L. (1984). "A new examination of the validity of the principle of beta radiation absorption for determination of ambient air dust concentrations". *Journal of Aerosol Science*, *15*(3), 391–395. doi:10.1016/0021-8502(84)90124-1

Knutson, E., & Whitby, K. (1975). "Aerosol classification by electric mobility: apparatus, theory, and applications". *Journal of Aerosol Science*, *6*(6), 443–451. doi:10.1016/0021-8502(75)90060-9

Knutson, E. (1976). "Extended Electrical Mobility Method For Measuring Aerosol Particle Size And Concentration". In B. Y. H. Liu (Ed.), *Fine Particles: Aerosol Generation, Measurement, Sampling, and Analysis* (pp. 739–762). Academic Press. doi:10.1016/B978-0-12-452950-2.50036-1

Knutson, E. O. (1999). "History of Diffusion Batteries in Aerosol Measurements". *Aerosol Science and Technology*, *31*(2-3), 83–128. doi:10.1080/027868299304192

Koehler, K. A, Clark, P., & Volckens, J. (2009). "Development of a sampler for total aerosol deposition in the human respiratory tract." *The Annals of Occupational Hygiene*, *53*(7), 731–8. doi:10.1093/annhyg/mep053

Koehler, K. A., & Volckens, J. (2013). "Development of a sampler to estimate regional deposition of aerosol in the human respiratory tract." *The Annals of Occupational Hygiene*, *57*(9), 1138–47. doi:10.1093/annhyg/met041

Kong, L., Zhang, P., Setlow, P., & Li, Y. (2011). "Multifocus confocal Raman microspectroscopy for rapid single-particle analysis". *Journal of Biomedical Optics*, *16*(12), 120503. doi:10.1117/1.3662456

Kostić, R., Aškrabić, S., Dohčević-Mitrović, Z., & Popović, Z. V. (2007). "Low-frequency Raman scattering from CeO_2 nanoparticles". *Applied Physics A*, *90*(4), 679–683. doi:10.1007/s00339-007-4345-6

Kousaka, Y., Niida, T., Okuyama, K., & Tanaka, H. (1982). "Development of a mixing type condensation nucleus counter". *Journal of Aerosol Science*, *13*(3), 231–240. doi:10.1016/0021-8502(82)90064-7

Krämer, L., Bozoki, Z., & Niessner, R. (2000). "Setup, calibration and characterization of a mobile photoacoustic soot sensor". *Journal of Aerosol Science*, *31* (Suppl. 1), S72–S73. doi:10.1016/S0021-8502(00)90079-X

Kreyling, W. G., Semmler, M., Erbe, F., Mayer, P., Takenaka, S., Schulz, H., & Ziesenis, A. (2002). "Translocation of ultrafine insoluble iridium particles from lung epithelium to extrapulmonary organs is size dependent but very low". *Journal of Toxicology and Environmental Health, Part A*, *65*(20), 1513–1530. doi:10.1080/00984100290071649

Kreyling, W. G., Semmler-Behnke, M., & Möller, W. (2006a). "Health implications of nanoparticles". *Journal of Nanoparticle Research*, *8*(5), 543–562. doi:10.1007/s11051-005-9068-z

Kreyling, W. G., Semmler-Behnke, M., & Möller, W. (2006b). "Ultrafine particle-lung interactions: does size matter?" *Journal of Aerosol Medicine*, *19*(1), 74–83. doi:10.1089/jam.2006.19.74

Kreyling, W. G., Semmler-Behnke, M., Seitz, J., Scymczak, W., Wenk, A., Mayer, P., Oberdörster, G. (2009). "Size dependence of the translocation of inhaled iridium and carbon nanoparticle aggregates from the lung of rats to the blood and secondary target organs." *Inhalation Toxicology*, *21 Suppl 1*(April), 55–60. doi:10.1080/08958370902942517

Krueger, B. J., Grassian, V. H., Iedema, M. J., Cowlin, J. P., & Laskin, A. (2003). "Probing heterogeneous chemistry of individual atmospheric particles using scanning electron microscopy and energy-dispersive X-ray analysis". *Analytical Chemistry*, *75*(19), 5170–5179. doi:10.1021/ac034455t

Ku, B. K., & Maynard, A. D. (2005). "Comparing aerosol surface-area measurements of monodisperse ultrafine silver agglomerates by mobility analysis, transmission electron microscopy and diffusion charging". *Journal of Aerosol Science*, *36*(9), 1108–1124. doi:10.1016/j.jaerosci.2004.12.003

Ku, B. K. (2010). "Determination of the ratio of diffusion charging-based surface area to geometric surface area for spherical particles in the size range of 100–900nm". *Journal of Aerosol Science*, *41*(9), 835–847. doi:10.1016/j.jaerosci.2010.05.008

Ku, B. K., & Evans, D. E. (2012). "Investigation of Aerosol Surface Area Estimation from Number and Mass Concentration Measurements: Particle Density Effect". *Aerosol Science and Technology*, *46*(4), 473–484. doi:10.1080/02786826.2011.639316

Ku, B. K., & Kulkarni, P. S. (2012). "Comparison of diffusion charging and mobility-based methods for measurement of aerosol agglomerate surface area". *Journal of Aerosol Science*, *47*, 100–110. doi:10.1016/j.jaerosci.2012.01.002

Kuhlbusch, T. A. J., Asbach, C., Fissan, H., Göhler, D., & Stintz, M. (2011). "Nanoparticle exposure at nanotechnology workplaces: a review." *Particle and Fibre Toxicology*, *8*(1), 22. doi:10.1186/1743-8977-8-22

Kuhlbusch, T. A. J., Quincey, P., Fuller, G. W., Kelly, F., Mudway, I., Viana, M., Querol, X., Alastuey, A., Katsouyanni, K., Weijers, E., Borowiak, A., Gehrig, R., Hueglin, C., Bruckmann, P., Favez, O., Sciare, J., Hoffmann, B., EspenYttri, K., Torseth, K., Sager, U., Asbach, C., Quass, U. (2014). "New Directions: The future of European urban air quality monitoring". *Atmospheric Environment*, *87*(April), 258–260. doi:10.1016/j.atmosenv.2014.01.012

Kulkarni, P., & Wang, J. (2006a). "New fast integrated mobility spectrometer for real-time measurement of aerosol size distribution: II. Design, calibration, and performance characterization". *Journal of Aerosol Science*, *37*(10), 1326–1339. doi:10.1016/j.jaerosci.2006.01.010

Kulkarni, P., & Wang, J. (2006b). "New fast integrated mobility spectrometer for real-time measurement of aerosol size distribution—I: Concept and theory". *Journal of Aerosol Science*, *37*(10), 1303–1325. doi:10.1016/j.jaerosci.2006.01.005

Kulmala, M., Pirjola, L., & Makela, J. (2000). "Stable sulphate clusters as a source of new atmospheric particles". *Nature*, *404*(6773), 66–69. doi:10.1038/35003550

Kulmala, M., & Kerminen, V.-M. (2008). "On the formation and growth of atmospheric nanoparticles". *Atmospheric Research*, *90*(2-4), 132–150. doi:10.1016/j.atmosres.2008.01.005

Kulzer, F., Laurens, N., Besser, J., Schmidt, T., Orrit, M., & Spaink, H. P. (2008). "Photothermal detection of individual gold nanoparticles: perspectives for high-throughput screening." *Chemphyschem : A European Journal of Chemical Physics and Physical Chemistry*, *9*(12), 1761–6. doi:10.1002/cphc.200800127

Labouta, H. I., & Schneider, M. (2013). "Interaction of inorganic nanoparticles with the skin barrier: current status and critical review." *Nanomedicine : Nanotechnology, Biology, and Medicine*, *9*(1), 39–54. doi:10.1016/j.nano.2012.04.004

Lach, K., B., Steer, Gorbunov, B., Mička, V., Muir, R. B. (2014). "Evaluation of exposure to airborne heavy metals at gun shooting ranges". *Annals of Occupational Hygiene*, (In press).

Lack, D., Lovejoy, E., Baynard, T., Pettersson, A., & Ravishankara, A. (2006). "Aerosol Absorption Measurement using Photoacoustic Spectroscopy: Sensitivity, Calibration, and Uncertainty Developments". *Aerosol Science and Technology*, *40*(9), 697–708. doi:10.1080/02786820600803917

Laden, F., Neas, L. M., Dockery, D. W., & Schwartz, J. (2000). "Association of fine particulate matter from different sources with daily mortality in six U.S. cities." *Environmental Health Perspectives*, *108*(10), 941–7. doi: 10.2307/3435052

Laden, F., Schwartz, J., Speizer, F. E., & Dockery, D. W. (2006). "Reduction in fine particulate air pollution and mortality: Extended follow-up of the Harvard Six Cities study". *American Journal of Respiratory and Critical Care Medicine*, *173*(6), 667–72. doi:10.1164/rccm.200503-443OC

Lahaye, J., Boehm, S., Chambrion, P., & Ehrburger, P. (1996). "Influence of cerium oxide on the formation and oxidation of soot". *Combustion and Flame*, *104*(1-2), 199–207. doi:10.1016/0010-2180(95)00176-X

Lamminen, E. (2011). "Accurate measurement of nanoparticle charge, number and size with the ELPI+ ™ instrument". *Journal of Physics: Conference Series*, *304*(1), 012064. doi:10.1088/1742-6596/304/1/012064

Larese, F. F., D'Agostin, F., Crosera, M., Adami, G., Renzi, N., Bovenzi, M., & Maina, G. (2009). "Human skin penetration of silver nanoparticles through intact and damaged skin." *Toxicology*, *255*(1-2), 33–7. doi:10.1016/j.tox.2008.09.025

Larner, F., Dogra, Y., Dybowska, A., Fabrega, J., Stolpe, B., Bridgestock, L. J., Goodhead, R., Weiss, D. J., Moger, J., Lead, J. R., Valsami-Jones, E., Tyler, C. R., Galloway, T. S., Rehkämper, M. (2012). "Tracing bioavailability of ZnO nanoparticles using stable isotope labeling." *Environmental Science & Technology*, *46*(21), 12137–45. doi:10.1021/es302602j

Larner, F., Gulson, B., McCall, M., Oytam, Y., & Rehkämper, M. (2014). "An inter-laboratory comparison of high precision stable isotope ratio measurements for nanoparticle tracing in biological samples". *Journal of Analytical Atomic Spectrometry*, *29*(3), 471. doi:10.1039/c3ja50322d

Laskin, A., Iedema, M. J., & Cowin, J. P. (2002). "Quantitative time-resolved monitoring of nitrate formation in sea salt particles using a CCSEM/EDX single particle analysis". *Environmental Science & Technology*, *36*(23), 4948–55. doi:10.1021/es020551k

Laskin, A., Cowin, J. P., & Iedema, M. J. (2006). "Analysis of individual environmental particles using modern methods of electron microscopy and X-ray microanalysis". *Journal of Electron Spectroscopy and Related Phenomena*, *150*(2-3), 260–274. doi:10.1016/j.elspec.2005.06.008

Laskin, J., Laskin, A., & Nizkorodov, S. A. (2013). "New mass spectrometry techniques for studying physical chemistry of atmospheric heterogeneous processes". *International Reviews in Physical Chemistry*, *32*(1), 128–170. doi:10.1080/0144235X.2012.752904

Law, M., Greene, L. E., Johnson, J. C., Saykally, R., & Yang, P. (2005). "Nanowire dye-sensitized solar cells." *Nature Materials*, *4*(6), 455–9. doi:10.1038/nmat1387

LeBlanc, A. J., Moseley, A. M., Chen, B. T., Frazer, D., Castranova, V., & Nurkiewicz, T. R. (2010). "Nanoparticle inhalation impairs coronary microvascular reactivity via a local reactive oxygen species-dependent mechanism". *Cardiovascular Toxicology*, *10*(1), 27–36. doi:10.1007/s12012-009-9060-4.Nanoparticle

Lee, J. H., Hopke, P. K., Holsen, T. M., Lee, D.-W., A. Jaques, P., Sioutas, C., & Ambs, J. L. (2005a). "Performance evaluation of continuous mass concentration monitors". *Journal of Aerosol Science*, *36*(1), 95–109. doi:10.1016/j.jaerosci.2004.07.006

Lee, J. H., Hopke, P. K., Holsen, T. M., & Polissar, A. V. (2005b). "Evaluation of Continuous and Filter-Based Methods for Measuring PM 2.5 Mass Concentration". *Aerosol Science and Technology*, *39*(4), 290–303. doi:10.1080/027868290929323

Lee, A. K. Y., & Chan, C. K. (2007). "Single particle Raman spectroscopy for investigating atmospheric heterogeneous reactions of organic aerosols". *Atmospheric Environment*, *41*(22), 4611–4621. doi:10.1016/j.atmosenv.2007.03.040

Lehmann, U., Niemelä, V., & Mohr, M. (2004). "New method for time-resolved diesel engine exhaust particle mass measurement." *Environmental Science & Technology*, *38*(21), 5704–11. doi:10.1021/es035206p

Li, D., Zhuo, W., Yi, Y., Chen, B., & Liu, H. (2008). "A new sampler for simulating aerosol deposition in the respiratory tract". *Nuclear Science and Techniques*, *19*(3), 169–173. doi:10.1016/S1001-8042(08)60045-7

Li, L., Chen, D.-R., Qi, C., & Kulkarni, P. S. (2009). "A miniature disk electrostatic aerosol classifier (mini-disk EAC) for personal nanoparticle sizers". *Journal of Aerosol Science*, *40*(11), 982–992. doi:10.1016/j.jaerosci.2009.09.003

Li, M., Zhang, R., Zhang, H., Feng, W., & Liu, X. (2010). "Synthesis, structural and magnetic properties of CeO_2 nanoparticles". *Micro & Nano Letters*, *5*(2), 95. doi:10.1049/mnl.2009.0092

Li, N., Sioutas, C., Cho, A., Schmitz, D., Misra, C., Sempf, J., Wang, M., Oberley, T., Froines, J., Nel, A. (2002a). "Ultrafine Particulate Pollutants Induce Oxidative Stress and Mitochondrial Damage". *Environmental Health Perspectives*, *111*(4), 455–460. doi:10.1289/ehp.6000

Li, R., Yabe, S., Yamashita, M., & Momose, S. (2002b). "Synthesis and UV-shielding properties of ZnO-and CaO-doped CeO_2 via soft solution chemical process". *Solid State Ionics*, *151*(1-4), 235–241. doi:10.1016/S0167-2738(02)00715-4

Li, R., Yabe, S., Yamashita, M., Momose, S., Yoshida, S., Yin, S., & Sato, T. (2002c). "UV-shielding properties of zinc oxide-doped ceria fine powders derived via soft solution chemical routes". *Materials Chemistry and Physics*, *75*(1-3), 39–44. doi:10.1016/S0254-0584(02)00027-5

Li, W., & Shao, L. (2009). "Transmission electron microscopy study of aerosol particles from the brown hazes in northern China". *Journal of Geophysical Research*, *114*(D9), D09302. doi:10.1029/2008JD011285

Liang, Z., Wei, G., Irwin, R. L., Walton, A. P., Michel, R. G., & Sneddon, J. (1990). "Determination of subnanogram per cubic meter concentrations of metals in the air of a

trace metal clean room by impaction graphite furnace atomic absorption and laser excited atomic fluorescence spectrometry". *Analytical Chemistry*, *62*(14), 1452–1457. doi:10.1021/ac00213a020

Liao, L., Lu, H. B., Li, J. C., He, H., Wang, D. F., Fu, D. J., Liu, C., Zhang, W. F. (2007). "Size Dependence of Gas Sensitivity of ZnO Nanorods". *Journal of Physical Chemistry C*, *111*(5), 1900–1903. doi:10.1021/jp065963k

Lidén, G., Juringe, L., & Gudmundsson, A. (1998). "Workplace validation of a laboratory determination of the sampling efficiency of personal samplers". *Journal of Aerosol Science*, *29* (Supplement 1), S335–S336. doi:10.1016/S0021-8502(98)00498-4

Lilienfeld, P. (1970). "Beta-Absorption-Impactor Aerosol Mass Monitor". *American Industrial Hygiene Association Journal*, *31*(6), 722–729. doi:10.1080/0002889708506320

Lin, C. I., Baker, M., & Charlson, R. J. (1973). "Absorption coefficient of atmospheric aerosol: a method for measurement." *Applied Optics*, *12*(6), 1356–63. doi:10.1364/AO.12.001356

Lin, C., Chen, C., Pan, S., Weng, H., & Yu, T. (2008). "Development of the Primary Nanoparticle Measurement Standard by the Electro-Gravitational Aerosol Balance". *American Society for Precision Engineering*, (2), 2–5. Retrieved from http://www.aspe.net/publications/Annual_2008/POSTERS/05DMET/2589.PDF

Ling, L., & Li, Y. (2013). "Measurement of Raman spectra of single airborne absorbing particles trapped by a single laser beam". *Optics Letters*, *38*(4), 416–8. doi:10.1364/OL.38.000416

Lison, D., Lardot, C., Huaux, F., Zanetti, G., & Fubini, B. (1997). "Influence of particle surface area on the toxicity of insoluble manganese dioxide dusts". *Archives of Toxicology*, *71*, 725–729. doi:10.1007/s002040050453

Lithgow, G. A., Robinson, A. L., & Buckley, S. G. (2004). "Ambient measurements of metal-containing PM2.5 in an urban environment using laser-induced breakdown spectroscopy". *Atmospheric Environment*, *38*(20), 3319–3328. doi:10.1016/j.atmosenv.2004.03.017

Liu, B. Y. H., Whitby, K. T., & Pui, D. Y. H. (1974). "A Portable Electrical Analyzer for Size Distribution Measurement of Submicron Aerosols". *Journal of the Air Pollution Control Association*, *24*(11), 1067–1072. doi:10.1080/00022470.1974.10470016

Liu, Y., Yang, Z., Desyaterik, Y., Gassman, P. L., Wang, H., & Laskin, A. (2008). "Hygroscopic Behavior of Substrate-Deposited Particles Studied by micro-FT-IR Spectroscopy and Complementary Methods of Particle Analysis". *Analytical Chemistry*, *80*(1148), 633–642. doi:10.1021/ac701638r

Liu, Y., & Laskin, A. (2009). "Hygroscopic properties of CH_3SO_3NA, $CH_3SO_3NH_4$, $(CH_3SO_3)_2Mg$, and $(CH_3SO_3)_2Ca$ particles studied by micro-FTIR spectroscopy". *The Journal of Physical Chemistry A*, *113*, 1531–1538. doi:10.1021/jp8079149

Lomer, M. C. E., Thompson, R. P. H., Commisso, J., Keen, C. L., & Powell, J. J. (2000). "Determination of titanium dioxide in foods using inductively coupled plasma optical emission spectrometry". *The Analyst*, *125*(12), 2339–2343. doi:10.1039/b006285p

Lomer, M. C. E., Thompson, R. P. H., & Powell, J. J. (2007). "Fine and ultrafine particles of the diet: influence on the mucosal immune response and association with Crohn's disease". *Proceedings of the Nutrition Society*, *61*(01), 123–130. doi:10.1079/PNS2001134

Lu, T., Lee, H., Chen, T., Herchak, S., Kim, J.-H., Fraser, S. E., Flagan, R. C., Vahala, K. (2011). "High sensitivity nanoparticle detection using optical microcavities." *Proceedings of the National Academy of Sciences of the United States of America*, *108*(15), 5976–9. doi:10.1073/pnas.1017962108

Lucarelli, F., Nava, S., Calzolai, G., Chiari, M., Udisti, R., & Marino, F. (2011). "Is PIXE still a useful technique for the analysis of atmospheric aerosols? The LABEC experience". *X-Ray Spectrometry*, *40*(3), 162–167. doi:10.1002/xrs.1312

Lundborg, M., Dahlén, S.-E., Johard, U., Gerde, P., Jarstrand, C., Camner, P., & Låstbom, L. (2006). "Aggregates of ultrafine particles impair phagocytosis of microorganisms by human alveolar macrophages." *Environmental Research*, *100*(2), 197–204. doi:10.1016/j.envres.2005.08.007

Ma, C.-J., & Kim, K.-H. (2008). "A combination of size-resolved particle samplers and XRF microprobe technique for single particle study". *Atmospheric Environment*, *42*(29), 7022–7026. doi:10.1016/j.atmosenv.2008.04.045

Ma, Z., Merkus, H. G., de Smet, J. G. A. E. ., Heffels, C., & Scarlett, B. (2000). "New developments in particle characterization by laser diffraction: size and shape". *Powder Technology*, *111*(1-2), 66–78. doi:10.1016/S0032-5910(00)00242-4

Ma, Z., Merkus, H. G., & Scarlett, B. (2001). "Extending laser diffraction for particle shape characterization: technical aspects and application". *Powder Technology*, *118*(1-2), 180–187. doi:10.1016/S0032-5910(01)00309-6

Madelin, T. (1992). "Design, construction, testing and use of an artificial lung for sampling biological aerosols". *Journal of Aerosol Science*, *23* (Supplement 1), 675–678. doi:10.1016/0021-8502(92)90502-M

Mallina, R. V., Wexler, A. S., Rhoads, K. P., & Johnston, M. V. (2000). "High Speed Particle Beam Generation: A Dynamic Focusing Mechanism for Selecting Ultrafine Particles". *Aerosol Science and Technology*, *33*(1-2), 87–104. doi:10.1080/027868200410868

Marijnissen, J., Scarlett, B., & Verheijen, P. (1988). "Proposed on-line aerosol analysis combining size determination, laser-induced fragmentation and time-of-flight mass spectroscopy". *Journal of Aerosol Science*, *19*(7), 1307–1310. doi:10.1016/0021-8502(88)90161-9

Marjamäki, M., Keskinen, J., Chen, D.-R., & Pui, D. Y. H. (2000). "Performance evaluation of the electrical low-pressure impactor (ELPI)". *Journal of Aerosol Science*, *31*(2), 249–261. doi:10.1016/S0021-8502(99)00052-X

Marple, V. A., Rubow, K. L., & Behm, S. M. (1991). "A Microorifice Uniform Deposit Impactor (MOUDI): Description, Calibration, and Use". *Aerosol Science and Technology*, *14*(4), 434–446. doi:10.1080/02786829108959504

Marquard, A., Meyer, J., & Kasper, G. (2006). "Characterization of unipolar electrical aerosol chargers—Part II:Application of comparison criteria to various types of nanoaerosol

charging devices". *Journal of Aerosol Science*, *37*(9), 1069–1080. doi:10.1016/j.jaerosci.2005.09.002

Marriott, C., MacRitchie, H. B., Zeng, X.-M., & Martin, G. P. (2006). "Development of a laser diffraction method for the determination of the particle size of aerosolised powder formulations." *International Journal of Pharmaceutics*, *326*(1-2), 39–49. doi:10.1016/j.ijpharm.2006.07.021

Marshall, I., Mitchell, J., & Griffiths, W. (1990). "Calibration of a TSI aerodynamic particle sizer with monodisperse non-spherical particles". *Journal of Aerosol Science*, *21* (Supplement 1), S613–S616. doi:10.1016/0021-8502(90)90317-Q

Marshall, I. A., Mitchell, J. P., & Griffiths, W. D. (1991). "The behaviour of regular-shaped non-spherical particles in a TSI aerodynamic particle sizer". *Journal of Aerosol Science*, *22*(1), 73–89. doi:10.1016/0021-8502(91)90094-X

Marshall, I. A., & Mitchell, J. P. (1992). "The behaviour of spheroidal particles in time-of-flight aerodynamic particle sizers". *Journal of Aerosol Science*, *23* (Supplement 1), S297–S300. doi:10.1016/0021-8502(92)90408-N

Marti, J. J., Weber, R. J., Saros, M. T., Vasiliou, J. G., & McMurry, P. H. (1996). "Modification of the TSI 3025 Condensation Particle Counter for Pulse Height Analysis". *Aerosol Science and Technology*, *25*(2), 214–218. doi:10.1080/02786829608965392

Martínez-Lozano, P., & Labowsky, M. (2009). "An experimental and numerical study of a miniature high resolution isopotential DMA". *Journal of Aerosol Science*, *40*(5), 451–462. doi:10.1016/j.jaerosci.2009.01.004

Matatov-Meytal, Y. I., & Sheintuch, M. (1998). "Catalytic abatement of water pollutants". *Industrial & Engineering Chemistry Research*, *37*(2), 309–326. doi:10.1021/ie9702439

Matsko, A. B., Savchenkov, A. A., Strekalov, D., Ilchenko, V. S., & Maleki, L. (2005). "Review of Applications of Whispering-Gallery Mode Resonators in Photonics and Nonlinear Optics". *IPN Progress Report*, *42*(162), 1–51.

Matter, U., Paul, J., Scherrer, L., & Siegmann, K. (1998). "Dynamic characterization of diesel particulate emissions using two portable sensors". *Journal of Aerosol Science*, *29* (Supplement 1), S951–S952. doi:10.1016/S0021-8502(98)90658-9

Matter, U., Siegmann, H. C., & Burtscher, H. (1999). "Dynamic Field Measurements of Submicron Particles from Diesel Engines". *Environmental Science & Technology*, *33*(11), 1946–1952. doi:10.1021/es981095w

Matthäus, C., Boydston-White, S., Miljković, M., Romeo, M., & Diem, M. (2006). "Raman and Infrared Microspectral Imaging of Mitotic Cells". *Applied Spectroscopy*, *60*(1), 1–8. doi:10.1366/000370206775382758

Mattimaricq, M. (2007). "Chemical characterization of particulate emissions from diesel engines: A review". *Journal of Aerosol Science*, *38*(11), 1079–1118. doi:10.1016/j.jaerosci.2007.08.001

May, K. (1945). "The cascade impactor: an instrument for sampling coarse aerosols". *Journal of Scientific Instruments*, *22* (October), 187. doi:10.1088/0950-7671/22/10/303

May, K. (1982). "A personal note on the history of the cascade impactor". *Journal of Aerosol Science*, *13*(1), 37–47. doi:10.1016/0021-8502(82)90006-4

Maynard, A. D. (1995). "The application of electron energy-loss spectroscopy to the analysis of ultrafine aerosol particles". *Journal of Aerosol Science*, *26*(5), 757–777. doi:10.1016/0021-8502(95)00006-X

Maynard, A. D. (2000). "Overview of Methods for Analysing Single Ultrafine Particles". *Philosophical Transactions: Mathematical, Physical and Engineering Sciences*, *358*(1775), 2593–2610. doi:10.2307/2666942

Maynard, A. D. (2003). "Estimating Aerosol Surface Area from Number and Mass Concentration Measurements". *Annals of Occupational Hygiene*, *47*(2), 123–144. doi:10.1093/annhyg/meg022

Maynard, A. D., Baron, P. A., Foley, M., Shvedova, A. A., Kisin, E. R., & Castranova, V. (2004). "Exposure to Carbon Nanotube Material: Aerosol Release During the Handling of Unrefined Single-Walled Carbon Nanotube Material". *Journal of Toxicology and Environmental Health, Part A*, *67*(1), 87–108. doi:10 1080/15287390490253688

Maynard, A. D., & Kuempel, E. D. (2005). "Airborne Nanostructured Particles and Occupational Health". *Journal of Nanoparticle Research*, *7*(6), 587–614. doi:10.1007/s11051-005-6770-9

Maynard, A. D., & Aitken, R. J. (2007). "Assessing exposure to airborne nanomaterials: Current abilities and future requirements". *Nanotoxicology*, *1*(1), 26–41. doi:10.1080/17435390701314720

Mazumder, M. K., & Kirsch, K. J. (1977). "Single particle aerodynamic relaxation time analyzer". *Review of Scientific Instruments*, *48*(6), 622. doi:10.1063/1.1135094

Mazzei, A., Götzinger, S., Menezes, L. de S., Zumofen, G., Benson, O., & Sandoghdar, V. (2007). "Controlled Coupling of Counterpropagating Whispering-Gallery Modes by a Single Rayleigh Scatterer: A Classical Problem in a Quantum Optical Light". *Physical Review Letters*, *99*(17), 1–4. doi:10.1103/PhysRevLett.99.173603

McLean, K. J. (1988). "Electrostatic precipitators". *IEE Proceedings A Physical Science, Measurement and Instrumentation, Management and Education, Reviews*, *135*(6), 347. doi:10.1049/ip-a-1.1988.0056

McMurry, P. H. (2000a). "A review of atmospheric aerosol measurements". *Atmospheric Environment*, *34*(12-14), 1959–1999. doi:10.1016/S1352-2310(99)00455-0

McMurry, P. H. (2000b). "The History of Condensation Nucleus Counters". *Aerosol Science and Technology*, *33*(4), 297–322. doi:10.1080/02786820050121512

McMurry, P. H., Wang, X., Park, K., & Ehara, K. (2002). "The Relationship between Mass and Mobility for Atmospheric Particles: A New Technique for Measuring Particle Density". *Aerosol Science and Technology*, *36*(2), 227–238. doi:10.1080/027868202753504083

Mehl, B. P., House, R. L., Uppal, A., Reams, A. J., Zhang, C., Kirschbrown, J. R., & Papanikolas, J. M. (2010). "Direct imaging of optical cavity modes in ZnO rods using

second harmonic generation microscopy". *The Journal of Physical Chemistry A*, *114*(3), 1241–6. doi:10.1021/jp9009614

Menzel, N., Schramel, P., & Wittmaack, K. (2002). "Elemental composition of aerosol particulate matter collected on membrane filters: A comparison of results by PIXE and ICP-AES". *Nuclear Instruments and Methods in Physics Research B*, *189*(1-4), 94–99. doi:10.1016/S0168-583X(01)01013-8

Mertes, S., Dippel, B., & Schwarzenböck, A. (2004). "Quantification of graphitic carbon in atmospheric aerosol particles by Raman spectroscopy and first application for the determination of mass absorption efficiencies". *Journal of Aerosol Science*, *35*(3), 347–361. doi:10.1016/j.jaerosci.2003.10.002

Mészáros, A., & Vissy, K. (1974). "Concentration, size distribution and chemical nature of atmospheric aerosol particles in remote oceanic areas". *Journal of Aerosol Science*, *5*(1), 101–109. doi:10.1016/0021-8502(74)90011-1

Meyer, D. E., Curran, M. A., & Gonzalez, M. A. (2009). "An Examination of Existing Data for the Industrial Manufacture and Use of Nanocomponents and Their Role in the Life Cycle Impact of Nanoproducts". *Environmental Science & Technology*, *43*(5), 1256 – 1263. doi:10.1021/es8023258

Min, B., Ostby, E., Sorger, V., Ulin-Avila, E., Yang, L., Zhang, X., & Vahala, K. (2009). "High-Q surface-plasmon-polariton whispering-gallery microcavity." *Nature*, *457*(7228), 455–8. doi:10.1038/nature07627

Minemawari, H., Yamada, T., Matsui, H., Tsutsumi, J., Haas, S., Chiba, R., Kumai, R., Hasegawa, T. (2011). "Inkjet printing of single-crystal films". *Nature*, *475*(7356), 364–7. doi:10.1038/nature10313

Mitra, A., Deutsch, B., Ignatovich, F. V., Dykes, C., & Novotny, L. (2010). "Nano-optofluidic Detection of Single Viruses and Nanoparticles." *ACS Nano*, *4*(3), 1305–12. doi:10.1021/nn901889v

Mitra, A., Ignatovich, F., & Novotny, L. (2012). "Real-time optical detection of single human and bacterial viruses based on dark-field interferometry." *Biosensors & Bioelectronics*, *31*(1), 499–504. doi:10.1016/j.bios.2011.11.025

Mitsakou, C., Helmis, C., & Housiadas, C. (2005). "Eulerian modelling of lung deposition with sectional representation of aerosol dynamics". *Journal of Aerosol Science*, *36*(1), 75–94. doi:10.1016/j.jaerosci.2004.08.008

Mizuno, A. (2000). "Electrostatic precipitation". *IEEE Transactions on Dielectrics and Electrical Insulation*, *7*(5), 615–624. doi:10.1109/94.879357

Moezzi, A., McDonagh, A. M., & Cortie, M. B. (2012). "Zinc oxide particles: Synthesis, properties and applications". *Chemical Engineering Journal*, *185-186*, 1–22. doi:10.1016/j.cej.2012.01.076

Moffet, R. C., Henn, T., Laskin, A., & Gilles, M. K. (2010). "Automated Chemical Analysis of Internally Mixed Aerosol Particles Using X-ray Spectromicroscopy at the Carbon K-Edge†". *Analytical Chemistry*, *82*(19), 7906–7914. doi:10.1029/2002GL014874.(21)

Moisio, M., & Niemelä, V. (2002). "Device for continuous measurement of density and mass concentration of vehicle exhaust aerosol". *International Aerosol Conference, Taipai, Taiwan*, 33700. Retrieved from http://micro-campaign.com/solma/wp-content/uploads/2012/11/IAC2002-DMM.pdf

Molenar, J. (2005). "Theoretical analysis of PM2. 5 mass measurements by nephelometry - # 110", 1–21. Retrieved from http://vista.cira.colostate.edu/improve/Publications/GrayLit/014_AerosolByNeph/AerosolbyNeph.pdf

Möller, W., Hofer, T., Ziesenis, A., Karg, E., & Heyder, J. (2002). "Ultrafine particles cause cytoskeletal dysfunctions in macrophages". *Toxicology and Applied Pharmacology*, *182*(3), 197–207. doi:10.1006/taap.2002.9430

Möller, W., Felten, K., Sommerer, K., Scheuch, G., Meyer, G., Meyer, P., Häussinger, K., Kreyling, W. G. (2008). "Deposition, retention, and translocation of ultrafine particles from the central airways and lung periphery." *American Journal of Respiratory and Critical Care Medicine*, *177*(4), 426–32. doi:10.1164/rccm.200602-301OC

Moosmüller, H., Arnott, W., & Rogers, C. (1997). "Methods for real-time, in situ measurement of aerosol light absorption". *Journal of the Air & Waste Management Association*, *47*(February), 157–166. doi:10.1080/10473289.1997.10464430

Moosmüller, H., Arnott, W. P., Rogers, C. F., Bowen, J. L., Gillies, J. A., Pierson, W. R., Collins, J. F., Durbin, T. D., Norbeck, J. M. (2001). "Time resolved characterization of diesel particulate emissions. 1. Instruments for particle mass measurements." *Environmental Science & Technology*, *35*(4), 781–7. doi:10.1021/es0013935

Moosmüller, H., Chakrabarty, R. K., & Arnott, W. P. (2009). "Aerosol light absorption and its measurement: A review". *Journal of Quantitative Spectroscopy and Radiative Transfer*, *110*(11), 844–878. doi:10.1016/j.jqsrt.2009.02.035

Morawska, L., Wang, H., Ristovski, Z., Jayaratne, E. R., Johnson, G., Cheung, H. C., Ling, X, He, C. (2009). "JEM spotlight: Environmental monitoring of airborne nanoparticles." *Journal of Environmental Monitoring : JEM*, *11*(10), 1758–73. doi:10.1039/b912589m

Morimoto, T., Tomonaga, H., & Mitani, A. (1999). "Ultraviolet ray absorbing coatings on glass for automobiles". *Thin Solid Films*, *351*(1-2), 61–65. doi:10.1016/S0040-6090(98)01779-9

Mortensen, A. (2006). *Concise Encyclopedia of Composite Materials* (2nd Edition). Elsevier, Oxford, UK and Amsterdam, The Netherlands.

Mouli, P. C., Mohan, S. V., Balaram, V., Kumar, M. P., & Reddy, S. J. (2006). "A study on trace elemental composition of atmospheric aerosols at a semi-arid urban site using ICP-MS technique". *Atmospheric Environment*, *40*, 136–146. doi:10.1016/j.atmosenv.2005.09.028

Müller, R., Laschober, C., Szymanski, W. W., & Allmaier, G. (2007). "Determination of molecular weight, particle size, and density of high number generation PAMAM dendrimers using MALDI-TOF-MS and nES-GEMMA". *Macromolecules*, *40*(15), 5599–5605. doi:10.1021/ma062599e

Murphy, D. (2007). "The Design of Single Particle Laser Mass Spectrometers". *Mass Spectrometry Reviews*, *26*(2), 150–165. doi:10.1002/mas.20113

Nader, J. S., & Allen, D. R. (1960). "A Mass Loading and Radioactivity Analyzer for Atmospheric Particulates". *American Industrial Hygiene Association Journal*, *21*(4), 300–307. doi:10.1080/00028896009343362

Nash, D. G., Baer, T., & Johnston, M. V. (2006). "Aerosol mass spectrometry: An introductory review". *International Journal of Mass Spectrometry*, *258*(1-3), 2–12. doi:10.1016/j.ijms.2006.09.017

Nedosekin, D. A, Galanzha, E. I., Dervishi, E., Biris, A. S., & Zharov, V. P. (2014). "Super-resolution nonlinear photothermal microscopy." *Small*, *10*(1), 135–42. doi:10.1002/smll.201300024

Nel, A., Xia, T., Mädler, L., & Li, N. (2006). "Toxic potential of materials at the nanolevel". *Science*, *311*(5761), 622–7. doi:10.1126/science.1114397

Nelson, M. P., Zugates, C. T., Treado, P. J., Casuccio, G. S., Exline, D. L., & Schlaegle, S. F. (2001). "Combining Raman chemical imaging and scanning electron microscopy to characterize ambient fine particulate matter". *Aerosol Science & Technology*, *34*(1), 108–117. doi:10.1080/02786820120709

Neuhauser, R., Panne, U., & Niessner, R. (1997a). "Elemental characterization of heavy metal aerosols by Laser-induced Plasma Spectroscopy (LIPS)". *Journal of Aerosol Science*, *28* (Suppl. 1), S437–S438. doi:10.1016/S0021-8502(97)85218-4

Neuhauser, R. E., Panne, U., Niessner, R., Petrucci, G. A., Cavalli, P., & Omenetto, N. (1997b). "On-line and in-situ detection of lead aerosols by plasma-spectroscopy and laser-excited atomic fluorescence spectroscopy". *Analytica Chimica Acta*, *346*(1), 37–48. doi:10.1016/S0003-2670(97)00244-4

Neuhauser, R. E., Panne, U., Niessner, R., Petrucci, G., Cavalli, P., & Omenetto, N. (1997c). "On-line and in situ detection of lead in ultrafine aerosols by laser-excited atomic fluorescence spectroscopy". *Sensors and Actuators B: Chemical*, *39*(1-3), 344–348. doi:10.1016/S0925-4005(97)80231-6

Neuhauser, R. ., Panne, U., & Niessner, R. (1999). "Laser-induced plasma spectroscopy (LIPS): a versatile tool for monitoring heavy metal aerosols". *Analytica Chimica Acta*, *392*(1), 47–54. doi:10.1016/S0003-2670(99)00053-7

Newman, M. D., Stotland, M., & Ellis, J. I. (2009). "The safety of nanosized particles in titanium dioxide- and zinc oxide-based sunscreens." *Journal of the American Academy of Dermatology*, *61*(4), 685–92. doi:10.1016/j.jaad.2009.02.051

Niu, J., Rasmussen, P. E., Wheeler, A., Williams, R., & Chénier, M. (2010). "Evaluation of airborne particulate matter and metals data in personal, indoor and outdoor environments using ED-XRF and ICP-MS and co-located duplicate samples". *Atmospheric Environment*, *44*(2), 235–245. doi:10.1016/j.atmosenv.2009.10.009

Nizkorodov, S. A, Laskin, J., & Laskin, A. (2011). "Molecular chemistry of organic aerosols through the application of high resolution mass spectrometry." *Physical Chemistry Chemical Physics : PCCP*, *13*(9), 3612–29. doi:10.1039/c0cp02032j

Noble, C. A., & Prather, K. A. (1996). "Real-Time Measurement of Correlated Size and Composition Profiles of Individual Atmospheric Aerosol Particles". *Environmental Science & Technology*, *30*(9), 2667–2680. doi:10.1021/es950669j

Noble, C. A., & Prather, K. A. (1998). "Aerosol Time-of-Flight Mass Spectrometry: A New Method for Performing Real-Time Characterization of Aerosol Particles". *Applied Occupational and Environmental Hygiene*, *13*(6), 439–443. doi:10.1080/1047322X.1998.10389569

Noble, C., & Prather, K. (2000). "Real-time single particle mass spectrometry: a historical review of a quarter century of the chemical analysis of aerosols". *Mass Spectrometry Reviews*, *19*(4), 248–74. doi:10.1002/1098-2787(200007)19:4<248::AID-MAS3>3.0.CO;2-I

Nordmeyer, T., & Prather, K. (1994). "Real-time measurement capabilities using aerosol time-of-flight mass spectrometry". *Analytical Chemistry*, *66*(20), 3540–3542. doi:10.1021/ac00092a040

Nottrodt, K. H., Georgii, H. W., & Groeneveld, K. O. (1978). "Absolute element concentrations in aerosols analysed by atomic-absorption-spectroscopy and by proton-induced X-ray emission, a comparison". *Journal of Aerosol Science*, *9*(2), 169–173. doi:10.1016/0021-8502(78)90076-9

Novotny, L. (2007). "The history of near-field optics". *Progress in Optics*, *50*, 137. Retrieved from http://www.optics.rochester.edu/workgroups/novotny/papers/history4.pdf

O'Brien, R. E., Laskin, A., Laskin, J., Liu, S., Weber, R., Russell, L. M., & Goldstein, A. H. (2013). "Molecular characterization of organic aerosol using nanospray desorption/electrospray ionization mass spectrometry: CalNex 2010 field study". *Atmospheric Environment*, *68* (April), 265–272. doi:10.1016/j.atmosenv.2012.11.056

O'Dowd, C. D., Aalto, P. P., Yoon, Y. J., & Hämeri, K. (2004). "The use of the pulse height analyser ultrafine condensation particle counter (PHA-UCPC) technique applied to sizing of nucleation mode particles of differing chemical composition". *Journal of Aerosol Science*, *35*(2), 205–216. doi:10.1016/j.jaerosci.2003.08.003

Ober, F., Mayer, M., Büttner, H., & Ebert, F. (2002). "Aerosol Measurement in Low-Pressure Systems with Standard Scanning Mobility Particle Sizers". *Particle & Particle Systems Characterization*, *19*(4), 229–239. doi:10.1002/1521-4117(200208)19:4<229::AID-PPSC229>3.0.CO;2-8

Oberdörster, G., Ferin, J., & Lehnert, B. (1994a). "Correlation between particle size, in vivo particle persistence, and lung injury." *Environmental Health Perspectives*, *102* (Supplement 5), 173–179. doi:10.2307/3432080

Oberdörster, G., Ferin, J., Soderholm, S., Gelein, R., Cox, C., Baggs, R., & Morrow, P. E. (1994b). "Increased Pulmonary Toxicity of Inhaled Ultrafine Particles: Due to Lung Overload Alone?". *Annals of Occupational Hygiene*, *38* (Supplement 1), 295–302. doi:10.1093/annhyg/38.inhaled_particles_VII.295

Oberdörster, G., Gelein, R. M., Ferin, J., & Weiss, B. (1995). "Association of particulate air pollution and acute mortality: involvement of ultrafine particles?" *Inhalation Toxicology*, *7*(1), 111–24. doi:10.3109/08958379509014275

Oberdörster, G., Sharp, Z., Atudorei, V., Elder, A., Gelein, R., Lunts, A., Kreyling, W., Cox, C. (2002). "Extrapulmonary translocation of ultrafine carbon particles following whole-body inhalation exposure of rats". *Journal of Toxicology and Environmental Health, Part A*, *65*(20), 1531–1543. doi:10.1080/0098410029007165

Oberdörster, G., Sharp, Z., Atudorei, V., Elder, A, Gelein, R., Kreyling, W. G., & Cox, C. (2004). "Translocation of inhaled ultrafine particles to the brain." *Inhalation Toxicology*, *16*(6-7), 437–45. doi:10.1080/08958370490439597

Oberdörster, G., Maynard, A. D., Donaldson, K., Castranova, V., Fitzpatrick, J., Ausman, K., Carter, J., Karn, B., Kreyling, W. G., Lai, D., Olin, S., Monteiro-Riviere, N., Warheit, D. Yang, H. (2005). "Principles for characterizing the potential human health effects from exposure to nanomaterials: elements of a screening strategy." *Particle and Fibre Toxicology*, *2*(1), 8. doi:10.1186/1743-8977-2-8

Okamoto, H., & Imura, K. (2009). "Near-field optical imaging of enhanced electric fields and plasmon waves in metal nanostructures". *Progress in Surface Science*, *84*(7-8), 199–229. doi:10.1016/j.progsurf.2009.03.003

Olfert, J. S., & Collings, N. (2005). "New method for particle mass classification—the Couette centrifugal particle mass analyzer". *Journal of Aerosol Science*, *36*(11), 1338–1352. doi:10.1016/j.jaerosci.2005.03.006

Olfert, J. S., Reavell, K. S., Rushton, M. G., & Collings, N. (2006). "The experimental transfer function of the Couette centrifugal particle mass analyzer". *Journal of Aerosol Science*, *37*(12), 1840–1852. doi:10.1016/j.jaerosci.2006.07.007

Olfert, J. S., Kulkarni, P., & Wang, J. (2008). "Measuring aerosol size distributions with the fast integrated mobility spectrometer". *Journal of Aerosol Science*, *39*(11), 940–956. doi:10.1016/j.jaerosci.2008.06.005

Olin, J. G., & Sem, G. J. (1971). "Piezoelectric microbalance for monitoring the mass concentration of suspended particles". *Atmospheric Environment*, *5*(8), 653–668. doi:10.1016/0004-6981(71)90123-5

Ono-Ogasawara, M., Serita, F., & Takaya, M. (2009). "Distinguishing nanomaterial particles from background airborne particulate matter for quantitative exposure assessment". *Journal of Nanoparticle Research*, *11*(7), 1651–1659. doi:10.1007/s11051-009-9703-1

Ottesen, D., Wang, J., & Radziemski, L. (1989). "Real-time laser spark spectroscopy of particulates in combustion environments". *Applied Spectroscopy*, *43*(6), 967–976. Retrieved from http://www.opticsinfobase.org/abstract.cfm?uri=as-43-6-967

Ottesen, D. K., Baxter, L. L., Radziemski, L. J., & Burrows, J. F. (1991). "Laser spark emission spectroscopy for in-situ, real-time monitoring of pulverized coal particle composition". *Energy & Fuels*, *5*(4), 304–312. doi:10.1021/ef00026a014

Özgür, U., Alivov, Y. I., Liu, C., Teke, A., Reshchikov, M. A., Doğan, S., Avrutin, V., Cho, S.-J., Morkoç, H. (2005). "A comprehensive review of ZnO materials and devices". *Journal of Applied Physics*, *98*(4), 041301. doi:10.1063/1.1992666

Pandis, S. N., Baltensperger, U., Wolfenbarger, J. K., & Seinfeld, J. H. (1991). "Inversion of aerosol data from the epiphaniometer". *Journal of Aerosol Science*, *22*(4), 417–428. doi:10.1016/0021-8502(91)90002-Y

Panne, U., Neuhauser, R., & Theisen, M. (2001). "Analysis of heavy metal aerosols on filters by laser-induced plasma spectroscopy". *Spectrochimica Acta Part B: Atomic Spectroscopy*, *56*(6), 839–850. doi:10.1016/S0584-8547(01)00209-9

Pant, P., & Harrison, R. M. (2013). "Estimation of the contribution of road traffic emissions to particulate matter concentrations from field measurements: A review". *Atmospheric Environment*, *77*(October), 78–97. doi:10.1016/j.atmosenv.2013.04.028

Park, B., Martin, P., Harris, C., Guest, R., Whittingham, A., Jenkinson, P., & Handley, J. (2007). "Initial in vitro screening approach to investigate the potential health and environmental hazards of Enviroxtrade mark - a nanoparticulate cerium oxide diesel fuel additive." *Particle and Fibre Toxicology*, *4*, 12. doi:10.1186/1743-8977-4-12

Park, B., Donaldson, K., Duffin, R., Tran, L., Kelly, F., Mudway, I., Morin, J.-P., Guest, R., Jenkinson, P., Samaras, Z., Giannouli, M., Kouridis, H., Martin, P. (2008). "Hazard and risk assessment of a nanoparticulate cerium oxide-based diesel fuel additive - a case study". *Inhalation Toxicology*, *20*(6), 547–66. doi:10.1080/08958370801915309

Park, H., Byeon, K.-J., Yang, K.-Y., Cho, J.-Y., & Lee, H. (2010). "The fabrication of a patterned ZnO nanorod array for high brightness LEDs". *Nanotechnology*, *21*(35), 355304. doi:10.1088/0957-4484/21/35/355304

Park, K., Cao, F., Kittelson, D. B., & McMurry, P. H. (2003). "Relationship between particle mass and mobility for diesel exhaust particles." *Environmental Science & Technology*, *37*(3), 577–83. doi:10.1021/es025960v

Park, K., Cho, G., & Kwak, J. (2009). "Development of an Aerosol Focusing-Laser Induced Breakdown Spectroscopy (Aerosol Focusing-LIBS) for Determination of Fine and Ultrafine Metal Aerosols". *Aerosol Science and Technology*, *43*(5), 375–386. doi:10.1080/02786820802662947

Park, S. S., & Wexler, A. S. (2007). "Particle deposition in the pulmonary region of the human lung: A semi-empirical model of single breath transport and deposition". *Journal of Aerosol Science*, *38*(2), 228–245. doi:10.1016/j.jaerosci.2006.11.009

Park, S. S., & Wexler, A. S. (2008). "Size-dependent deposition of particles in the human lung at steady-state breathing". *Journal of Aerosol Science*, *39*(3), 266–276. doi:10.1016/j.jaerosci.2007.11.006

Patashnick, H., & Hemenway, C. L. (1969). "Oscillating Fiber Microbalance". *Review of Scientific Instruments*, *40*(8), 1008. doi:10.1063/1.1684137

Patashnick, H. (1975). "Microbalance". US Patent 3,926,271. Retrieved from http://www.google.co.uk/patents/US3926271

Patashnick, H., & Rupprecht, G. (1983). *Personal Dust Exposure Monitor Based on the Tapered Element Oscillating Microbalance*. Bureau of Mines, U.S. Department of the Interior. Retrieved from http://books.google.co.uk/books?id=9psPGwAACAAJ

Patashnick, H., & Rupprecht, E. G. (1991). "Continuous PM-10 Measurements Using the Tapered Element Oscillating Microbalance". *Journal of the Air & Waste Management Association*, *41*(8), 1079–1083. doi:10.1080/10473289.1991.10466903

Paulo, P. M. R., Gaiduk, A., Kulzer, F., Krens, S. F. G., Spaink, H. P., Schmidt, T., & Orrit, M. (2009). "Photothermal Correlation Spectroscopy of Gold Nanoparticles in Solution". *The Journal of Physical Chemistry C*, *113*(27), 11451–11457. doi:10.1021/jp806875s

Person, S., Deutsch, B., Mitra, A., & Novotny, L. (2011). "Material-specific detection and classification of single nanoparticles." *Nano Letters*, *11*(1), 257–61. doi:10.1021/nl103656y

Peters, A., Wichmann, H. E., Tuch, T., Heinrich, J., & Heyder, J. (1997). "Respiratory effects are associated with the number of ultrafine particles." *American Journal of Respiratory and Critical Care Medicine*, *155*(4), 1376–83. doi:10.1164/ajrccm.155.4.9105082

Peters, T. M., & Leith, D. (2003). "Concentration measurement and counting efficiency of the aerodynamic particle sizer 3321". *Journal of Aerosol Science*, *34*(5), 627–634. doi:10.1016/S0021-8502(03)00030-2

Petzold, A., & Niessner, R. (1996). "Photoacoustic soot sensor for in-situ black carbon monitoring". *Applied Physics B*, *63*(2), 191–197. doi:10.1007/BF01095272

Petzold, A., & Schönlinner, M. (2004). "Multi-angle absorption photometry—a new method for the measurement of aerosol light absorption and atmospheric black carbon". *Journal of Aerosol Science*, *35*(4), 421–441. doi:10.1016/j.jaerosci.2003.09.005

Pfefferkorn, F. E., Bello, D., Haddad, G., Park, J.-Y., Powell, M., McCarthy, J., Bunker, K. L., Fehrenbacher, A., Jeon, Y., Virji, M. A., Gruetzmacher, G., Hoover, M. D. (2010). "Characterization of exposures to airborne nanoscale particles during friction stir welding of aluminum." *The Annals of Occupational Hygiene*, *54*(5), 486–503. doi:10.1093/annhyg/meq037

Plakhotnik, T. (2007). "Seeing small". *Journal of Luminescence*, *127*(1), 204–208. doi:10.1016/j.jlumin.2007.02.024

Politis, M., Pilinis, C., & Lekkas, T. D. (2008). "Ultrafine Particles (UFP) and Health Effects. Dangerous. Like No Other PM? Review and Analysis." *Global NEST Journal*, *10*(3), 439–452. Retrieved from https://gnest.org/Journal/Vol10_No3/439-452_579_POLITIS_10-3.pdf

Pope, C. A. III, & Dockery, D. W. (2006). "Health effects of fine particulate air pollution: lines that connect". *Journal of the Air & Waste Management Association*, *56*(6), 709–742. doi:10.1080/10473289.2006.10464485

Pöschl, U. (2005). "Atmospheric aerosols: composition, transformation, climate and health effects". *Angewandte Chemie (International Ed. in English)*, *44*(46), 7520–40. doi:10.1002/anie.200501122

Powers, K. W., Palazuelos, M., Moudgil, B. M., & Roberts, S. M. (2007). "Characterization of the size, shape, and state of dispersion of nanoparticles for toxicological studies". *Nanotoxicology*, *1*(1), 42–51. doi:10.1080/17435390701314902

Prather, K. A., Nordmeyer, T., & Salt, K. (1994). "Real-time characterization of individual aerosol particles using time-of-flight mass spectrometry". *Analytical Chemistry*, *66*(9), 1403–1407. doi:10.1021/ac00081a007

Pratt, K. A., Mayer, J. E., Holecek, J. C., Moffet, R. C., Sanchez, R. O., Rebotier, T. P., Furutani, H., Gonin, M., Fuhrer, K., Su, Y., Guazzotti, S., Prather, K. A. (2009). "Development and characterization of an aircraft aerosol time-of-flight mass spectrometer". *Analytical Chemistry*, *81*(5), 1792–1800. doi:10.1029/2003JD004198.(11)

Pratt, K., & Prather, K. (2012a). "Mass spectrometry of atmospheric aerosols—Recent developments and applications. Part I: Off-line mass spectrometry techniques". *Mass Spectrometry Reviews*, *31*(1), 1–16. doi:10.1002/mas.20322

Pratt, K. A., & Prather, K. A. (2012b). "Mass spectrometry of atmospheric aerosols—Recent developments and applications. Part II: On-line mass spectrometry techniques". *Mass Spectrometry Reviews*, *31*(1), 17–48. doi:10.1002/mas.20330

PROSPEcT (2009) - http://www.nanotechia.org/prospect-project-20090101/prospectproject20090101

Pruppacher, H., & Klett, J. (1978). *Microphysics of Clouds and Precipitation* (p. 714). Reidel, Boston.

Qi, C., Asbach, C., Shin, W. G., Fissan, H., & Pui, D. Y. H. (2009). "The Effect of Particle Pre-Existing Charge on Unipolar Charging and Its Implication on Electrical Aerosol Measurements". *Aerosol Science and Technology*, *43*(3), 232–240. doi:10.1080/02786820802587912

Qi, Q., Zhang, T., Liu, L., Zheng, X., Yu, Q., Zeng, Y., & Yang, H. (2008). "Selective acetone sensor based on dumbbell-like ZnO with rapid response and recovery". *Sensors and Actuators B: Chemical*, *134*(1), 166–170. doi:10.1016/j.snb.2008.04.024

Qian, L., Zhu, J., Du, W., & Qian, X. (2009). "Solvothermal synthesis, electrochemical and photocatalytic properties of monodispersed CeO2 nanocubes". *Materials Chemistry and Physics*, *115*(2-3), 835–840. doi:10.1016/j.matchemphys.2009.02.047

Quant, F. R., Flagan, R. C., & Horton, K. D. (1993). "Implementation of a Scanning Mobility Particle Sizer (SMPS)". *Journal of Aerosol Science*, *24* (Supplement 1), S83–S84. doi:10.1016/0021-8502(93)90134-U

Rader, D. J. (1990). "Momentum slip correction factor for small particles in nine common gases". *Journal of Aerosol Science*, *21*(2), 161–168. doi:10.1016/0021-8502(90)90001-E

Radziemski, L. J., Loree, T. R., Cremers, D. a., & Hoffman, N. M. (1983). "Time-resolved laser-induced breakdown spectrometry of aerosols". *Analytical Chemistry*, *55*(8), 1246–1252. doi:10.1021/ac00259a016

Ranjan, M., & Dhaniyala, S. (2007). "Theory and design of a new miniature electrical-mobility aerosol spectrometer". *Journal of Aerosol Science*, *38*(9), 950–963. doi:10.1016/j.jaerosci.2007.07.005

Ranjan, M., & Dhaniyala, S. (2008). "A new miniature electrical aerosol spectrometer (MEAS): Experimental characterization". *Journal of Aerosol Science*, *39*(8), 710–722. doi:10.1016/j.jaerosci.2008.04.005

Renwick, L. C., Donaldson, K., & Clouter, A. (2001). "Impairment of alveolar macrophage phagocytosis by ultrafine particles". *Toxicology and Applied Pharmacology*, *172*(2), 119–27. doi:10.1006/taap.2001.9128

Richard, A. (2011). *Determination of trace elements in ambient aerosols with synchrotron induced X-ray fluorescence spectrometry and subsequent source apportionment*. ETH Zürich. Retrieved from http://e-collection.library.ethz.ch/view/eth:2907

Ristimäki, J., Virtanen, A., Marjamäki, M., Rostedt, A., & Keskinen, J. (2002). "On-line measurement of size distribution and effective density of submicron aerosol particles". *Journal of Aerosol Science*, *33*(11), 1541–1557. doi:10.1016/S0021-8502(02)00106-4

Ristovski, Z. D., Morawska, L., Hitchins, J., & Barron, W. (1998). "Influence of the sheath air humidity on the SMPS measurements of hygroscopic aerosols". *Journal of Aerosol Science*, *29*, S327–S328. doi:10.1016/S0021-8502(98)00488-1

Robinson, C. B., Kimmel, J. R., David, D. E., Jayne, J. T., Trimborn, A., Worsnop, D. R., & Jimenez, J. L. (2011). "Thermal desorption metastable atom bombardment ionization aerosol mass spectrometer". *International Journal of Mass Spectrometry*, *303*(2-3), 164–172. doi:10.1016/j.ijms.2011.01.027

Rodríguez, S., Alastuey, A., & Querol, X. (2012). "A review of methods for long term in situ characterization of aerosol dust". *Aeolian Research*, *6* (October), 55–74. doi:10.1016/j.aeolia.2012.07.004

Rogak, S. N., Baltensperger, U., & Flagan, R. C. (1991). "Measurement of Mass Transfer to Agglomerate Aerosols". *Aerosol Science and Technology*, *14*(4), 447–458. doi:10.1080/02786829108959505

Rosen, H., & Novakov, T. (1977). "Raman scattering and the characterisation of atmospheric aerosol particles". *Nature*, *266* (21 April), 708–710. doi:10.1038/266708a0

Ruppecht, E., Meyer, M., & Patashnick, H. (1992). "The tapered element oscillating microbalance as a tool for measuring ambient particulate concentrations in real time". *Journal of Aerosol Science*, *23* (Suppl. 1), S635–S638. doi:10.1016/0021-8502(92)90492-E

Rusak, D. A., Castle, B. C., Smith, B. W., & Winefordner, J. D. (1997). "Fundamentals and Applications of Laser-Induced Breakdown Spectroscopy". *Critical Reviews in Analytical Chemistry*, *27*(4), 257–290. doi:10.1080/10408349708050587

Ryu, H.-W., Park, B.-S., Akbar, S. A., Lee, W.-S., Hong, K.-J., Seo, Y.-J., Shin, D.-C., Park, J.-S., Choi, G.-P. (2003). "ZnO sol–gel derived porous film for CO gas sensing". *Sensors and Actuators B: Chemical*, *96*(3), 717–722. doi:10.1016/j.snb.2003.07.010

Ryu, J., & Ro, C. (2009). "Attenuated total reflectance FT-IR imaging and quantitative energy dispersive-electron probe X-ray microanalysis techniques for single particle analysis of atmospheric aerosol particles". *Analytical Chemistry*, *81*(16), 6695–6707. doi:10.1021/ac9007545

Sager, T. M., Kommineni, C., & Castranova, V. (2008). "Pulmonary response to intratracheal instillation of ultrafine versus fine titanium dioxide: role of particle surface area." *Particle and Fibre Toxicology*, *5*, 17. doi:10.1186/1743-8977-5-17

Sager, T. M., & Castranova, V. (2009). "Surface area of particle administered versus mass in determining the pulmonary toxicity of ultrafine and fine carbon black: comparison to ultrafine titanium dioxide." *Particle and Fibre Toxicology*, *6*, 15. doi:10.1186/1743-8977-6-15

Sakata, K., Sakaguchi, A., Tanimizu, M., Takaku, Y., Yokoyama, Y., & Takahashi, Y. (2014). "Identification of sources of lead in the atmosphere by chemical speciation using X-ray absorption near-edge structure (XANES) spectroscopy". *Journal of Environmental Sciences*, *26*(2), 343–352. doi:10.1016/S1001-0742(13)60430-1

Salma, I., Pósfai, M., Kovács, K., Kuzman, E., Homonnay, Z., & Posta, J. (2009). "Chemical species of transition metals in the aerosol particles of a metropolitan underground railway station". In *European Aerosol Conference 2009*, Abstract T051A06.

Salt, K., Noble, C. A, & Prather, K. A. (1996). "Aerodynamic Particle Sizing versus Light Scattering Intensity Measurement as Methods for Real-Time Particle Sizing Coupled with Time-of-Flight Mass Spectrometry." *Analytical Chemistry*, *68*(1), 230–4. doi:10.1021/ac950396a

Sánchez, E. J., Novotny, L., & Xie, X. S. (1999). "Near-field fluorescence microscopy based on two-photon excitation with metal tips". *Physical Review Letters*, *82*(20), 4014–4017. doi:10.1103/PhysRevLett.82.4014

Sanchez-Valencia, J. R., Alcaire, M., Romero-Gómez, P., Macias-Montero, M., Aparicio, F. J., Borras, A., Gonzalez-Elipe, A. R., Barranco, A. (2014). "Oxygen Optical Sensing in Gas and Liquids with Nanostructured ZnO Thin Films Based on Exciton Emission Detection". *The Journal of Physical Chemistry C*, *118*(18), 9852–9859. doi:10.1021/jp5026027

Sanderson, P., Delgado-Saborit, J. M., & Harrison, R. M. (2014). "A review of chemical and physical characterisation of atmospheric metallic nanoparticles". *Atmospheric Environment*, *94*, 353–365. doi:10.1016/j.atmosenv.2014.05.023

Sandoghdar, V., Klotzsch, E., Jacobsen, V., Renn, A., Håkanson, U., Agio, M., Gerhardt, I., Seelig, J., Wrigge, G. (2006). "Optical Detection of Very Small Nonfluorescent Nanoparticles". *CHIMIA International Journal for Chemistry*, *60*(11), 761–764. doi:10.2533/chimia.2006.761

Santos, J. P., Hontañón, E., Ramiro, E., & Alonso, M. (2009). "Performance evaluation of a high-resolution parallel-plate differential mobility analyzer". *Atmospheric Chemistry and Physics*, *9*(7), 2419–2429. doi:10.5194/acp-9-2419-2009

Sayes, C. M., Reed, K. L., & Warheit, D. B. (2007). "Assessing toxicity of fine and nanoparticles: comparing in vitro measurements to in vivo pulmonary toxicity profiles." *Toxicological Sciences : An Official Journal of the Society of Toxicology*, *97*(1), 163–80. doi:10.1093/toxsci/kfm018

SCCS (Scientific Committee on Consumer Safety). (2012). "Opinion on ZnO (nano form), 18". *European Commission*, (18 September). Retrieved from http://ec.europa.eu/health/scientific_committees/consumer_safety/docs/sccs_o_103.pdf

Schadt, C. F., & Cadle, R. D. (1957). "Thermal forces on aerosol particles in a thermal precipitator". *Journal of Colloid Science*, *362*(4), 356–362. doi:10.1016/0095-8522(57)90035-1

Schmid, O., Trueblood, M. B., Gregg, N., Hagen, D. E., & Whitefield, P. D. (2002). "Sizing of Aerosol in Gases Other Than Air Using a Differential Mobility Analyzer". *Aerosol Science and Technology*, *36*(3), 351–360. doi:10.1080/027868202753504452

Schmidt-Ott, A., & Federer, B. (1981). "Photoelectron emission from small particles suspended in a gas". *Surface Science*, *106*(1-3), 538–543. doi:10.1016/0039-6028(81)90248-X

Schwab, J. J., Felton, H. D., Rattigan, O. V, & Demerjian, K. L. (2006). "New York State urban and rural measurements of continuous PM2.5 mass by FDMS, TEOM, and BAM." *Journal of the Air & Waste Management Association*, *56*(4), 372–83. doi:10.1080/027868202753504452

Schwarzmeier, K., Knauer, M., Ivleva, N. P., Niessner, R., & Haisch, C. (2013). "Bioaerosol analysis based on a label-free microarray readout method using surface-enhanced Raman scattering". *Analytical and Bioanalytical Chemistry*, *405*(16), 5387–92. doi:10.1007/s00216-013-6984-0

Schweiger, G. (1990). "Raman scattering on single aerosol particles and on flowing aerosols: a review". *Journal of Aerosol Science*, *21*(4), 483–509. doi:10.1016/0021-8502(90)90126-I

Secker, D., Hirst, E., & Kaye, P. (2000). "Measurements of deformed droplets and droplets with inclusions in an aerodynamic particle sizer". *Journal of Aerosol Science*, *31* (Supplement 1), S971–S972. doi:10.1016/S0021-8502(00)90981-9

Selmke, M., Braun, M., & Cichos, F. (2012a). "Gaussian beam photothermal single particle microscopy." *Journal of the Optical Society of America. A, Optics, Image Science, and Vision*, *29*(10), 2237–41. doi:10.1364/JOSAA.29.002237

Selmke, M., Braun, M., & Cichos, F. (2012b). "Photothermal single-particle microscopy: detection of a nanolens." *ACS Nano*, *6*(3), 2741–9. doi:10.1021/nn300181h

Selmke, M., Schachoff, R., Braun, M., & Cichos, F. (2013). "Twin-focus photothermal correlation spectroscopy". *RSC Advances*, *3*(2), 394. doi:10.1039/c2ra22061j

Sem, G. (2002). "Design and performance characteristics of three continuous-flow condensation particle counters: a summary". *Atmospheric Research*, *62*(3-4), 267–294. doi:10.1016/S0169-8095(02)00014-5

Senthil, T. S., Kim, A.-Y., Muthukumarasamy, N., & Kang, M. (2013). "Improved performance of dye sensitized ZnO nanorod solar cells prepared using TiO2 seed layer". *Journal of Sol-Gel Science and Technology*, *67*(2), 420–427. doi:10.1007/s10971-013-3083-9

Shah, S., & Cocker, D. (2005). "A Fast Scanning Mobility Particle Spectrometer for Monitoring Transient Particle Size Distributions". *Aerosol Science and Technology*, *39*(6), 519–526. doi:10.1080/027868291004652

Shao, L., Jiang, X., Yu, X., Li, B., Clements, W. R., Vollmer, F., Wang, W., Xiao, Y.-F., Gong, Q. (2013). "Detection of single nanoparticles and lentiviruses using microcavity resonance broadening". *Advanced Materials*, *25*(39), 5616–5620. doi:10.1002/adma201302572

Shen, J., Yu, B., Xu, Y., Liu, L., Riebel, U., & Guo, X. (2008). "Fundamentals of particle size analysis by fluctuating transmission autocorrelation with an extremely narrow beam". *Measurement*, *41*(1), 55–64. doi:10.1016/j.measurement.2006.11.021

Shen, S., Jaques, P. A., Zhu, Y., Geller, M. D., & Sioutas, C. (2002). "Evaluation of the SMPS–APS system as a continuous monitor for measuring PM2.5, PM10 and coarse (PM2.5-10) concentrations". *Atmospheric Environment*, *36*(24), 3939–3950. doi:10.1016/S1352-2310(02)00330-8

Shen, Y., Chen, D.-R., & Shen, J.-T. (2012). "Statistical theory of nanoparticle sensing using a whispering-gallery-mode resonator". *Physical Review A*, *85*(6), 063808. doi:10.1103/PhysRevA.85.063808

Shi, J. P., Harrison, R. M., & Evans, D. (2001). "Comparison of ambient particle surface area measurement by epiphaniometer and SMPS/APS". *Atmospheric Environment*, *35*(35), 6193–6200. doi:10.1016/S1352-2310(01)00382-X

Shim, J., Seok Kang, H., Park, W.-S., Han, S.-H., Kim, J., & Chang, I.-S. (2004). "Transdermal delivery of mixnoxidil with block copolymer nanoparticles." *Journal of Controlled Release : Official Journal of the Controlled Release Society*, *97*(3), 477–84. doi:10.1016/j.jconrel.2004.03.028

Shin, W. G., Pui, D. Y. H., Fissan, H., Neumann, S., & Trampe, A. (2006). "Calibration and numerical simulation of Nanoparticle Surface Area Monitor (TSI Model 3550 NSAM)". *Journal of Nanoparticle Research*, *9*(1), 61–69. doi:10.1007/s11051-006-9153-y

Simeonova, P. P., & Erdely, A. (2009). "Engineered nanoparticle respiratory exposure and potential risks for cardiovascular toxicity: predictive tests and biomarkers". *Inhalation Toxicology*, *21*(Supplement 1), 68–73. doi:10.1080/08958370902942566

Sinclair, D., & Hoopes, G. S. (1975a). "A Novel Form of Diffusion Battery". *American Industrial Hygiene Association Journal*, *36*(1), 39–42. doi:10.1080/0002889758507205

Sinclair, D., & Hoopes, G. (1975b). "A continuous flow condensation nucleus counter". *Journal of Aerosol Science*, *6*(1), 1–7. doi:10.1016/0021-8502(75)90036-1

Singh, S., Shi, T., Duffin, R., Albrecht, C., van Berlo, D., Höhr, D., Fubini, B., Martra, G., Fenoglio, I., Borm, P. J. A., Schins, R. P. F. (2007). "Endocytosis, oxidative stress and IL-8 expression in human lung epithelial cells upon treatment with fine and ultrafine TiO2: role of the specific surface area and of surface methylation of the particles." *Toxicology and Applied Pharmacology*, *222*(2), 141–51. doi:10.1016/j.taap.2007.05.001

Sioutas, C., Abt, E., Wolfson, J. M., & Koutrakis, P. (1999). "Evaluation of the Measurement Performance of the Scanning Mobility Particle Sizer and Aerodynamic Particle Sizer". *Aerosol Science and Technology*, *30*(1), 84–92. doi:10.1080/027868299304903

Smijs, T. G., & Pavel, S. (2011). "Titanium dioxide and zinc oxide nanoparticles in sunscreens: focus on their safety and effectiveness". *Nanotechnology, Science and Applications*, *4*, 95–112. doi:10.2147/NSA.S19419

Smirnov, V. V. (2006). "Nature and Evolution of Ultrafine Aerosol Particles in the Atmosphere". *Izvestiya, Atmospheric and Oceanic Physics*, *42*(6), 663–687. doi:10.1134/S0001433806060016

Smith, B. W., Womack, J. B., Omenetto, N., & Winefordner, J. D. (1989). "Approaching single atom detection with atomic fluorescence in a glow discharge atom reservoir". *Applied Spectroscopy*, *43*(5), 873–876. Retrieved from http://www.opticsinfobase.org/abstract.cfm?uri=as-43-5-873

Smith, S., Ward, M., Lin, R., Brydson, R., Dall'Osto, M., & Harrison, R. M. (2012). "Comparative study of single particle characterisation by Transmission Electron Microscopy and time-of-flight aerosol mass spectrometry in the London atmosphere". *Atmospheric Environment*, *62*, 400–407. doi:10.1016/j.atmosenv.2012.08.028

Sobanska, S., Falgayrac, G., Laureyns, J., & Brémard, C. (2006). "Chemistry at level of individual aerosol particle using multivariate curve resolution of confocal Raman image". *Spectrochimica Acta. Part A, Molecular and Biomolecular Spectroscopy*, *64*(5), 1102–9. doi:10.1016/j.saa.2005.11.038

Sobanska, S., Hwang, H., Choël, M., Jung, H.-J., Eom, H.-J., Kim, H., Barbillat, J., Ro, C.-U. (2012). "Investigation of the chemical mixing state of individual Asian dust particles by the combined use of electron probe X-ray microanalysis and Raman microspectrometry". *Analytical Chemistry*, *84*(7), 3145–54. doi:10.1021/ac2029584

Sobanska, S., Falgayrac, G., Rimetz-Planchon, J., Perdrix, E., Brémard, C., & Barbillat, J. (2014). "Resolving the internal structure of individual atmospheric aerosol particle by the combination of Atomic Force Microscopy, ESEM–EDX, Raman and ToF–SIMS imaging". *Microchemical Journal*, *114*(May), 89–98. doi:10.1016/j.microc.2013.12.007

Solomon, P. A., & Sioutas, C. (2008). "Continuous and Semicontinuous Monitoring Techniques for Particulate Matter Mass and Chemical Components: A Synthesis of Findings from EPA's Particulate Matter Supersites Program and Related Studies". *Journal of the Air & Waste Management Association*, *58*(2), 164–195. doi:10.3155/1047-3289.58.2.164

Song, Y., Ryu, J., Malek, M. A., Jung, H., Ro, C., & Malek, A. (2010). "Chemical Speciation of Individual Airborne Particles by the Combined Use of Quantitative Energy-Dispersive Electron Probe X-ray Microanalysis and Attenuated Total Reflection Fourier Transform-Infrared Imaging Techniques †". *Analytical Chemistry*, *82*(19), 7987–7998. doi:10.1021/ac1014113

Song, Y., Eom, H.-J., Jung, H.-J., Malek, M. A., Kim, H. K., Geng, H., & Ro, C.-U. (2013). "Investigation of aged Asian dust particles by the combined use of quantitative ED-EPMA and ATR-FTIR imaging". *Atmospheric Chemistry and Physics*, *13*(6), 3463–3480. doi:10.5194/acp-13-3463-2013

Spangler, G. (2000). "Fundamental considerations for the application of miniature ion mobility spectrometry to field analytical applications". *Field Analytical Chemistry & Technology*, *4*(5), 255–267. doi:10.1002/1520-6521(2000)4:5<255::AID-FACT5>3.0.CO;2-R

Spanier, J., Robinson, R., Zhang, F., Chan, S.-W., & Herman, I. (2001). "Size-dependent properties of CeO2-y nanoparticles as studied by Raman scattering". *Physical Review B*, *64*(24), 1–8. doi:10.1103/PhysRevB.64.245407

Spurny, K. R. (2000). "Atmospheric Condensation Nuclei PJ Coulier 1875 and J. Aitken 1880 (Historical Review)". *Aerosol Science & Technology*, *32*(3), 243–248. doi:10.1080/027868200303777

Srivastava, V., Gusain, D., & Sharma, Y. C. (2013). "Synthesis, characterization and application of zinc oxide nanoparticles (n-ZnO)". *Ceramics International*, *39*(8), 9803–9808. doi:10.1016/j.ceramint.2013.04.110

Stanmore, B. R., Brilhac, J. F., & Gilot, P. (2001). "The oxidation of soot: a review of experiments, mechanisms and models". *Carbon*, *39*(15), 2247–2268. doi:10.1016/S0008-6223(01)00109-9

Stchur, P., Yang, K. X., Hou, X., Sun, T., & Michel, R. G. (2001). "Laser excited atomic fluorescence spectrometry—a review". *Spectrochimica Acta Part B: Atomic Spectroscopy*, *56*(9), 1565–1592. doi:10.1016/S0584-8547(01)00265-8

Steer, B., Gorbunov, B. Z., Rowles, J., & Green, D. (2012). Surface area controlled heterogeneous nucleation. The Journal of Chemical Physics, 136(5), 054704. doi:10.1063/1.3681400

Steer, B., Gorbunov, B., Muir, R., Ghimire, A., & Rowles, J. (2014). "Portable Planar DMA: Development and Tests". Aerosol Science and Technology, 48(3), 251–260. doi:10.1080/02786826.2013.868863

Stefaniak, E. A., Worobiec, A., Potgieter-Vermaak, S., Alsecz, A., Török, S., & Van Grieken, R. (2006). "Molecular and elemental characterisation of mineral particles by means of parallel micro-Raman spectrometry and Scanning Electron Microscopy/Energy Dispersive X-ray Analysis". *Spectrochimica Acta Part B: Atomic Spectroscopy*, *61*(7), 824–830. doi:10.1016/j.sab.2006.04.009

Stein, S. W., Gabrio, B. J., Oberreit, D., Hairston, P., Myrdal, P. B., & Beck, T. J. (2002). "An Evaluation of Mass-Weighted Size Distribution Measurements with the Model 3320 Aerodynamic Particle Sizer". *Aerosol Science and Technology*, *36*(7), 845–854. doi:10.1080/02786820290092087

Stevens, D. C. (1971). "An assessment of the oscillating fibre microbalance of Patashnick and Hemenway". *Journal of Aerosol Science*, *2*(3), 315–324. doi:10.1016/0021-8502(71)90056-5

Stoeger, T., Reinhard, C., Takenaka, S., Schroeppel, A., Karg, E., Ritter, B., Heyder, J., Schulz, H. (2005). "Instillation of Six Different Ultrafine Carbon Particles Indicates a Surface Area Threshold Dose for Acute Lung Inflammation in Mice". *Environmental Health Perspectives*, *114*(3), 328–333. doi:10.1289/ehp.8266

Stolzenburg, M. R., & McMurry, P. H. (1991). "An Ultrafine Aerosol Condensation Nucleus Counter". *Aerosol Science and Technology*, *14*(1), 48–65. doi:10.1080/02786829108959470

Sturges, W., & Harrison, R. (1989). "Semi-quantitative X-ray diffraction analysis of size fractionated atmospheric particles". *Atmospheric Environment*, *23*(5), 1083–1098. doi:10.1016/0004-6981(89)90309-0

Su, Y., Sipin, M., Furutani, H., & Prather, K. (2004). "Development and characterization of an aerosol time-of-flight mass spectrometer with increased detection efficiency". *Analytical Chemistry*, *23*(3), 712–719. doi:10.1029/2001JD001211.(12)

Suehiro, J., Nakagawa, N., Hidaka, S.-I., Ueda, M., Imasaka, K., Higashihata, M., Okada, T., Hara, M. (2006). "Dielectrophoretic fabrication and characterization of a ZnO nanowire-based UV photosensor". *Nanotechnology*, *17*(10), 2567–73. doi:10.1088/0957-4484/17/10/021

Suess, D. T., & Prather, K. A. (1999). "Mass spectrometry of aerosols." *Chemical Reviews*, *99*(10), 3007–36. doi:10.1021/cr980138o

Suh, D.-I., Lee, S.-Y., Kim, T.-H., Chun, J.-M., Suh, E.-K., Yang, O.-B., & Lee, S.-K. (2007). "The fabrication and characterization of dye-sensitized solar cells with a branched structure of ZnO nanowires". *Chemical Physics Letters*, *442*(4-6), 348–353. doi:10.1016/j.cplett.2007.05.093

Suh, D.-I., Lee, S.-Y., Hyung, J.-H., Kim, T.-H., & Lee, S.-K. (2008). "Multiple ZnO Nanowires Field-Effect Transistors". *Journal of Physical Chemistry C*, *112*(4), 1276–1281. doi:10.1021/jp709673s

Sun, T., Liu, Z., Zhu, G., Liu, H., Xu, Q., Li, Y., Wang, G., Sun, H., Luo, P., Pan, Q., Ding, X. (2009). "Identification of origin of single aerosol particles using polycapillary X-ray lens". *Nuclear Instruments and Methods in Physics Research Section B: Beam Interactions with Materials and Atoms*, *267*(1), 171–174. doi:10.1016/j.nimb.2008.11.032

Sun, X., Huang, J., Wang, J., & Xu, Z. (2008). "A ZnO Nanorod Inorganic/Organic Heterostructure Light-Emitting Diode Emitting at 342 nm". *Nano Letters*, *8*(4), 1219–1223. doi:10.1021/nl080340z

Sverdrup, G., & Whitby, K. (1977). "Determination of submicron atmospheric aerosol size distributions by use of continuous analog sensors". *Environmental Science & Technology*, *11*(13), 1171–1176. doi:10.1021/es60136a007

Symonds, J. P. R., Reavell, K. S. J., Olfert, J. S., Campbell, B. W., & Swift, S. J. (2007). "Diesel soot mass calculation in real-time with a differential mobility spectrometer". *Journal of Aerosol Science*, *38*(1), 52–68. doi:10.1016/j.jaerosci.2006.10.001

Szilágyi, V., & Hartyáni, Z. (2005). "Development of an X-ray fluorescence spectrometric method for the analysis of atmospheric aerosol samples". *Microchemical Journal*, *79*(1-2), 37–41. doi:10.1016/j.microc.2004.09.002

Szymanski, W. W., & Liu, B. Y. H. (1986). "On the sizing accuracy of laser optical particle counters". *Particle & Particle Systems Characterization*, *3*(1), 1–7. doi:10.1002/ppsc.19860030102

Szymanski, W. W., & Allmaier, G. (2009). Measurement and Characterization of Aerosol Nanoparticles. *Nanoparticles in medicine and environment* (pp. 91–112). Dordrecht: Springer Netherlands. doi:10.1007/978-90-481-2632-3

Takahashi, Y., Kanai, Y., Kamioka, H., Ohta, A., Maruyama, H., Song, Z., & Shimizu, H. (2006). "Speciation of sulfate in size-fractionated aerosol particles using sulfur K-edge X-ray absorption near-edge structure." *Environmental Science & Technology*, *40*(16), 5052–7. doi:10.1021/es060497y

Talbot, J. H. (1966). "A diffraction size-frequency analyser with automatic recording of size-frequency distributions and total and respirable surface areas". *Journal of Scientific Instruments*, *43*, 744–749. doi:10.1088/0950-7671/43/10/318

Talbot, J. H. (1967). "Automated dust measurement: The diffraction size-frequency analyser". *Journal of Mine Ventilation Society of South Africa*, 20:21-30.

Tammet, H., Mirme, A., & Tamm, E. (2002). "Electrical aerosol spectrometer of Tartu University". *Atmospheric Research*, *62*(3-4), 315–324. doi:10.1016/S0169-8095(02)00017-0

Tammet, H. (2011). "Symmetric Inclined Grid Mobility Analyzer for the Measurement of Charged Clusters and Fine Nanoparticles in Atmospheric Air". *Aerosol Science and Technology*, *45*(4), 468–479. doi:10.1080/02786826.2010.546818

Tani, B., Siegel, S., Johnson, S., & Kumar, R. (1983). "X-ray diffraction investigation of atmospheric aerosols in the 0.3–1.0 μm aerodynamic size range". *Atmospheric Environment*, *17*(11), 2277–2283. doi:10.1016/0004-6981(83)90226-3

Tanninen, V.-P., Hyvärinen, H.-K., Grekula, A., & Kalliomäki, P.-L. (1985). "Experimental improvements in analysis of aerosol samples by x-ray powder diffraction". *Journal of Aerosol Science*, *16*(5), 373–378. doi:10.1016/0021-8502(85)90048-5

Terhune, R. W., & Anderson, J. E. (1977). "Spectrophone measurements of the absorption of visible light by aerosols in the atmosphere." *Optics Letters*, *1*(2), 70–2. doi:10.1364/OL.1.000070

Theodore, L., & Kunz, R. (2005). *Nanotechnology: Environmental Implications and Solutions* (pp. 25–98). Wiley, New Jersey. ISBN: 978-0-471-69976-7

Thölén, A. R. (1995). "Electron microscopy of small particles". *Journal of Aerosol Science*, *26* (Supplement 1), S901–S902. doi:10.1016/0021-8502(95)97358-L

Thompson, A., Jaklevic, J., O'Connor, B., & Morris, C. (1982). "X-ray powder diffraction system for chemical speciation of particulate aerosol samples". *Nuclear Instruments and Methods*, *198*(2-3), 539–546. doi:10.1016/0167-5087(82)90297-6

Tinke, A. P., Carnicer, A., Govoreanu, R., Scheltjens, G., Lauwerysen, L., Mertens, N., Vanhoutte, K., Brewster, M. E. (2008). "Particle shape and orientation in laser diffraction and static image analysis size distribution analysis of micrometer sized rectangular particles". *Powder Technology*, *186*(2), 154–167. doi:10.1016/j.powtec.2007.11.017

Tokonami, S., & Knutson, E. O. (2000). "The Scan Time Effect on the Particle Size Distribution Measurement in the Scanning Mobility Particle Sizer System". *Aerosol Science and Technology*, *32*(3), 249–252. doi:10.1080/027868200303786

Tomić, S., Valković, V., Budnar, M., Starc, V., & Smit, Ž. (1987). "Comparison of XRF and PIXE on Aerosol Samples". *Nuclear Instruments and Methods in Physics Research B*, *24-25*(2), 609–612. doi:10.1016/S0168-583X(87)80207-0

Toyoda, M., Kaibuchi, K., Nagasono, M., Terada, Y., Tanabe, T., Hayakawa, S., & Kawai, J. (2004). "X-ray analysis of a single aerosol particle with combination of scanning electron

microscope and synchrotron radiation X-ray microscope". *Spectrochimica Acta Part B: Atomic Spectroscopy*, *59*(8), 1311–1315. doi:10.1016/j.sab.2004.05.023

Trimborn, A., Hinz, K.-P., & Spengler, B. (2000). "Online Analysis of Atmospheric Particles with a Transportable Laser Mass Spectrometer". *Aerosol Science and Technology*, *33*(1-2), 191–201. doi:10.1080/027868200410921

Tripathi, A., Jabbour, R. E., Guicheteau, J. A., Christesen, S. D., Emge, D. K., Fountain, A. W., Bottiger, J. R., Emmons, E. D., Snyder, A. P. (2009). "Bioaerosol analysis with Raman chemical imaging microspectroscopy". *Analytical Chemistry*, *81*(16), 6981–90. doi:10.1021/ac901074c

Trovarelli, A., de Leitenburg, C., Boaro, M., & Dolcetti, G. (1999). "The utilization of ceria in industrial catalysis". *Catalysis Today*, *50*(2), 353–367. doi:10.1016/S0920-5861(98)00515-X

Tsai, C.-J., Chen, S.-C., Huang, C.-H., & Chen, D.-R. (2004). "A Universal Calibration Curve for the TSI Aerodynamic Particle Sizer". *Aerosol Science and Technology*, *38*(5), 467–474. doi:10.1080/02786820490460725

TSI: http://www.tsi.com/uploadedFiles/_Site_Root/Products/Literature/Spec_Sheets/SMPS3936-3034.pdf (Visited November 2012)

Tsukazaki, A., Ohtomo, A., Onuma, T., Ohtani, M., Makino, T., Sumiya, M., Ohtani, K., Chichibu, S. F., Fuke, S., Segawa, Y., Ohno, H., Koinuma, H., Kawasaki, M. (2004). "Repeated temperature modulation epitaxy for p-type doping and light-emitting diode based on ZnO". *Nature Materials*, *4*(1), 42–46. doi:10.1038/nmat1284

Tunved, P., Hansson, H.-C., Kerminen, V.-M., Ström, J., Maso, M. D., Lihavainen, H., Viisanen, Y., Aalto, P. P., Komppula, M., Kulmala, M. (2006). "High natural aerosol loading over boreal forests." *Science*, *312*(5771), 261–3. doi:10.1126/science.1123052

van Dijk, M. A., Lippitz, M., & Orrit, M. (2005). "Far-field optical microscopy of single metal nanoparticles." *Accounts of Chemical Research*, *38*(7), 594–601. doi:10.1021/ar0401303

van Dijk, M. A., Tchebotareva, A. L., Orrit, M., Lippitz, M., Berciaud, S., Lasne, D., Cognet, L., Lounis, B. (2006). "Absorption and scattering microscopy of single metal nanoparticles." *Physical Chemistry Chemical Physics : PCCP*, *8*(30), 3486–95. doi:10.1039/b606090k

van Hoecke, K., Quik, J. T. K., Mankiewicz-Boczek, J., De Schamphelaere, K. A. C., Elsaesser, A., Van der Meeren, P., Barnes, C., McKerr, G., Howard, C. V., Van de Meent, D., Rydzyński, K., Dawson, K. A., Salvati, A., Lesniak, A., Lynch, I., Silversmit, G., De Samber, B., Vincze, L., Janssen, C. R. (2009). "Fate and effects of CeO2 nanoparticles in aquatic ecotoxicity tests." *Environmental Science & Technology*, *43*(12), 4537–46. doi:10.1021/es9002444

van Niekerk, W. C. A., & Fourie, M. H. (2004). "Ultrafine Particles: Aggravating Exposure Factor?". In *Tenth International Ferroalloys Congress; INFACON X: 'Transformation through Technology* (pp. 787–795). Retrieved from http://www.pyrometallurgy.co.za/InfaconX/097.pdf

van Veldhuizen, EM, and WR Rutgers. (2001). “Corona Discharges: Fundamentals and Diagnostics.” *Invited Paper, Proc. Frontiers in Low Temp. Plasma Diagn. IV, Rolduc, Netherlands*: 40–49. http://www.phys.tue.nl/FLTPD/invited/veldhuizen.pdf

Vandebriel, R. J., & De Jong, W. H. (2012). "A review of mammalian toxicity of ZnO nanoparticles". *Nanotechnology, Science and Applications*, *5*, 61–71. doi:10.2147/NSA.S23932

Vehring, R. (1998). "Linear Raman spectroscopy on aqueous aerosols: influence of nonlinear effects on detection limits". *Journal of Aerosol Science*, *29*(1-2), 65–79. doi:10.1016/S0021-8502(97)00292-9

Vehring, R., Aardahl, C. L., Schweiger, G., & Davis, E. J. (1998). "The characterization of fine particles originating from an uncharged aerosol: Size dependence and detection limits for Raman analysis". *Journal of Aerosol Science*, *29*(9), 1045–1061. doi:10.1016/S0021-8502(98)80002-5

Venables, J. A. (2000). *Introduction to surface and thin film processes* (pp. 25–97). Cambridge University Press, Cambridge, England. doi:10.1017/CBO9780511755651

Vincent, J. (1998). "International occupational exposure standards: a review and commentary". *American Industrial Hygiene Association*, *59* (May 2014), 37–41. doi:10.1080/15428119891010910

Volmer, M., & Weber, A. (1926). "Keimbildung in übersättigten Gebilden". *Zeitschrift Für Physikalische Chemie*, *119*, 277–301. http://www.degruyter.com/view/j/zpch

Volmer, M. (1939). *Kinetik der Phasenbildung*. Theodor Steinkopff, Dresden.

Waggoner, A., & Weiss, R. (1980). "Comparison of fine particle mass concentration and light scattering extinction in ambient aerosol". *Atmospheric Environment*, *14*(5), 623–626. doi:10.1016/0004-6981(80)90098-0

Wake, D., Thorpe, A., Bostock, G. J., Davies, J. K. W., & Brown, R. C. (1991). "Apparatus for measurement of the electrical mobility of aerosol particles: computer control and data analysis". *Journal of Aerosol Science*, *22*(7), 901–916. doi:10.1016/0021-8502(91)90083-T

Waldram, J. M. (1945). "Measurement of the photometric properties of the upper atmosphere". *Quarterly Journal of the Royal Meteorological Society*, *71*(309-310), 319–336. doi:10.1002/qj.49707130910

Walton, W. H., & Vincent, J. H. (1998). "Aerosol Instrumentation in Occupational Hygiene: An Historical Perspective". *Aerosol Science and Technology*, *28*(5), 417–438. doi:10.1080/02786829808965535

Wan, Q., Li, Q. H., Chen, Y. J., Wang, T. H., He, X. L., Li, J. P., & Lin, C. L. (2004). "Fabrication and ethanol sensing characteristics of ZnO nanowire gas sensors". *Applied Physics Letters*, *84*(18), 3654. doi:10.1063/1.1738932

Wang, D., Seo, H. W., Tin, C.-C., Bozack, M. J., Williams, J. R., Park, M., & Tzeng, Y. (2006). "Lasing in whispering gallery mode in ZnO nanonails". *Journal of Applied Physics*, *99*(9), 093112. doi:10.1063/1.2196148

Wang, H.-C., & John, W. (1987). "Particle Density Correction for the Aerodynamic Particle Sizer". *Aerosol Science and Technology*, *6*(2), 191–198. doi:10.1080/02786828708959132

Wang, H.-C., & John, W. (1989). "A Simple Iteration Procedure to Correct for the Density Effect in the Aerodynamic Particle Sizer". *Aerosol Science and Technology*, *10*(3), 501–505. doi:10.1080/02786828908959290

Wang, J., Guo, P., Li, X., Zhu, J., Reinert, T., Heitmann, J., Spemann, D., Vogt, J., Flagmeyer, R.-H., Butz, T. (2000). "Identification of air pollution sources by single aerosol particle fingerprints–micro-PIXE spectra". *Nuclear Instruments and Methods in Physics Research B*, *161-163* (March), 830–835. doi:10.1016/S0168-583X(99)00979-9

Wang, J. (2009). "A fast integrated mobility spectrometer with wide dynamic size range: Theoretical analysis and numerical simulation". *Journal of Aerosol Science*, *40*(10), 890–906. doi:10.1016/j.jaerosci.2009.06.005

Wang, J. C. F., Patashnick, H., & Rupprecht, G. (1980). "A New Real-Time Isokinetic Dust Mass Monitoring System". *Journal of the Air Pollution Control Association*, *30*(9), 1018–1021. doi:10.1080/00022470.1980.10465140

Wang, S. (2001). "Study of the Raman spectrum of CeO_2 nanometer thin films". *Materials Chemistry and Physics*, *68*(1-3), 246–248. doi:10.1016/S0254-0584(00)00357-6

Wang, S. C., & Flagan, R. C. (1990). "Scanning electrical mobility spectrometer". *Aerosol Science and Technology*, *13*(2), 230–240. doi:10.1080/02786829008959441

Wang, X., Song, J., Liu, J., & Wang, Z. L. (2007). "Direct-current nanogenerator driven by ultrasonic waves." *Science*, *316*(5821), 102–5. doi:10.1126/science.1139366

Wang, Z. L. (2004). "Zinc oxide nanostructures: growth, properties and applications". *Journal of Physics: Condensed Matter*, *16*(25), R829–R858. doi:10.1088/0953-8984/16/25/R01

Warheit, D. B., Webb, T. R., Reed, K. L., Frerichs, S., & Sayes, C. M. (2007). "Pulmonary toxicity study in rats with three forms of ultrafine-TiO2 particles: differential responses related to surface properties". *Toxicology*, *230*(1), 90–104. doi:10.1016/j.tox.2006.11.002

Watson, J., Chow, J., & Chen, L. (2005). "Summary of Organic and Elemental Carbon / Black Carbon Analysis Methods and Intercomparisons". *Aerosol and Air Quality Research*, *5*(1), 65–102. Retrieved from http://www.aaqr.org/Doi.php?id=6_AAQR-05-06-OA-0006

Weber, A. P., Baltensperger, U., Gäggeler, H. W., & Schmidt-Ott, A. (1996). "In situ characterization and structure modification of agglomerated aerosol particles". *Journal of Aerosol Science*, *27*(6), 915–929. doi:10.1016/0021-8502(96)00013-4

Weingartner, E., Saathoff, H., Schnaiter, M., Streit, N., Bitnar, B., & Baltensperger, U. (2003). "Absorption of light by soot particles: determination of the absorption coefficient by means of aethalometers". *Journal of Aerosol Science*, *34*(10), 1445–1463. doi:10.1016/S0021-8502(03)00359-8

Weingartner, E., Burtscher, H., Hüglin, C., & Ehara, K. (2011). "Semi-Continuous Mass Measurement". In Kulkarni, P., Baron, P.A., & Willeke, K. (Eds.), *Aerosol Measurement: Principles, Techniques, and Applications, Third Edition* (pp. 255–268). John Wiley & Sons, Inc. doi:10.1002/9781118001684.ch12

Welz, B., & Sperling, M. (2007). *Atomic absorption spectrometry* (Third Edit.). Wiley-VCH Verlag GmbH. doi:10.1002/9783527611690

Wennmalm, S., & Widengren, J. (2012). "Interferometry and fluorescence detection for simultaneous analysis of labeled and unlabeled nanoparticles in solution." *Journal of the American Chemical Society*, *134*(48), 19516–9. doi:10.1021/ja308213q

Whitby, K., Clark, W. W. E., Whitby, B. K. T., Clark, W. W. E., & Departmnt, M. E. (1966). "Electric aerosol particle counting and size distribution measuring system for the 0.015 to 1 μm size range". *Tellus*, *18*(2-3), 573–586. doi:10.1111/j.2153-3490.1966.tb00272.x

Wiedensohler, A. (1988). "Technical note: an approximation of the bipolar charge distribution for particles in the submicron size range". *Journal of Aerosol Science*, *19*(3), 387–389. doi:10.1016/0021-8502(88)90278-9

Wiedensohler, A., Aalto, P., Covert, D., Heintzenberg, J., & McMurry, P. H. (1993). "Intercomparison of three methods to determine size distributions of ultrafine aerosols with low number concentrations". *Journal of Aerosol Science*, *24*(4), 551–554. doi:10.1016/0021-8502(93)90038-B

Wiedensohler, A., Aalto, P., Covert, D., Heintzenberg, J., & McMurry, P. H. (1994). "Intercomparison of Four Methods to Determine Size Distributions of Low-Concentration (~100 cm^{-3}), Ultrafine Aerosols ($3 < D_p < 10$ nm) with Illustrative Data from the Arctic". *Aerosol Science and Technology*, *21*(2), 95–109. doi:10.1080/02786829408959700

Wiedensohler, A., Birmili, W., Nowak, A., Sonntag, A., Weinhold, K., Merkel, M., Wehner, B., Tuch, T., Pfeifer, S., Fiebig, M., Fjäraa, A. M., Sellegri, K., Depuy, R., Venzac, H., Villani, P., Laj, P., Aalto, P., Ogren, J. A., Swietlicki, E., Williams, P., Roldin, P., Quincey, P., Hüglin, C., Fierz-Schmidhauser, R., Gysel, M., Weingartner, E., Riccobono, F., Santos, S., Grüning, C., Faloon, K., Beddows, D., Harrison, R. M., Monahan, C., Jennings, S. G., O'Dowd, C. D., Marinoni, A., Horn, H.-G., Keck, L., Jiang, J., Scheckman, J., McMurry, P. H., Deng, Z., Zhao, C. S., Moerman, M., Henzing, B., de Leeuw, G., Löschau, G., Bastian, S. (2012). "Mobility particle size spectrometers: harmonization of technical standards and data structure to facilitate high quality long-term observations of atmospheric particle number size distributions". *Atmospheric Measurement Techniques*, *5*(3), 657–685. doi:10.5194/amt-5-657-2012

Willander, M., Nur, O., Zhao, Q. X., Yang, L. L., Lorenz, M., Cao, B., Zúñiga Pérez, J., Czekalla, C., Zimmermann, G., Grundmann, M., Bakin, A., Behrends, A., Al-Suleiman, M., El-Shaer, A., Che Mofor, A., Postels, B., Waag, A., Boukos, N., Travlos, A., Kwack, H. S., Guinard, J., Le Si Dang, D. (2009). "Zinc oxide nanorod based photonic devices: recent progress in growth, light emitting diodes and lasers." *Nanotechnology*, *20*(33), 332001. doi:10.1088/0957-4484/20/33/332001

Willeke, K. (1976). "Temperature dependence of particle slip in a gaseous medium". *Journal of Aerosol Science*, *7*(3), 381–387. doi:10.1016/0021-8502(76)90024-0

Willeke, K. and Liu, B.Y.H. (1976). Single Particle Optical Counter: Principle and Application. In B. Y. H. Liu (Ed.), *Fine Particles – Aerosol Generation, Measurement, Sampling, and Analysis* (pp. 697–729). Academic Press, New York, San Francisco, London.

Willeke, K., & Brockmann, J. (1977). "Extinction coefficients for multimodal atmospheric particle size distributions". *Atmospheric Environment*, *11*(10), 995–999. doi:10.1016/0004-6981(77)90029-4

Wilson, C. T. R. (1897). "Condensation of Water Vapour in the Presence of Dust-Free Air and Other Gases". *Philosophical Transactions of the Royal Society A: Mathematical, Physical and Engineering Sciences*, *189* (January), 265–307. doi:10.1098/rsta.1897.0011

Wilson, J., & Liu, B. (1980). "Aerodynamic particle size measurement by laser-Doppler velocimetry". *Journal of Aerosol Science*, *11*(2), 139–150. doi:10.1016/0021-8502(80)90030-0

Wilson, W. E., Chow, J. C., Claiborn, C., Fusheng, W., Engelbrecht, J., & Watson, J. G. (2002). "Monitoring of particulate matter outdoors." *Chemosphere*, *49*(9), 1009–43. doi:10.1016/S0045-6535(02)00270-9

Wilson, W. E., Han, H. S., Stanek, J., Turner, J., & Pui, D. H. Y. (2003). "The Fuchs surface area, as measured by charge acceptance of atmospheric particles, may be a useful indicator of the surface area of particles deposited in the lung". *Journal of Aerosol Science*, *34* (Supplement 1), S421–S422. doi:10.1016/S0021-8502(03)00137-X

Wilson, W. E., Stanek, J., Han, H.-S. (Ryan), Johnson, T., Sakurai, H., Pui, D. Y. H., Turner, J., Chen, D.-R. and Duthie, S. (2007). "Use of the Electrical Aerosol Detector as an Indicator of the Surface Area of Fine Particles Deposited in the Lung". *Journal of the Air & Waste Management Association*, *57*(2), 211–220. doi:10.1080/10473289.2007.10465321

Winchester, J. W., Ivanov, V. A., Prokofyev, M. A., Zhukovski, D. A., Shlikhta, A., Zhvalev, V. F., Zhukovski, A. N., Stroganov, D. M., Nelson, J. W., Bauman, S. E., Nakhgaltsev, L. N. (1990). "An Intercomparison of PIXE and XRF for Statistically Resolving Aerosol Components in Leningrad and Environs". *Nuclear Instruments and Methods in Physics Research B*, *49*(1-4), 351–359. doi:10.1016/0168-583X(90)90275-Y

Winklmayr, W., Reischl, G. P., Lindner, A. O., & Berner, A. (1991). "A new electromobility spectrometer for the measurement of aerosol size distributions in the size range from 1 to 1000 nm". *Journal of Aerosol Science*, *22*(3), 289. doi:10.1016/S0021-8502(05)80007-2

Woo, K.-S., Chen, D.-R., Pui, D. Y. H., & Wilson, W. E. (2001). "Use of Continuous Measurements of Integral Aerosol Parameters to Estimate Particle Surface Area". *Aerosol Science and Technology*, *34*(1), 57–65. doi:10.1080/02786820117549

Worobiec, A., Potgieter-Vermaak, S., Brooker, A., Darchuk, L., Stefaniak, E., & Van Grieken, R. (2010). "Interfaced SEM/EDX and micro-Raman Spectrometry for characterisation of heterogeneous environmental particles — Fundamental and practical challenges". *Microchemical Journal*, *94*(1), 65–72. doi:10.1016/j.microc.2009.09.003

Xu, Y., Shen, J., Cai, X., Riebel, U., & Guo, X. (2008). "Particle size analysis by transmission fluctuation spectrometry with band-pass filters". *Powder Technology*, *184*(3), 291–297. doi:10.1016/j.powtec.2007.08.016

Yabe, S., Yamashita, M., Momose, S., Tahira, K., Yoshida, S., Li, R., Yin, S., Sato, T. (2001). "Synthesis and UV-shielding properties of metal oxide doped ceria via soft solution chemical processes". *International Journal of Inorganic Materials*, *3*(7), 1003–1008. doi:10.1016/S1466-6049(01)00198-2

Yamamoto, H., Matsuyama, T., & Wada, M. (2002). "Shape distinction of particulate materials by laser diffraction pattern analysis". *Powder Technology*, *122*(2-3), 205–211. doi:10.1016/S0032-5910(01)00417-X

Yang, W., Peters, J. I., & Williams, R. O. (2008). "Inhaled nanoparticles--a current review". *International Journal of Pharmaceutics*, *356*(1-2), 239–47. doi:10.1016/j.ijpharm.2008.02.011

Zamengo, L., Barbiero, N., Gregio, M., & Orrù, G. (2009). "Combined scanning electron microscopy and image analysis to investigate airborne submicron particles: a comparison between personal samplers." *Chemosphere*, *76*(3), 313–23. doi:10.1016/j.chemosphere.2009.03.065

Zelenyuk, A., Cai, Y., Chieffo, L., & Imre, D. (2005). "High Precision Density Measurements of Single Particles: The Density of Metastable Phases". *Aerosol Science and Technology*, *39*(10), 972–986. doi:10.1080/02786820500380206

Zhang, F., Chan, S.-W., Spanier, J. E., Apak, E., Jin, Q., Robinson, R. D., & Herman, I. P. (2002). "Cerium oxide nanoparticles: Size-selective formation and structure analysis". *Applied Physics Letters*, *80*(1), 127. doi:10.1063/1.1430502

Zhang, L. W., Yu, W. W., Colvin, V. L., & Monteiro-Riviere, N. A. (2008). "Biological interactions of quantum dot nanoparticles in skin and in human epidermal keratinocytes." *Toxicology and Applied Pharmacology*, *228*(2), 200–11. doi:10.1016/j.taap.2007.12.022

Zhao, J., Eisele, F. L., Titcombe, M., Kuang, C., & McMurry, P. H. (2010). "Chemical ionization mass spectrometric measurements of atmospheric neutral clusters using the cluster-CIMS". *Journal of Geophysical Research*, *115*(D8), D08205. doi:10.1029/2009JD012606

Zharov, V., & Lapotko, D. (2005). "Photothermal imaging of nanoparticles and cells". *IEEE Journal of Selected Topics in Quantum Electronics*, *11*(4), 733–751. doi:10.1109/JSTQE.2005.857382

Zhong, X., Li, Q., Hu, J., & Lu, Y. (2008). "Characterization and corrosion studies of ceria thin film based on fluorinated AZ91D magnesium alloy". *Corrosion Science*, *50*(8), 2304–2309. doi:10.1016/j.corsci.2008.05.016

Zhou, E. H., Watson, C., Pizzo, R., Cohen, J., Dang, Q., de Barros, P. M. F., Park, C. Y., Chen, C., Brain, J. D., Butler, J. P., Ruberti, J. W., Fredberg, J. J., Demokritou, P. (2014). "Assessing the impact of engineered nanoparticles on wound healing using a novel in vitro bioassay." *Nanomedicine*, (Posted online on May 13, 2014), 1–13. doi:10.2217/nnm.14.40

Zhu, J., Ozdemir, S. K., Xiao, Y.-F., Li, L., He, L., Chen, D.-R., & Yang, L. (2009). "On-chip single nanoparticle detection and sizing by mode splitting in an ultrahigh-Q microresonator". *Nature Photonics*, *4*(1), 46–49. doi:10.1038/nphoton.2009.237

Zhu, J., Özdemir, Ş. K., He, L., Chen, D.-R., & Yang, L. (2011). "Single virus and nanoparticle size spectrometry by whispering-gallery-mode microcavities." *Optics Express*, *19*(17), 16195–206. doi:10.1364/OE.19.016195

Zimmermann, S., Abel, N., Baether, W., & Barth, S. (2007). "An ion-focusing aspiration condenser as an ion mobility spectrometer". *Sensors and Actuators B: Chemical*, *125*(2), 428–434. doi:10.1016/j.snb.2007.02.038

Zimmermann, S., Barth, S., Baether, W. K. M., & Ringer, J. (2008). "Miniaturized low-cost ion mobility spectrometer for fast detection of chemical warfare agents". *Analytical Chemistry*, *80*(17), 6671–6. doi:10.1021/ac800559h